Optimisation of *Phaeodactylum tricornutum* as a Microalgal Expression Host for Industrial Biotechnology

A thesis submitted to University College London for the degree of Doctor of Philosophy

By

Zhongdi Song

Department of Biochemical Engineering
University College London
Gower Street
London
WC1E 6BT

2020

Declaration

I, Zhongdi Song confirm that the work presented in this thesis is my own. Where information has been derived from other sources, I confirm that this has been indicated in the thesis.

Signature:

Acknowledgement

I would like to express my sincere gratitude to all those who helped me during the four years studying as a PhD student at University College London.

I sincerely thank my principal supervisor, Dr. Brenda M Parker, for her great encouragement and patience to me, and for her great support and guidance on my PhD work. She gave me the freedom to explore things that I am interested in and encourages us to attend the algae-related conferences. During writing up, she shared us her experience in time management, paper drafting and paper revision and gave me valuable feedback. I would also like to thank my secondary supervisor, Prof. Gary Lye, who offered me great help during my application of scholarship and gave me valuable suggestions on my project, first year report and paper manuscript.

I am very thankful to the lab members who gave me training and assistance during my experimental work. They are Victor Sanchez Tarre, Dr. Baolong Wang, Dr. Haoran Yu, Greta Csalane Besenyei, Anaëlle Vilatte, Dr. Cheng Zhang, Dr. Maria Bawn, Dr. Max Cardenas Fernandez, Roberto Chiocchio, Dr. Xenia Spencer Milnes, Alexander Cotton and Alex Olivares Molina. I especially thank Dr. Andrea Rayat for her training on shear device and guidance on result analysis. In addition, I am grateful to Dr. Michael Sulu, Dr. Gareth Mannall and Dr. Brian O'Sullivan for managing the labs and maintaining the instruments in good condition.

It would not have been possible for me to study abroad without the financial support from the Chinese Scholarship Councils (CSC) for my living allowance and the UCL Overseas Research Scholarships (UCL-ORS) award for my tuition fees. I am truly grateful for this support.

Lastly, I would like to give thanks to my friends Dr. Chuanjie Du, Yang Lu, and Dr. Yiling Zhu for their help during my language learning. Most of all, I am very thankful to my parents, Qingguo Song and Fengzhi Han, my sisters,

Zhongwei Song and Dr. Zhongxin Song, and my husband, Dr. Haoran Yu, for their endless love and constant support, encouragement and understanding.

Abstract

Phaeodactylum tricornutum is a polymorphic marine diatom and can undergo morphological conversions between cell morphotypes, mainly fusiform, triradiate and oval. However, limited information is available about the conditions that can be used for controlling cell morphology and maintaining a specific cell morphotype with high growth rate and biomass productivity. In this study, the effects of culture medium and culture age on morphological changes in *P. tricornutum* were first investigated. Mann and Myers' medium was identified as eliciting significant morphotype conversion from fusiform to oval in *P. tricornutum*. Liquid cultures containing more than 90% oval cells were obtained and well-maintained in this medium under the constant shaking condition, allowing high dry biomass concentration (0.73 g L^{-1}) to be achieved. The subsequent biochemical composition analyses of different cell morphotypes revealed that pigments, particularly fucoxanthin and chlorophyll *a*, were markedly accumulated and higher protein content (% dry weight) was obtained in oval cell cultures maintained in M & M medium compared to fusiform cell cultures maintained in f/2 medium, where lipid and carbohydrate were significantly accumulated over 21 days cultivation. The further investigation of downstream processing of different cell morphotypes using ultra scale-down approaches predicted that a high cell recovery efficiency (>93%) without evident cell damage could be obtained for both morphotypes when using either a hermetically or a non-hermetically sealed disc-stack centrifuge. Additionally, cell disruption analysis by focused acoustics demonstrated that oval cells were much more robust against mechanical forces, requiring a longer treatment time for complete cell rupture than fusiform cells. This study offered an effective and practical way to achieve high biomass production of oval cells in liquid cultures and provided significant implications for upstream cultivation strategies and downstream bioprocessing to optimise the manufacture of different classes of products in different morphotypes of *P. tricornutum*.

Impact statement

Phaeodactylum tricornutum is a polymorphic marine diatom, displaying three main cell morphotypes: fusiform, triradiate and oval. It may be important to be able to selectively control growth of a particular morphotype for a particular industrial application. However, limited information is available about the conditions that can be used for controlling and maintaining cell morphology. In this study, a culture medium called Mann and Myers' medium was identified to induce significant morphotype transformation from fusiform to oval in *P. tricornutum*. Liquid cultures abundant with >90% oval cells were finally obtained and well-maintained in this medium under constant agitation, which enhances the mass and gas transfer and light availability allowing high cell concentration and biomass yield to be achieved. This work is considered to be significant for offering a novel way to regulate and maintain cell morphology of *P. tricornutum*, which can be used by *Phaeodactylum* researchers to establish stable phenotypes for deeper exploration on molecular mechanisms of cell morphology control. By demonstrating that M & M medium was effective and practical for high oval cell production in liquid cultures, this work enables further assessment of oval *P. tricornutum* cells for potential industrial applications.

P. tricornutum is of great interest for industrial application as a natural rich source of high-value eicosapentaenoic acid (EPA) and fucoxanthin. Its highly interesting pleiomorphic property motivated us to characterise the biochemical profiles in fusiform and oval cells. Oval *P. tricornutum* cells maintained in M & M medium were shown to be promising for high pigment and protein production whereas fusiform *P. tricornutum* cells cultured in f/2 medium were found to be a potential feedstock for biofuel production due to the marked accumulation of lipid and carbohydrate over time. This work provides insights into biochemical profiles of different cell morphotypes in response to culture media, which is essential for nutritional value evaluation and for better utilisation of algal biomass, in support of *Phaeodactylum* biorefinery for industrial exploitation.

The further investigation of downstream processing of different cell morphotypes indicated that a predicted high cell recovery efficiency (>93%) without evident cell damage was obtained for both morphotypes when using either a hermetically or a non-hermetically sealed disc-stack centrifuge. It was also found that oval cells were much more robust, requiring a longer treatment time by focused acoustics for complete cell rupture than fusiform cells. This work provides new insights into the impacts of cell morphotypes on *P. tricornutum* downstream bioprocessing. *P. tricornutum* is currently under development as an expression host for therapeutic proteins, bioplastics, etc. This study might have important implications on upstream cultivation strategies and downstream bioprocessing for the optimisation of product manufacture in *P. tricornutum*, which would be very useful for scale-up bioprocess design and for *P. tricornutum* application in industry.

The results from the third and fourth chapters have been published in a scholarly journal. The results from the fifth chapter will also be expected to be published. By disseminating outputs through publication, this study would potentially be known by international scholars with the impact being extended.

Table of Contents

Table of Figures

Table of Tables

Abbreviations

AFA	Adaptive focused acoustics
BSA	Bovine Serum Albumin
CCAP	Culture Collection of Algae and Protozoan
CFD	Computational fluid dynamics
DHA	Docosahexaenoic acid
DMF	*N, N*-dimethylformamide
DMSO	Dimethyl sulfoxide
DW	Dry weight
E. coli	*Escherichia coli*
EDTA	Ethylenediaminetetraacetic acid
EPA	Eicosapentaenoic acid
EPS	Exopolymeric substances/ Exopolysaccharides
EST	Expressed sequence tag
FAME	Fatty acid methyl ester
FID	Flame ionisation detector
GC	Gas chromatography
HCl	Hydrochloric acid
HPAEC	High-performance anion exchange chromatography
HPLC	High-performance liquid chromatography
LED	Light emitting diodes
MUFA	Monounsaturated fatty acid
M & M medium	Mann and Myers' medium
NaOH	Sodium hydroxide
NLs	Neutral lipids
OD	Optical density
PBRs	Photobioreactors
PES	Polyethersulfone
PHB	Poly-3-hydroxybutyrate
PLs	Polar lipids
PMSF	Phenylmethylsulfonylfluoride

ppt	Parts per thousand
PSA	Phenol sulphuric acid
Pt1 8.6	*Phaeodactylum tricornutum* CCAP 1055/1
Pt4	*Phaeodactylum tricornutum* CCAP 1052/6
PTFE	Polytetrafluoroethylene
PUFA	Polyunsaturated fatty acid
RO	Reverse osmosis
SDS-PAGE	Sodium dodecyl sulphate polyacrylamide gel electrophoresis
SFA	Saturated fatty acid
SQDG	sulfoquinovosyl diacylglycerol
TAG	Triacylglyceride
TAP	Tris-acetate-phosphate
TFA	Total fatty acid
Tris	Hydroxymethylaminomethane
USD	Ultra scale-down

1 Introduction

1.1 Microalgae

Algae are a large group of diverse photosynthetic organisms containing macroalgae (seaweed) and microalgae. They can efficiently use solar energy and the greenhouse gas carbon dioxide for photoautotrophic growth, contributing approximately half of the planet's oxygen production and the global net primary production (Chapman, 2013, Field et al., 1998). Microalgae are unicellular microscopic algae containing a huge biodiversity of both prokaryotic (cyanobacteria) and eukaryotic species (Figure 1-1). They are widely abundant in every biome on the planet, found in freshwater, marine and terrestrial environments. It has been estimated that over 300,000 microalgal species exist of which only 30,000 have been documented (Mobin and Alam, 2017). Microalgae are broadly divided into several groups: Cyanobacteria (blue-green algae), Rhodophyta (red algae), Chlorophyta (green algae), Bacillariophyta (diatoms) and others (Keeling, 2010, Hallmann, 2015).

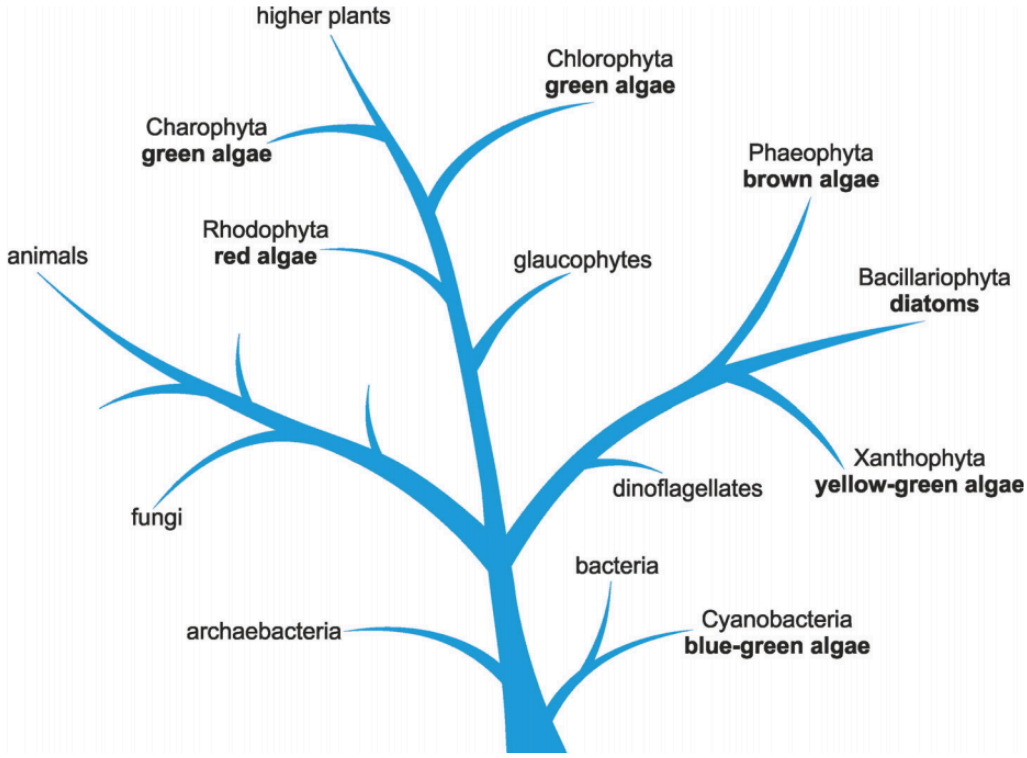

Figure 1-1 A schematic diagram of tree of life with emphasis on algae showing the diversity of phylogeny (Hallmann, 2015).

1.1.1 Potential application of microalgae

Considerable attention has recently been paid to microalgal exploitation and utilisation since they can efficiently use solar energy and inorganic carbon for sustainable biosynthesis of high-value compounds such as proteins, pigments, polysaccharides, lipids and vitamins. These microalgae-derived products have applications in various industries (Figure 1-2). For example, microalgae biomass as feed in aquaculture or as nutritional supplement for animals and humans (Hemaiswarya et al., 2011, Caporgno and Mathys, 2018), pigments as natural colourants in food and cosmetics (Begum et al., 2016), lipids and carbohydrates for renewable biofuel production (Ziolkowska and Simon, 2014), and microalgal extracts for nutraceutical and pharmaceutical applications (Jha et al., 2017).

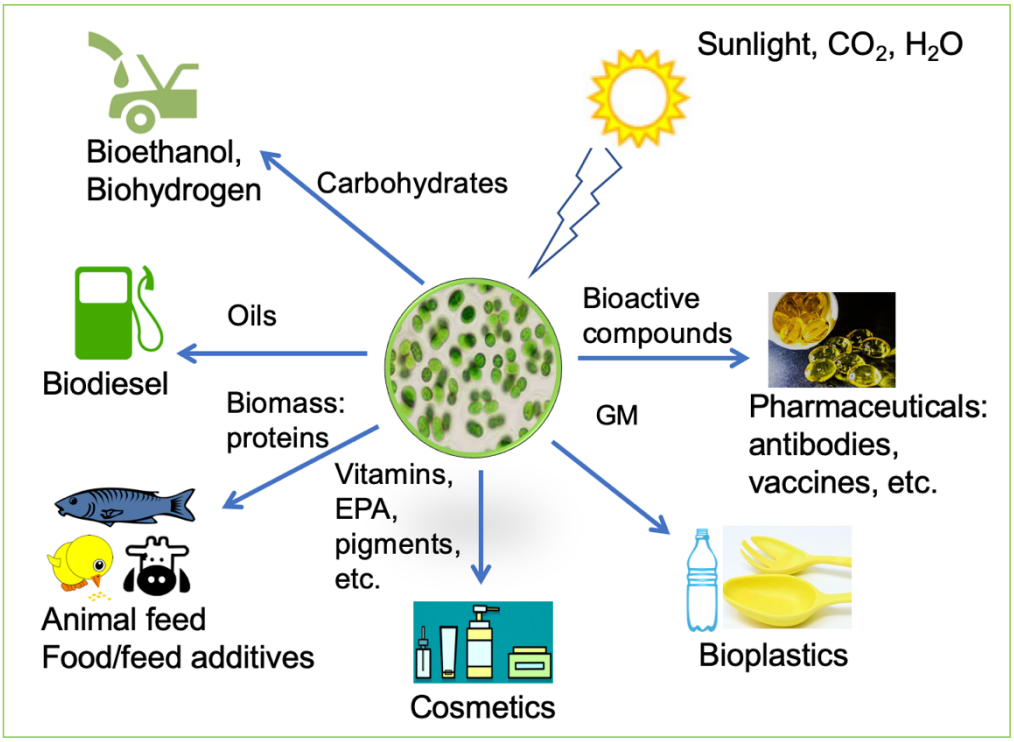

Figure 1-2 Biotechnological applications of microalgae.

A schematic diagram showing the biotechnological potential of microalgae. GM, genetically modified.

Today only a few products are commercially produced from microalgae. One notable application is the cultivation of the freshwater green microalga

Haematococcus pluvialis for high-level production of astaxanthin (4-5% of dry weight (DW)), a carotenoid widely used as a feed additive in fish aquaculture. Astaxanthin has superior antioxidant properties compared to other carotenoids for pharmaceutical and cosmetic applications (Shah et al., 2016). Other examples include β-carotene production (up to 14% DW) from the halotolerant green microalga *Dunaliella salina* (Spolaore et al., 2006, Xu et al., 2018), and docosahexaenoic acid (DHA) production from the marine heterotrophic dinoflagellate *Crypthecodinium cohnii* (Gong et al., 2015). In addition, the green algal species *Chlorella* and the cyanobacteria *Arthrospira platensis*, more widely known as *Spirulina* are produced globally in large quantities every year for human and animal consumption in view of their excellent nutritive value and health benefits (Spolaore et al., 2006).

Dried whole algae *Spirulina* accounts for the largest market volume of microalgae-based products. The annual production of *Spirulina* biomass exceeds 12 000 tons, followed by an estimated 5000 tons of *Chlorella*, 3000 tons of *D. salina* for carotene, 700 tons of *H. pluvialis* for astaxanthin and 500 tons of *C. cohnii* for DHA (Garcia et al., 2017). The global market value of microalgae is estimated to be US$5-7 billion, out of which about US$2.5 billion is from the health food, US$2 billion from the high-value products (cosmetics, nutraceuticals and pharmaceuticals) and US$0.7 billion by aquaculture (Mobin and Alam, 2017, Khanra et al., 2018).

Microalgae biomass is rich in lipids and carbohydrates, which can be converted into biofuels such as biodiesel, bioethanol, biohydrogen and methane (Ziolkowska and Simon, 2014). The microalgae used in practical applications typically have a lipid content of 20–50% DW, with higher oil productivities than those from traditional crops like corn, soybeans and oil palm (Medipally et al., 2015, Ziolkowska and Simon, 2014). Therefore, microalgae have emerged as an attractive alternative to the conventional crop-based feedstock for sustainable biofuel production, which in some extent would relieve the fossil fuel-based energy crisis and the food/feed crop-fuel crop crisis. However, the production of biofuels from microalgae in commercial scale is not economically viable at present.

The definition of biorefinery is the sustainable biomass processing to obtain energy biofuels and high-value products through a series of processes and equipment for biomass transformation (Gonzalez-Delgado and Kafarov, 2011). The biorefinery concept allows to make full utilisation of raw materials at low cost for the sustainable production of diverse bioproducts. Different kinds of biomass can be utilised in biorefinery such as agricultural crops (first generation), lignocellulosic biomass like straw and bark (second generation), and aquatic biomass of algae (third generation) (de Jong et al., 2009, Hossain et al., 2017). Microalgae can be used as an efficient and economical biorefinery feedstock. Based on the biorefinery concept, co-production of multiple value-added products with biofuels is considered as an approach to obtain a maximum financial profit for microalgal application. The remaining biomass can be used as feed, fertilizer or for energy co-generation (Brennan and Owende, 2010).

Several microalgae species such as *Spirulina*, *Chlorella*, *Dunaliella*, *Haematococcus*, *C. cohnii* and *Schizochytrium* have been classified as Generally Recognized As Safe (GRAS) organisms (Garcia et al., 2017), which eases microalgal use in nutraceutical and pharmaceutical industries. Microalgae could produce a vast range of bioactive compounds such as β-carotene, astaxanthin, fucoxanthin, lutein, DHA, EPA (eicosapentaenoic acid), polysaccharides and phenolics, with the extracts showing antibacterial, antiviral, antifungal, anticancer, anti-inflammatory, and antioxidant properties (Jha et al., 2017). In addition to the application of microalgae as a production platform for a host of naturally-produced compounds, genetically modified (GM) microalgae have been eliciting considerable interest for the augmentation of desired product yield or for the production of recombinant proteins, which are in great demand in various industrial and pharmaceutical applications. For example, successful genetic engineering in the expression of bioplastics or therapeutic proteins such as vaccines, antibodies and immunotoxins has been achieved in microalgae *Chlamydomonas reinhardtii* and *Phaeodactylum tricornutum* (Gangl et al., 2015, Hempel et al., 2011a, Hempel et al., 2017).

Furthermore, microalgae can also be used for bioremediation, for example, removal of nitrogen, phosphorus and heavy metals for wastewater treatment (Ummalyma et al., 2018) and removal of CO_2 by bio-fixation from flue gas emissions (Devi et al., 2014). CO_2 capture by microalgae plays a significant role in reducing greenhouse gas and mitigating the climate change of global warming.

1.1.2 Advantages of microalgae as a production platform

Microalgae are considered promising as an emerging industrial production platform for the light-driven synthesis of high-value compounds and recombinant proteins. They hold numerous economic, environmental and technical advantages. As photoautotrophs, they combine advantages of both microorganisms and higher plants (Potvin and Zhang, 2010). They have simple, inexpensive nutrient requirements and short generation time, and can be grown in seawater, brackish water or wastewater (Mata et al., 2010, Ziolkowska and Simon, 2014).

Currently, the well-established expression systems that are commonly employed to produce commercial bioproducts, particularly recombinant proteins, include bacteria, yeasts, plants, insect and mammalian cells (Yan et al., 2016). However, there are limitations with each system. Bacterial expression hosts lack the ability of post-transcriptional and post-translational modifications such as intron-splicing, glycosylation and multimeric protein assembly, which means that the majority of functional eukaryotic proteins could not be produced in prokaryotic systems (Yan et al., 2016). Furthermore, the presence of bacterial endotoxins enhances difficulty in purification and has adverse effect on human health (Walker et al., 2005). Although yeasts possess protein modification systems, the pattern of glycosylation usually involves hypermannosylation, different from that occurring in higher organisms (Chiba and Jigami, 2007). Mammalian bioreactors remain the system used for the production of the majority of pharmaceutical proteins due to their ability to express large and complex functional proteins with proper post-translational modifications (Tripathi and

Shrivastava, 2019). However, the production cost is very high as mammalian cells require sophisticated and expensive growth media and are difficult to culture at large scale and high-level purification requiring large volumes of cell culture is expensive (Puetz and Wurm, 2019, Yan et al., 2016). The mammalian systems also have the contamination risk by animal viruses (Owczarek et al., 2019). Transgenic plants come into focus due to their ability to perform photosynthesis, ease of scale up and resistance to most human pathogens. However, they have low growth rate, compete for agricultural land and may cause flow of transgenes to environment when cultivated in open and semi-enclosed greenhouses (Hempel et al., 2011b, Stoffels et al., 2019). It is therefore still appealing to develop novel, safe and low-cost expression platforms for industrial biotechnology.

Microalgae hold several advantages as an emerging host for the light-driven production of recombinant proteins. Microalgae do not involve human pathogens, being an advantage for the expression of pharmaceutical proteins (Yan et al., 2016, Hempel et al., 2011b). Compared to transgenic plants, microalgae represent a much simpler system and hence more efficient genetic manipulations, have much shorter doubling times, do not compete for arable land and freshwater with agricultural crops, and can be grown in enclosed photobioreactors (PBRs) to prevent the release of transgenes to the environment (Raja et al., 2008, Gangl et al., 2015). Eukaryotic microalgae are able to perform post-transcriptional and post-translational modifications which is species-specific (Dumontier et al., 2018). Investigation of *P. tricornutum* producing human anti-Hepatitis B monoclonal antibodies revealed that proteins carry high mannose-type *N*-glycans ranging from Man-5 to Man-9 (Vanier et al., 2015). In another study, one N-acetylglucosaminyltransferase I (GnT I) gene which is able to convert Man-5 into complex-type *N*-glycans was predicted in *P. tricornutum* genome and traces of other glycan types such as Man-3, Man-4 and fucosylated Man-3 were also detected for proteins from *P. tricornutum* (Baïet et al., 2011). Although the reported protein *N*-glycosylation occurring in microalgae differs from that described in mammals, genetic engineering tools are available and may be used to engineer the glycosylation pathways in microalgae to

produce biopharmaceuticals compatible for use in human therapy (Dumontier et al., 2018). From industrial perspective, the ease of cultivation makes microalgae particularly suitable for mass cultivation with comparatively low operating cost, and potentially cost-efficient product production (Stoffels et al., 2019). High cell density and biomass yield can be achieved in simple PBRs with sufficient supply of light and carbon source (El-Baz and El Baky, 2018). These demonstrated the great potential of microalgae to serve as a cost-effective, safe and eco-friendly expression platform for industrial biotechnology.

1.1.3 Microalgal cultivation

Microalgae can efficiently convert solar energy into chemical energy through photosynthesis. As photoautotrophic organisms, microalgae have simple growth requirements. They require inorganic carbon like CO_2 and light energy, together with macronutrients like nitrogen and phosphorus for growth (Singh and Patidar, 2018). Nitrogen and phosphorus are constituents of proteins and nucleic acids and are therefore essential nutrients for cell growth. They are generally provided in the inorganic form like nitrate, ammonium and phosphate, although depending on the species and metabolism organic compounds such as urea, amino acids and nucleosides can also be assimilated (Neilson and Larsson, 1980). Besides macronutrients, microalgae also require a variety of micronutrients such as iron, zinc, cobalt, manganese and mostly B vitamins (Markou et al., 2014). Diatoms generally also require silicate for growth. In addition, cultivation parameters including light intensity, temperature, agitation, aeration and pH have significant influence on algal growth (Khan et al., 2018).

In addition to the photoautotrophic cultivation in which light is used as an energy source and inorganic carbon mainly CO_2 is used as a carbon source, some microalgae can grow heterotrophically or mixotrophically. In heterotrophic growth, microalgae utilise only organic compounds such as glucose, acetate and glycerol as both energy and carbon source under dark conditions (Guidhe et al., 2017). Mixotrophic growth involves both

phototrophic and heterotrophic cell metabolisms, in which microalgae perform photosynthesis for phototrophic growth, complemented with an organic compound as an extra energy and carbon source (Zhan et al., 2017). Studies have shown that *P. tricornutum* can grow in mixotrophic mode on glycerol, acetate, lactate, and glucose (Villanova et al., 2017, Garcıa et al., 2005, Smith et al., 2020), which is a good cultivation strategy to enhance cell growth and biomass production. *P. tricornutum* is an obligate photoautotrophic organism and unable to grow heterotrophically. However, through metabolic engineering to introduce a gene encoding a glucose transporter, successful heterotrophic growth of *P. tricornutum* on glucose was achieved, reaching a five-fold higher cell density relative to the phototrophic control (Zaslavskaia et al., 2001).

Large-scale cultivation of microalgae is mainly performed in two types of systems: open-culture systems and closed photobioreactors (PBRs) (Khanra et al., 2018). Open-culture systems such as raceway ponds have a low capital expenditure requirement and a large volumetric production capacity. They are normally located outdoors and rely on natural sunlight and temperature, thus being susceptible to weather conditions. Open ponds allow little control of process conditions such as temperature, illumination and evaporation, have a high contamination risk, have poor mixing, occupy large land area, and have difficulty in growing algae for long periods (Mata et al., 2010). The open systems are thus limited to a small quantity of algae species which can tolerate extreme environmental conditions to reduce contamination risks, such as *Spirulina, Chlorella* and *Dunaliella* belonging to fast growers and capable of thriving in highly alkaline or saline environments (Zhou et al., 2015, Tan et al., 2020). A variety of PBRs including flat-panel, tubular, airlift, bubble column PBRs and plastic bags are available for microalgae cultivation (El-Baz and El Baky, 2018). Closed PBRs are more commonly located outdoors to make use of free sunlight but may also be located indoors. They hold several advantages. For example, they offer a high degree of control over cultivation parameters (e.g. temperature, pH, mixing, CO_2), provide a closed environment protecting the culture from contamination or invasion by competing microorganisms and preventing evaporation, allow high cell

densities and high volumetric productivities to be attained and make it feasible to cultivate microalgae for some high-value products like pharmaceuticals. Their main limitations include high capital and operating costs, cell damage by shear stress due to mechanical or air bubbling mixing, oxygen accumulation, biofouling, and deterioration of construction material for photo-stage (Mata et al., 2010, Cruz et al., 2018). In PBRs, microalgal adhesion on the transparent PBR surfaces leads to biofouling. The process of biofouling is dynamic and sequential, including 1) the formation of a conditioning film on the exposed surface, 2) microfouling with colonies of microalgae and bacteria, and 3) macrofouling with a high number of microalgae and microorganisms. PBR biofouling reduces the sunlight penetration in the PBR and therefore decreases the photosynthetic efficiency and biomass productivity of the cultivation system (Zeriouh et al., 2017, Harris et al., 2013). Industrial microalgae production is typically conducted in non-axenic conditions. Some bacteria involved in the algal microbiome could induce biofilm formation and attachment of algae on the substrate through exopolymeric substances (EPS) production, leading to biofouling and reduced biomass productivity during industrial cultivation of microalgae in PBRs (Giraldo et al., 2019).

Microalgae can be cultivated in batch or continuous mode. Large-scale production of microalgal biomass is costly, requiring a large volume of seed culture to ensure the purity of cultures (Chisti, 2016). In order to reduce production costs, strategies to improve the nutrient utilisation efficiency have been tested. By adopting a circular economy approach, the sustainability of microalgal production could be improved by combining the microalgae cultivation with pollution control processes for recycling of waste nutrients, for instance, utilisation of CO_2 from flue gas emissions or nitrogen and phosphorus from a wastewater effluent (Odjadjare et al., 2017).

Microalgae and bacteria have existed together since the early stages of evolution (Ramanan et al., 2016). In both natural and industrial processes, there is evidence of microalgae living together with bacteria in complex microbial communities. Microalgae and bacteria synergistically affect each

other's physiology and metabolism mainly by exchanging metabolites and nutrients (Yao et al., 2019). The algae-bacterial interactions involve diverse symbiotic relationships including mutualism, commensalism and parasitism (Ramanan et al., 2016, Tandon et al., 2017). Studies have shown that bacteria may positively or negatively influence microalgal growth through a variety of mechanisms (Shi et al., 2018). For example, in mutualism, symbiotic bacteria could stimulate microalgal growth by producing B vitamins, phytohormones, siderophores to improve iron availability or inorganic nitrogen in exchange for fixed organic carbon such as EPS and glycolate from microalgae (Yao et al., 2019, Fuentes et al., 2016). Alternatively, in parasitism, parasitic bacteria may inhibit algal growth by competing for existing nutrients and may kill algae by secreting algicidal compounds to degrade algal cell wall (Ramanan et al., 2016, Tandon et al., 2017). Vitamins, acting as enzyme cofactors, play a vital part in the development of cellular biochemistry of microalgae. However, the majority of microalgae is vitamin B auxotroph since they cannot synthesise B vitamins and require the exogenous supply of vitamin B_{12} (cobalamin), B_1 (thiamine) and B_7 (biotin) in different combinations as growth factors (Tandon et al., 2017). These B vitamins can be produced by bacteria, archaea, and marine cyanobacteria and may serve as part of synergistic interactions between microalgae and bacteria (Yao et al., 2019).

The bacterial community naturally associated to algae is species-specific (Eigemann et al., 2013). A study on the microbiome of non-axenic *P. tricornutum* cultures from a culture collection revealed that the associated bacterial community is highly dynamic with four bacterial families playing major roles depending on growth phase and culture conditions. The authors showed that in complete f/2 medium, Pseudoalteromonadaceae dominated in lag phase, Flavobacteriaceae dominated in log phase and the stationary phase was dominated by Flavobacteriaceae and Pseudoalteromonadaceae. By contrast, in minimal medium containing only nitrogen (N) and phosphorus (P), Alteromonadaceae, Pseudoalteromonadaceae and Pseudomonadaceae dominated in log phase supporting good growth of *P. tricornutum* and the stationary phase was dominated by Alteromonadaceae (Moejes et al., 2017).

Another study showed that in N-deficient *P. tricornutum* cultures, the relative abundance of three gammaproteobacterial genera *Marinobacter, Methylophaga* and *Algiphilus,* belonging to families Alteromonadacea, Piscirickettsiaceae and Algiphilaceae respectively, increased markedly while the abundance of species *Sinorickettsia chlamys* markedly decreased (Shi et al., 2018). Marine methylotrophic bacteria were found to support the photoautotrophic growth of *P. tricornutum* by providing ammonium from degradation of methylamines which occur ubiquitously in oceans (Suleiman et al., 2016). Moreover, a marine bacterium *Stappia* sp. K01 (family Rhodobacteraceae), isolated from xenic cultures of *P. tricornutum,* was identified to promote growth and fucoxanthin biosynthesis of this diatom through utilising the extracellular fatty acids secreted by *P. tricornutum* (Vuong et al., 2019). These studies have important implications for industrial algal cultivation, where working in axenic conditions is hardly feasible. Appropriate control of the biological interactions between microalgae and bacteria would help to improve microalgal biomass production or control algal blooms.

1.2 *Phaeodactylum tricornutum*

Phaeodactylum tricornutum is a marine diatom. Diatoms constitute the most abundant eukaryotic phytoplankton in marine environments (Kooistra et al., 2007). They are estimated to contribute approximately 40% of marine primary productivity (Nelson et al., 1995) and up to 25% of global primary productivity (Falkowski et al., 1998, Lebeau and Robert, 2003). Diatoms also play an ecologically significant role in biogeochemical cycles of silicon, carbon, nitrogen and phosphorus (Treguer et al., 1995). Typically, a diatom cell is enclosed in a silicified shell, which is composed of two valves and connecting bands. According to the shape of cell walls known as frustules, diatoms can be divided into two major classes: the centrics which tend to appear radially symmetric and the pennates which display bilateral symmetry (Bowler et al., 2008).

P. tricornutum is a pennate raphid diatom, belonging to the division Heterokontophyta, class Bacillariophyceae, order Bacillariales, family Phaeodactylaceae and genus *Phaeodactylum* (De Martino et al., 2007).

1.2.1 Polymorphism of *Phaeodactylum tricornutum*

Three main cell morphotypes

P. tricornutum is a polymorphic diatom, displaying three distinct morphotypes: fusiform, triradiate and oval (Figure 1-3). The polymorphic feature and different cell morphotypes of *P. tricornutum* were first described by Wilson D. P. under the name of *Nitzschia closterium* (Wilson, 1946). The fusiform morphotype with two arms is 15-35 μm in length and 2.5-5 μm in width and appears to be most stable and frequently observed in liquid cultures. The triradiate cell with three arms being often unequal in length (6-8 μm), was shown to be rare and difficult to maintain in laboratory cultures (De Martino et al., 2007). The third type, oval cell, has no arms and is 6-10 μm long and 2.5-5 μm broad. This morphotype usually occurs on the bottom and sides of a flask, on solid media or under suboptimal conditions such as hyposalinity and low temperature (Wilson, 1946, De Martino et al., 2007).

The ultrastructure of each cell morphotype has also been described (Borowitzka and Volcani, 1978). It was shown that the three cell morphotypes contain similar cytoplasmic organelles in organisation and structure except for the vacuolar organisation and cell wall. The fusiform and triradiate cells are better adapted to planktonic lifestyle (Tesson et al., 2009a), which might be mediated by the vacuoles occupying the space within their arms (Borowitzka and Volcani, 1978), the cellular lipid content and the evolution of arms that increase the surface area to volume ratio (Bowler et al., 2010). By contrast, the oval morphotype is preferentially benthic, having a higher sedimentation rate compared to the other two morphotypes (De Martino et al., 2011). Almost the whole space inside oval cells was taken up by plastids or chromatophores (Wilson, 1946). Furthermore, oval cells can secrete mucilaginous EPS and possess a raphe (Lewin et al., 1958), favouring cell adhesion and gliding motility on surface (Tesson et al., 2009a, De Martino et

al., 2011). The raphe, commonly found on the hypotheca (Figure 1-4), is a slit along the frustule that facilitates gliding movement via the secretion of EPS (Kooistra et al., 2007, Bowler et al., 2010). EPS are metabolic products comprising polysaccharides, glycoproteins and other biopolymers. EPS, attached to the cell surface or released into environment, play important ecological roles including cell adhesion, motility of benthic diatoms, biofilm formation, as a carbon and energy source and cell protection against stresses such as UV radiation, oxidative stress or water deficiency (Xiao and Zheng, 2016, Han et al., 2019). It has been observed that oval cells tend to aggregate in clusters surrounded by mucilage, sink and adhere to culture flasks in stressed cultures, which suggested that cell aggregation and EPS secretion could represent protective mechanisms of cells against stresses like low temperature and nutrient starvation (De Martino et al., 2007, De Martino et al., 2011).

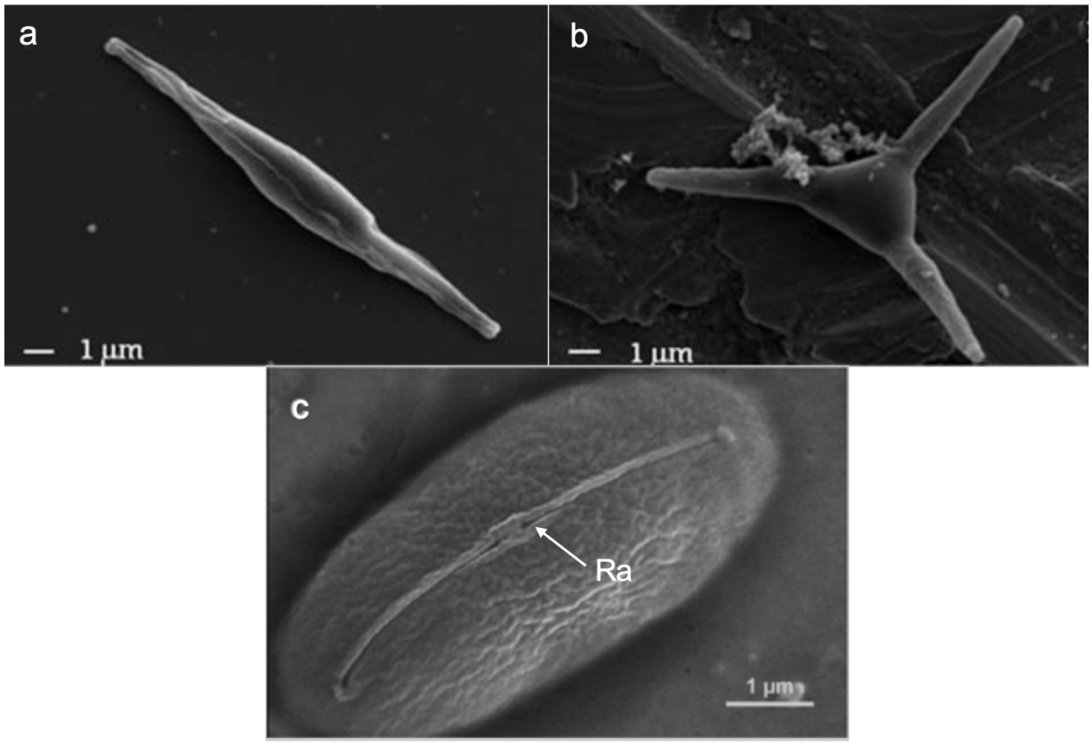

Figure 1-3 Scanning electron microscopy images of three morphotypes of *P. tricornutum.*

Scanning electron micrographs showing the fusiform (a), triradiate (b) and oval (c) morphotypes of *P. tricornutum*. Ra, raphe, a silicified structure found only in oval morphotype. Images are cited from (Martin-Jezequel and Tesson, 2013, Francius et al., 2008)

Cell wall structure and constituent

P. tricornutum has a three-layer cell wall structure: an outer opaque organic layer (3 nm), an intermediate organic or silicified layer (4-6 nm) and an inner opaque organic layer (3 nm) (Reimann and Volcani, 1967, Borowitzka and Volcani, 1978). The inner layer, called diatotepum, is described previously as fibrillar material within an amorphous matrix, composed of polyanionic polysaccharides (Borowitzka and Volcani, 1978, Tesson et al., 2009a). Sulphated glucuronomannan, commonly found in diatom cell walls, has shown to be the major component of *Phaeodactylum* cell wall (Ford and Percival, 1965b, Le Costaouec et al., 2017) and was described as fibrils deposited in the inner layer of the cell wall (Tesson et al., 2009b).

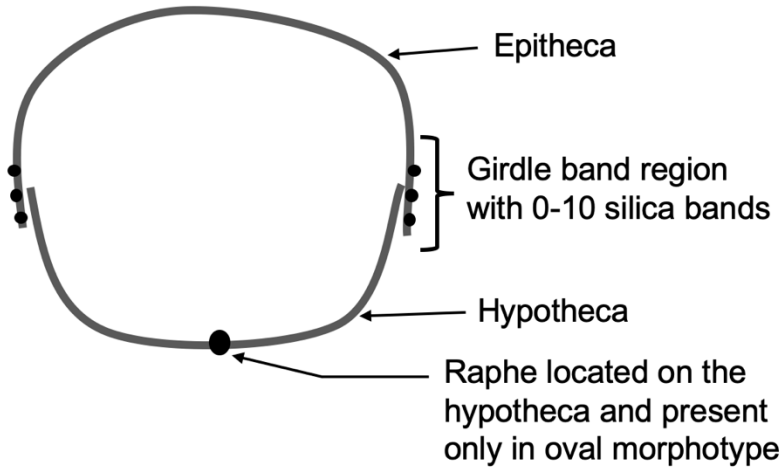

Figure 1-4 A schematic diagram showing the cell wall of *P. tricornutum.*

P. tricornutum can grow well without the addition of silicon (Zhao et al., 2014). In contrast with the siliceous frustules of other diatoms, the cell wall of *P. tricornutum* is only weakly silicified and the silica frustule is synthesised facultatively. Only the oval form can generate an opaque siliceous valve equipped with a raphe when grown in the presence of silicate (Lewin et al., 1958). The degree of silicification of oval cell walls ranges from only a raphe to a silicified valve with a raphe (Tesson et al., 2009a). By contrast, the frustules in fusiform and triradiate cells are entirely organic apart from the girdle region, the area at the junction of two valves, containing several silica bands. These bands are usually located on the epitheca embedded in the

organic material with the number varying from 0 to 10 (Figure 1-4) (Borowitzka and Volcani, 1978, Tesson et al., 2009a). Despite the above observations, the amounts of silicon obtained in oval and fusiform cells were reported to be similar, representing 0.4-0.5% DW (Lewin et al., 1958). X-ray photoelectron spectroscopy (XPS) analysis on cell surface chemicals in *P. tricornutum* revealed that the majority of silicon found in the fusiform and triradiate morphotypes was in the form of weakly polymerised silicate whereas the oval cells had a higher silicon concentration in the form of condensed silica compared to weakly polymerised silicate (Tesson et al., 2009b).

Overall, the organic constituents of *Phaeodactylum* cell wall comprise lipids, polysaccharides (mainly sulphated glucuronomannans), proteins and polyamines, similar to other diatoms. Frustulins, diatom cell wall proteins, form the organic constituents and are located at the surface of diatom cell walls (Kroger and Poulsen, 2008). Long chain polyamines and proteins (silaffins, silacidins and cingulins), located inside the silica matrix, have been identified to be involved in the silicification processes like silica polymerisation and morphogenesis in diatom cell walls (Kroger and Poulsen, 2008, Wenzl et al., 2008, Scheffel et al., 2011). A gene of bacterial origin encoding agmatinase, which may be involved in polyamine biosynthesis, a gene encoding a silaffin-like protein and frustulin genes have been identified in *P. tricornutum* genome but lacking homologues of silacidin (Martin-Jezequel and Tesson, 2013, Bowler et al., 2008).

Other morphotypes

In addition to the three commonly found morphotypes, other types of *P. tricornutum* cells have also been observed occasionally. Round cells were typically observed in the centre of oval cell clusters exposed to prolonged periods of stress conditions such as low temperature, low salinity and stationary-phase culture (De Martino et al., 2007, De Martino et al., 2011). In contrast to the above three morphotypes, round cells showed features of resting cells with a thick cell wall, increased lipid granules and

disorganisation of the plastid. Moreover, round cells adhered to surfaces and could develop biofilms, but they had no raphe and were not motile (De Martino et al., 2011). More recently, it was reported that only the rounded morphotype with a width-to-length ratio of 0.4-0.6 was observed in *P. tricornutum* cultures grown under red light. These rounded cells showed expansion of thylakoid membrane system and developed a red-shifted antenna to enhance light harvesting in response to red-enhanced illumination (Herbstova et al., 2017). Furthermore, a cruciform morphotype with four arms was reported previously (Wilson, 1946) and a culture of *P. tricornutum* strain CCMM 2004 containing approximately 40% of cruciform cells was obtained when grown in L1 medium (He et al., 2014). However, this shape needs further confirmation as it is rare and unstable, indicating that this may be an intermediate morphotype of *P. tricornutum*.

1.2.2 Morphological plasticity of *Phaeodactylum tricornutum*

Cell morphotype interconversion

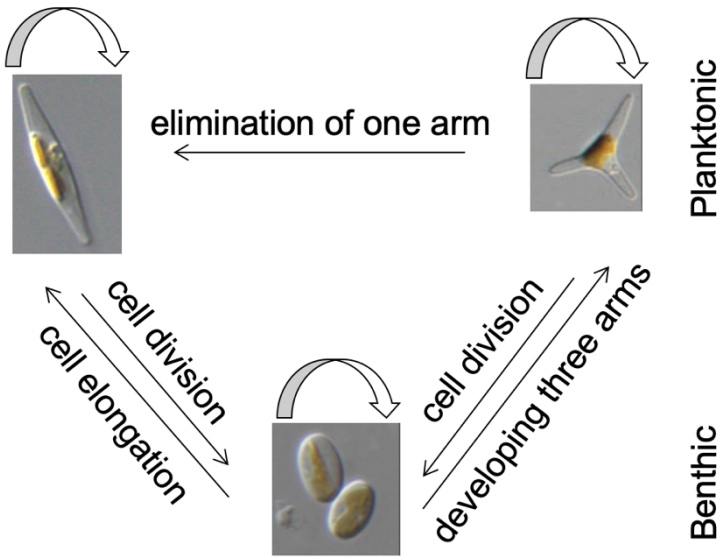

Figure 1-5 Morphological transformation between three morphotypes of *P. tricornutum.*

A schematic diagram showing the life cycle of *P. tricornutum*. Images of three morphotypes of cells were cited from (Vardi et al., 2008).

In addition to the unique polymorphic property, *P. tricornutum* exhibits another peculiarity of morphological plasticity, which is probably related to its atypical nature of facultatively and poorly silicified frustule. Several studies have described the processes of morphological interconversions between three cell morphotypes of *P. tricornutum* (Wilson, 1946, Lewin et al., 1958, De Martino et al., 2011, Martin-Jezequel and Tesson, 2013). Specifically, oval cells can be generated within the central region of both fusiform and triradiate cells by the retraction of protoplasm and multiply by successive divisions and are ultimately released by rupture of parental cell walls along the girdle band region. The produced oval cells can divide to give rise to further ovals or can grow either two or three arms, generally two, to change into fusiform or triradiate in shape. Similarly, fusiform cells can be produced by division of fusiform cells, elongation of ovals or gradual elimination of one arm of triradiate cells (Figure 1-5). In terms of the formation of triradiate cells, besides oval cells growing three arms, little evidence is available to support the transformation of fusiform cells to triradiate cells by developing a third arm (De Martino et al., 2011). The relation of these changes in morphology to the reproduction of *P. tricornutum* remains unknown. Based on the genome sequences and the assumption that at least 20 core meiosis genes are required for an alga to maintain sexual reproduction, it was proposed that asexual reproduction strategy was mainly adopted by *P. tricornutum* (Guo and Yang, 2015). Furthermore, no obvious evidence has been found to date in support of sexual reproduction of *P. tricornutum*.

Eleven accessions of *P. tricornutum*

P. tricornutum strains, isolated from different geographic locations worldwide, are deposited in culture collections with different accession numbers. The reported information on the genetic and morphological characteristics of eleven commonly used *P. tricornutum* strains are summarised in Table 1-1.

Table 1-1 Characterisation of *P. tricornutum* strains

Strains	Accession numbers in culture collections	Location of sampling	Dominant morphotype	Cell size[a] (length & width, μm)
Pt1-A	CCMP632 CCAP 1055/3	Blackpool, UK	Fusiform (>95%)	19-24 2.9-3.9
Pt1 8.6	CCAP 1055/1 CCMP2561	Monoclonal culture of Pt1	Fusiform (90%[b])	
Pt2-A	CCAP 1052/1A UTEX 642	Plymouth, UK	Fusiform (>95%)	19-24 2.8-3.3
Pt3-A	CCAP 1052/1B UTEX 640	Brackish clonal culture of Pt2	Oval (60-75%)	7.7-9.3 2.5-3.9
Pt4-B	CCAP 1052/6 UTEX 646	Island of Segelskar, Finland	Fusiform (>95%)	19-24 2.5-3.6
Pt5-C	CCMP630 CCAP 1055/2	Cape Cod Bay, West Dennis, USA	Fusiform (>95%)	25-30 2.5-3.4
Pt6-D	CCMP631 CCAP 1055/4	Nantucket Bay, Woods Hole, USA	Fusiform (>95%)	15-19 2.8-4.1
Pt7-D	CCMP1327 CCAP 1055/6	Great South Bay, Long Island, USA	Fusiform (>95%)	15-19 3.2-4.8
Pt8-D	CCMP2560 CCAP 1055/7	Jericho Beach, Vancouver, Canada	Triradiate (80-85%)	6.6-8.4 (arm)
Pt9-A	CCMP633 CCAP 1055/5	Territory of Guam, Northern Mariana Islands, Micronesia	Oval (60-75%) at 15-19 °C; Fusiform (80-95%) at 25-28 °C	5.9-8.2, 2.8-5.1 16-20, 3.1-5.2
Pt10-C	CCAP 1055/8 CCMP2928	Yellow Sea, Dalian, China	Fusiform (>95%)	15-20 2.6-4.6

The information indicated here are from a previous report (De Martino et al., 2007).
CCMP, Provasoli-Guillard National Center for Culture of Marine Phytoplankton; CCAP, Culture Collection of Algae and Protozoa; UTEX, Culture Collection of Algae at the University of Texas at Austin.
A, B, C, D represent four different genotypes.
[a]Size of the major type of cells.
[b]Our Pt1 8.6 stock cultures contained approximately 90% fusiform cells upon arrival from CCAP.

Ten axenic strains of *P. tricornutum* (Pt1-Pt10) have been characterised systematically in genotype and phenotype (De Martino et al., 2007). Another strain Pt1 8.6 is one monoclonal culture derived from Pt1 and shows mainly

the fusiform morphotype. This clone has been selected for genome sequencing and is available at CCAP and CCMP with the accession numbers CCAP 1055/1 and CCMP2561 respectively (De Martino et al., 2007, Bowler et al., 2008). Eight of these strains exist predominantly in fusiform morphotype (>90%) while one strain (Pt3) exhibits mainly the oval form (>60%) and one strain (Pt8) is principally in triradiate (>80%) (Table 1-1). Further analyses of the fast-evolving internal transcribed spacer 2 (ITS2) sequences and amplified fragment length polymorphism (AFLP) revealed that these strains represent four different genotypes, denoted as A, B, C and D (Table 1-1) (De Martino et al., 2007).

Pt2 was first identified as *Nitzschia closterium* W. Sm. forma *minutissima* and was subsequently revised to *P. tricornutum* Bohlin emend by Lewin J. C. in 1958 (Lewin, 1958) and has been officially renamed as *P. tricornutum* since then. Numerous physiological and biochemical studies were carried out with this Plymouth strain and published under the name of *N. Closterium* (Wilson, 1946, Leigh-Clare, 1927). Pt3 is a subclonal culture, initially isolated from Pt2 with its ability to grow in freshwater media. It comprises mainly oval cells (>60%) even when grown in artificial seawater medium (De Martino et al., 2007). The Finnish strain Pt4 was described as a brackish strain collected from a supralittoral rock pool. Pt5 was collected in a shallow tidal creek with fluctuations in salinity in the Gulf of Maine (De Martino et al., 2007). The Woods Hole strain Pt6 was isolated from a seawater tank by Lewin J. C. and Lewin R. A. in 1956 and was then described morphologically, structurally and biochemically in 1958 (Lewin et al., 1958). The collection site of Pt7 was described as an enclosed bay with low salinity. Although Pt8 with the accession name NEPCC 640 (North East Pacific Culture Collection) was described to show a fusiform morphotype, De Martino et al. reported that the subculture of this strain they received from CCCM (Canadian Centre for the Culture of Microorganisms) was mainly in triradiate (>80%) and oval cells were not found in this accession (De Martino et al., 2007). The tropical strain Pt9 is typically grown at 20-26 ^{o}C. Interestingly, it shows different cell morphotypes when grown under different temperatures, displaying mainly the fusiform morphotype (>80%) at 25-28 ^{o}C in comparison to the predominant

oval form (>60%) at 15-19 ^{o}C. In addition, the oval cells of Pt9 are shorter and wider than those in Pt3 cultures (Table 1-1). The Chinese strain Pt10 was also described as *N. closterium* W. Sm. forma *minutissima*, containing >95% fusiform cells.

Conditions influencing cell morphological conversion

Changing culture conditions has been shown to elicit morphological changes in *P. tricornutum*. Observations in the marine environment revealed that *P. tricornutum* is typically found in unstable coastal environments such as estuaries and rock pools where temperature and salinity change rapidly due to tidal effect (De Martino et al., 2007). Its unique characteristics of polymorphism and morphological plasticity could thus represent acclimation strategies employed by *P. tricornutum* to the highly changing environmental conditions (De Martino et al., 2011). Several studies have identified some factors triggering the cell morphotype variations in this species, as summarised in Table 1-2.

Cell morphotype transformation from fusiform to oval on solid agar medium was first discovered by Barker with Pt2 (Barker, 1935). Enrichment of oval cells (100%) was observed through successive passaging on solid agar plate. This approach has been confirmed and applied in some studies to obtain oval cells in Pt1, Pt2, Pt6 and Pt7 (Abdullahi et al., 2006, Gutenbrunner et al., 1994, Borowitzka and Volcani, 1978, Francius et al., 2008, Tesson et al., 2009b). This process of morphological change was shown to be reversible by inoculating oval cells back into liquid media with the observed gradual reversion during subculturing transfers to fusiform cells (Barker, 1935). In addition, colonies on agar plate derived from oval cells were found to be more diffuse and irregular due to the ability of oval cells to spread over the surface, compared to those of fusiform cells being rounded with smooth margins (Lewin et al., 1958). Although solid media favour oval cell production, it was reported that some oval strains could grow faster in liquid media than on solid (Borowitzka and Volcani, 1978).

Table 1-2 Reported conditions triggering cell morphotype conversion in *P. tricornutum*

Strains	Conditions	Conversion	References
Pt1, Pt2, Pt6, Pt7	Solid media	F→O	Barker, 1935 Lewin et al., 1958 Borowitzka and Volcani, 1978 Gutenbrunner et al., 1994 Abdullahi et al., 2006 Francius et al., 2008 Tesson et al., 2009b
Pt2	Low calcium	F→O	Cooksey and Cooksey, 1974
Pt1 8.6, Pt3, Pt8	Low salinity	F→O T→F, O	De Martino et al., 2007 De Martino et al., 2011 Ovide et al., 2018
Pt3, Pt8, Pt9	Low temperature	F→O T→F	De Martino et al., 2007 De Martino et al., 2011
Pt2	High pH or High dissolved inorganic carbon	F→T	Bartual et al., 2008
Pt2	Red light	F→O	Herbstova et al., 2017
Pt1-Pt10	Adhering to flasks Stationary phase Static condition plus repeated medium exchange	F→O	De Martino et al., 2007 Stanley and Callow, 2007 Willis et al., 2013 Buhmann et al., 2016
Pt1 8.6	Marine bacteria	F→O	Buhmann et al., 2016

F, O and T represent fusiform, oval and triradiate respectively.

Under optimal conditions, fusiform and triradiate cells generally predominate in liquid media whereas oval cells usually occur on solid media or adhere to flasks through secreting mucilage. However, cells tend to convert to the oval form in response to stress conditions such as hyposalinity and low temperature (Table 1-2). An increase in the oval cell abundance from 30% to above 50% was observed in Pt2 after 5 days cultivation in liquid ASP-2 medium with the calcium concentration being below 15 mg L^{-1} whereas the oval percentage decreased to 10% when the calcium concentration in the medium was 25-85 mg L^{-1} (Cooksey and Cooksey, 1974). However, the effect of calcium on cell morphotype was not confirmed in another study

(Borowitzka and Volcani, 1978). Seawater based culture media contain approximately 400 mg L^{-1} calcium. Furthermore, significant cell morphotype changes from fusiform to oval occurred in strains Pt1 8.6 and Pt3 induced by hyposaline conditions (De Martino et al., 2011, De Martino et al., 2007, Ovide et al., 2018). After cultivation for 30 days under low salinities of 10sw (3.3 g/L) and 0sw, the oval cell abundance was approximately 10% and 20% respectively in Pt1 8.6 and were >85% in Pt3. Further extension of culture time to 90 days, 100% oval cells were observed in both Pt1 8.6 and Pt3. Low temperature (15 ^{o}C) was also reported to induce oval cell production in strains Pt3 and Pt9 (De Martino et al., 2011, De Martino et al., 2007). When the temperature was shifted from 15 ^{o}C to 28 ^{o}C, a cell morphotype reversion to fusiform cells from 20% to >70% was observed in Pt3 and Pt9. However, Pt1 8.6 existed still mainly in fusiform (>70%) when subjected to the low temperature of 15 ^{o}C (De Martino et al., 2011) and no significant cell morphotype changes were observed in strains Pt1, Pt2, Pt6 and Pt7 grown under various salinities (Wilson, 1946, Gutenbrunner et al., 1994, Abdullahi et al., 2006, Borowitzka and Volcani, 1978). These results suggested that morphotype variations can be regulated by changing culture conditions but depend on strains. It was reported that some strains of *P. tricornutum* had a greater tendency to be pleiomorphic and to undergo morphotype conversion than others (Borowitzka and Volcani, 1978, Tesson et al., 2009a).

It is noteworthy that only rounded cells with a width-to-length ratio of 0.4-0.6 were observed in Pt2 grown under red light. The authors concluded that the rounded form represented a general response to adverse conditions, showing a tendency towards aggregation and biofilm formation. The rounded cells expanded thylakoid membrane system and developed a red-shifted antenna to enhance light harvesting in acclimation to red-enhanced illumination, which is expected in habitats with diminished availability of visible light such as benthic environments and eutrophic waters and could be viewed as a response to the lack of other photosynthetically usable wavelengths (Herbstova et al., 2017). However, these rounded cells in red light are similar in size to Pt9 oval cells having a width-to-length ratio of 0.45-0.63 but different from the previously reported round cells which showed a

ball shape under microscopy (De Martino et al., 2007). Other unfavourable conditions such as stationary growth phase and static condition combined with repeated medium exchange were reported to promote oval cell production as well (De Martino et al., 2007, Stanley and Callow, 2007, Willis et al., 2013). Interestingly, a study on a diatom/bacteria model community revealed that a marine *Roseobacter* strain, feeding on secreted diatom exopolymers, could influence cell aggregation by inducing a morphotype conversion from fusiform to oval and secretion of mucin-like proteins in Pt1 8.6 whereas Pt4 was not significantly affected (Buhmann et al., 2016).

Triradiate cells are sensitive to suboptimal conditions and rarely observed in laboratory cultures except for the strain Pt8 (De Martino et al., 2007). Low salinity and low temperature conditions were shown to elicit significant cell morphotype changes from triradiate to fusiform in Pt8. Different from Pt3 and Pt9, there was no evident morphotype reversion to triradiate cells in Pt8 when the temperature for growth was shifted from 15 ^{o}C to 28 ^{o}C (De Martino et al., 2011). High pH or high dissolved inorganic carbon were reported to increase the abundance of triradiate cells in Pt2, particularly under subsaturating illumination for growth (Bartual et al., 2008). Other factors such as N and P sources or concentrations, silicate concentrations, light intensity and agitation did not produce evident change in cell morphotype of Pt6 and Pt7 (Borowitzka and Volcani, 1978). P-limitation had no significant effect on cell morphotype of Pt1 (Abdullahi et al., 2006).

1.2.3 A model species: *Phaeodactylum tricornutum*

P. tricornutum has been extensively studied as a model system for diatom biology, physiology and ecology. It is also a good model species for functional genomic studies due to the growing availability of genetic tools for this microalga. The complete genome of *P. tricornutum* has been sequenced, which is available through the Joint Genome Institute (JGI) Genome Portal at http://genome.jgi.doe.gov/portal/phaeodactylum (Bowler et al., 2008). *P. tricornutum* has a comparatively small genome, approximately 27.4 megabases (Mb) in size, and is predicted to contain 10,402 genes. Of these

genes, 1,328 genes were diatom-specific, at least 164 genes were of red algal origin and 587 genes were proposed from bacteria, revealing diverse origins of diatom genes. Furthermore, a diatom expressed sequence tag (EST) database (http://www.biologie.ens.fr/diatomics/EST3) containing 130,000 *P. tricornutum* ESTs derived from cells grown under 16 different conditions has been constructed (Maheswari et al., 2005, Maheswari et al., 2009, Maheswari et al., 2010). The ITS2 sequences of *P. tricornutum* (Pt1-Pt10), which have been deposited in GenBank, were highly conserved among *P. tricornutum* strains and were highly divergent from other diatom ITS2 sequences (De Martino et al., 2007). Specific primers (forward: 5'-tctggctgctgttcaagtgt-3' and reverse: 5'-tcggtttccgtctccagt-3') to amplify a specific region of *P. tricornutum* ITS2 have been developed previously and successfully used to detect *P. tricornutum* in natural environments (De Martino et al., 2007). In addition, a range of molecular tools required for transgenic strain construction have become available for *P. tricornutum* (Table 1-3).

Genetic transformation

A stable nuclear transformation system has been developed for *P. tricornutum* (Apt et al., 1996, Falciatore et al., 1999, Miyagawa et al., 2009, Niu et al., 2012, Zhang and Hu, 2014). Apt et al. successfully introduced a selectable marker gene (*sh ble*) into Pt4 cells using microparticle bombardment with the transformation efficiency of 1-10/10^7 cells and demonstrated that the *cat* reporter gene could also be introduced with this method and expressed at high levels (Apt et al., 1996). Co-transformation of Pt1 with two different plasmids, one containing the *sh ble* gene and another containing the firefly *luciferase* gene (*luc*), has also been achieved using the microparticle bombardment approach. It turned out that the cotransformation efficiencies were high, 60-70% of transformed clones containing both genes (Falciatore et al., 1999). Both studies demonstrated the genetic transformation for the fusiform morphotype of *P. tricornutum*. As described in section 1.2.1, *P. tricornutum* is pleiomorphic. In order to develop *P. triornutum* as a microalgal expression system and explore the relationship between cell

morphology and its ability to act as an expression host, it is important to be able to transform all three morphotypes. Successful genetic transformation of all three morphotypes with different *P. tricornutum* strains has been achieved using the microparticle bombardment method at highly similar transformation efficiencies. However, the triradiate transformants were difficult to maintain, only 25% of the transformants derived from 100% triradiate cells being triradiate while the rest being fusiform (De Martino et al., 2007). These studies indicated the feasibility of *P. tricornutum* to be transformed using the method of microparticle bombardment and the possibility of expressing heterologous genes in *P. tricornutum.*

Table 1-3 Molecular tools available for *P. tricornutum*

Molecular tools	Name of genes/vectors	References
Selectable marker genes	*sh ble* (phleomycin/zeocin) *nat* (nourseothricin) *sat-1* (nourseothricin) *npt*II (G418, kanamycin)	Apt et al., 1996 Zaslavskaia et al., 2000
Reporter genes	*cat* (chloramphenicol acetyltransferase) *luc* (luciferase) *uidA* (β-glucuronidase) *eGFP* (green fluorescent protein) *eYFP* (yellow fluorescent protein)	Apt et al., 1996 Falciatore et al., 1999 Zaslavskaia et al., 2000 De Martino et al., 2007
Promoter/ Terminator	*fcp* (fucoxanthin chlorophyll binding protein, light & circadian regulated) *NR* (nitrate reductase, nitrate inducible) *rbcL/S* (rubisco large/small subunit) *EF2* (elongation factor 2) *HASP1* (highly abundant secreted protein 1)	Apt et al., 1996 Miyagawa et al., 2009 Niu et al., 2012 Xie et al., 2014 Seo et al., 2015 Erdene-Ochir et al., 2019
Vector	pBluescript SK- pBluescript KS^+ pPha-T1 pHY11 pMD19	Apt et al., 1996 Falciatore et al., 1999 Zaslavskaia et al., 2000 Niu et al., 2012 Xie et al., 2014
Transformation method	Microparticle bombardment Electroporation Bacterial conjugation	Apt et al., 1996 Niu et al., 2012 Karas et al., 2015
Reference genes	*RPS* (30S ribosomal protein subunit) *TBP* (TATA box binding protein) Histone *H4*	Siaut et al., 2007

Another nuclear transformation method with high efficiency has been established for *P. tricornutum*. Niu et al. first reported the successful genetic transformation of *P. tricornutum* via electroporation at an efficiency of approximately 100/10^7 cells (Niu et al., 2012). This nuclear transformation method was further confirmed and optimised for *P. tricornutum* by Zhang and Hu. They introduced the plasmid pPha-T1 into Pt1 8.6 cells through electroporation and achieved a high transformation efficiency of 280/10^7 cells by optimising the electric field strength and using a linearised vector with carrier DNA added. Furthermore, Pt1 8.6 was successfully co-transformed with two plasmids containing the *sh ble* selectable marker gene and the *uidA* reporter gene respectively using the electroporation method, showing a co-transformation efficiency of 60% (Zhang and Hu, 2014). In another study, Pt2 cells grown in the presence of silicate were successfully transformed with two reporter genes (*sgfp, uidA*) using a multi-pulse electroporation system and a high transformation efficiency of approximately 450/10^7 cells was achieved through the optimisation of pulse conditions (Miyahara et al., 2013).

In addition to the nuclear transformation, a high-efficiency plastid transformation system was also reported for *P. tricornutum*. The plastid genome of *P. tricornutum* has been completely sequenced, showing the presence of inverted repeat (IR) regions (Oudot-Le Secq et al., 2007). A novel plastid expression vector based on pMD19 was constructed and the *cat* and *eGFP* reporter genes were introduced into cells using electroporation and integrated into the plastid genome through homologous recombination, reaching a transformation efficiency of about 1/10^3 cells (Xie et al., 2014). This study demonstrated the expression of foreign genes in plastids of *P. tricornutum*. A novel nuclear episomal vector transferred by conjugation from *Escherichia coli* to *P. tricornutum* at a high efficiency of 4/10^4 cells was described previously (Karas et al., 2015).

Selectable markers, Reporter genes and Promoters/Terminators

During the development of genetic transformation systems, a variety of expression elements such as selectable markers and reporter genes have

been identified and effectively expressed in *P. tricornutum* (Table 1-3). Selectable markers are usually genes that encode proteins conferring resistance to antibiotics and are widely used in genetic engineering for primary selection of transformants, indicating the successful genetic transformation of cells. Reporter genes can confer some easily identified and measured characteristics on expression hosts, commonly used as an indication of the successful expression of target genes or the subcellular location of specific proteins in cells. The *sh ble* gene from the bacterium *Streptoalloteichus hindustanus* confers resistance to phleomycin and zeocin and has been proven to be a reliable selectable marker in Pt4 (Apt et al., 1996). Three other genes, *nat* encoding nourseothricin acetyltransferase from *Streptomyces noursei* and *sat-1* encoding streptothricin acetyltransferase from *E. coli* confer resistance to the antibiotic nourseothricin, and *npt*II encoding neomycin phosphotransferase from the transposon Tn5 confers resistance to G418 (Geneticin). They have also been reported as effective selectable markers for identifying primary transformants of Pt4 (Zaslavskaia et al., 2000). Several reporter genes have been successfully expressed in *P. tricornutum*, including the genes encoding chloramphenicol acetyltransferase (*cat*), luciferase (*luc*), β-glucuronidase (*uidA*), green fluorescent protein (e*gfp*) and yellow fluorescent protein (e*yfp*) (Apt et al., 1996, Falciatore et al., 1999, Zaslavskaia et al., 2000, De Martino et al., 2007). The *gfp* gene is widely used due to the direct visualization of target proteins within cells through green fluorescence. Notably, codon usage has a significant impact on the efficient expression of *gfp* in *P. tricornutum* (Zaslavskaia et al., 2000).

In the above studies, three types of promoters and terminators from *P. tricornutum* were used to drive expression of exogenous genes in *P. tricornutum*. One is the light-regulated promoters/terminators from the highly expressed *P. tricornutum fcp* genes (Pt-*fcp*) encoding fucoxanthin chlorophyll binding proteins (Apt et al., 1996, Falciatore et al., 1999). FCPs are major components of the light-harvesting complexes of photosynthetic apparatus. Another is the *P. tricornutum nitrate reductase* (*NR*) promoter/terminator (Pt-*NR*), which is induced by nitrate and repressed when ammonium is used as

the only nitrogen source (Niu et al., 2012). This inducible system can be used to control the expression of heterologous genes. The *fcp* and *NR* promoters/terminators derived from the pennate diatom *Cylindrotheca fusiformis* (Cf-*fcp* & Cf-*NR*) were also tested in *P. tricornutum* for driving expression of the zeocin resistance gene (*ble*) and the *egfp* gene respectively in one plasmid. Pt4 was transformed by microparticle bombardment and both promoters worked with a transformation efficiency of $65/10^7$ cells obtained, higher than those with Pt-*fcp* promoters/terminators, suggesting that the Cf-*fcp* promoter activity might be stronger than that of Pt-*fcp* promoter (Miyagawa et al., 2009). In addition, the promoter of the rubisco large subunit (*rbcL*) and the terminator of the rubisco small subunit (*rbcS*) from *P. tricornutum* plastid genome were employed to drive the *eGFP* expression in plastids of *P. tricornutum* (Xie et al., 2014). Recently, a novel expression vector containing the *luc* reporter gene fused to the constitutive *P. tricornutum* elongation factor 2 (*EF2*) promoter was constructed and introduced in *P. tricornutum* via microparticle bombardment, resulting in a higher luciferase expression level compared to the Pt-*fcpB* promoter (Seo et al., 2015). An endogenous promoter *HASP1* (highly abundant secreted protein 1) was also found to strongly drive *GFP* expression in *P. tricornutum* (Erdene-Ochir et al., 2019).

Additionally, several housekeeping genes such as *RPS* (30S ribosomal protein subunit), *TBP* (TATA-box binding protein) and histone *H4* were identified as rather stable internal references for gene expression analysis by quantitative real-time PCR (qRT-PCR) in *P. tricornutum* (Siaut et al., 2007). These advanced resources will enhance the potential use of *P. tricornutum* for both basic biological research and industrial applications through gene manipulation. The available whole-genome sequences and molecular tools will facilitate exploration of gene function and diatom biology thereby understanding more about their ecological roles in aquatic environments. The highly developed transgenic technologies for *P. tricornutum* will allow the expression of value-added proteins in *P. tricornutum* and drive its utilisation for industrial biotechnology. Therefore, it is important that the impact of its

pleiomorphism is investigated in order to optimise productivity of valuable compounds or recombinant proteins for *P. tricornutum* biotechnology.

1.2.4 Biotechnological applications of *Phaeodactylum tricornutum*

The aim of the microalgal biorefinery is to create an industrial process to extract high-value products while converting lipids or carbohydrates within microalgal biomass feedstock into biofuels or platform chemicals then further converting the residual biomass to additional value-added marketable products (Hossain et al., 2017). This process aims to take full advantage of microalgal biomass to achieve sustainable and economical production of bio-based products at an industrial scale. Microalgae represent a renewable source of valuable compounds such as proteins, pigments, lipids and polysaccharides (section 1.1.1).

P. tricornutum, as a marine microalga, has great industrial significance both for industrial biorefinery and for synthetic biology. This species grows in brackish to saline water with a high growth rate of 0.09 h^{-1} under optimal conditions (Perez et al., 2008). *P. tricornutum* has been commercially cultivated for aquaculture and shows important potential applications in nutritional and pharmaceutical industries. This species has been identified as a natural rich source of the high-value omega-3 fatty acid EPA (C20:5) and the marine carotenoid fucoxanthin (Yongmanitchai and Ward, 1991, Kim et al., 2012). It is commonly known that omega-3 polyunsaturated fatty acids (PUFAs), particularly EPA and DHA, are essential for brain and eye development of infants and they have been shown to prevent or reduce the risk of some diseases, such as cardiac disease, inflammation and cancers (Leaf et al., 2003, Calder, 2006, Larsson et al., 2004). Fucoxanthin has also been found to have multiple bioactivities including antioxidant, anti-cancer, anti-inflammatory, anti-obesity and anti-diabetic effects (Peng et al., 2011, Maeda, 2015). In addition, *P. tricornutum* is considered as a potential renewable feedstock for biofuel production due to its capability to accumulate high lipids (up to 42.5% DW) and carbohydrates (~50% DW), particularly triacylglycerides (TAGs) and chrysolaminarin under nitrogen starvation (Gao

et al., 2017, Breuer et al., 2012). However, the authors did not specify the cell morphotype of *P. tricornutum* in their studies.

Microalgal lipids can generally be classified into two categories: neutral lipids (NLs) comprising acylglycerides and free fatty acids, and polar lipids (PLs) including glycolipids and phospholipids (Cuellar-Bermudez et al., 2015). TAGs, a storage pool of energy existing as lipid bodies in cells, are precursors for biodiesel production (Bilbao et al., 2017) and PLs are important components of various cellular membrane structures (van Meer et al., 2008). Both the biomass yield and the biochemical profile of microalgae vary greatly depending on culture conditions such as nutrients, temperature and light. It has been widely reported that NLs, primarily TAGs, were significantly accumulated under N starvation in microalgae, representing up to 90% of total fatty acid (TFA) content and over 40% DW in some species (Breuer et al., 2012). In *P. tricornutum*, EPA is present in all lipid classes, mainly in PLs. Among PLs, the highest EPA content was found in the glycolipid fraction of sulfoquinovosyl diacylglycerol (SQDG) (Yang et al., 2017). *P. tricornutum* has been reported to contain about 1.7-4.4% DW EPA (30-40% of TFAs) depending on strains and growth conditions (Medina et al., 1998, Steinrucken et al., 2018). Vitamins B_1 and B_{12} did not significantly affect growth of *P. tricornutum*, but B_{12} supplementation was shown to enhance the EPA production (Yongmanitchai and Ward, 1991). *P. tricornutum* does not absolutely require cobalamin, thiamine and biotin for growth (Moejes et al., 2017). Vitamin B_{12} is only produced by some bacteria, cyanobacteria and archaea but is required by many eukaryotic microalgae as a cofactor for the enzyme methionine synthase. The available genome sequence of *P. tricornutum* indicates that its genome encodes both the B_{12}-dependent methionine synthase (MetH) and the B_{12}-independent methionine synthase (MetE), thus *P. tricornutum* having a flexible cobalamin demand (Bertrand et al., 2012).

Application of transgenic *P. tricornutum*

The advanced genetic toolkits developed for *P. tricornutum* greatly facilitate

the exploitation of this species for industrial biotechnology (section 1.2.3). Apart from the naturally accumulated products in wild strain, genetically engineered strains can potentially be used to improve the commercial value of *P. tricornutum* through expressing genes with specific interest. Strategies for genetic engineering of *P. tricornutum* include modification of existing biosynthetic pathways to overproduce desired molecules and direct biosynthesis of recombinant proteins by introducing exogenous genes or overexpressing endogenous genes. Table 1-4 shows several bioproducts with yields achieved in transgenic *P. tricornutum*.

Several research groups have succeeded in overproduction of lipids in *P. tricornutum* by adopting a metabolic engineering approach. Yao et al. enhanced glycerol and NLs production in fusiform *P. tricornutum* through overexpressing endogenous glycerol-3-phosphate dehydrogenase (GPDH). This study showed that there was a 6.8-fold increase in glycerol concentration, and a 1.6-fold increase in total lipid (TL) content reaching 39.7% DW in transgenic *P. tricornutum*. However, the final transgenic cell concentration decreased by 20% and the EPA content decreased by 24% (Yao et al., 2014). One challenge in developing microalgal strains for biodiesel production is the achievement of both biomass yield and interested lipids such as TAGs. The malic enzyme (ME) catalyzes the conversion of malate to pyruvate and its transcript level in *P. tricornutum* increased by over 7-fold upon N starvation (Yang et al., 2013). Overexpression of the endogenous ME in fusiform Pt1 8.6 resulted in a 2.7-fold increase in NLs and a 2.5-fold increase in TL content to 57.8% DW at a similar growth rate to the wild-type cells. Treatment of transgenic cells under N starvation further increased the NL content by 31%, 66% higher than that in wild-type cells (Xue et al., 2015). Moreover, an enhanced lipid-producing strain of Pt1 8.6 with 45-fold increase in TAG accumulation was generated via disruption of the UDP-glucose pyrophosphorylase gene using the molecular scissor transcription activator-like effector nucleases (TALEN) for targeted mutagenesis (Daboussi et al., 2014). *P. tricornutum* has a low amount of DHA while accumulating EPA. Augmentation of DHA production in Pt4 has been achieved by expressing the heterologous Δ5-elongase, which catalyzes

Table 1-4 Bioproducts produced by transgenic *P. tricornutum*

Product	Transformation system	Yield	Strain & morphotype	Reference
Human IgG1 antibody CL4mAb, HBsAg (Hepatitis B surface antigen)	Vector: pPha-NR (*sh ble*) Pro/Ter: Pt-*NR* Reporter gene: *eGFP* Microparticle bombardment	Antibody: 8.7% TSP, 2.1% DW, 1.6 mg L^{-1} per week Antigen: 0.7% TSP	Pt4 Fusiform	Hempel et al., 2011b
Bioplastic PHB	Vector: pPha-NR (*sh ble*) Pro/Ter: Pt-*NR* Reporter gene: *eGFP* Microparticle bombardment	10.6% DW	NA Fusiform	Hempel et al., 2011a
DHA	Vector: pPha-T1 (*sh ble*) Target: *Δ5-elongase* Pro/Ter: *fcpA* Microparticle bombardment	10.4% TFAs (8-fold increase)	Pt4 NA	Hamilton et al., 2014
Glycerol NLs TLs	Vector: pHY11 (*cat*) Target: *GPDH* Pro/Ter: *fcpC/fcpA* Electroporation	Glycerol: 6.8-fold increase NLs: 1.9-fold increase TLs: 39.7% DW	FACHB-863 Fusiform	Yao et al., 2014
TLs NLs	Vector: pHY11 (*cat*) Target: *ME* Pro/Ter: *fcpC/fcpA* Electroporation	TLs: 57.8% DW (2.5-fold increase) NLs: 66% increase	Pt1 8.6 Fusiform	Xue et al., 2015
Fucoxanthin	Vector: pPha-T1 (*sh ble*) Pro/Ter: *fcpA, NR* Microparticle bombardment	2.4% DW (2.4-fold increase)	Pt4 NA	Eilers et al., 2016
Triterpenoids (lupeol and betulin)	Vector: pPha-T1 (*sh ble*) Pro/Ter: *fcpA* Microparticle bombardment	Lupeol: 0.1 mg L^{-1}, 2 days Betulin: NA	Pt1 8.6 NA	D'Adamo et al., 2019
Phytase DHA	Vector: pPhOS2 (*sh ble*) Pro/Ter: *fcpA, EF2 or CIP1*/*fcpA* Microparticle bombardment	Phytase activity: 23-40 FTU mg^{-1} soluble protein DHA: 8-11% TFAs EPA:19-26% TFAs	Pt4 Fusiform	Pudney et al., 2019

NA, not available; TSP, total soluble protein; DW, dry weight; PHB, poly-3-hydroxybutyrate; TFAs, total fatty acids; NLs, neutral lipids; TLs, total lipids; Pro/Ter, promoter/terminator; GPDH, glycerol-3-phosphate dehydrogenase; ME, malic

enzyme; CIP1, an algal virus promoter of a putative replication-associated gene from *Chaetocero lorenzianus*-infecting DNA virus; FTU, phytase activity units.

the elongation of EPA to convert into DHA. With this method, the DHA accumulation was markedly increased by 8-fold, averaging 10.4% of TFAs and the transgene-generated DHA was accumulated in TAGs (Hamilton et al., 2014). In addition, the fucoxanthin production was enhanced by up to 2.4-fold to 2.4% DW in Pt4 via overexpressing the endogenous 1-deoxy-D-xylulose 5-phosphate synthase (*dxs*) or phytoene synthase (*psy*) (Eilers et al., 2016).

Successful genetic engineering has been achieved in fusiform Pt4 for the expression of high-value therapeutic recombinant proteins such as a monoclonal human IgG antibody and the respective antigen of Hepatitis B surface protein. Both the antibody and antigen were proved to be fully-assembled and functional and accumulated to 8.7% and 0.7% of total soluble protein, respectively (Hempel et al., 2011b). *P. tricornutum* could also perform as a microalgal bioreactor for biodegradable bioplastic production. The heterologous expression of bacterial enzymes, introducing the poly-3-hydroxybutyrate (PHB) biosynthetic pathway from *Ralstonia eutropha* H16, resulted in successful accumulation of the bioplastic PHB, reaching up to 10.6% DW in fusiform *P. tricornutum* (Hempel et al., 2011a). In addition, Pt1 8.6 was successfully engineered to express plant enzymes including a *Lotus japonicus* oxidosqualene cyclase and a *Medicago truncatula* cytochrome P450 along with its reductase for the production of triterpenoids, betulin and lupeol (D'Adamo et al., 2019). The co-expression of Δ5-elongase from *Ostreococcus tauri* and phytase from either *E. coli* or *Aspergillus niger* led to accumulation of high levels of EPA and DHA together with phytase in fusiform Pt4 without influencing cell growth rate (Pudney et al., 2019).

These studies demonstrated the feasibility of synthesising bioproducts in *P. tricornutum* through genetic manipulation. Such progress in genetic engineering could drive forward not only our understanding on the molecular mechanisms of product accumulation in *P. tricornutum* but also the

development of *P. tricornutum* as a microalgal expression platform for commercial production of high-value compounds.

1.3 Downstream bioprocessing of microalgae

Microalgae represent great potential for commercial production of bioproducts such as pigments (chlorophylls and carotenoids), proteins, carbohydrates, lipids and biopolymers (Khanra et al., 2018, Kim et al., 2013). Development of efficient downstream processing technologies is one of the key factors that determine the quality and economic feasibility of microalgae-based products. The key steps involved in the industrial production process of microalgal biomolecules generally include cell cultivation, cell harvest, pre-treatment, extraction and purification (Figure 1-6). The downstream process was reported to contribute to 60% of the total production cost of biodiesel (Kim et al., 2013). After cultivation, harvesting and cell disruption are the essential downstream steps for intracellular product recovery.

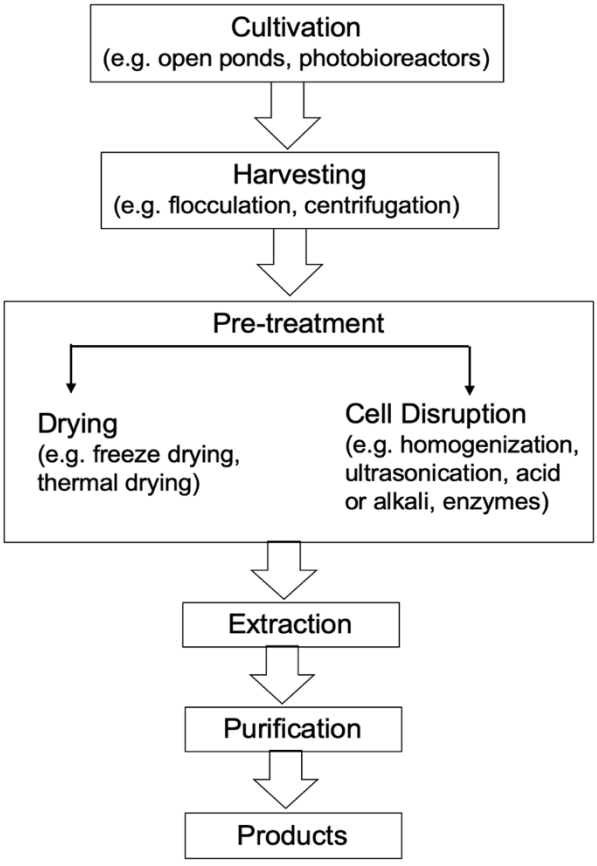

Figure 1-6 A schematic diagram showing the general industrial production process of microalgal biomolecules.

1.3.1 Cell harvest

Harvesting is the initial step for recovery of microalgal biomass from the growth medium, which requires one or more solid-liquid separation techniques. Microalgal cells are typically small in size (3-30 μm in diameter) and culture broths are generally relatively dilute (<0.5 g L^{-1} dry biomass in some commercial production systems) with large volumes, making the recovery of microalgal biomass challenging (Grima et al., 2003, Sharma et al., 2013). The harvesting process of microalgae from dilute suspension at large scale is costly and energy intensive, contributing to 20-30% of the total cost of biomass production (Grima et al., 2003). Selection of harvesting techniques for microalgae processing is largely depending on the species, culture conditions, end products and cell density of microalgal cultures.

A range of techniques are available for microalgae harvesting, including flocculation, centrifugation, filtration, flotation, gravity sedimentation and so forth (Singh and Patidar, 2018). The diverse microalgae harvesting and concentrating techniques are well documented, categorised into chemical, mechanical, biological and electrical based methods (Grima et al., 2003, Kim et al., 2013, Milledge and Heaven, 2013). These techniques can be used alone or in combination for more efficient and cost-effective cell harvest. Microalgal cells usually possess a negatively charged surface through zeta potential measurement, a similar density to the culture medium and a dispersed state, resulting in slow natural settling of cells by gravity (Gonçalves et al., 2015, Singh and Patidar, 2018). According to the Stokes' law, the settling speed of spherical particles in fluid is described as follows:

$$\boldsymbol{V_g = \frac{\Delta\rho}{18\mu} d_p{}^2 g} \qquad \textbf{Equation 1-1}$$

where the settling speed of particles, V_g, is a function of the density difference between the solid and liquid phase, $\Delta\rho$, the viscosity μ, the diameter of settling particles d_p and the gravitational force g.

Centrifugation is one of the most commonly used methods for harvesting microalgal biomass by replacing gravity with centrifugal force. This mechanical method is applicable to all microalgae. Large volume of dilute microalgal culture broth can be easily processed by centrifugation in a fast and effective way with high recovery efficiency (>90%) and chemical-free biomass obtained (Singh and Patidar, 2018). However, centrifugation requires high energy consumption and has high capital, operational and maintenance costs due to the fast-moving mechanical parts of the equipment (Uduman et al., 2010). Centrifugation is thus considered as an expensive technique and suitable for recovery of high-value microalgal products such as omega-3 PUFAs (Grima et al., 2003). Biodiesel production by centrifugation is not recommended as more energy is consumed than that produced (Milledge and Heaven, 2013). In addition, the high degree of shear forces generated in industrial centrifuges due to the rapid acceleration of feed stream to the set spinning speed and the high discharge velocity of solids could disrupt algal cells, and consequently lower the attainable product productivity (Titchener-Hooker et al., 2008, Uduman et al., 2010).

Flocculation has been proposed as a superior pre-harvesting method for concentrating the dilute algal suspension to an algal slurry of 2-7% total suspended solids (Uduman et al., 2010, Sharma et al., 2013). Flocculation can be induced by addition of flocculants such as aluminium sulphate, ferric chloride, sodium hydroxide and chitosan based on the mechanism of surface charge neutralisation, leading to agglomeration of microalgal cells (Branyikova et al., 2018). The flocculation efficiency of *P. tricornutum* cultures was dramatically improved at pH of 9.75 after 10 min settling time or when chitosan was added at 20 mg L^{-1} with an adjusted pH of 9.9 (Sirin et al., 2012). The flocculation method has a low energy requirement and can be used for large scale with a wide range of species. However, the chemical flocculants may be expensive and contaminate the obtained biomass (Singh and Patidar, 2018). Filtration yields high-quality algal biomass, but this method is time consuming with high capital and operating costs to avoid filter fouling and suitable for harvesting large microalgae (Yellapu et al., 2018). It has been proven that flocculation combined with the subsequent dewatering

steps by centrifugation or filtration could improve harvesting efficiencies and reduce process costs (Sharma et al., 2013).

There is no one superior harvesting method applicable to all cases. From the perspective of microalgae application, different orders of suitability of the harvesting techniques were proposed for production of biofuels, human and animal food, and high-value products. Flocculation was recommended for biofuel production considering biomass quantity and cost. By contrast, for human and animal food and high-value products, the best options for harvesting were filtration and centrifugation, respectively, considering biomass quality and toxicity (Singh and Patidar, 2018). Nutrient recycling after separation is helpful for reducing the harvest process cost. Development of efficient and economical harvesting process, which may be microalgae strain specific, is still necessary for the production of metabolites from microalgae.

1.3.2 Cell disruption

After cultivation and harvesting, pre-treatment methods such as drying and cell disruption are most commonly used for microalgal biomass processing based on the extraction procedure and the final product. Most of the bioproducts including chlorophylls, carotenoids, fatty acids and proteins are intracellular in nature and can generally only be recovered by solvent extraction (Halim et al., 2019). Cell disruption is an essential downstream step for intracellular product recovery. It is a crucial step to rupture the cell wall thereby enhancing extraction efficiency of biomolecules from microalgae. However, the cell wall structure and composition of microalgae is complex and has a significant impact on the disruption efficiency (Alhattab et al., 2019). Microalgal cell walls are diverse and sometimes structurally robust, composed of interlinking biopolymers (polysaccharides and glycoprotein) (Halim et al., 2019). Diatoms possess rigid silicified cell wall with complex sulphated polysaccharides as the major component (Le Costaouec et al., 2017). High energy consumption or large quantities of chemicals are required to disrupt cells in order to maximise intracellular product recovery from

microalgae, which remains a major barrier to the commercial application of microalgae (Alhattab et al., 2019). However, this could be advantageous in some cases where intact microalgal cells are required for whole cell products like edible vaccines (Rosales-Mendoza et al., 2016).

Cell disruption of microalgae can be performed with a variety of techniques, classified into two categories: mechanical and non-mechanical. Mechanical methods include bead milling, high-pressure homogenisation, ultrasonication, microwave, autoclaving, steam explosion, etc. This type of cell disruption methods result in non-specific cell wall breakdown due to high mechanical forces and were found effective for large-scale operations (Gunerken et al., 2015). The non-mechanical methods including chemical and enzymatic treatments are using chemicals such as acids, alkalis and surfactants, or enzymes like cellulase, lysozyme and snailase, or osmotic shock to lyse microalgal cells. The enzymes, papain and bromelain, were shown to be effective in facilitating lipid extraction from *P. tricornutum* (Horst et al., 2012). Enzymatic lysis has the advantages of biological specificity, mild operating conditions and low energy requirement. However, this method is restricted by the high cost of enzymes, long process time and low enzyme availability for algae disruption (Al hattab and Ghaly, 2015). Chemical additions for cell disruption are potentially toxic and not environmental-friendly and may affect cell constitutes, such as protein denaturation by alkali and pigment degradation by acid (Gunerken et al., 2015, Wang et al., 2014).

High-pressure homogenisation is commonly employed in the biotechnology industry to break cells, releasing valuable intracellular products. This cell disruption method involves passing the cell suspension at high pressure and low temperature, through an adjustable valve with a narrow cavity. Cell breakage is thus achieved with several mechanisms including fluid shear forces, cavitation from a rapid pressure drop and high velocity impact on the impact ring (Blaha et al., 2018). This process can be repeated for several passes increasing the levels of cell disruption. Models have been developed for the protein release accompanying cell disruption from high-pressure homogenisation as follows (Follows et al., 1971, Blaha et al., 2018):

$$\ln\left(\frac{R_{max}}{R_{max}-R}\right) = kNp^{\alpha}$$ **Equation 1-2**

where R_{max} represents the maximum amount of protein releasable, R is the amount of protein released after N passes through the valve, k is a temperature dependent rate constant, p is the operating pressure and α is a constant, a measure of a microbe's resistance to disruption. High-pressure homogenisation is a preferred method for the large-scale disruption of microalgal cells with effective cell rupture, low risk of thermal degradation. The specific energy consumption varies (0.25-147 kWh kg^{-1} of biomass) depending on algae species, biomass concentration and growth conditions (Gunerken et al., 2015).

Ultrasonication is one of the most widely used methods for laboratory-scale rupture of microalgal cells. Several mechanisms contribute to the cell disruption by ultrasonication (Priego-Capote and de Castro, 2007). The high intensity ultrasonic waves initiate cavitation bubbles and the propagating shock waves generate jet streams in the surrounding suspension causing high shear forces (Al hattab and Ghaly, 2015). Furthermore, the formation of free radicals due to the thermolysis of water also contributes to cell rupture (Zhang et al., 2007b). Ultrasonication has been demonstrated to be effective in assisting lipid extraction from microalgae with the specific energy consumption ranging from 0.06 kWh kg^{-1} to 119 kWh kg^{-1} for different species (Al hattab and Ghaly, 2015, Gunerken et al., 2015). Sonication was found to be less efficient compared to homogenisation when a partially miscible solvent system, hexane-methanol was used for lipid extraction from *P. tricornutum* (Balasubramanian et al., 2013). To increase cell disruption efficiency and reduce the energy demand, ultrasonication could be combined with other cell disruption methods like chemical methods, which would be interesting for the mild microalgae biorefinery.

A previous study comparing various cell disruption methods indicated that bath sonication, steam explosion and microwave radiation were suitable for microalgae pre-treatment and for large-scale operations while freeze drying, autoclaving and enzymatic techniques were considered as unsuitable due to

the high costs, long treatment time or scale up difficulty (Al hattab and Ghaly, 2015). Evaluation of different cell rupture methods on lipid extraction from *P. tricornutum* showed that lipid extraction efficiency was higher after steam explosion treatment compared to autoclaving, ultrasound and microwave techniques (Lorente et al., 2015). Recently, some new technologies such as explosive decompression, laser treatment, microfluidizer, high frequency focused ultrasonication and cationic polymer coated membranes are emerging in microalgae cell disruption and are being applied to aid the extraction of bioactive molecules from microalgae (McMillan et al., 2013, Gunerken et al., 2015, Wang et al., 2014, Yoo et al., 2014).

1.4 Ultra scale-down (USD) techniques

Evaluation of the performance of large-scale bioprocessing by direct experimental method is material, time and cost consuming and labour-intensive. In bioprocess development, ultra scale-down (USD) technologies enable to use experimentation at the millilitre scale to rapidly assess the large-scale bioprocessing performance with greater ease and low cost (Rayat et al., 2016). Different from conventional scale-down approaches with similar geometry and flow characteristics, USD techniques mimic critical parameters that will dominate and determine performance when scale changes are made in the bioprocessing (Titchener-Hooker et al., 2008). Evaluation of these dominant effects at small scale will allow prediction of large-scale performance. A series of USD approaches have been developed for investigation of a range of downstream processing operations including flocculation, centrifugal clarification, dewatering and discharge, homogenisation, filtration and pump transfers (del Real et al., 2014, Boychyn et al., 2004, Lopes and Keshavarz-Moore, 2012, Aucamp et al., 2014, Fernandez-Cerezo et al., 2019, Zhang et al., 2007a, Li et al., 2013).

1.4.1 Ultra scale-down centrifugation

The USD centrifugation is using an USD rotating-disc shear device, which was designed to mimic the hydrodynamic environments experienced by cells in the feed zone of industrial centrifuges, followed by a bench-top

centrifugation to predict the performance of large-scale centrifugation (Figure 1-7) (Boychyn et al., 2001).

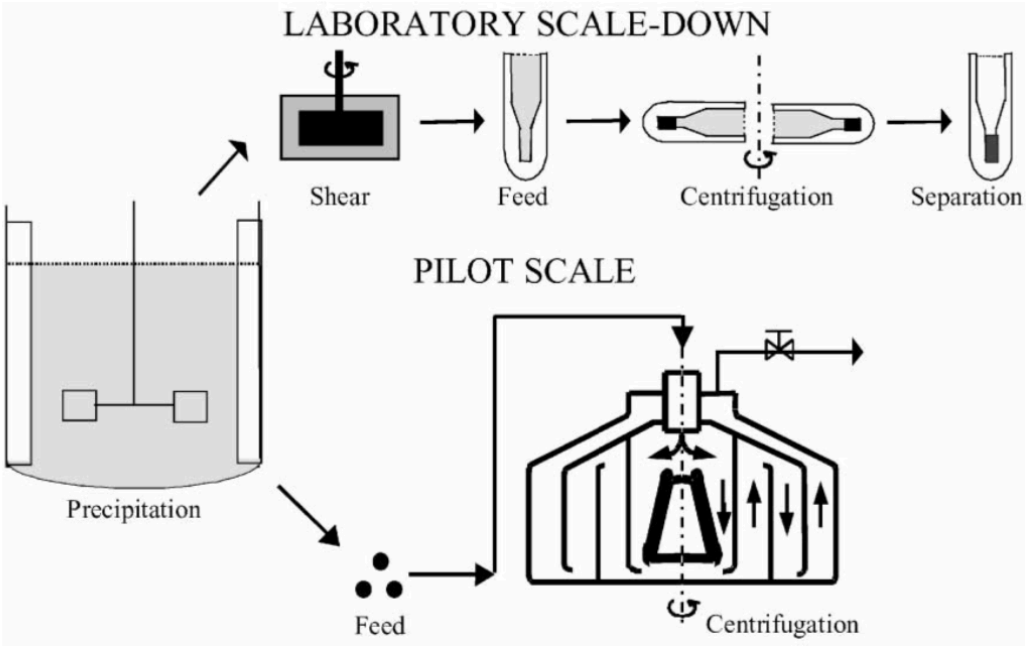

Figure 1-7 Ultra scale-down centrifugation to mimic and predict the large-scale centrifugation performance.

The utilisation of a high-speed rotating-disc shear device combined with a laboratory-scale centrifugation to predict the large-scale centrifugal recovery. The image is cited from a previous report (Boychyn et al., 2001).

The performance of large-scale centrifuges can be predicted using the USD centrifugation based on the Sigma Theory (Ambler, 1959) as follows:

$$\frac{\boldsymbol{Q_{LS}}}{\boldsymbol{C_{LS}\Sigma_{LS}}} = \frac{\boldsymbol{V_{USD}}}{\boldsymbol{C_{USD}t_{USD}\Sigma_{USD}}} \qquad \textbf{Equation 1-3}$$

where Q_{LS}, C_{LS}, Σ_{LS} represent the flow rate, calibration factor and equivalent settling area of large-scale (subscript $_{LS}$) centrifuges and V_{USD}, C_{USD}, t_{USD}, Σ_{USD} represent the centrifuged sample volume, calibration factor (C_{USD}=1), centrifugation time, and equivalent settling area of bench-top (subscript $_{USD}$) centrifuges.

According to the Sigma Theory, the ratio of flow rate to equivalent settling area ($Q/(C\Sigma)$) is constant across centrifuges of different types and scales.

The flow rate for a batch centrifuge can be expressed as the sample volume divided by the centrifugation time, thus enabling to compare the performance of continuous and batch centrifuges with the above Equation 1-3.

The equivalent settling area of the bench-top centrifuge (Σ_{USD}) can be determined with the following equation (Maybury et al., 2000):

$$\boldsymbol{\Sigma_{USD}} = \frac{\boldsymbol{V_{USD}\omega^2(3-2x-2y)}}{\boldsymbol{6gln\left(\frac{2R_2}{R_2+R_1}\right)}} \qquad \textbf{Equation 1-4}$$

where V_{USD} represents the centrifuged sample volume, ω (rad s^{-1}) represents the angular velocity (=$2\pi N$, where N is the rotational speed of centrifugation), x and y represent the fractional acceleration and deceleration time respectively, g is the gravitational acceleration and R_1 and R_2 are the inner and outer radii of rotation. An example sigma calculation can be found in Appendix.

The use of laboratory centrifuges for direct prediction of the large-scale centrifugation performance is challenging because the high levels of flow stresses occurring in large-scale centrifuges may cause damage to shear-sensitive biological materials. As a consequence, the proportion of fine particles could increase leading to a reduction in the recovery efficiency and overprediction of large-scale centrifuge performance (Maybury et al., 2000). Advances in computational fluid dynamics (CFD) enable the complex flow and energy dissipation patterns in continuous industrial centrifuges to be quantified. A maximum energy dissipation rate of 2-14x10^5 W kg^{-1} was reported in the feed zone, where breakage primarily occurred, of the industrial centrifuges including disc-stack centrifuge, multichamber-bowl centrifuge and CARR PowerfugeTM centrifuge (Boychyn et al., 2001, Boychyn et al., 2004). A small high-speed rotating-disc shear device (Figure 1-8) has been designed to reproduce the energy dissipation rates in industrial centrifuges with the aid of CFD analysis (Levy et al., 1999, Boychyn et al., 2001). The degree of shear stress generated in the device is controlled by the speed of disc rotation. Millilitre quantities of feed material are shear-

treated in the USD shear device operating at a speed that mimics the flow stress experienced by cells in the feed zone of large-scale centrifuges. This step enables to assess the impact of centrifugation conditions on the recovery performance of shear-sensitive materials with a subsequent bench-top centrifugation.

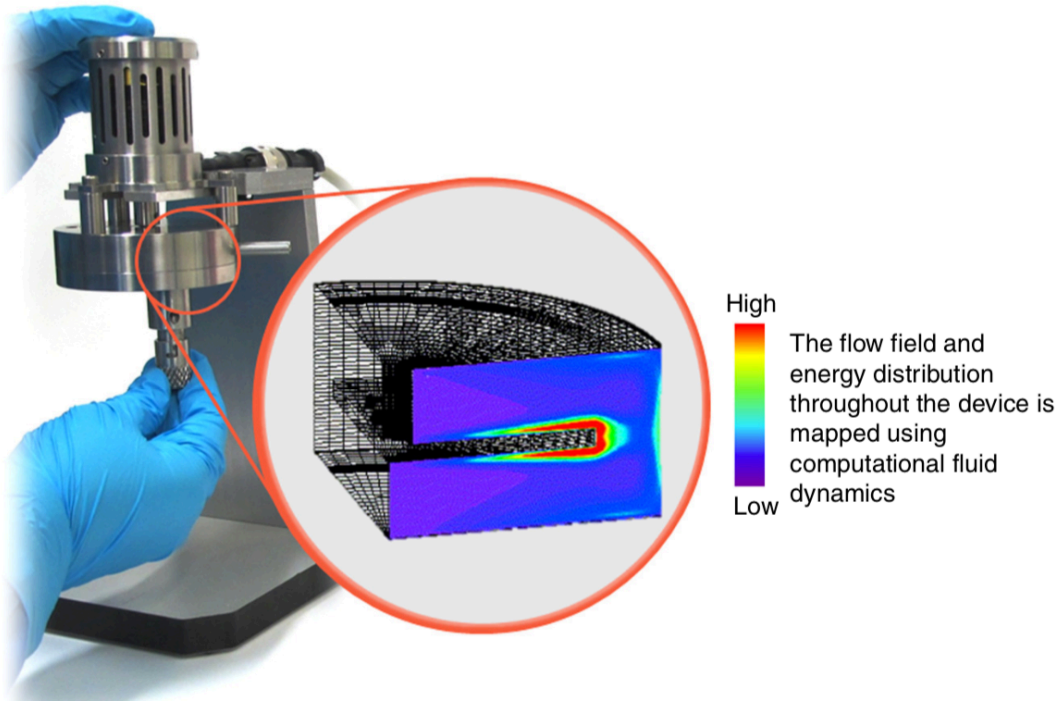

Figure 1-8 A diagram of an USD rotating-disc shear device (kompAs^{TM}) with the energy dissipation rates predicted by CFD. The image is from a previous report (Rayat et al., 2016)

The USD centrifugation approach has been successfully applied to predict the clarification performance of various large-scale continuous-flow centrifuges with diverse biological materials. For example, separation of a green microalga, *Chlamydomonas reinhardtii* using disc-stack centrifuges (Stoffels et al., 2019), recovery of protein precipitates using multichamber-bowl centrifuges, a disc-stack centrifuge and a CARR PowerfugeTM centrifuge (Boychyn et al., 2001, Boychyn et al., 2004), mammalian cell separation in disc-stack centrifuges (Hutchinson et al., 2006, Zaman et al., 2009), separation of the flocculated *E. coli* heat extract using a disc-stack centrifuge (Berrill et al., 2008) and separation of the flocculated recombinant *E. coli* broths in a disc-stack centrifuge and a tubular bowl centrifuge

(Voulgaris et al., 2016). From these studies, all the predicted results from the USD centrifugation method were verified at a pilot or industrial scale. This approach can also be used to investigate the interactions between centrifugation and other processing unit operations such as interactions of flocculation, centrifugation and depth filtration (Voulgaris et al., 2016, Joseph et al., 2016) and interactions of homogenisation and centrifugation (Chatel et al., 2014, Rayat et al., 2016).

In addition, the USD rotating-disc shear device has been applied to assess the effects of shear stress on the properties of valuable biological materials such as aluminium phosphate adjuvant, adjuvant-containing vaccine drug products (Kolade et al., 2015), human cells for cancer vaccine therapy (Mccoy et al., 2009) and an antibody fusion protein expressed by X33 *Pichia pastoris* for colorectal cancer treatment (Blas et al., 2018). Moreover, this device was used to simulate the shear conditions in pump transfers to predict the shear damage of supercoiled circular plasmid DNA (Zhang et al., 2007a) and the shear conditions during formulation and vial filling operations to assess responses of human cancer vaccine cells (Mccoy et al., 2010).

During large-scale centrifugation, an additional level of breakage could occur due to the centrifugal discharge, which has proven to be correlated with the impact velocity (Chan et al., 2006). Discharge from disc-stack centrifuges was shown to result in 10-20% disruption of *E. coli* (Gary et al., 1972) and cell breakage of a cell wall-reduced strain of the green microalga *C. reinhardtii* (Stoffels et al., 2019). A capillary discharge device has been used to mimic centrifugal discharge to predict damage of bioengineered *E. coli* strains for Fab production (Aucamp et al., 2014).

1.4.2 Ultra scale-down cell disruption

Release of protein or enzymes from bakers' yeast by cell disruption using an industrial high-pressure homogeniser or agitator mill had been studied in the 1970s (Follows et al., 1971, Currie et al., 1972). Models for rupture of microorganisms by high-pressure homogenisation were developed,

describing the changes in particle size distribution accompanying cell disruption under various homogenising conditions (Shamlou et al., 1995, Siddiqi et al., 1996). The high-pressure homogenisation models established using natural yeast were further refined for a recombinant yeast strain using a scale-down unit, a Manton Gaulin Lab40 high-pressure homogeniser. The use of this scale-down device enabled model parameters to be collected rapidly from small volume (40 mL) of feed materials and enables to predict and optimise large-scale performance of high-pressure homogenisation in disrupting recombinant yeast to yield an intracellular protein (Varga et al., 1998). A CFD model was applied to characterise the fluid dynamics in an industrial high-pressure homogeniser for *E. coli* disruption (Miller et al., 2002). These studies provided the basis for the development of USD cell disruption technologies.

More recently, an USD cell disruption method based on adaptive focused acoustics (AFA) (Figure 1-9) has been used to mimic the high-pressure homogenisation of recombinant *E. coli* for recovery of an intracellular antibody fragment. Given the same fractional release of the antibody fragment or overall protein, the cell debris particle size distribution of the disruptate produced by AFA was in good agreement with that of the homogenate produced by pilot high-pressure homogenisation. This was further verified by USD centrifugation (as described in section 1.4.1) of both disruptates, demonstrating the same sedimentation characteristics (Li et al., 2012). Moreover, this research group studied the interaction of fermentation, homogenisation and centrifugation using a combination of AFA-based USD cell disruption approach followed by microwell-based USD centrifugation. Successful verification was achieved using a pilot high-pressure homogeniser followed by a pilot disc-stack centrifuge through comparing the faction of antibody fragment release, particle size distribution and solid carryover in the supernatant (Li et al., 2013). The particle size distribution information is especially essential because increasing cell rupture to achieve near complete protein product release will decrease particle size with the subsequent micronised debris removal by centrifugation challenging. Another group applied this USD cell disruption platform to *Pichia pastoris* for recovery

of intracellular recombinant protein. Models of cell rupture by AFA were developed based on five different performance criteria, allowing to mimic the large-scale homogenisation processes (Blaha et al., 2018).

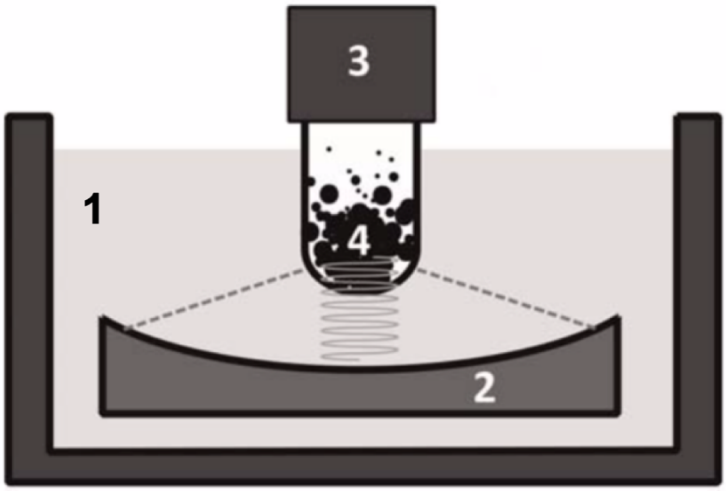

Figure 1-9 A diagram showing the Covaris focused acoustic ultrasonicator.

1, cooled water bath in a tank at 10 °C; 2, acoustic transducer; 3, sample vessel, e.g. 1 mL millitube (Covaris, USA); 4, acoustic focal zone. The image is adapted from a figure in a previous report (Blaha et al., 2018).

1.5 Aims and objectives

P. tricornutum is of growing interest as a production system for sustainable manufacture of lipids and small molecules, as well as recombinant proteins. The overall aim of this thesis was to explore how the cell morphotypes of *P. tricornutum* might influence its industrial applications, thereby optimising *P. tricornutum* as a microalgal expression host for industrial biotechnology. To achieve these, the objectives are as follows.

The first objective was to determine if culture conditions are capable of triggering cell morphotype change of the selected ecotypes of *P. tricornutum,* Pt1 8.6 and Pt4, in liquid cultures and maintain the obtained morphotype in high abundance. These two strains were selected because the advanced genetic toolkits available for *P. tricornutum* were mostly established using these two strains (section 1.2.3). Pt1 8.6 has been selected for genome sequencing and 12,000 ESTs have been generated

from this strain and organised in a queryable database. Pt4 has a different genotype from Pt1 8.6 (Table 1-1) and may behave differently to varying environmental conditions. Pt4 has also been frequently used for developing genetic tools including genetic transformation method, selectable markers and reporter genes and for recombinant protein expression (Table 1-4). Overall, valuable genetic information is available for both strains to study cell shape control and to construct GM strains. Two culture media, f/2 medium and Mann & Myers' medium, were used for *P. tricornutum* cultivation to investigate the impacts of culture media on cell morphology. f/2 medium is most widely used for *P. tricornutum* storage and cultivation in culture collections and by other researchers. Mann & Myers' medium was previously reported to grow *P. tricornutum* as well and usually used for scale-up cultivation due to its rich nutrient. These two media contain very different nutrients and thus were chosen to determine if marked changes in medium composition would influence cell morphology of *P. tricornutum*. Mann & Myers' medium was observed to elicit significant morphotype conversion from fusiform to oval in liquid cultures and successive transfers in this medium enriched oval cells. The reversibility of the morphological changes was also investigated by inoculating the oval cells back into f/2 medium to understand if cell morphology could be flexibly controlled through changing cultivation strategy.

The second objective was to explore the relationship between cell morphotype and classes of product formation in *P. tricornutum*, to support its biorefinery for industrial exploitation. In response to the changing culture conditions, distinct morphotypes of cells could have different gene expression levels, leading to different cell biochemical compositions. Biochemical profiles including pigment, protein, lipid and carbohydrate in fusiform and oval morphotypes under their respective growth medium were investigated. Biochemical composition in various cell morphotypes is also essential for nutritional value evaluation and optimisation of *P. tricornutum* for industrial biotechnology.

The third objective was to explore the downstream processing of different cell morphotypes of *P. tricornutum*, considering their potential use as expression hosts. To our knowledge, little is known about the shear resistance of diverse *P. tricornutum* morphotypes and no study has been carried out to compare the rupture of various cell morphotypes. The initial steps of downstream processing including harvest and disruption of fusiform and oval cells were investigated in order to recover intracellular bioproducts. The ultra scale-down (USD) platform developed at UCL was employed to characterise the robustness of fusiform and oval cells against shear stresses and to predict the cell recovery in large-scale centrifuges. The cell disruption efficiency of the two morphotypes was studied using the USD method based on adaptive focused acoustics (AFA).

2 Materials and methods

2.1 Microorganisms, culture media and solutions preparation

2.1.1 *Phaeodactylum tricornutum* strains

Phaeodactylum tricornutum strains Pt1 8.6 (CCAP 1055/1) and Pt4 (CCAP 1052/6) were acquired from the Culture Collection of Algae and Protozoa (CCAP, Oban, UK). From CCAP website (http://www.ccap.ac.uk/), *P. tricornutum* cultures were non-axenic. Pt1 8.6 is a monoclonal culture derived from Pt1 isolated off Blackpool, UK, in 1956 and Pt4 was isolated from a supralittoral rock pool on the Island of Segelskar, Finland, in 1951 and was described as a brackish strain (De Martino et al., 2007). Upon arrival from CCAP, the stock cultures of both strains consisted mainly of the fusiform morphotype, accounting for approximately 88% in Pt1 8.6 and 97% in Pt4.

2.1.2 f/2 medium and stock solutions

The f/2 medium (Guillard, 1975), f/2-enriched artificial seawater here, was prepared by dissolving 33 g Aquarium Systems Instant Ocean salt (Instant Ocean, Blacksburg, USA), 75 mg $NaNO_3$ and 5 mg $NaH_2PO_4 \cdot H_2O$ in 1 litre of reverse osmosis (RO) water. The pH was adjusted to 8.0-8.1 with HCl or NaOH. The medium was sterilised at 121 ^oC for 20 min. Trace elements and vitamins were added at 1 mL L^{-1} and 0.5 mL L^{-1} respectively prior to use (Table 2-1).

The f/2 trace elements stock solution was prepared by dissolving the following additives: Na_2EDTA 4.16 g, $FeCl_3 \cdot 6H_2O$ 3.15 g, $CuSO_4 \cdot 5H_2O$ 0.01 g, $ZnSO_4 \cdot 7H_2O$ 0.022 g, $CoCl_2 \cdot 6H_2O$ 0.01 g, $MnCl_2 \cdot 4H_2O$ 0.18 g and $Na_2MoO_4 \cdot 2H_2O$ 0.006 g in 1 litre of Milli-Q water (Milli-Q Advantage A10 purification system, Merck Millipore, Germany). The stock solution was autoclaved for sterilisation and stored at 4 ^oC.

The vitamins stock solution was prepared by dissolving 0.2 g thiamine HCl (vitamin B_1), 0.001 g cyanocobalamin (vitamin B_{12}) and 0.001 g biotin

(vitamin H or B_7) in 1 litre of Milli-Q water, which was sterilised by filtering through 0.2 μm filter and stored at 4 °C.

Table 2-1 Chemical composition of f/2 medium and Mann and Myers' medium.

	f/2 medium		Mann and Myers' medium	
	Component	Concentration	Component	Concentration
Salinity	Instant Ocean salt [a]	33 g L^{-1}	NaCl	5 g L^{-1}
			$MgSO_4 \cdot 7H_2O$	1.2 g L^{-1}
			KCl	0.6 g L^{-1}
			$CaCl_2$	0.3 g L^{-1}
Nitrate	$NaNO_3$	0.88 mM	$NaNO_3$	11.76 mM
Phosphate	$NaH_2PO_4 \cdot H_2O$	0.036 mM	K_2HPO_4	0.574 mM
Tris			Tris	1 g L^{-1}
Trace element	Na_2EDTA	1.24 x 10^{-5} M	Na_2EDTA	8.92 x 10^{-5} M
	$Na_2MoO_4 \cdot 2H_2O$	2.48 x 10^{-8} M	H_3BO_3	9.70 x 10^{-5} M
	$FeCl_3 \cdot 6H_2O$	1.17 x 10^{-5} M	$FeSO_4 \cdot 7H_2O$	7.19 x 10^{-6} M
	$MnCl_2 \cdot 4H_2O$	9.09 x 10^{-7} M	$MnCl_2 \cdot 4H_2O$	1.11 x 10^{-5} M
	$ZnSO_4 \cdot 7H_2O$	7.65 x 10^{-8} M	$ZnSO_4 \cdot 7H_2O$	1.15 x 10^{-6} M
	$CoCl_2 \cdot 6H_2O$	4.20 x 10^{-8} M	$Co(NO_3)_2 \cdot 6H_2O$	2.40 x 10^{-8} M
	$CuSO_4 \cdot 5H_2O$	4.00 x 10^{-8} M	$CuSO_4 \cdot 5H_2O$	8.01 x 10^{-9} M
Vitamin	Vitamin B_{12}	0.0005 mg L^{-1}		
	Vitamin B_1	0.1 mg L^{-1}		
	Biotin	0.0005 mg L^{-1}		

[a] The f/2 medium was prepared in artificial seawater made from Instant Ocean Salt at 33 g L^{-1} which contains 1.2 g L^{-1} magnesium ion, 0.35 g L^{-1} potassium ion and 0.4 g L^{-1} calcium ion.

2.1.3 Mann & Myers' medium and stock solutions

The Mann & Myers' medium (hereafter M & M medium) (Mann and Myers, 1968), was prepared by dissolving 5 g NaCl, 1.2 g $MgSO_4 \cdot 7H_2O$, 0.6 g KCl, 0.3 g $CaCl_2$, 1 g $NaNO_3$, 0.1 g K_2HPO_4 and 1 g Tris in 1 litre of RO water. The pH was adjusted to 8.0-8.1 with HCl or NaOH and the medium was

sterilised at 121 °C for 20 min. Trace elements was added at 10 mL L^{-1} prior to use (Table 2-1).

The M & M trace elements stock solution was prepared by dissolving 3 g Na_2EDTA, 0.6 g H_3BO_3, 0.2 g $FeSO_4 \cdot 7H_2O$, 0.22 g $MnCl_2 \cdot 4H_2O$, 0.033 g $ZnSO_4 \cdot 7H_2O$, 0.0002 g $CuSO_4 \cdot 5H_2O$ and 0.0007 g $Co(NO_3)_2 \cdot 6H_2O$ in 1 litre of Milli-Q water. The stock solution was autoclaved for sterilisation and stored at 4 °C.

2.1.4 Cell lysis buffer

Lysis buffer was prepared by dissolving 50 mM Tris-HCl, pH 8.0 (7.88 g), 10 mM EDTA (2.92 g), and 0.1% (v/v) TritonX-100 (1 mL) in 1 litre of Milli-Q water. EDTA as a chelating agent binds to metal ions like Mg^{2+}, thereby reducing the activity of enzymes such as DNase and protease. TritonX-100 is a nonionic surfactant and could dissolve cell membrane, changing membrane permeability or causing cell structure collapse. Phenylmethylsulfonylfluoride (PMSF, 36978, Thermo Scientific, UK) acting as a protease inhibitor that reacts with serine residues was added at a working concentration of 0.5 mM prior to use.

100 mM PMSF stock solution was prepared by dissolving 0.174 g PMSF in 10 mL of isopropanol. Stock was aliquoted into 1.5 mL eppendorf tubes and stored at -20 °C.

2.1.5 Solvents for pigment analysis

Analysis of pigment composition in *P. tricornutum* was carried out by reverse phase high-performance liquid chromatography (RP-HPLC). The mobile phase solvent A (80% v/v methanol containing 0.5 M ammonium acetate) was prepared by mixing 800 mL of methanol (HPLC grade) with 200 mL of filtered 0.5 M ammonium acetate.

0.5 M ammonium acetate solution was prepared by dissolving 19.27 g ammonium acetate (HPLC grade, ⩾99%, Honeywell Fluka, UK) in 500 mL of

Milli-Q water. The pH was adjusted to 7.2 with acetic acid or ammonium hydroxide. The solution was filtered through 0.22 µm polyethersulfone (PES) membrane (Stericup, Merck Millipore, Germany).

The solvent B (90% v/v acetonitrile) was prepared by mixing 900 mL of acetonitrile (CHROMASOLV® HPLC gradient grade) with 100 mL of Milli-Q water.

2.1.6 Reagents for carbohydrate determination

1 M sulphuric acid solution was prepared by slowly adding 5 mL of 98% pure H_2SO_4 into 85 mL of Milli-Q water in a glass vessel.

5% (w/v) phenol solution was prepared by dissolving 5 g phenol in 100 mL of Milli-Q water. The solution was mixed thoroughly using a magnetic stirrer for 30 min.

2.1.7 BODIPY 505/515 stock solution

A 1 mg mL^{-1} stock solution of a green lipophilic fluorescence dye, BODIPY 505/515 (4,4-difluoro-1,3,5,7-tetramethyl-4-bora-3a,4a-diaza-s-indacene, D3921, Invitrogen, UK) was made by dissolving the dye in dimethyl sulfoxide (DMSO). The stock was aliquoted and stored in the dark at -20 ^oC.

2.1.8 Solutions for fatty acid determination

The chloroform: methanol (2:1, v/v) mixture was prepared fresh on day by mixing 40 mL of chloroform and 20 mL of methanol in a glass bottle in fume hood.

Pentadecanoic acid (C15:0) stock solution was prepared by dissolving 10 mg C15:0 free fatty acid in 1 mL of n-heptane. The stock was aliquoted and stored at -20 ^oC.

2.5% (v/v) H_2SO_4 in methanol was made by slowly adding 2 mL of concentrated sulphuric acid into 78 mL of methanol.

2.2 Cultivation and analytical methods

2.2.1 Standard cultivation conditions

Stock cultures of Pt1 8.6 and Pt4 were maintained in f/2 medium upon arrival from CCAP. Since *P. tricornutum* is facultative for silicate, it was not added for cultivation of both strains throughout this study. All cultures were grown at 20 °C with 100 rpm shaking under continuous light illumination at 80 µmol photons m^{-2} s^{-1} from fluorescent lamps (P0300-0221, Grolux T8 15W Sylvania, Eppendorf, UK) factory-installed in the shaker (New Brunswick™ Innova® 44, Eppendorf, UK).

2.2.2 Cell growth and dry biomass determination

The growth of *P. tricornutum* cells was determined by optical density measurement at 750 nm (OD_{750}) using a visible spectrophotometer (Ultrospec 500 pro, GE Healthcare Life Sciences, USA). The cell density was also monitored by microscopic cell counting using a haemocytometer (Bright-Line 1492, Hausser Scientific, USA) (Figure 2-1).

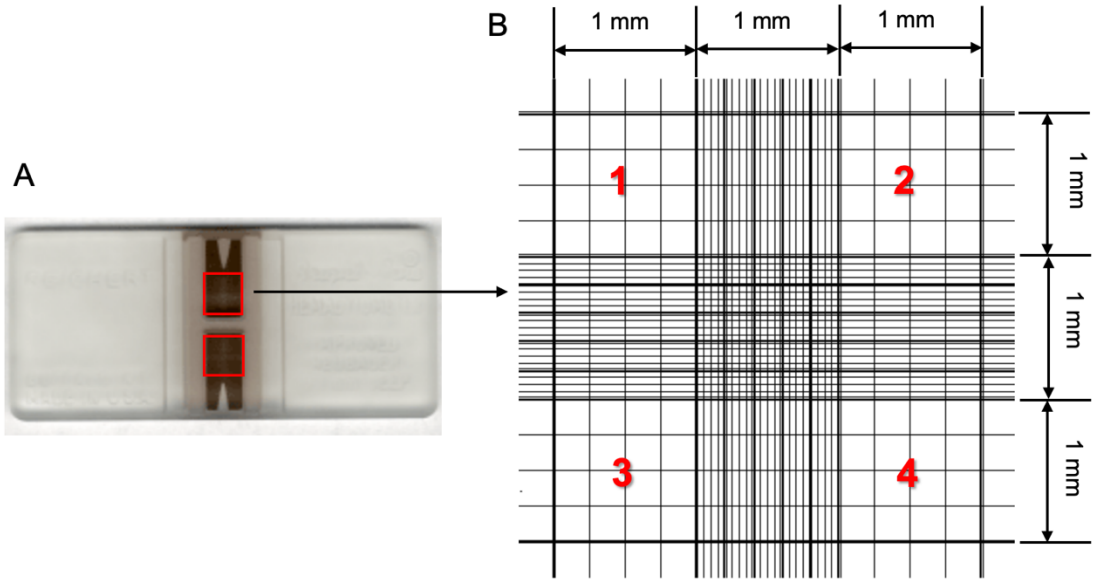

Figure 2-1 A diagram of a haemocytometer for cell counting.

A photograph of a haemocytometer (A) and a diagram showing the counting chamber (B). Red boxes label the regions where samples were added and counted. For each sample, cells in the four corner boxes (1, 2, 3 and 4) with the length and

width being 1 mm were counted. The depth of chambers is 0.1 mm. Thus, the cell density (cells mL^{-1}) = the averaged cell number per box x dilution factor x 10,000.

The specific growth rate (*k*), which generally refers to the growth rate of cells in exponential phase, is calculated with the equation:

$$\boldsymbol{k = \frac{lnN_2 - lnN_1}{t_2 - t_1}} \qquad \textbf{Equation 2-1}$$

where *N* is the cell density (cells mL^{-1}) and *t* is the time after inoculation at time 1 and 2 respectively. Thus, the doubling time can be calculated with following the equation.

$$\boldsymbol{t = \frac{ln2}{k}} \qquad \textbf{Equation 2-2}$$

Dry biomass concentration (g L^{-1}) was measured as follows. Culture samples (20 mL) were centrifuged at 3,200 x g for 15 min, washed with RO water to remove non-biological materials like mineral salts and then resuspended in a small volume of RO water. Cell suspensions were filtered through the pre-dried and pre-weighed GF/C glass microfiber filters (Whatman, GE Healthcare Life Sciences, USA) and were dried in an oven (Heraeus T6060, Thermo Scientific, UK) at 80 ^{o}C until a constant mass was achieved.

2.2.3 Microscopic examination

P. tricornutum samples were imaged using an inverted microscope (TE2000-U, Nikon, Japan) under phase contrast at 30x magnification. Micrographs were captured and acquired with NIS-Elements BR 3.2 software.

2.2.4 Protein quantification

P. tricornutum samples before and after focused acoustic disruption or shear treatment in the rotating disc shear device were centrifuged at 21,000 x g for 20 min at 4 ^{o}C to remove cells and debris. The released soluble protein in the supernatant was quantified using the Coomassie (Bradford) Protein Assay kit

(No. 23200, Thermo Scientific, UK) (Bradford, 1976). In acidic conditions, the Coomassie G-250 dye binds to primarily the basic amino acids (arginine, lysine and histidine) of proteins due to the presence of ammonia in their side chains. The number of Coomassie dye ligands bound to each protein molecule is proportional to the number of positive charges found on the protein. The formation of protein-dye complex causes a shift in absorption maximum from 465 nm to 595 nm with a colour change from brown to blue. The measurement was performed in microplate format. Specifically, 5 µL of each sample was pipetted into microplate wells (96-well plate, Sarstedt, UK), followed by adding 250 µL of the Coomassie reagent. The plate was mixed for 30 s with a plate shaker (Eppendorf ThermoMixer C, Eppendorf, UK) and incubated for 10 min at room temperature. The absorbance at or near 595 nm was then measured with a microplate reader (BMG Fluostar Optima, BMG LABTECH Ltd., UK). The protein concentration was calculated using the equation from the standard curve of bovine serum albumin (BSA). The standard curve was made in each assay with the BSA concentration ranging from 0.025 mg mL^{-1} to 0.75 mg mL^{-1}.

2.2.5 Carbohydrate quantification

The carbohydrate content was quantified using the phenol sulphuric acid (PSA) assay as described in the EnAlgae protocol, SOP 4.2.a (Silkina et al., 2015), modified from the DuBois assay (Dubois et al., 1956). Briefly, 0.1 mL of each sample was pipetted into a glass test tube. To the sample, 2.5 mL of 98% H_2SO_4 was added directly, quickly followed by adding 0.5 mL of 5% phenol solution. This was then mixed and left for 20 min to cool. The samples were carefully poured into acid resistant cuvettes (Brand UV-Cuvette, 1.5 mL, Brand, Germany) and read at 485 nm. The carbohydrate content was calculated using the equation from a D-glucose standard curve.

2.2.6 Particle size distribution measurement

The particle size distribution of *P. tricornutum* samples was measured using the laser diffraction particle size analyser (Mastersizer 3000, Malvern Panalytical Ltd., Malvern, UK), with a particle size detection range of 0.01-

3,500 µm. Samples were added dropwise into Milli-Q water in the dispersion unit operating at 2000 rpm until a laser obscuration value of >5% was reached. A refractive index of 1.03 relative to water and an absorption index of 0.01 were used. The particle size distribution profile obtained for each sample represented the average of five measurements.

2.3 Chromatographic analysis

All solvents used for chromatographic analysis were HPLC grade or GC grade and Milli-Q water was used throughout the chromatographic analysis.

2.3.1 High-performance liquid chromatography (HPLC) for pigment analysis

Pigment analysis by reverse phase HPLC (RP-HPLC) was conducted on an UltiMate 3000 HPLC system (Dionex, Thermo Scientific, UK). Separation was achieved in an ACE 5 C18 reverse phase column (150 mm x 4.6 mm ID, 5 µm particle size, Advanced Chromatography Technologies Ltd, UK) which was maintained at 30 °C. Twenty microlitres of each sample was injected into the system. The mobile phase was pumped in at a flow rate of 1 mL min^{-1} programmed as follows (Wright et al., 1991): an initial 4 min linear gradient from 100% solvent A (80% (v/v) methanol containing 0.5 M ammonium acetate, pH 7.2) to 100% solvent B (90% (v/v) acetonitrile), followed by a linear gradient to 20% solvent B and 80% solvent C (100% ethyl acetate) in 14 min. The column was returned to the initial conditions by a 3 min linear gradient to 100% solvent B and another 3 min linear gradient to 100% solvent A and then re-equilibrated in 100% solvent A for 5 min before the next injection. The eluted pigments were detected at 440 nm using a diode array detector.

2.3.2 Gas chromatography (GC) for fatty acid analysis

Fatty acid composition was analysed by GC on a Trace 1300 gas chromatograph (Thermo Scientific, UK) equipped with an automatic sampler, a Rxi-5Sil MS column (30 m × 0.25 mm ID, 0.5 µm film thickness, Restek,

UK) and a flame ionisation detector (FID). One microlitre of sample was injected into the column with a 35:1 split ratio. Helium was used as the carrier gas at a flow rate of 1.2 mL min^{-1}. Injector and detector temperatures were set at 230 ^{o}C and 250 ^{o}C, respectively. The oven temperature was programmed as follows: held at 80 ^{o}C for 2 min, ramped at 15 ^{o}C min^{-1} to 180 ^{o}C, ramped to 240 ^{o}C at 2.5 ^{o}C min^{-1} and held for 10 min.

2.3.3 High-performance anion exchange chromatography (HPAEC) for carbohydrate analysis

Carbohydrate analysis by HPAEC was conducted using an ICS 5000+ system (Dionex, Thermo Scientific, UK) equipped with an AminoPac PA10 column (250 mm x 4 mm, Dionex, Thermo Scientific, UK) and a pulsed amperometric (electrochemical) detector. Ten microlitres of each sample was injected into the column maintained at 30 °C. Monosaccharide separation was achieved following the procedure of an isocratic elution of 1 mM KOH for 25 min at a flow rate of 0.25 mL min^{-1}.

2.4 Statistical analysis

In this study, statistical analyses were performed using one-way student's t-test in Microsoft Office Excel (Microsoft, Redmond, Washington, USA). Data were considered significantly different at a significance level of 0.05.

3 Morphological changes in *Phaeodactylum tricornutum* triggered by culture media

3.1 Introduction

P. tricornutum has a unique property of polymorphism, displaying three main morphotypes: fusiform, triradiate and oval (Figure 1-3) (Wilson, 1946). The fusiform and triradiate types are better adapted to the planktonic lifestyle whereas the oval form tends to be benthic, having a higher sedimentation rate (De Martino et al., 2011). Oval cells possess a raphe and can secrete mucilaginous exopolymeric substances, favouring gliding motility and cell adhesion on surface (De Martino et al., 2011, Tesson et al., 2009a). Unlike typical diatoms, *P. tricornutum* does not have an absolute requirement of silicate for growth. The cell wall of *P. tricornutum* is weakly silicified with organic valves formed in fusiform and triradiate cells and organic or one silicified valve synthesised in oval cells (Borowitzka and Volcani, 1978, Vartanian et al., 2009). This may be an advantage for *P. tricornutum* biotechnology in terms of genetic transformation and intracellular product recovery during bioprocessing, compared to other diatoms with rigid cell walls.

P. tricornutum has been shown to undergo cell morphological conversions in response to fluctuations in growth conditions such as salinity, temperature and pH (De Martino et al., 2011, Bartual et al., 2008). Observations in the natural environment revealed that *P. tricornutum* is typically found in unstable coastal environments such as estuaries and rock pools where temperature and salinity change rapidly (De Martino et al., 2007). Ten strains of *P. tricornutum* (Pt1-Pt10) isolated from different geographic locations worldwide were characterised genetically and phenotypically (De Martino et al., 2007). Another strain Pt1 8.6 is one monoclonal culture derived from Pt1 and has been selected for genome sequencing (Bowler et al., 2008). Among these strains, the fusiform morphotype was found to be most stable and frequently observed in cell cultures (Table 1-1). However, significant cell morphotype change from fusiform to oval occurred in strains Pt1 8.6, Pt3 and Pt9,

induced by hyposaline conditions or low temperature (15 °C) (De Martino et al., 2011, De Martino et al., 2007, Ovide et al., 2018). Enrichment of oval cells was also observed through successive transfers on solid agar medium (Barker, 1935) and this method has been confirmed and applied in some studies to obtain oval cells (Gutenbrunner et al., 1994, Abdullahi et al., 2006, Francius et al., 2008, Tesson et al., 2009b). Under these suboptimal conditions, despite the significant conversion in cell morphotype to oval, the overall total cell growth rate experienced an evident decrease (De Martino et al., 2011), which is not beneficial for industrial applications. Moreover, reversible transformation from oval to fusiform was observed when temperature was shifted from 15 °C to 28 °C (De Martino et al., 2011) or when oval cells were transferred from solid medium to liquid culture (Barker, 1935). More recently, a significant morphological change from fusiform to round (a cell width-to-length ratio of 0.4-0.6) was reported in Pt2 grown under red light (Herbstova et al., 2017). Other unfavourable conditions such as nutrient limitation, low light intensity and low calcium concentration (< 15 mg L^{-1}) were reported to promote oval cell production as well, but the changes in cell morphotype were not marked or the results still need verification (De Martino et al., 2007, Cooksey and Cooksey, 1974, Borowitzka and Volcani, 1978). Triradiate cells are rarely observed in laboratory cultures except for the strain Pt8 (De Martino et al., 2007), though high pH or high dissolved inorganic carbon were reported to increase their abundance particularly under subsaturating illumination (Bartual et al., 2008).

Despite the above observations, limited information is available about the conditions that can be used for controlling cell morphology and maintenance of each cell morphotype of *P. tricornutum*. The molecular mechanisms behind the phenotypic changes are also poorly understood. In order to optimise the polymorphic *P. tricornutum* as a production platform for industrial biotechnology, it may be important to be able to selectively control growth of a particular morphotype for a particular industrial application. In this chapter, the effects of culture media on cell morphology of *P. tricornutum* were first investigated. A culture medium triggering significant cell morphotype conversion from fusiform to oval and suitable for maintenance of

oval cells in liquid cultures was identified. The reversibility of this morphological change was also detected. Finally, the impacts of various medium components on cell morphology of *P. tricornutum* were investigated in order to gain some insights into the factors inducing cell morphotype change in *P. tricornutum*.

3.2 Materials and methods

All chemicals were obtained from Sigma-Aldrich unless mentioned otherwise.

3.2.1 Cell morphological changes study

Stock cultures of Pt1 8.6 and Pt4 were maintained in f/2 medium (Guillard, 1975). Experimental cultures were grown in either f/2 medium or Mann and Myers' medium (Mann and Myers, 1968) to investigate the impact of culture media on cell morphology and growth of *P. tricornutum*. Log-phase cultures of Pt1 8.6 and Pt4 grown in f/2 medium were centrifuged at 3,200 x g for 10 min. Cells were transferred to fresh f/2 medium or M & M medium to pre-acclimate for 6 days (denoted as the 1st transfer). The pre-acclimated cultures were then inoculated in 250 mL Erlenmeyer flasks containing 100 mL of respective culture medium with an initial cell density of 8-10x10^5 cells mL^{-1} (denoted as the 2nd transfer). Subculturing treatments denoted as the 3rd, 4th and 5th transfer were performed when it was estimated that late stationary phase was reached (~day 21), giving an initial cell density as above. Cultivation conditions were detailed in Chapter 2, section 2.2.1. Morphological studies were performed in biological duplicate. The relative proportions of fusiform, oval and triradiate morphotypes in cultures were determined after each transfer using a haemocytometer. A minimum of 500 cells across 4 corner boxes were counted per replica (Figure 2-1). Cell growth and pH changes during cultivation were also monitored by cell counting and using a pH meter (SevenEasy S20 pH meter, Mettler Toledo, Switzerland) respectively. Images of *P. tricornutum* cells grown in f/2 medium or M & M medium were obtained under the microscope as described in Chapter 2, section 2.2.3.

3.2.2 Reversibility characterisation of morphological change

In order to investigate the reversibility of the morphological changes occurred in Pt1 8.6 and Pt4, the obtained stable cells maintained in M & M medium were inoculated back into the f/2 medium where the fusiform morphotype is maintained. Specifically, aliquots of log-phase cell cultures of both strains maintained in M & M medium were centrifuged at 3,200 x g for 10 min and cells were then inoculated into 250 mL Erlenmeyer flasks containing 100 mL of f/2 medium at an initial cell density of approximately $1x10^6$ cell mL^{-1}. Subculturing transfers were conducted as mentioned above (section 3.2.1). The morphotype of *P. tricornutum* cells was checked periodically through microscopy. Experiment was carried out in biological duplicate.

3.2.3 Factorial experiments

Salinity and Tris experiments

When compared to f/2 medium, M & M medium has a much lower salinity and contains Tris (Table 2-1) which is often used to stabilise pH in microalgal cultures. Therefore, the impacts of salinity and Tris on cell growth and morphology of *P. tricornutum* were initially investigated with Pt4. Experimental cultures were prepared by centrifuging log-phase cultures of Pt4 (OD_{750}=0.4-0.6) grown in f/2 medium at 3,200 x g for 10 min and inoculating cells into 250 mL Erlenmeyer flasks containing 100 mL of respective modified f/2 medium, giving an initial cell density of approximately $1x10^6$ cells mL^{-1} (OD_{750}=0.1). For salinity experiments, salinities of 0 ppt, 15 ppt, 33 ppt and 40 ppt were tested by preparing f/2 medium with different amount of Instant Ocean salt (0 g L^{-1}, 15 g L^{-1}, 33 g L^{-1} and 40 g L^{-1}), which represent a gradient from freshwater (0-5 ppt), brackish water (5-30 ppt) and seawater (30-50 ppt). For Tris experiments, f/2 medium was modified by addition of Tris at 0 mM, 5 mM, 10 mM and 20 mM respectively. All cultures were grown under the conditions as detailed in Chapter 2, section 2.2.1. Three biological replicates were conducted for each condition. Cell growth was monitored in short term (~10 days) by OD_{750} and dry biomass measurement while cell morphotype abundance was monitored in long term

(>30 days) by cell counting or microscopic examination. The effect of Tris on culture pH variation was also examined using a pH meter.

Study on components of M & M medium influencing cell morphology

In order to explore the environmental factors inducing morphological changes of *P. tricornutum* grown in M & M medium, several experiments including single-factor and triple-factor methods (Table 3-1) were designed for a rapid evaluation of the impacts of various medium components on cell morphotype of Pt1 8.6 and Pt4.

Table 3-1 Modifications to f/2 medium for factorial experiment.

	f/2 medium → M & M medium
S-	33 g L^{-1} → 7.1 g L^{-1}
N+	0.88 mM → 11.76 mM
P+	0.036 mM $NaH_2PO_4 \cdot H_2O$ → 0.57 mM K_2HPO_4
T+	0 g L^{-1} → 1 g L^{-1}
Trace	f/2 trace elements → M & M trace elements
Vit-	No vitamins added
S N P	33 g L^{-1}, 0.88 mM, 0.036 mM → 7.1 g L^{-1}, 11.76 mM, 0.57 mM
S N T	33 g L^{-1}, 0.88 mM, 0 g L^{-1} → 7.1 g L^{-1}, 11.76 mM, 1 g L^{-1}
S P T	33 g L^{-1}, 0.036 mM, 0 g L^{-1} → 7.1 g L^{-1}, 0.57 mM, 1 g L^{-1}
N P T	0.88 mM, 0.036 mM, 0 g L^{-1} → 11.76 mM, 0.57 mM, 1 g L^{-1}

The medium recipes can be found in Table 2-1.
S, salinity; N, nitrate; P, phosphate; T, Tris, Trace, trace elements; Vit, vitamins.
S-, decreasing the salinity of f/2 medium from 33 g L^{-1} Instant Ocean salt to 5 g L^{-1} NaCl, 1.2 g L^{-1} $MgSO_4 \cdot 7H_2O$, 0.6 g L^{-1} KCl and 0.3 g L^{-1} $CaCl_2$.

Nutrients were divided into fractions of salinity (S), nitrate (N), phosphate (P), Tris (T), trace elements (Trace) and vitamins (Vit). Single-factor experiments represent changing one nutrient fraction of f/2 medium each time to the amount and component of that in M & M medium. That is the modified f/2 media respectively containing 7.1 g L^{-1} salinity, 11.76 mM $NaNO_3$, 0.57 mM

K_2HPO_4, 1 g L^{-1} Tris, M & M trace elements and no vitamins. Triple-factor experiments represent changing three nutrient fractions of f/2 medium each time to the amount and component of those in M & M medium. Here, four combinations of S N P, S N T, S P T and N P T were tested (Table 3-1). The inoculation method and growth conditions are same as described above for salinity and Tris experiments. All cultures were carried through two successive transfers representing a cultivation period of 55 days, in which the second transfer was conducted on day 23. Cultures after the first transfer were maintained for 34 days and Cultures after the second transfer were maintained for 32 days. OD_{750} was measured by the end of cultivation and cell morphotype was examined by microscopy.

3.3 Results and discussion

3.3.1 Impact of culture media on cell morphology of *P. tricornutum*

As *P. tricornutum* is pleiomorphic, it may be important to be able to selectively control growth of a particular morphotype for a particular industrial application. Two previously reported culture media, f/2 medium and M & M medium containing very different nutrients (Table 2-1), were chosen for *P. tricornutum* cultivation in order to determine if marked changes in medium composition would influence cell morphology of *P. tricornutum*.

Upon arrival from CCAP, the genome sequenced strain Pt1 8.6 consisted of approximately 88% fusiform, 10% triradiate and less than 3% oval cells, and another strain Pt4, possessing a different genotype from Pt1 8.6, contained mainly the fusiform morphotype as well (~97% fusiform, 3% oval and <0.5% triradiate), as mentioned in Chapter 2, section 2.1.1. Cultivation for 30 days in liquid f/2 medium did not significantly change the cell morphotype abundance in either strain ($p>0.05$), showing stability for many cell divisions (Figure 3-1 A & C). Contrastingly, when cells were transferred and grown for 30 days in M & M medium, a significant increase in the abundance of oval cells from 2.9% to 38.4% in Pt1 8.6 and from 5.7% to 18.4% in Pt4 was observed ($p<0.05$). Correspondingly, the proportions of fusiform (from 91.3% to 58.5% in Pt1 8.6 and from 94.0% to 81.6% in Pt4) and triradiate (from 6.1% to 3.1% in Pt1 8.6

and <0.1% in Pt4) morphotypes were decreased gradually over time (Figure 3-1 B & D). These results suggested that the oval morphotype was preferred by *P. tricornutum* as a response and an adaption to the M & M medium and confirmed that cell morphological transformation in *P. tricornutum* could be triggered by changing growth conditions.

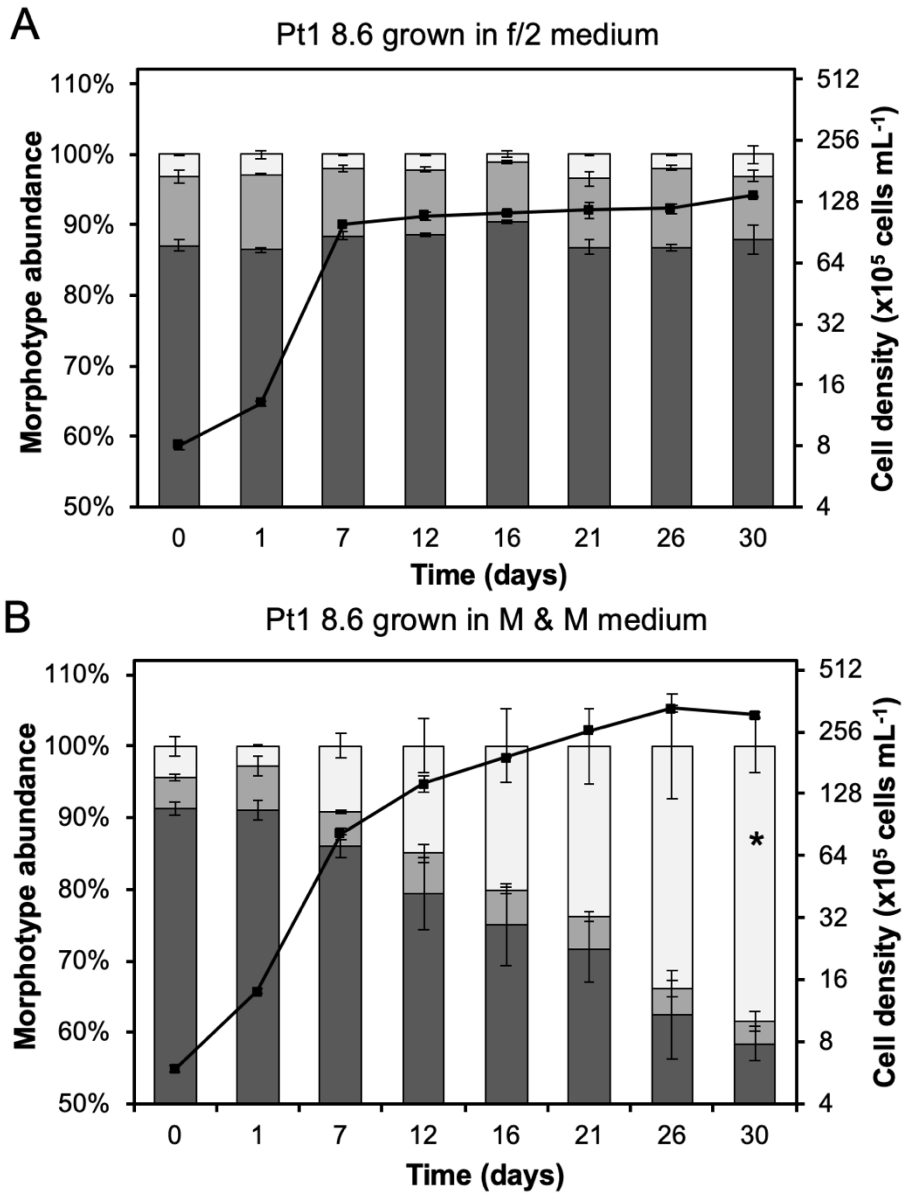

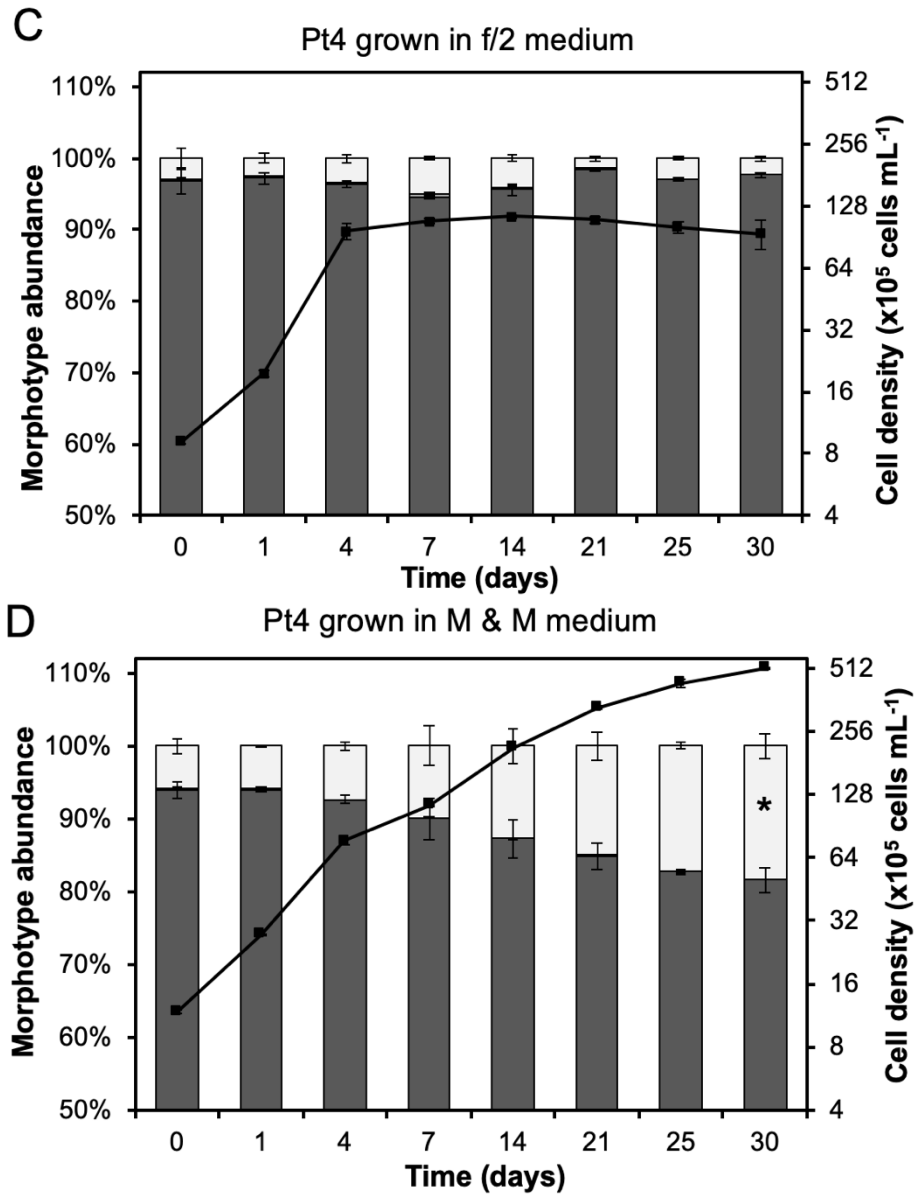

Figure 3-1 Effects of culture media on cell morphology and growth of two *P. tricornutum* strains.

Relative abundance of fusiform (dark grey bars), triradiate (light grey bars) and oval cells (white bars) in Pt1 8.6 and Pt4 cultures maintained in f/2 medium (A, C) and after a transfer from f/2 medium to M & M medium (with a pre-acclimation to M & M medium for 6 days) (B, D). Growth curves of total cells are represented by solid lines. Data shown are averages from two biological replicates. Error bars represent differences from the means, indicating the minimum and the maximum values. *$p<0.05$ when comparing the oval cell abundance on day 30 with that on day 0.

3.3.2 Enrichment of oval cells through successive transfers

Successive transfers on solid medium were previously reported to enrich oval cells in Pt2 (Barker, 1935). In order to obtain oval cell-dominant cultures,

successive transfers in liquid M & M medium were conducted in this study and the quantitative analysis of cell morphotype abundance was performed after each transfer. The oval morphotype appeared to be enriched in both strains with subculturing treatments in liquid M & M medium (Figure 3-2), accompanied by the decrease in the abundance of fusiform and triradiate cells. After five successive transfers over a cultivation period of approximately four months, 90.8% of cells were oval in Pt1 8.6 cultures and almost all the cells (99.9%) were oval in Pt4 cultures grown in M & M medium (Figure 3-2). Microscopic images clearly showed the different fusiform or oval morphotype in the two strains maintained in liquid f/2 medium or M & M medium (Figure 3-3). This new cell morphotype abundance obtained in both strains remained stable during subsequent passages in M & M medium, indicating that this culture medium is suitable for oval morphotype maintenance in liquid cultures.

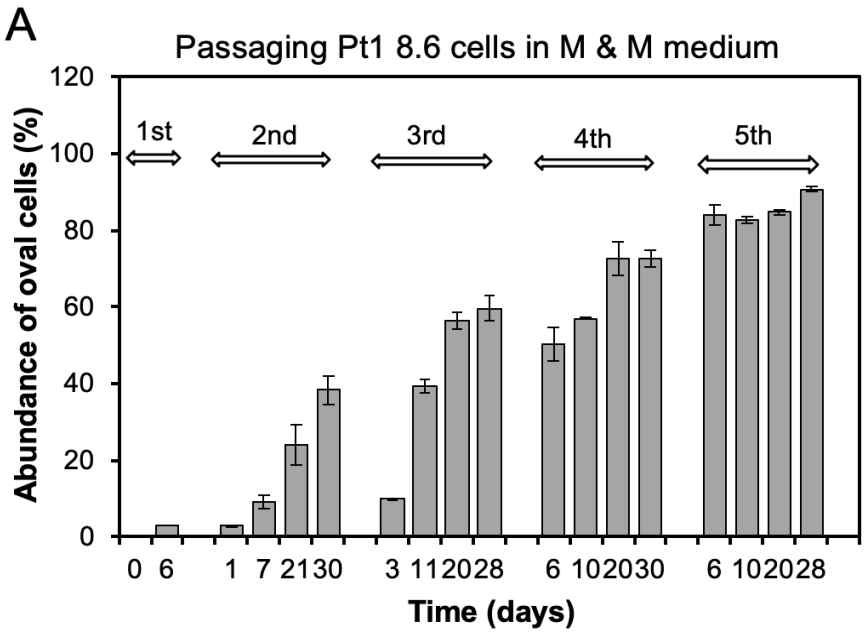

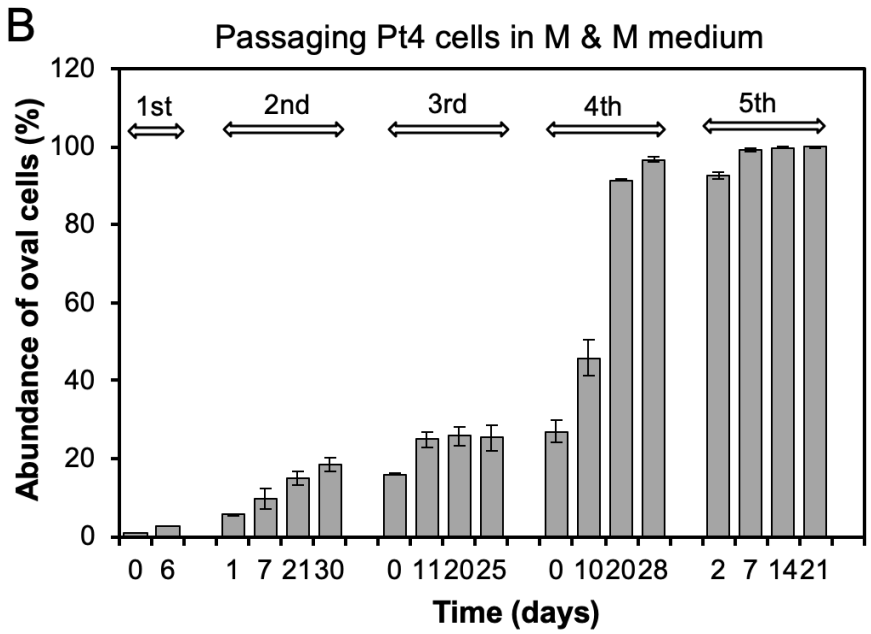

Figure 3-2 Impact of M & M medium on the abundance of oval morphotype in two *P. tricornutum* strains.

Relative abundance of oval cells in Pt1 8.6 (A) and Pt4 (B) cultures during five successive transfers in liquid M & M medium. Data shown are averages from two biological replicates. Error bars represent differences from the means, indicating the minimum and the maximum values.

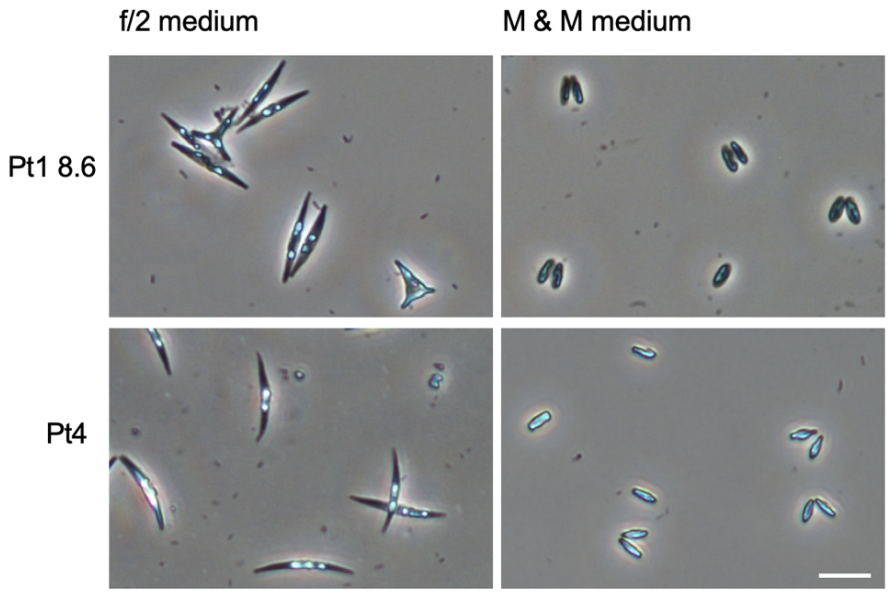

Figure 3-3 Microscopic images of *P. tricornutum* cells after successive transfers in different culture media.

Micrographs showing representative examples of different cell morphotypes of Pt1 8.6 and Pt4 maintained in f/2 medium or M & M medium. Samples for imaging were taken from cultures after the fifth transfer. Scale bar: 20 µm.

Despite the significant change in cell morphology occurred in both strains, there were differences between them worth noting. The proportion of oval cells achieved 38.4% in Pt1 8.6 compared to the 18.6% in Pt4 by the end of cultivation of the second transfer in M & M medium (Figure 3-1 B & D), which implies that Pt1 8.6 might have a greater tendency to conduct morphotype conversion than Pt4 in response to this culture medium. In addition, Pt1 8.6 was shown to undergo morphological transformation gradually while the morphotype variation in Pt4 occurred suddenly with the percentage of oval cells increasing markedly from 26.9% to 96.6% after the fourth transfer (Figure 3-2). In contrast to Pt4, the fusiform cells did not disappear entirely in Pt1 8.6 cultures maintained in M & M medium. These differences between them are more likely due to their different genotypes, with genotype A of Pt1 8.6 and genotype B of Pt4 (Table 1-1) (De Martino et al., 2007).

M & M medium has been previously used for *P. tricornutum* cultivation (Yongmanitchai and Ward, 1991, Acien Fernandez et al., 2003). However, the fact that this culture medium-triggered cell morphological change from fusiform to oval was first reported in this study and the specific factors capable of initiating oval cell production remain unknown. The M & M medium has a different nutrient content compared with f/2 medium. It contains 1 g L^{-1} Tris and has a relatively low salinity (7.1 g L^{-1}) but high concentrations of nitrate and phosphate without any vitamins added (Table 2-1). Hyposaline conditions were previously reported to induce significant cell morphotype change to the oval form in Pt1 8.6 and Pt3. However, under low salinity (3.8 g L^{-1}, 10sw), the proportion of oval cells was less than 10% in Pt1 8.6 on day 30 (De Martino et al., 2011), much lower than the 38% obtained here in M & M medium. This suggested that low salinity of M & M medium might be a contributing factor to the observed morphotype change in Pt1 8.6 but not the main one. Furthermore, under hyposaline conditions, no evident morphotype conversion to oval was found in Pt1, Pt6 and Pt7 (Abdullahi et al., 2006, Borowitzka and Volcani, 1978), indicating that morphological variation can be regulated by changing culture conditions but depends on strains.

It is commonly reported that *P. tricornutum* cells tend to convert to oval morphotype under stress conditions such as nutrient limitation (De Martino et al., 2007). Compared with f/2 medium, although M & M medium contains more than 13-fold higher concentrations of nitrate and phosphate, it has lower Ca, Mg, Fe, Co, Mo and Cu content and no B vitamins (Table 2-1). There have been many studies focusing on the impact of nitrate concentration (0-33.6 mM) on *P. tricornutum* cells (Gao et al., 2017, Breuer et al., 2012). However, no cell morphotype change was reported under high nitrate concentrations. Growth of *P. tricornutum* has been shown to be significantly limited by low Fe availability (Allen et al., 2008, Bertrand et al., 2012). It could be the balance of all nutrients which is important. Under relatively high nitrate and phosphate conditions, other nutrients such as Fe, Cu, Ca and Mg might become limited, which could be responsible for the observed phenomena. *P. tricornutum* does not have an absolute requirement for cobalamin, thiamine and biotin for growth (Moejes et al., 2017, Bertrand et al., 2012). The omission of B vitamins might therefore not be responsible for the observed morphotype changes. In addition, Tris was shown to be inhibitory for some algal species (Ursi et al., 2008). Further studies are required to elucidate the specific inducing factors to the observed cell morphotype conversions in *P. tricornutum* induced by M & M medium, which will be further presented in section 3.3.4, and to confirm the universality of this method in other *P. tricornutum* strains.

3.3.3 Reversibility of morphological change

It has been previously demonstrated that the transformation of *P. tricornutum* cells between different morphotypes could be reversible (Barker, 1935, De Martino et al., 2011). Apart from the stability of cell morphotype that should be taken into account, it will be important to be able to flexibly control cell morphology through changing cultivation strategy from the perspective of scale-up cultivation. Thus, the reversibility of morphological changes was characterised by growing the obtained stable oval cells of Pt1 8.6 and Pt4 maintained in M & M medium back into the f/2 medium.

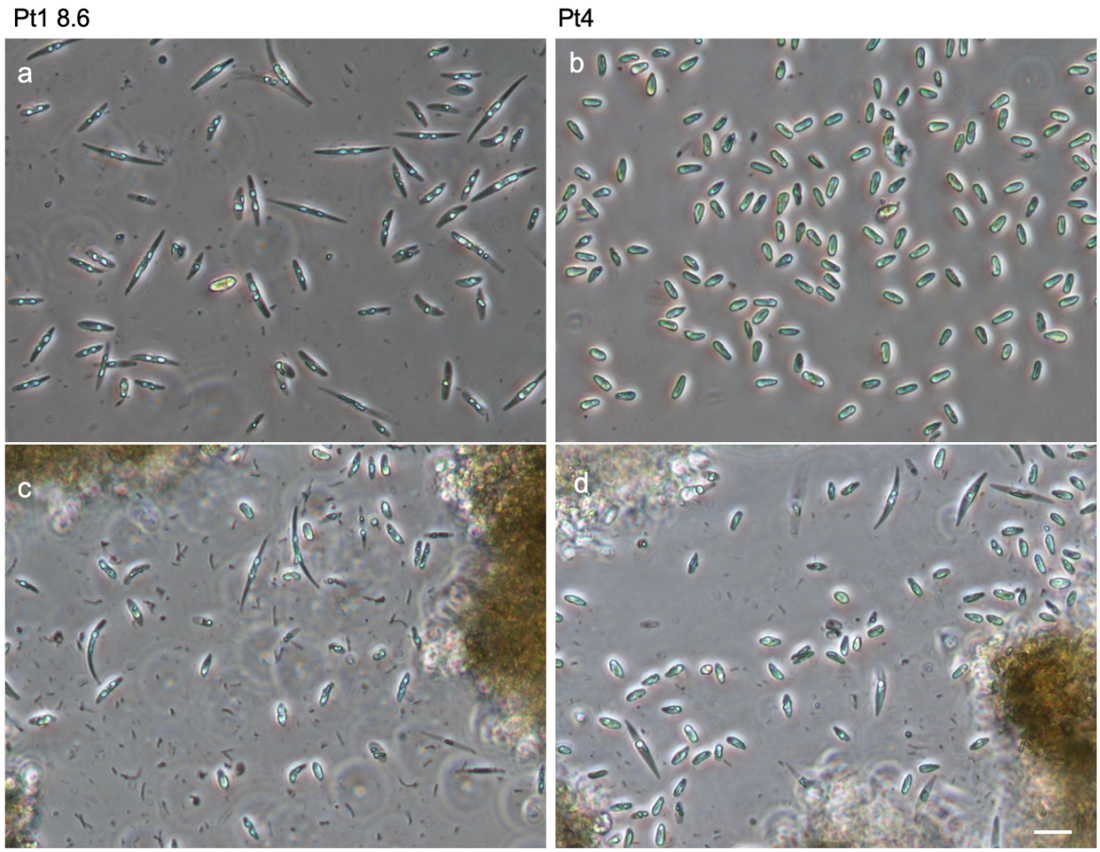

Figure 3-4 Microscopic images showing the reversibility of cell morphological conversion in two *P. tricornutum* strains.

Micrographs showing the morphology of Pt1 8.6 cells (a, c) and Pt4 cells (b, d) after four successive transfers in f/2 medium, in which the cells were initially transferred from M & M medium. Each transfer lasted around 30 days and the cultures were sampled for imaging on day 13 after the fourth transfer, 103 days in total cultured in f/2 medium. Two images were taken for each strain to show cells in suspension (a, b) and near the large aggregation (c, d). Scale bar, 20 μm.

With successive transfers in f/2 medium, a gradually reversible conversion from oval to fusiform was observed in Pt1 8.6 cultures by microscopy (Figure 3-4 a). After five subculturing treatments representing a cultivation period of more than four months, the relative abundance of Pt1 8.6 fusiform cells achieved above 90%. A number of Pt1 8.6 cells with intermediate morphology between oval and fusiform were observed (Figure 3-4 a), revealing the reported elongation of oval cells to generate fusiform cells (Wilson, 1946, De Martino et al., 2011). However, few triradiate cells were observed in this culture (Figure 3-4 a & c), different from the original Pt1 8.6 culture on arrival from CCAP. Interestingly, biofilm formation was observed in

both strains after the first and second transfers back in fresh f/2 medium (Figure 3-5 A). With subsequent passaging, Pt1 8.6 cultures were an even golden colour with fusiform cells distributed in suspension (Figure 3-5 B). By contrast, Pt4 cell cultures displayed severe cell aggregation (Figure 3-5 B) and the majority of cells (>95%) existed still in the oval form even after several subculturing treatments (Figure 3-4 b & d). This indicated that the morphological conversion induced by M & M medium was reversible in Pt1 8.6 and might be irreversible in Pt4 under the tested conditions. It also further suggests that the mechanisms employed by cells for morphological changes may differ between the two *P. tricornutum* strains possessing different genotypes.

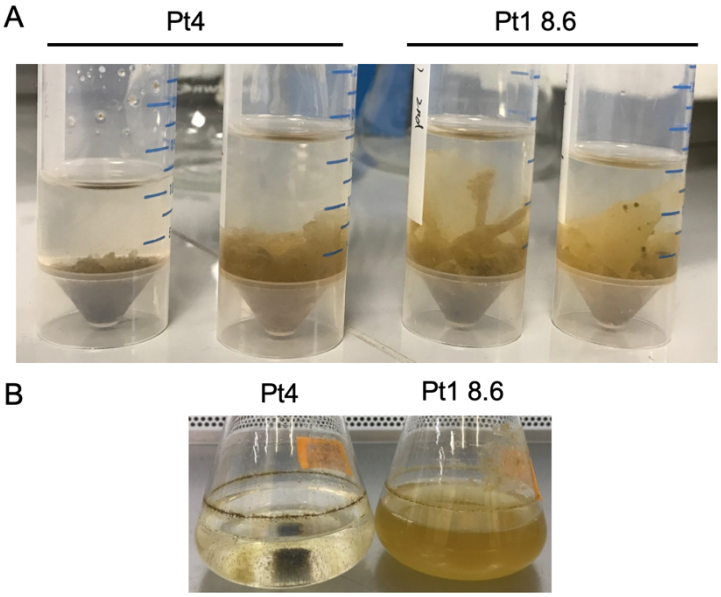

Figure 3-5 Cultures of two *P. tricornutum* strains after inoculation of cells from M & M medium back into f/2 medium.

A, biofilm formation observed in Pt1 8.6 and Pt4 cultures after two successive transfers of cells back in f/2 medium (65 days). B, culture flasks of Pt1 8.6 showing the distributed cells in suspension and of Pt4 showing the severe cell aggregation after five successive transfers back in f/2 medium (135 days).

3.3.4 Investigation of factors influencing cell growth and morphology

M & M medium has been identified to trigger significant cell morphotype change in *P. tricornutum*. In order to gain a better understanding about the major factors triggering this process, the influence of various medium

components on cell growth or morphology of *P. tricornutum* were investigated. Salinity and Tris were initially explored for their impacts on cell growth and cell morphotype abundance using Pt4. The f/2 medium was then modified based on the nutrient components of M & M medium for rapid assessment of the effects of various medium components including salinity, Tris, nitrate, phosphate, trace elements and vitamins on cell morphology of *P. tricornutum*.

Salinity analysis

Salinity is an important factor for the growth of marine microorganisms. *P. tricornutum* is found to be occurring naturally in unstable marine environment such as rock pools and estuaries, where the salinity changes rapidly due to the tidal effect or human activities (De Martino et al., 2007). Salinity has also been reported to influence cell morphology of Pt1 8.6, Pt3 and Pt8 (De Martino et al., 2011, Ovide et al., 2018). Pt4 was isolated from a rock pool on the Island of Segelskar and was described as a brackish strain. Here, the modified f/2 media with four salinities (0 ppt, 15 ppt, 33 ppt and 40 ppt) representing freshwater, brackish water and seawater were used to explore the impact of salinity on cell growth and morphotype of Pt4. The original f/2 medium has a salinity of 33 ppt.

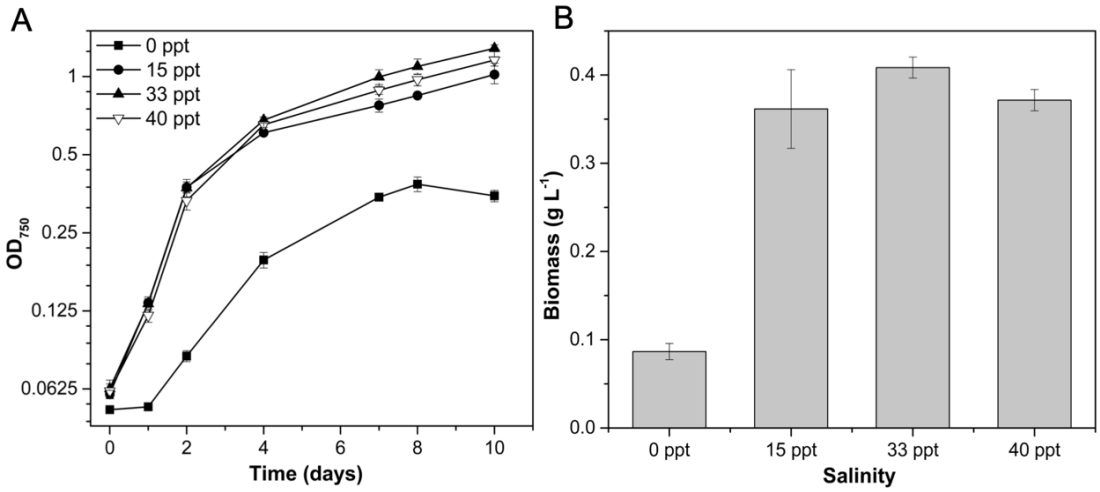

Figure 3-6 Impact of salinity on cell growth of Pt4.

Growth curves from OD_{750} measurement (A) and dry biomass concentration measured on day 10 (B) of Pt4 cells grown in modified f/2 media with different salinities (0 ppt, 15 ppt, 33 ppt and 40 ppt). Data are shown as mean± one standard

deviation from three biological replicates. ppt (parts per thousand), equal to g L^{-1} here.

The results showed that Pt4 cells were capable of growing at all the four tested salinity conditions (Figure 3-6). Similar growth was observed for cells cultured at salinities of 15 ppt, 33 ppt and 40 ppt, although the optimal growth with the highest dry biomass concentration (0.41±0.01 g L^{-1}) was obtained from cells grown at the salinity of 33 ppt, compared to the 0.36±0.04 g L^{-1} and 0.37±0.01 g L^{-1} at salinities of 15 ppt and 40 ppt respectively. Interestingly, this marine diatom could even survive in freshwater, though a much slower growth and a more than 4-fold decreased biomass concentration (0.09±0.01 g L^{-1}) were obtained at this condition (0 ppt) compared to other salinity conditions. These results indicate that Pt4 cells can survive over a wide range of salinity conditions. Growth curves of total cells (Figure 3-7 A) are consistent with those from OD_{750} measurement.

The impact of salinity on cell morphotype abundance of Pt4 was analysed quantitatively by cell counting. After cultivation for 42 days in f/2 medium under various salinity conditions, all cultures displayed still mainly the fusiform morphotype (>96%) and no significant increase in the abundance of oval cells (<4%) was observed at the tested salinity conditions (Figure 3-7). However, the abundance of fusiform cells tended to increase at the high salinity conditions. For example, the proportion of fusiform cells reached almost 100% after 42 days cultivation at the salinity of 40 ppt (Figure 3-7 A). The result indicated that the fusiform morphotype was preferable in saline water. Hyposaline conditions representing brackish water or freshwater did not induce the significant increase in oval cell abundance in Pt4, which is different from the reported observations in Pt1 8.6, Pt3 and Pt8 (De Martino et al., 2011, Ovide et al., 2018), but consistent with previous reports in Pt6, Pt7, Pt2 and Pt1 (Borowitzka and Volcani, 1978, Gutenbrunner et al., 1994, Wilson, 1946, Abdullahi et al., 2006). Low calcium concentration (<15 mg L^{-1}) was reported to increase oval cell abundance (Cooksey and Cooksey, 1974). However, this was not confirmed in another study (Borowitzka and Volcani, 1978). Our observations at the salinity of 0 ppt implied that low Ca and Mg

content might not be the inducing factor to the observed morphotype change in Pt4 grown in M & M medium.

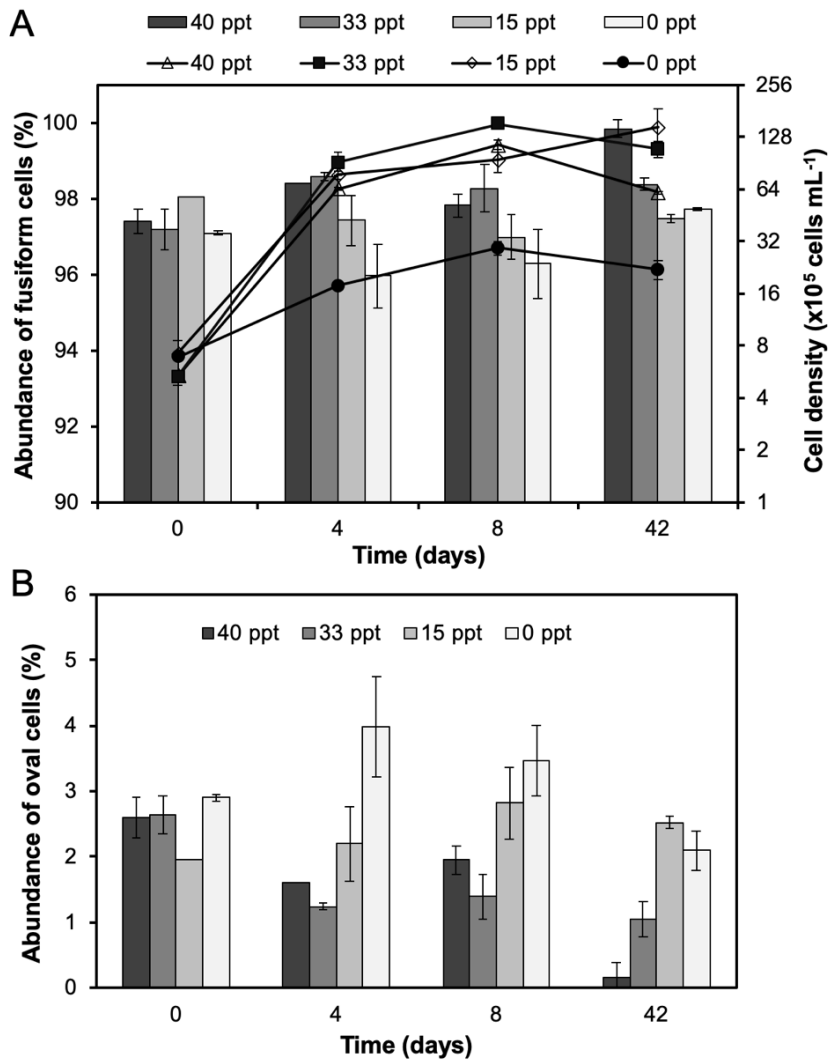

Figure 3-7 Impact of salinity on cell morphotype abundance of Pt4.

Relative abundance of fusiform cells (A) and oval cells (B) in Pt4 cultures grown in modified f/2 media with different salinities. Growth curves of total cells are shown by solid lines. Data are presented as mean± one standard deviation from three biological replicates. ppt (parts per thousand), equal to g L^{-1} here.

Tris and pH analysis

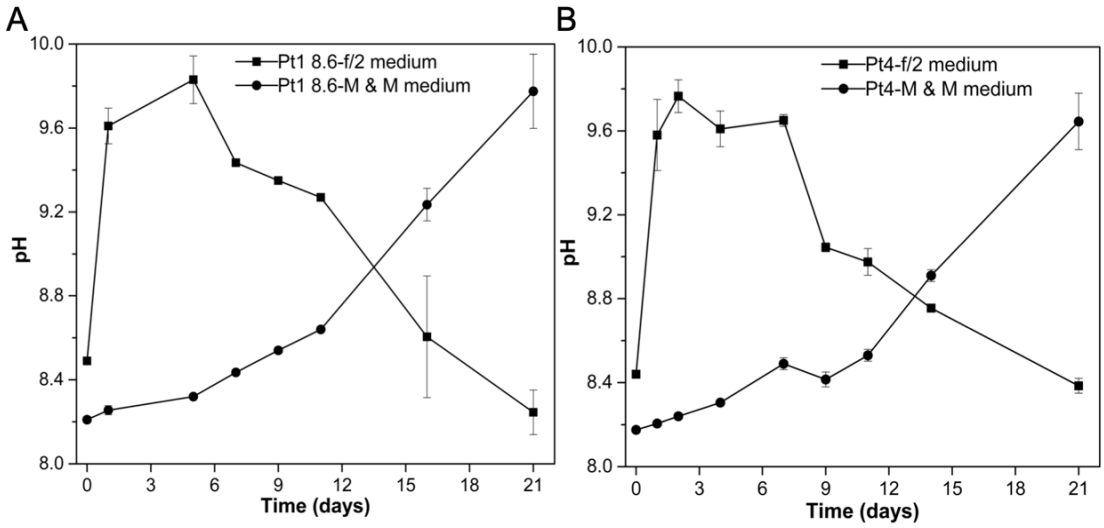

Figure 3-8 pH change pattern of *P. tricornutum* cultures grown in different media.

Changes in culture pH of Pt1 8.6 (A) and Pt4 (B) grown in f/2 medium or M & M medium. Data are shown as mean ± one standard deviation from three biological replicates.

In this study, during cultivation of *P. tricornutum* in f/2 medium and M & M medium, the changes in culture pH were also monitored for both Pt1 8.6 and Pt4. As shown in Figure 3-8, the pH change pattern varied greatly between cultures grown in f/2 medium and M & M medium. Specifically, when *P. tricornutum* cells were grown in f/2 medium, the culture pH increased rapidly to approximately 9.8 in the first several days cultivation. This could be explained by the photosynthesis and nitrate assimilation through reduction to ammonium ion, which were accompanied by CO_2 absorption and influx of protons from culture medium into cells (Scherholz and Curtis, 2013). The further assimilation of ammonium ion releases protons to culture medium, leading to a gradual drop in pH as observed in cultures grown in f/2 medium. By contrast, in cultures maintained in M & M medium, the pH showed a relatively stable level of below 8.6 over the initial 11 days cultivation due to the involvement of Tris (1 g L^{-1}) in this medium. After that, the pH increased evidently to above 9.6 in cultures of both strains, indicating that the pH buffering effect of Tris was not maintained. Failure of Tris in stabilising the

culture pH during cultivation was previously reported for growth of phytoplankton species (Harrison et al., 1980). This phenomenon might be due to the culture pH being out of the buffering capacity of Tris (7.0-9.0). Another reason is probably that Tris might be consumed. It has been shown that in non-axenic microalgal cultures, Tris could sustain bacterial growth (Fábregas et al., 1993, Nguyen et al., 2016).

F/2 medium has been commonly used for routine growth of *P. tricornutum* by many culture collections and researchers. Tris is often used as a pH buffer involved in culture media for growing microalgae. For example, the ASP-2 medium designed for photosynthetic marine algae is buffered by Tris (1 g L^{-1}) (Provasoli et al., 1957). Tris-acetate-phosphate (TAP) medium often used for growth of *Chlamydomonas reinhardtii* also contains Tris. Based on the above observations on pH changes in *P. tricornutum* cultures (Figure 3-8), it will be interesting to know whether the f/2 medium with stable pH would benefit cell growth and if the addition of Tris would influence cell morphotype abundance. Therefore, the modified f/2 media containing different concentrations of Tris were used to investigate the effect of Tris on cell growth, culture pH and cell morphology using Pt4.

Tris was shown to have a slightly negative effect on growth of Pt4. Although no significant difference in cell growth from OD_{750} readings was observed between Pt4 cultures grown in f/2 medium containing 0 mM and 5 mM Tris, slower growth between day 1 and day 2 with lower final OD_{750} values was observed for cells cultured in f/2 medium with addition of 10 mM or 20 mM Tris ($p<0.05$) (Figure 3-9 A). In order to confirm this, the biomass yields on day 9 were measured. It was found that the addition of Tris into f/2 medium resulted in a decrease in dry biomass concentration (Figure 3-9 B). Compared to the highest dry biomass concentration of 0.49±0.03 g L^{-1} obtained in f/2 medium without Tris, only 0.39±0.04 g L^{-1} and 0.36±0.01 g L^{-1} were obtained when 10 mM and 20 mM Tris were added respectively. The changes in culture pH with addition of Tris were also monitored. Similar to observations in Figure 3-8, the culture pH changed greatly in f/2 medium even when 5 mM Tris was added, experiencing an initial increase from 8.2 to

9.3 in 2 days cultivation before decreasing to 9.0 by day 9 (Figure 3-9 C). Addition of 10 mM and 20 mM Tris into f/2 medium were shown to be helpful for maintaining pH during Pt4 cultivation with the culture pH only increasing slightly from 8.2 to 8.8 and to 8.5 respectively by the end of cultivation (Figure 3-9 C). These results indicated that Tris could have an inhibitory effect on growth of Pt4, despite its contribution to a relatively stable culture pH. In addition, no significant cell morphotype change was observed in long-term Pt4 cultures (30 days) under the tested Tris conditions (data not shown).

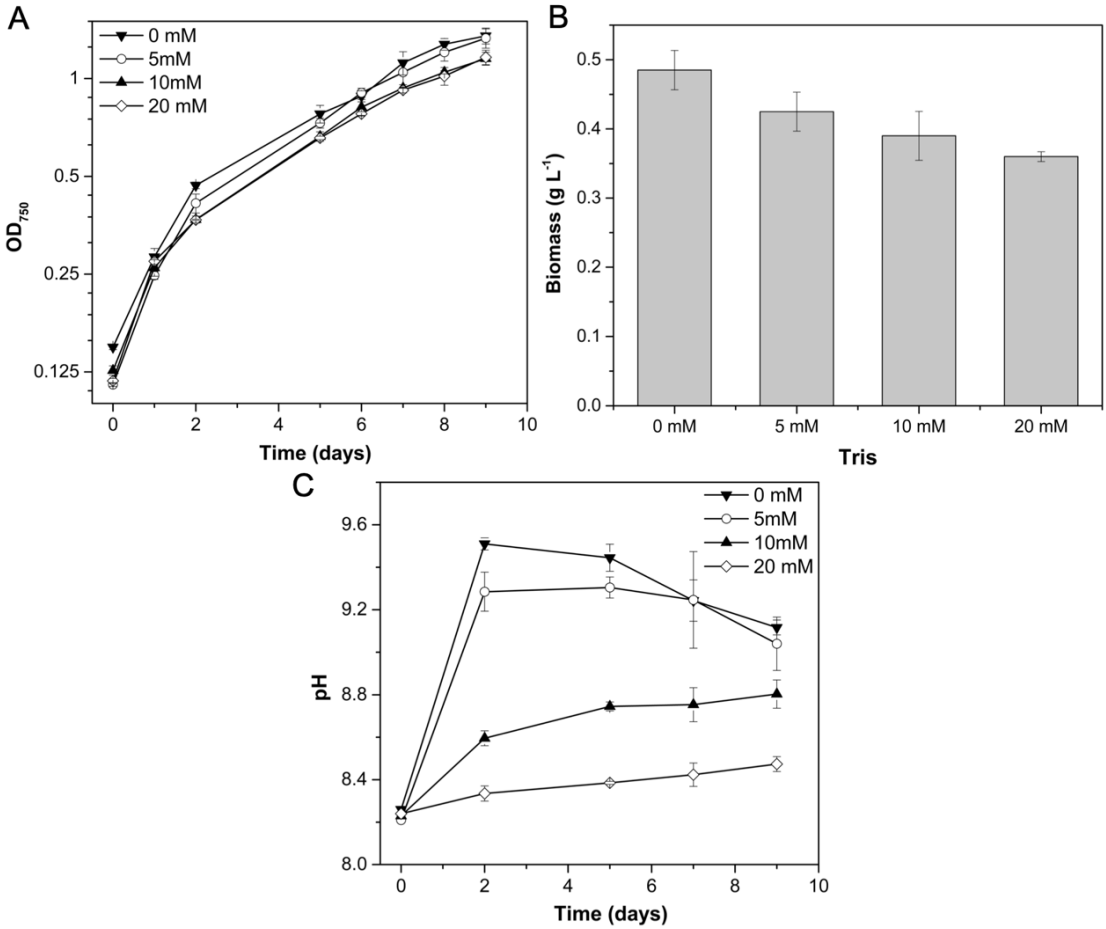

Figure 3-9 Effect of Tris on cell growth and culture pH of *P. tricornutum*.

Growth curves from OD_{750} measurement (A), dry biomass concentration measured on day 9 (B) and culture pH changes (C) of Pt4 grown in modified f/2 media with addition of different concentrations of Tris. Data are shown as mean± one standard deviation from three biological replicates.

In agreement with our observations, previous studies have shown that Tris became inhibitory at approximately 0.3% for growth of flagellate (Provasoli et

al., 1957) and had deleterious effects on growth of a red alga *Gracilaria birdiae* (Ursi et al., 2008), some phytoplankton species (Harrison et al., 1980) and freshwater blue-green algae (Smith and Foy, 1974). There are several mechanisms proposed for Tris inhibition in previous publications. One is that Tris, like other amines, was shown to inhibit growth of the lactic acid bacteria *Lactobacillus arabinosus* by interfering with the uptake of K^+ (Macleod and Onofrey, 1954). The inhibitory effect could be overcome or partially counteracted by increasing the amount of K^+ in the medium, which has been confirmed in microalgae *Phormidium persicinum* (Provasoli et al., 1957) and *Oscillatoria redekei* (Smith and Foy, 1974). Another is that Tris feeds bacteria in the presence of phosphate and the competition for phosphorus as well as the low pH values due to bacterial growth might cause inhibition of microalgae (Fábregas et al., 1993, Harrison et al., 1980). Moreover, Tris was indicated to inhibit photosynthesis by interfering with HCO_3^- utilisation probably through competition for H^+ in a brown alga *Laminaria saccharina* (Axelsson et al., 2000). *P. tricornutum* can tolerate high pH values up to 10.3 and grows well over a wide pH range (Goldman et al., 1982). This species is capable of direct uptake of HCO_3^- from the medium through K^+-dependent and -independent HCO_3^- transporters with the former one being predominant at high alkaline pH (Chen et al., 2006). Thus, the addition of Tris may not be necessary for *P. tricornutum* cultivation. Since there were no significant effects of salinity and Tris on cell morphotype change observed in Pt4, Pt1 8.6 was not further examined under these conditions.

Rapid assessment of medium components affecting cell morphology

In order to gain some insights into the cell morphotype change of *P. tricornutum* induced by M & M medium, we modified f/2 medium to the components of M & M medium in terms of salinity, nitrate, phosphate, Tris, trace elements and vitamins (Table 3-1). The modified f/2 media were employed for rapid assessment of the impacts of medium components on cell morphology of *P. tricornutum*.

Cultivation in modified f/2 media for 55 days, in which two successive transfers were carried out, showed that the tested low salinity (7.1 g L^{-1}), high concentration of nitrate or phosphate, addition of 1 g L^{-1} Tris (8.3 mM), M & M trace elements or omission of vitamins did not trigger evident cell morphotype change in both Pt1 8.6 and Pt4, with the fusiform morphotype being predominant (>90%) in cultures through microscopic examination (Figure 3-10). This result is consistent with our observations from salinity (Figure 3-7) and Tris experiments. Furthermore, the addition of Tris to f/2 medium was shown again to have a negative effect on *P. tricornutum* and the degree of Tris inhibition varies depending on strains. Pt1 8.6 appeared to be more sensitive to Tris than Pt4, evidenced by the more severe cell aggregation (Figure 3-10) and a much lower final cell density (OD_{750}, 1.25 versus 1.74; cell density, $4.8x10^6$ cells mL^{-1} versus $9.6x10^6$ cells mL^{-1}) (Table 3-2 T+). Only slight aggregation was observed in Pt4 cultures with addition of 8.3 mM Tris, consistent with our above results showing a slight inhibition of Pt4 from Tris experiment (Figure 3-9). As discussed above, Tris may interfere with K^+-dependent HCO_3^- utilisation or stimulate bacterial growth competing for phosphorus thereby inhibiting growth of *P. tricornutum*. Increasing nitrate content in f/2 medium was found to greatly increase the cell yield with the OD_{750} value reaching 2.33 for Pt1 8.6 and 2.42 for Pt4 by day 34 (Table 3-2 N+). Only increasing the phosphate content in f/2 medium led to the formation of abundant precipitates and had no significant impact on cell growth (Table 3-2 P+). As described in section 1.2.4, *P. tricornutum* does not absolutely require the cobalamin (vitamin B_{12}) for growth as its genome encodes the cobalamin-independent methionine synthase (MetE) (Bertrand et al., 2012). This species does not have an absolute requirement for thiamine (vitamin B_1) and biotin (vitamin B_7) either (Carlucci and Bowes, 1970, Droop, 1958, Moejes et al., 2017). Our results showed that cells grew well in f/2 medium without vitamins, reaching an OD_{750} value of 1.90 for Pt1 8.6 and 1.93 for Pt4 by day 34 (Table 3-2 Vit-). Since similar results were obtained for cultures after the second transfer, they are not reported here.

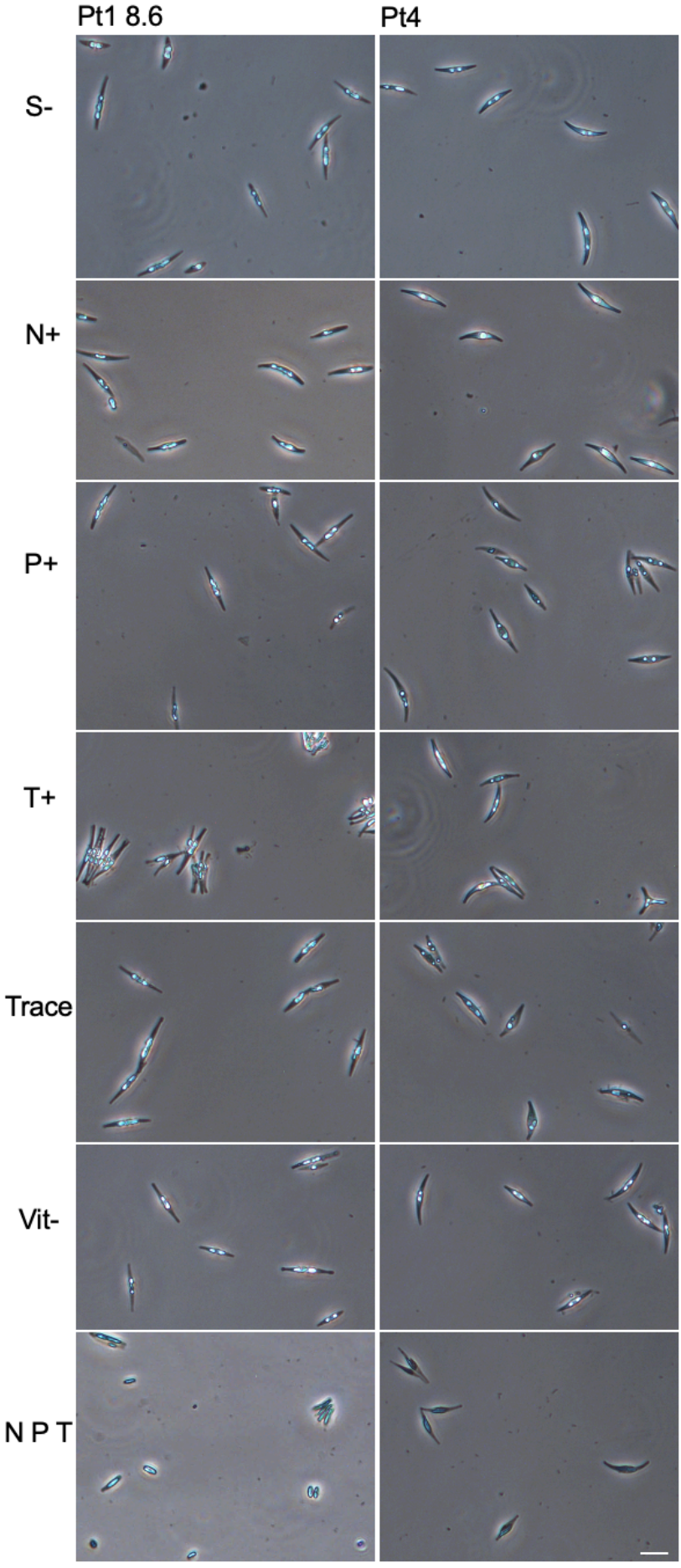
Pt1 8.6
Pt4
S-
N+
P+
T+
Trace
Vit-
N P T

Figure 3-10 Micrographs showing the impact of medium component on cell morphotype of *P. tricornutum*.

Representative microscopic images showing the cell morphotype of Pt1 8.6 and Pt4 cells after cultivation for 34 days in modified f/2 media. S-, f/2 medium with decreased salinity (7.1 g L^{-1}) as M & M medium; N+, f/2 medium with increased nitrate (11.76 mM $NaNO_3$); P+, f/2 medium with increased phosphate (0.57 mM K_2HPO_4); T+, f/2 medium with 1 g L^{-1} Tris added; Trace, replacing f/2 trace elements with M & M trace elements; Vit-, f/2 medium without vitamins added; N P T, f/2 medium containing 11.76 mM $NaNO_3$, 0.57 mM K_2HPO_4 and 1 g L^{-1} Tris (Table 3-1).

Table 3-2 OD_{750} readings for *P. tricornutum* cultures grown in modified f/2 media for 34 days.

OD_{750}	S-	N+	P+	T+	Trace
Pt1 8.6	1.502	2.328	1.604	1.246	1.836
Pt4	1.906	2.421	1.666	1.744	1.72
	Vit-	**N P T**	**S N T**	**S P T**	**S N P**
Pt1 8.6	1.904	1.779	0.59	1.378	2.52
Pt4	1.93	2.316	NA	NA	NA

Modifications to f/2 medium for each condition can be found in Table 3-1.
NA, not available.

The accumulative contribution of various components leads to an interesting result. An apparent increase in oval cell abundance to 72.5% was observed in Pt1 8.6 after two subculturing treatments in the modified f/2 medium with increased nitrate and phosphate content and Tris addition, which is not the case in Pt4 containing only 2.1% oval cells (Figure 3-10 N P T). Meanwhile, a relatively inhibitory effect on growth of Pt1 8.6 was observed, showing an OD_{750} value of 1.78 ($15.0x10^6$ cells mL^{-1}) in comparison to the 2.32 ($24.3x10^6$ cells mL^{-1}) for Pt4 by day 34 (Table 3-2 N P T). Bacteria were reported to actively feed on Tris and phosphate (Fábregas et al., 1993). Co-cultivation of Pt1 8.6 with the marine *Roseovarius* sp. strain 217 led to the formation of large cell aggregates through a bacteria-induced morphotype conversion from fusiform to oval and secretion of mucin-like proteins, while this phenomenon was not observed in Pt4 (Buhmann et al., 2016). It is therefore hypothesised that the interactions between *P. tricornutum* and bacteria might

contribute to the observed morphotype change in Pt1 8.6. However, there was no evident cell morphotype change observed for the combinational condition of S P T, where bacterial overgrowth might occur as well. Cultures grown under the nutritional combination of S N T were unhealthy with a low OD_{750} reading of 0.59 obtained after 34 days cultivation (Table 3-2). Microscopic examination revealed that most fusiform cells appeared to die with a few oval cells existing in groups under this condition, which implied that bacterial overgrowth might occur and the competition for limited phosphorus between *P. tricornutum* and bacteria might cause collapse of *P. tricornutum* cultures (Fábregas et al., 1993, Moejes et al., 2017). In addition, a high microalgal cell yield without evident morphotype change was obtained for the condition of S N P (Table 3-2).

A previous study on dynamics of bacterial community associated with *P. tricornutum* cultures revealed the presence of four major bacterial families with a number of bacterial species playing roles. Generally, metabolic exchanges such as the organic carbon supply from diatoms to bacteria, B vitamins supply from bacteria to diatoms and phosphorus competition occur between them (Moejes et al., 2017). However, which bacteria become dominant is dependent on the environmental conditions and the prevailing needs of the algae-bacterial community. There is not a consensus about Tris/bacteria effects existing because they vary among different species. Further confirmation of bacterial presence in tested *P. tricornutum* cultures and maybe a more detail investigation of the interactions between *P. tricornutum* and bacteria under the conditions like T+, S P T and N P T are required to understand the role of bacteria on cell morphotype and growth of *P. tricornutum*. Although the factorial combination of N P T was found to trigger significant morphotype change to oval in Pt1 8.6, this was not observed in Pt4. Variables of trace elements and vitamins are not involved for factorial combination. Other combinations like N P Trace and N P Vit maybe worth testing in the future to assess their effects on *P. tricornutum* morphology. In addition, DoE approach might be applied to optimise experimental design in the future for further systematic studies.

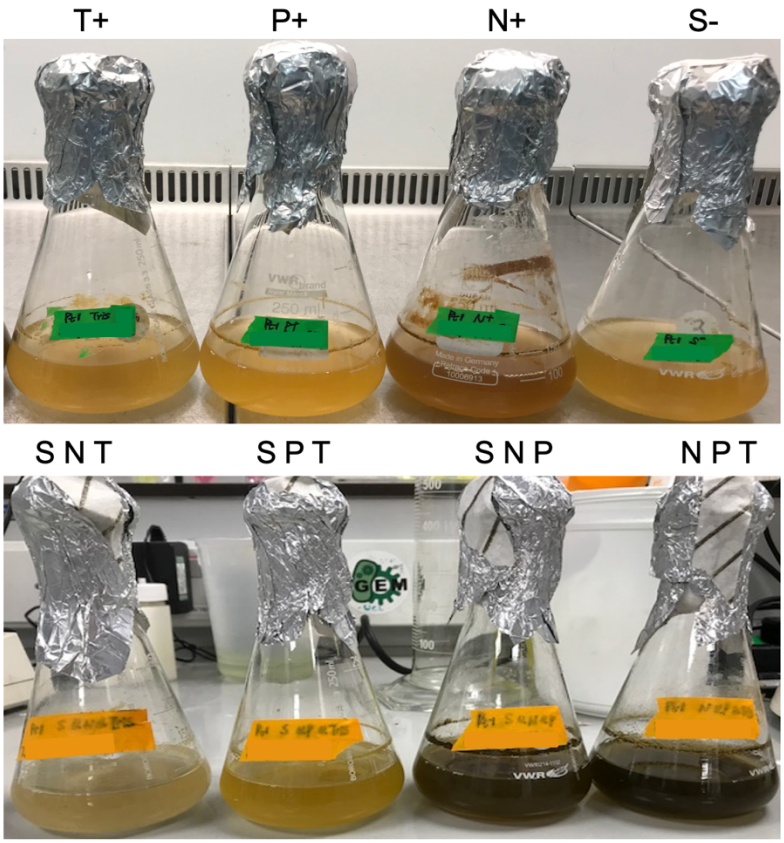

Figure 3-11 Images of representative culture flasks showing the impacts of medium component on cell growth of *P. tricornutum*.

Representative images of Pt1 8.6 cultures after cultivation for 32 days in modified f/2 media. T+, f/2 medium with 1 g L^{-1} Tris added; P+, f/2 medium with increased phosphate (0.57 mM K_2HPO_4); N+, f/2 medium with increased nitrate (11.76 mM $NaNO_3$); S-, f/2 medium with decreased salinity (7.1 g L^{-1}) as M & M medium; S N T, f/2 medium containing 7.1 g L^{-1} salinity, 11.76 mM $NaNO_3$ and 1 g L^{-1} Tris; S P T, f/2 medium containing 7.1 g L^{-1} salinity, 0.57 mM K_2HPO_4 and 1 g L^{-1} Tris; S N P, f/2 medium with 7.1 g L^{-1} salinity, 11.76 mM $NaNO_3$ and 0.57 mM K_2HPO_4; N P T, f/2 medium containing 11.76 mM $NaNO_3$, 0.57 mM K_2HPO_4 and 1 g L^{-1} Tris (Table 3-1).

3.4 Conclusion

Phaeodactylum tricornutum is a polymorphic marine diatom of interest for industrial biotechnology. In this chapter, two culture media were used for *P. tricornutum* cultivation in order to investigate the effects of culture media on cell morphotype of *P. tricornutum*. The fusiform morphotype was predominant in cultures of Pt1 8.6 and Pt4 grown in f/2 medium, representing approximately 88% and 97% respectively. Contrastingly, Mann and Myers' medium was identified as eliciting significant cell morphotype conversion from fusiform/triradiate to oval in *P. tricornutum*. Through successive subculturing in M & M medium, liquid cultures of Pt1 8.6 and Pt4 abundant with approximately 90% and 100% oval cells respectively were obtained and well-maintained in this medium under the constant shaking condition. In contrast to Pt4, the fusiform cells did not disappear entirely in Pt1 8.6 cultures maintained in M & M medium. The reversibility of this cell morphotype change in *P. tricornutum* induced by M & M medium was investigated by growing the obtained oval cells back in f/2 medium. It turned out that the cell morphotype conversion occurred in Pt1 8.6 was reversible and might be irreversible in Pt4 under the tested conditions.

In order to gain some insights into the major factors eliciting morphological transformation in *P. tricornutum*, the impacts of various medium components on cell growth or morphology were investigated. *P. tricornutum* could grow over a wide range of salinity conditions and the increase of fusiform cells was observed at the high salinity of 40 ppt. The addition of Tris in f/2 medium could have an inhibitory effect on growth of *P. tricornutum*. Pt1 8.6 appeared to be more sensitive to Tris than Pt4, showing apparent cell aggregation and a much lower cell density (OD_{750}, 1.25 versus 1.74; cell density, 4.8×10^6 cells mL^{-1} versus 9.6×10^6 cells mL^{-1}) after cultivation for 34 days in f/2 medium with 8 mM Tris added. The tested single factor of low salinity, addition of Tris, high concentration of nitrate or phosphate, M & M trace elements or omission of vitamins did not trigger evident cell morphotype change to oval in both Pt1 8.6 and Pt4 after two subculturing treatments (55 days). Interestingly, an apparent increase in oval cell abundance to 72.5% was observed in Pt1 8.6

after two successive transfers in the modified f/2 medium with increased nitrate and phosphate content and Tris addition (N P T). However, Pt4 was not significantly affected by the combinational condition of N P T, displaying still mainly the fusiform shape (97.9%).

This study offers a novel way to regulate cell morphology of *P. tricornutum* in liquid cultures. It is considered as important to establish stable phenotypes for deeper exploration on cell morphology control at genetic levels. By demonstrating the stability of oval morphotype in M & M medium, this work enables assessment of oval cells for potential industrial applications.

4 Biochemical characterisation in two *Phaeodactylum tricornutum* morphotypes

4.1 Introduction

P. tricornutum is a marine pennate diatom that grows well in brackish to saline water (Figure 3-6). As detailed in the section 1.2.4, *P. tricornutum* is of great interest for applications in nutritional, pharmaceutical and biofuel industries as it represents a natural rich source of the high-value marketable products, EPA and fucoxanthin, and can accumulate high lipids and carbohydrates, particularly TAGs and chrysolaminarin, under nitrogen starvation (Gao et al., 2017, Breuer et al., 2012). Furthermore, the advanced genetic tools available for *P. tricornutum* empower this species as a production platform for industrial biotechnology. *P. tricornutum* is polymorphic and can undergo cell morphological transformation induced by changing growth conditions such as temperature, salinity and light (De Martino et al., 2011, Herbstova et al., 2017). Meanwhile, biochemical profiles of microalgae also vary greatly depending on culture conditions such as nutrient, salinity, temperature, pH and light (Qiao et al., 2016, Bartual and Galvez, 2002). Cell morphology and biochemical profiles reflect the physiological and metabolic status of cells under the specific growth conditions. As a result of specific genes expression, they are responses made by *P. tricornutum* cells at phenotypic and metabolic levels to external stimuli. In order to define the technoeconomic feasibility of *Phaeodactylum* biorefinery, it is essential to characterise various compositions from cell biomass. Although product accumulation in *P. tricornutum* cells has been characterised under diverse culture conditions, few studies quantify the proportion of cell morphotypes. Little is therefore known about the biochemical differences between cell morphotypes.

While the phenomenon of polymorphism is intrinsically interesting, there has not been a systematic study linking this behaviour to the ability of *P. tricornutum* to perform as a solar-powered production platform for industrial biotechnology. This is largely due to the limited method available for

obtainment and maintenance of each cell form accompanied with high biomass production. In Chapter 3, Mann and Myers' medium was identified as triggering significant cell morphotype conversion in *P. tricornutum* from fusiform to oval and suitable for maintenance of oval cells in liquid cultures under the constant shaking condition, which enables us to explore the biochemical differences between cell morphotypes and to assess oval cells for potential industrial applications. In this chapter, the growth kinetics and biochemical profiles including pigment, protein, lipid and carbohydrate in fusiform and the obtained oval morphotypes under their respective growth medium were investigated in support of their further industrial exploitation.

4.2 Materials and methods

All chemicals were purchased from Sigma-Aldrich unless otherwise stated.

4.2.1 Cultivation for growth and biochemical analyses

As described in Chapter 3, after five successive transfers representing a cell cultivation of approximately four months, cultures of Pt1 8.6 and Pt4 grown in M & M medium were abundant with more than 90% oval cells. Here, experimental cultures were prepared by inoculating the well-maintained log-phase cultures of Pt1 8.6 and Pt4 grown in f/2 medium and M & M medium into 250 mL Erlenmeyer flasks containing 100 mL of respective culture medium with an initial cell density of 8-10x10^5 cells mL^{-1}. Cultures were monitored for 21 days for growth measurement with the method described in section 2.2.2 and 1 mL or 2 mL samples were taken on day 3, 7, 10, 14 and 21 for pigment analysis. For protein, carbohydrate and lipid analyses, experimental cultures were prepared in 500 mL Pyrex glass flasks containing 200 mL of respective culture medium with a same initial cell density as above. Culture samples were taken on day 3, 8, 14 and 21 by centrifugation at 3,200 x g for 15 min and stored at -80 ^oC until for further biochemical analyses. All cultures were grown under the conditions detailed in Chapter 2, section 2.2.1. Growth and biochemical analyses were conducted in biological triplicate.

4.2.2 Pigment analysis

The pigment content in *P. tricornutum* cells were analysed using both the colorimetric and the RP-HPLC methods. Pigment was extracted based on the EnAlgae protocol (SOP 4.4.c) (Silkina et al., 2015). Briefly, *P. tricornutum* cells were incubated in 1 mL of *N,N*-dimethylformamide (DMF) under orbital agitation at 250 rpm for 15 min at room temperature. Following centrifugation at 21,000 x g for 5 min, the extracts were collected with the remaining pellet being white. All extraction procedures were performed under dimmed light to avoid light-induced degradation of pigments. The pigment extracts were diluted and carefully poured into disposable DMF resistant cuvettes (Brand UV-Cuvette, 70-850 µL, Brand, Germany) to read in a spectrophotometer at 480, 647 and 664.5 nm. The chlorophyll *a* and total carotenoid content (µg mL^{-1}) were calculated with the following equations (Inskeep and Bloom, 1985, Wellburn, 1994).

$$\boldsymbol{Chl\ a = 12.70A_{664.5} - 2.79A_{647}} \qquad \textbf{Equation 4-1}$$

$$\boldsymbol{Chl\ b = 20.70A_{647} - 4.62A_{664.5}} \qquad \textbf{Equation 4-2}$$

$$\boldsymbol{Chl\ x\ +\ C\ (carotenoids) = \frac{1000A_{480} - 2.14Chl\ a - 70.16Chl\ b}{245}} \qquad \textbf{Equation 4-3}$$

The pigment profiles in different *P. tricornutum* morphotypes were further analysed by RP-HPLC. Prior to analysis, pigment extracts were filtered through 0.2 µm polytetrafluoroethylene (PTFE) syringe filters (DHI, Denmark), diluted and then analysed with the method detailed in Chapter 2, section 2.3.1. The pigments in samples were identified by a comparison of retention times of eluted peaks with those from a mixed pigment standard (PPS-MIX-1, DHI, Denmark). Quantitative analysis was achieved using the equations from standard curves of each individual pigment standard (chlorophyll *c2*, fucoxanthin, diadinoxanthin, chlorophyll *a* and β-carotene, DHI, Denmark).

4.2.3 Total soluble protein determination

P. tricornutum cell pellets from 4-20 mL of cell cultures, corresponding to approximately 1.5 mg biomass in dry weight, were resuspended in 1 mL of chilled lysis buffer made of 50 mM Tris-HCl pH 8.0, 10 mM EDTA, 0.5 mM phenylmethylsulfonylfluoride (PMSF) and 0.1% (v/v) TritonX-100 (section 2.1.4). Cell suspensions were transferred into 1 mL millitubes with AFA (adaptive focused acoustics) fibres (Covaris, USA) and subjected to focused acoustic disruption using a Covaris E210 focused-ultrasonicator (Covaris, USA) (Figure 1-9). The operation conditions are cycles per burst of 1000, power intensity of 10, duty factor of 20% and water bath at 10 ^{o}C. Treatment time employed was depending on the cell morphotype, allowing a cell disruption efficiency of more than 97% to be achieved. Specifically, fusiform cell suspensions were treated for 90 s while oval cell suspensions were sonicated for 8-10 min (Figure 5-5). More details could be found in Chapter 5, section 5.3.3. The total soluble protein content was determined with the Bradford assay as described in Chapter 2, section 2.2.4.

4.2.4 Neutral lipid and fatty acid analysis

Neutral lipids in *P. tricornutum* cells were qualitatively detected through BODIPY 505/515 cell staining (Cooper et al., 2010). Aliquots of a 1 mg mL^{-1} BODIPY 505/515 stock solution (section 2.1.7) were added directly to 1 mL of cell suspensions (~2x10^{6} cells mL^{-1}) to achieve a final dye concentration of 1 μg mL^{-1}. Each sample was well mixed and incubated in darkness for 10 min at room temperature. Intracellular lipid bodies stained with the dye were then viewed using an epifluorescence microscope (TE2000-U, Nikon, Japan). Fluorescent images were made with filter blocks of excitation set from 450 to 490 nm and emission set from 500 to 550 nm. Bright-field images were made simultaneously under phase contrast.

Fatty acid detection was performed following the procedure of lipid extraction, transesterification and gas chromatography (GC) analysis based on the EnAlgae protocols (SOP 4.3.c and SOP 4.7.c) with some modifications. Lipid was extracted from cell pellets (~3 mg in dry weight) by adding 8 mL of a

chloroform: methanol (2:1, v/v) mixture (Folch et al., 1957, Axelsson and Gentili, 2014). Pentadecanoic acid (200 µg) was added as an internal standard. Samples were then sonicated for 30 min in an ultrasonic iced bath (Branson 2800 ultrasonic bath, CPX2800H, Emerson, USA) and incubated for another 30 min in the iced bath. Two millilitres of deionized water was added and vortexed to mix thoroughly. Phase separation was achieved by centrifugation at 1500 x g for 5 min. The lower phase containing lipids was recovered, evaporated using GeneVac EZ-2 evaporator (GeneVac, UK) saturated with N_2 gas and resuspended in 200 µL of n-heptane. Transesterification was then performed by adding 3 mL of methanol containing 2.5% (v/v) H_2SO_4 into 60 µL of lipid extracts and incubating at 60 ^oC in a water bath for 4 h. The obtained fatty acid methyl esters (FAMEs) were analysed by GC-FID according to the method described in Chapter 2, section 2.3.2. FAMEs were identified by co-elution with a FAME standard mix (Supelco 37 Component FAME Mix, Sigma Aldrich, UK) and quantified from calibration curves of external standards (methyl esters of C14:0, C16:0, C16:1, etc). All FAME concentrations were normalised against the methyl pentadecanoate from the internal standard. Total FAME content was calculated as the sum of all individual FAMEs.

4.2.5 Carbohydrate determination

The carbohydrate content with three fractions including exopolysaccharides (EPS), soluble cellular carbohydrate and residual carbohydrate were determined according to the method described previously (Smith and Underwood, 2000) and the EnAlgae protocol (SOP 4.2.a) with some modifications. In brief, 8-18 mL of cell broth was centrifuged at 3,200 x g for 15 min. The supernatant (6-10 mL) was transferred to a new Falcon tube for EPS precipitation by adding 3 volumes of chilled ethanol and incubating at 4 ^oC overnight. Following centrifugation at 3,200 x g for 10 min, the precipitated EPS was resuspended in 1 mL of Milli-Q water and analysed for extracellular carbohydrate. Cell pellets (~1.5 mg in dry weight) were resuspended in 1 mL of Milli-Q water and transferred into 1 mL millitubes for focused acoustic ultrasonication. Samples were then transferred to glass test tubes followed

by adding 1 mL of 1 M sulphuric acid. Glass tubes were capped with stoppers, mixed thoroughly, and incubated at 90 ^{o}C for 1 h. After centrifugation at 21,000 x g for 10 min, the supernatants were collected for soluble cellular carbohydrate measurement. The residues were resuspended in 1 mL of 0.5 M sulphuric acid and analysed for residual carbohydrate. The carbohydrate content was quantified using the phenol sulphuric acid (PSA) assay, as detailed in Chapter 2, section 2.2.5.

The monosaccharide composition of cellular carbohydrate extracts was further analysed by high-performance anion exchange chromatography (HPAEC). Before HPAEC analysis, the extracts were hydrolysed in 0.5 M sulphuric acid for 1 h at 121 ^{o}C in an autoclave. After cooling to room temperature, the hydrolysates were neutralised with calcium carbonate and centrifuged at 3,200 x g for 10 min. The supernatants were filtered through 0.2 µm syringe filters, diluted and analysed using the HPAEC method as described in Chapter 2, section 2.3.3. Standards (fucose, glucose, galactose, mannose, etc) were used for identification and quantification.

4.3 Results and Discussion

The highly interesting pleiomorphic property of *P. tricornutum* motivated us to investigate other characteristics such as growth kinetics and biochemical profiles including pigment, protein, fatty acid and carbohydrate from various cell morphotypes in support of *Phaeodactylum* biorefinery for industrial exploitation.

4.3.1 Growth of fusiform and oval *P. tricornutum* cells

As mentioned in Chapter 3, fusiform cells are predominant in cultures grown in f/2 medium (denoted as fusiform cell cultures), representing approximately 88% in Pt1 8.6 and 97% in Pt4. By contrast, the oval form is most abundant in cultures maintained in M & M medium (denoted as oval cell cultures), accounting for approximately 90% in Pt1 8.6 and 100% in Pt4. From a bioprocessing perspective, it is important to be able to quantify cell growth rate and dry biomass yield with regard to bioprocess design and scale-up.

Consequently, we investigated the effects of culture media on growth and biomass production of the two obtained cell morphotypes.

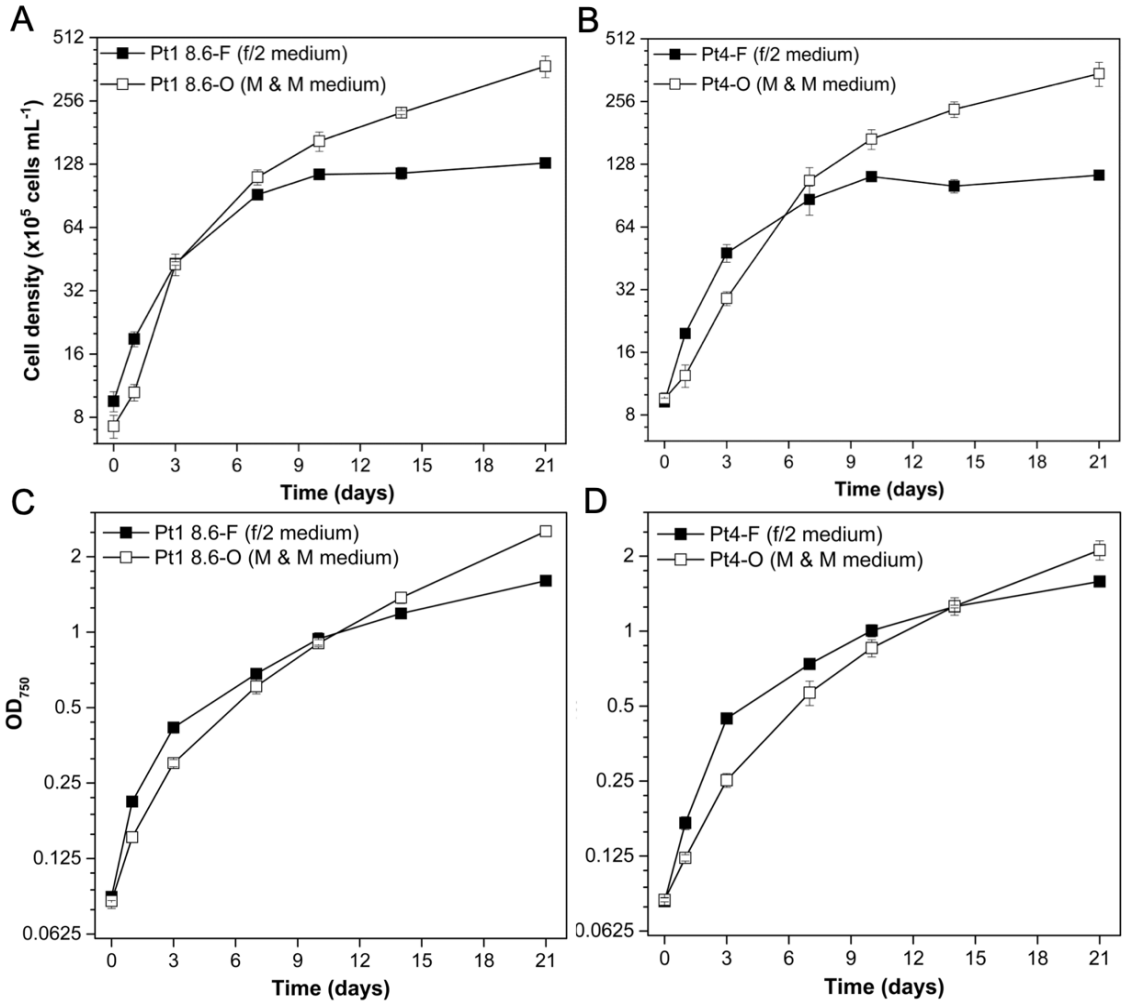

Figure 4-1 Growth profiles of fusiform and oval *P. tricornutum* cultures maintained in two different culture media.

Growth curves measured by cell density (A, B) or OD_{750} (C, D) for fusiform (F) cell cultures grown in f/2 medium or oval (O) cell cultures grown in M & M medium in Pt1 8.6 (A, C) and Pt4 (B, D). Data are shown as mean ± one standard deviation from three biological replicates.

The cell density was measured to monitor growth of fusiform and oval cells for Pt1 8.6 and Pt4. As shown in Figure 4-1 A, similar growth rates were obtained for fusiform and oval cell cultures of Pt1 8.6, with the maximum specific growth rates of 0.68 d^{-1} and 0.70 d^{-1}, corresponding to doubling times of 1.03 d and 0.99 d, respectively (Table 4-1). Fusiform cell cultures entered stationary phase from day 10, reaching a final cell density of approximately

$12x10^6$ cells mL^{-1}. In contrast, oval cell cultures experienced a longer lag phase, kept growing after 10 days cultivation and appeared to only reach the early stationary phase on day 21, where a 3-fold higher cell density of $37.4x10^6$ cells mL^{-1} was achieved. Similar growth patterns were observed for Pt4 cultures except that a higher maximum specific growth rate was obtained for fusiform cell cultures compared to oval cell cultures (0.76 d^{-1} versus 0.43 d^{-1}; doubling time, 0.92 d versus 1.65 d) (Figure 4-1 B & Table 4-1). Slower growth rate was previously reported for the oval strain (Pt3) in comparison to fusiform strains and the doubling times obtained here were similar to those reported previously (De Martino et al., 2007).

Table 4-1 Maximum specific growth rates (μ_{max}) and doubling times of fusiform (F) and oval (O) *P. tricornutum* cultures.

	μ_{max} (d^{-1})	Doubling time (d)
Pt1 8.6-F	0.68±0.10[a]	1.03±0.17
Pt1 8.6-O	0.70±0.04[b]	0.99±0.06
Pt4-F	0.76±0.04[a]	0.92±0.06
Pt4-O	0.43±0.07[b]	1.65±0.25

Data are shown as mean ± one standard deviation from three biological replicates.
[a] The μ_{max} values for fusiform cell cultures were calculated based on the cell density from day 0 to day 1 (Figure 4-1 A & B).
[b] The μ_{max} values for oval cell cultures were calculated based on the cell density from day 1 to day 3 (Figure 4-1 A & B).

As a simple and rapid method, optical density measurement can also be used to estimate cell growth based on Beer-Lambert's Law. For both strains tested, fusiform cell cultures showed higher OD_{750} readings for the first 10 days or 14 days cultivation, which were then overtaken by OD_{750} values for oval cell cultures (Figure 4-1 C & D). Similar trend was observed for the changes in dry biomass yield of the two cell morphotypes (Figure 4-2). Over three weeks cultivation, the highest biomass concentrations were obtained for oval cell cultures (0.73 g L^{-1} in Pt1 8.6 and 0.58 g L^{-1} in Pt4), compared to the 0.50 g L^{-1} obtained for fusiform cell cultures of the two strains. This demonstrated that M & M medium is suitable for oval cell maintenance and

production, allowing high biomass yield to be achieved for oval *P. tricornutum* cells.

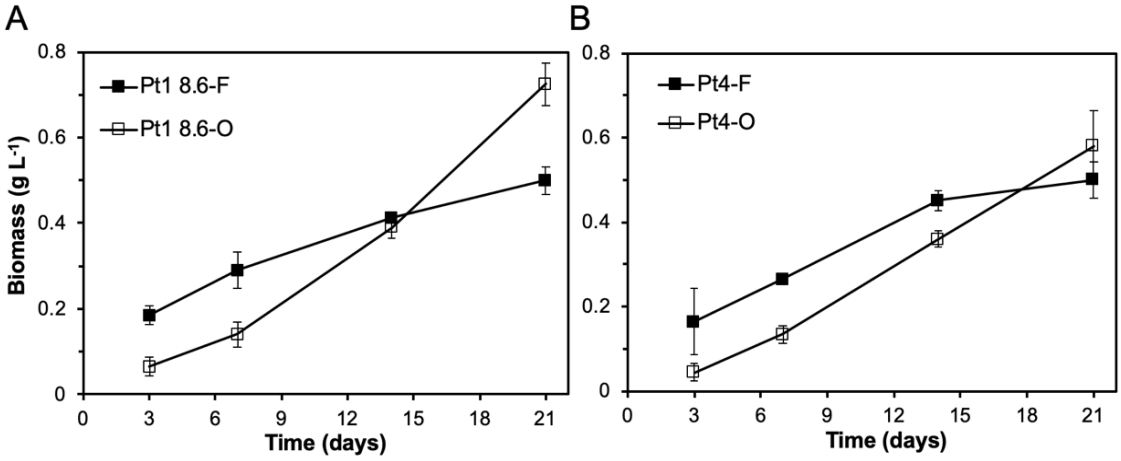

Figure 4-2 Dry biomass concentration of fusiform and oval *P. tricornutum* cultures.

Dry biomass concentration measured for fusiform (F) cell cultures grown in f/2 medium or oval (O) cell cultures grown in M & M medium in Pt1 8.6 (A) and Pt4 (B). Data are shown as mean ± one standard deviation from three biological replicates.

Interestingly, from day 7 to day 10 or 14, oval cell cultures displayed lower biomass concentrations (Figure 4-2) and OD_{750} values despite higher total cell numbers than fusiform cell cultures (Figure 4-1). This could be explained by the smaller cell size of oval morphotype (~10 μm) than fusiform morphotype (~30 μm) as well as the differences in biomass composition between them. For polymorphic microalgae, the relationship between OD and cell density is affected by cell morphology such as cell size and shape with the smaller particles usually having larger amount of transmitted and scattered light and thus lower absorbance. Moreover, the associated pigments in algae influence OD values as well, which is the reason why a wavelength of 750 nm, outside the absorption range of chlorophyll, is usually used for measuring OD. Since both the microalgal cell morphology and pigmentation are dependent on the physiological state of cells, which varies with changes in growth conditions such as light and nutrient availability and across the growth cycle, inaccuracies in the estimation of cell density by OD could occur (Griffiths et al., 2011). This may explain the observed differences

in kinetics of OD_{750} and cell count such as no lag phase showed for oval cells from OD_{750} measurement and a slight increase in OD_{750} of fusiform cells in stationary phase (Figure 4-1). A continuous increase in biomass concentration was also observed for fusiform cells after day 10 in stationary phase (Figure 4-2). Such an increase might be due to the accumulation of storage compounds such as carbohydrate and TAGs, caused by the initial nutrient starvation, as commonly reported for many microalgae (Breuer et al., 2012). This also indicates that calibration curves of cell density or dry biomass concentration versus OD_{750} should be generated for each cell morphotype across the entire growth cycle when using OD_{750} for growth estimation (Appendix, Figure A-1).

The evident longer growth phase and markedly higher final cell and biomass concentrations for oval cell cultures could be attributed to the higher macronutrient content, particularly nitrate and phosphate, in M & M medium when compared to f/2 medium used to grow fusiform cells (Table 2-1). The N:P assimilation ratio for phytoplankton growth is assumed to be 16:1 (Redfield, 1958). It has also been shown that the percentages of nitrate and phosphate remaining in f/2 medium were approximately 0% after 7 days cultivation of *P. tricornutum*, which exhibited a similar growth pattern as our results observed for fusiform cell cultures (Ridley et al., 2018). Nutrient deprivation in f/2 medium at the stationary phase might therefore inhibit the growth of fusiform cells. In addition, a 5-fold increase in the dry biomass concentration from 0.5 g L^{-1} to 2.5 g L^{-1} was observed for *P. tricornutum* grown for 7 days in M & M medium when the CO_2 concentration in the air supply increased from 0% to 1% (Yongmanitchai and Ward, 1991). From growth curves, stationary phase was not reached for oval cells even after 21 days cultivation (Figure 4-1). This implies that carbon might be an important limiting factor for fast growth of oval cells and further optimisation of cultivation parameters such as inorganic carbon supply may further increase the growth rate and biomass production of oval *P. tricornutum* cells.

4.3.2 Pigment content and composition from fusiform and oval *P. tricornutum* cells

Pigments, particularly fucoxanthin, represent potentially valuable products from *P. tricornutum* for food, cosmetics and pharmaceutical applications. Hence, it is essential to determine types of pigment produced and their concentrations. The effects of cultivation time and culture medium on pigment content and composition in fusiform and oval *P. tricornutum* cells were studied and the pigment content was calculated on a dry weight (DW) basis in order to estimate specific yields and productivities. Calibration curves of DW versus OD_{750} were created separately for fusiform and oval cells of Pt1 8.6 and Pt4 (Appendix, Figure A-1) and were used for DW estimation from OD_{750} readings.

The rapid spectrophotometric method and the HPLC method were employed to determine the pigment content in *P. tricornutum* and for comparison. The amounts of chlorophyll *a* (Chl *a*) and total carotenoids (Car) in the two cell morphotypes determined by spectrophotometry were calculated with the previously reported equations (Equations 4-1 & 4-3) and shown in Figure 4-3. Clearly, a gradual decline in the content of Chl *a* and Car from 17.5 to 3.3 mg g^{-1} DW and from 6.2 to 1.9 mg g^{-1} DW respectively was observed in Pt1 8.6 fusiform cell cultures in comparison to the increase from 15.1 to 25.2 mg g^{-1} DW for Chl *a* and from 5.1 to 8.8 mg g^{-1} DW for Car in Pt1 8.6 oval cell cultures over 21 days cultivation (Figure 4-3 A). Pt4 cell cultures showed a very similar change pattern in pigment content (Figure 4-3 B).

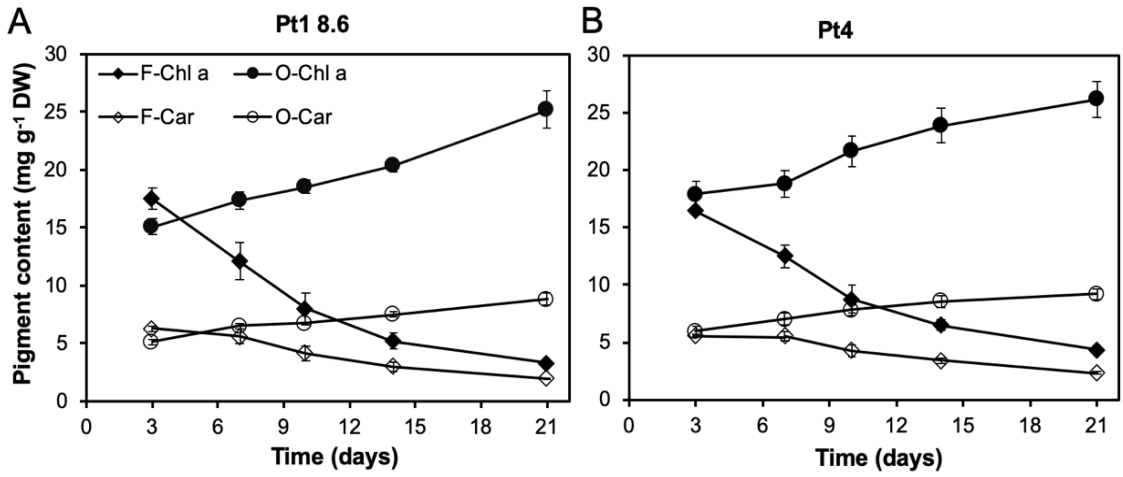

Figure 4-3 Pigment content in two morphotypes of *P. tricornutum* cells quantified with the spectrophotometric method.

Quantification of chlorophyll *a* (Chl *a*) and total carotenoids (Car) by the spectrophotometric method from fusiform (F) cell cultures grown in f/2 medium or oval (O) cell cultures grown in M & M medium in Pt1 8.6 (A) and Pt4 (B). Data are shown as mean ± one standard deviation from three biological replicates. DW, dry weight.

From HPLC analysis, five major diatom pigments including chlorophyll *c2* (Chl *c2*), fucoxanthin (Fuc), diadinoxanthin (Diad), chlorophyll *a* (Chl *a*) and β-carotene (β-car) were detected in both fusiform and oval *P. tricornutum* cultures (Figure 4-4), consistent with those commonly reported (Kosakowska et al., 2004, Ragni and D'Alcala, 2007). The results showed that Chl *a* and Fuc were the two predominant pigments produced in *P. tricornutum* (Figure 4-5), which have previously been identified as the principal light harvesting pigments in *P. tricornutum* (Mann and Myers, 1968). In agreement with measurements from spectrophotometry, the content of each pigment was found to decrease gradually in fusiform cell cultures but increase slightly in oval cell cultures for both strains over three weeks cultivation. For example, the amounts of two major pigments, Chl *a* and Fuc, represented 9.5 mg g^{-1} DW and 9.7 mg g^{-1} DW respectively in Pt1 8.6 fusiform cell cultures, and 8.2 mg g^{-1} DW and 7.5 mg g^{-1} DW respectively in Pt1 8.6 oval cell cultures on day 3. After 21 days cultivation, their amounts declined to 2.4 mg g^{-1} DW and 2.2 mg g^{-1} DW respectively in fusiform cell cultures, significantly lower than those from oval cell cultures which were 12.1 mg g^{-1} DW and 12.0 mg g^{-1} DW

respectively (Figure 4-5 A & B). Pigment content in Pt4 cultures followed a similar trend (Figure 4-5 C & D).

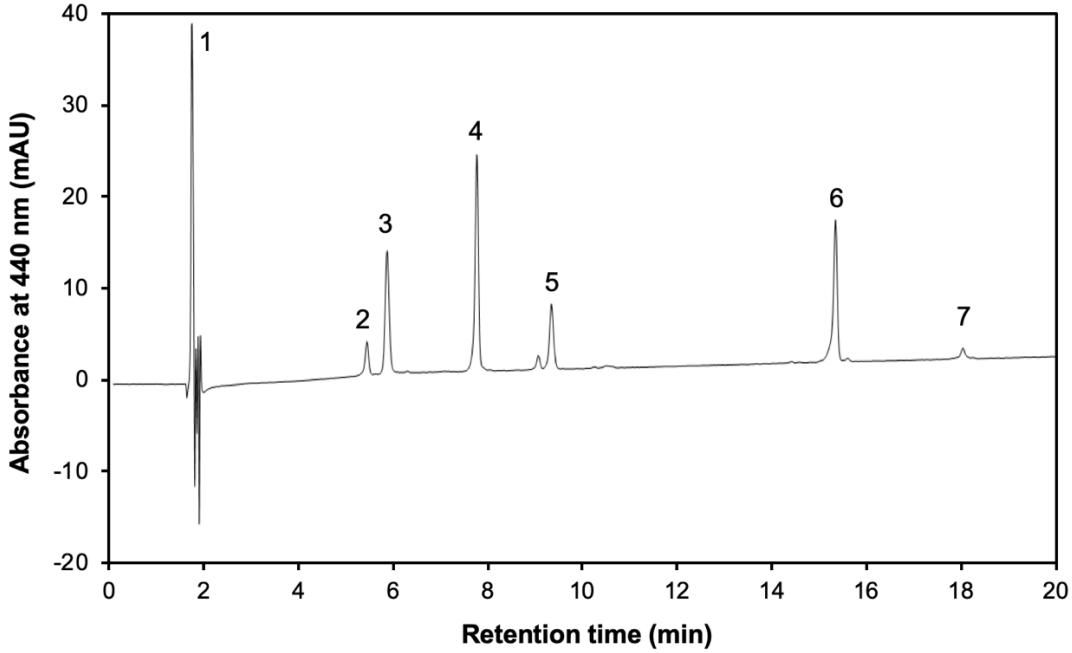

Figure 4-4 Representative reverse phase HPLC chromatogram of pigments extracted from *P. tricornutum* cultures.

Identified pigments with retention times: 1, solvent front; 2, chlorophyll derivative; 3, chlorophyll *c2*, 5.83 min; 4, fucoxanthin, 7.75 min; 5, diadinoxanthin, 9.35 min; 6, chlorophyll *a*, 15.36 min; 7, β-carotene, 18.07 min.

This physiological response of declining pigment content with culture age observed in fusiform cell cultures is consistent with observations in microalgae grown under nutrient deprivation (Pancha et al., 2014, Msanne et al., 2012). Specifically, high pigment was generally synthesised in actively growing microalgal cells under nutrient-replete conditions for efficient photosynthesis and cell division. When cells reached stationary phase accompanied with nutrient limitation, cell growth was inhibited and photosynthetic capacity was decreased. Furthermore, suppression of genes involved in photosynthesis and pigment biosynthesis has also been observed in *P. tricornutum* in response to N and P deprivation (Alipanah et al., 2015, Alipanah et al., 2018). Thus, the low nutrient availability in f/2 medium could be responsible for the decreased pigment levels observed in fusiform *P. tricornutum* cultures. By contrast, the M & M medium contains relatively high

nitrate and phosphate content, leading to the accumulation of pigment in oval *P. tricornutum* cultures under the tested conditions. The higher contents of pigments, particularly Chl *a* and Fuc, from oval cells are consistent with the ability to increase light harvesting in abundant nitrate and phosphate which leads to greater cell division rate and cell density.

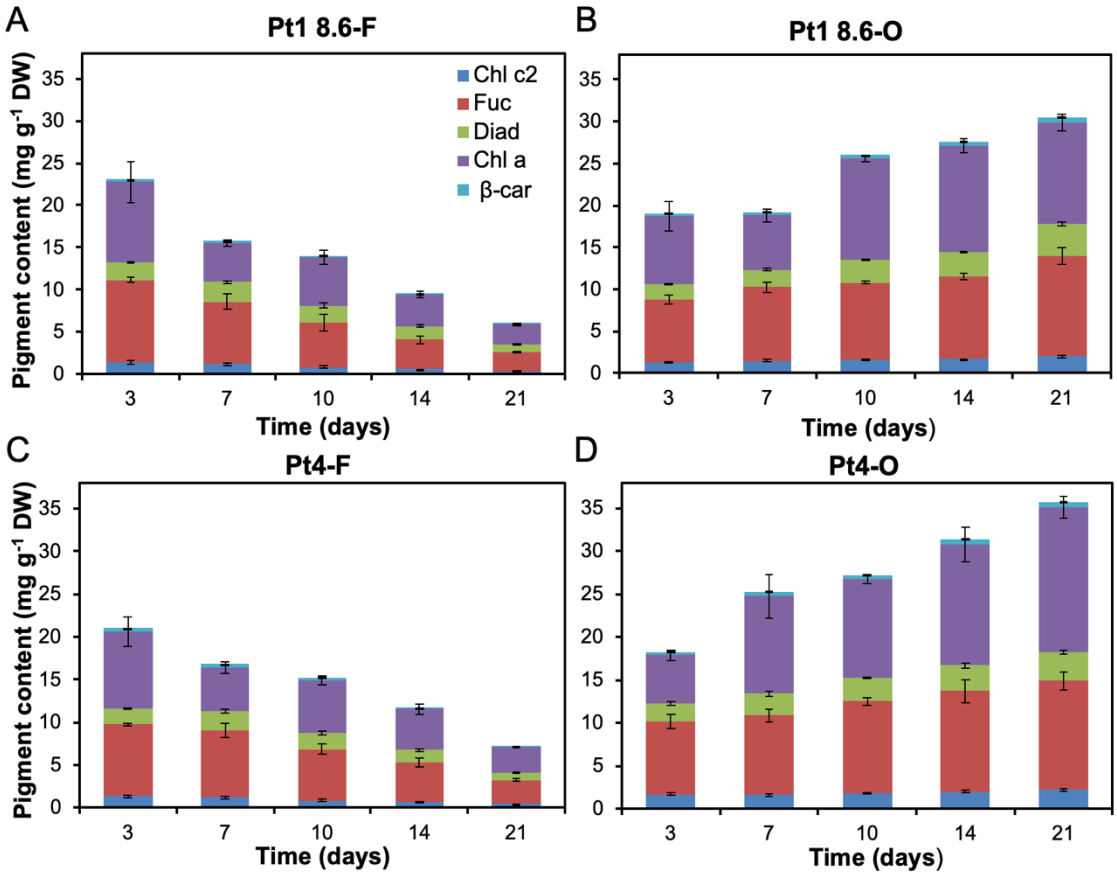

Figure 4-5 Pigment composition and content in two morphotypes of *P. tricornutum* cells quantified by the HPLC method.

Quantification of five major pigments including chlorophyll *c2* (Chl *c2*), fucoxanthin (Fuc), diadinoxanthin (Diad), chlorophyll *a* (Chl *a*) and β-carotene (β-car) by the HPLC method from fusiform (F) or oval (O) cell cultures of Pt1 8.6 (A, B) and Pt4 (C, D). Data are shown as mean ± one standard deviation from three biological replicates. DW, dry weight.

The total pigment content also clearly revealed the pigment accumulation over cultivation time in oval *P. tricornutum* cultures grown in M & M medium but not in the fusiform cell cultures grown in f/2 medium. On day 3, there was no significant difference in total pigment content between fusiform and oval cell cultures in both strains. Over three weeks cultivation, the total pigment

content quantified by HPLC in oval cell cultures increased by more than 1.6-fold, from 1.9% DW to 3.0% DW in Pt1 8.6 and from 1.8% DW to 3.6% DW in Pt4. By contrast, a gradual decrease from 2.3% DW to 0.6% DW in Pt1 8.6 and from 2.1% DW to 0.7% DW in Pt4 was observed in fusiform cell cultures (Table 4-2). Accordingly, the oval cell cultures showed dark brown colour compared to the golden colour for fusiform cell cultures after two weeks cultivation (Figure 4-6), implying the higher pigment production from oval cells than fusiform cells.

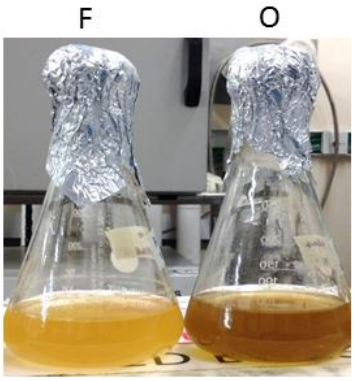

Figure 4-6 Representative flask image of fusiform and oval *P. tricornutum* cultures.

Representative culture flasks of Pt1 8.6 on day 14 showing the dark brown colour of oval (O) cell cultures grown in M & M medium compared to the golden colour of fusiform (F) cell cultures grown in f/2 medium.

Compared with the HPLC method, the spectrophotometric method gave a highly similar total pigment content of 2.4-0.5% DW and 2.0-3.4% DW for Pt1 8.6 fusiform and oval cell cultures respectively, and 2.2-0.7% DW and 2.4-3.5% DW for Pt4 fusiform and oval cell cultures respectively. However, this method appeared to overestimate the Chl *a* content and underestimate total carotenoids in *P. tricornutum* in comparison to the HPLC method (Figures 4-3 & 4-5). The HPLC method was believed to be more accurate since each pigment in the extract (chlorophylls and carotenoids) was separated and quantified from their respective standard calibration curve. By contrast, the spectrophotometric method is measuring the absorbance of the crude extract at wavelengths corresponding to the maximum absorption of the studied pigments and using equations with specific molar extinction coefficients for

quantification. The overestimation of Chl *a* by spectrophotometry might be due to the presence of Chl *c,* the absorption spectrum of which overlaps with that of Chl *a*, in *P. tricornutum* and the presence of Chl degradation derivatives (Figure 4-4) (Picazo et al., 2013). The Chl *a* overestimation will result in the underestimation of total carotenoids based on the Equation 4-3 shown in section 4.4.2. In addition, the accuracy of spectrophotometry also depends on the accuracy of the extinction coefficients, the spectral purity of pigments, the relative proportion of different Chls in the extract, the precision of spectrophotometer and the presence of water from the extracted cells which affects the maximum absorbance peak (Connan, 2015).

P. tricornutum has been identified as a natural source of the high-value marine carotenoid fucoxanthin (Kim et al., 2012). Our results confirmed the high content of fucoxanthin in *P. tricornutum.* The maximum fucoxanthin content was observed in oval cell cultures on day 21, reaching 12.0 mg g^{-1} DW in Pt1 8.6 and 12.7 mg g^{-1} DW in Pt4, corresponding to the highest volumetric concentrations of 8.5 mg L^{-1} and 7.0 mg L^{-1} respectively, which are more than 3.5-fold higher than those achieved in fusiform cell cultures (1.6 mg L^{-1} in Pt1 8.6 and 2.0 mg L^{-1} in Pt4). The fucoxanthin content obtained here from fusiform cell cultures is similar to those (2.1-5.5 mg g^{-1} DW) reported in *P. tricornutum* grown in f/2 medium (Wu et al., 2016). A higher amount of 6-15.7 mg g^{-1} DW was observed previously in *P. tricornutum* at a large scale of over 30 L depending on the nutrient conditions and extraction methods (Kim et al., 2012, Gao et al., 2017), suggesting that optimisation of cultivation time and scale-up parameters may further enhance the pigment production from oval *P. tricornutum* cultures.

4.3.3 Protein content from fusiform and oval *P. tricornutum* cells

The protein content (% DW) from the two morphotypes of cell cultures over cultivation time was investigated. Overall, significantly higher protein content was obtained in oval cell cultures than in fusiform cell cultures for both strains under the tested conditions ($p<0.05$) (Figure 4-7), implying the potential nutritional value of oval cells. Specifically, the protein content from oval cell

cultures grown in M & M medium reached a plateau after experiencing an initial increase in the first 8 days cultivation, representing 24.1% DW in Pt1 8.6 and 20.4% DW in Pt4. In contrast, the protein content from fusiform cell cultures grown in f/2 medium increased initially as well, reaching a maximum amount of 16.0% DW in Pt1 8.6 and 14.1% DW in Pt4 on day 8. After that, the values decreased gradually to 8.1% DW and 8.6% DW respectively by the end of cultivation (Table 4-2).

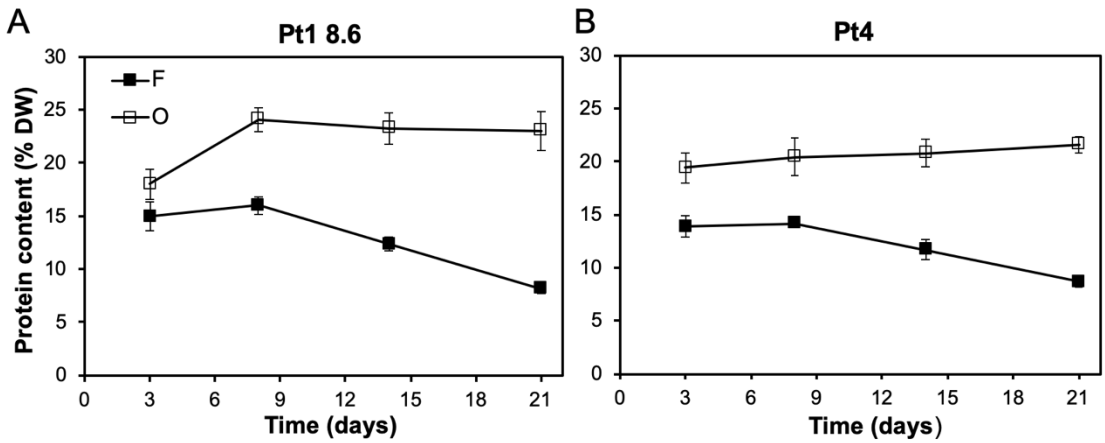

Figure 4-7 Protein content in two morphotypes of *P. tricornutum* cells.

Total soluble protein content quantified on a dry weight (DW) basis from fusiform (F) or oval (O) cell cultures of Pt1 8.6 (A) and Pt4 (B). Data are shown as mean ± one standard deviation from three biological replicates.

In a study on Pt3 sampled in the mid-log phase, it was shown that 68% of the 2,326 differentially expressed genes were up-regulated and the nucleotide biosynthesis and protein processing were more active in oval cells maintained in 10% seawater, compared to fusiform and triradiate cells grown in 100% seawater (Ovide et al., 2018). This may explain the higher protein content detected in oval cell cultures than in fusiform cell cultures for both strains even at the log phase of day 3 (Figure 4-7). Highest protein content was observed at late log phase (~day 8), consistent with previous observations in microalgae (Gatenby et al., 2003). Nutrient limitation, particularly nitrate and phosphate deprivation, in f/2 medium as cultures reached stationary phase, is likely the main reason for the decrease in protein content observed in fusiform *P. tricornutum* cultures. This corroborates previous reports which have shown that genes involved in

protein biosynthesis and folding were repressed and recycling of organic N resources such as protein, chlorophyll and nucleotide was increased in *P. tricornutum* grown under N and P deprivation (Alipanah et al., 2015, Alipanah et al., 2018). On the other hand, the observed high protein content from oval cells than from fusiform cells could be co-founded by the high initial N and P in M & M medium. It would be helpful to culture fusiform cells in f/2 medium with increased N and P or to grow oval cells in M & M medium with decreased N and P to understand the protein content in the two morphotypes of *P. tricornutum* in the future.

4.3.4 Lipid and fatty acid composition from fusiform and oval *P. tricornutum* cells

In the context of lipid-based biodiesel production from microalgae, the neutral lipids stored as lipid bodies in the two morphotypes of *P. tricornutum* cells were analysed qualitatively through BODIPY 505/515 cell staining. Representative images showed that with the increasing culture time, more and larger lipid bodies with stronger fluorescence intensity were found in fusiform cells grown in f/2 medium whereas no obvious formation of lipid bodies was observed in oval cells cultured in M & M medium (Figure 4-8). This implies higher neutral lipid accumulation in fusiform cells than in oval cells under the tested conditions. In agreement with the observations from BODIPY staining, FAME analysis showed that fusiform cells grown in f/2 medium accumulated a high amount of lipid over time with the FAME-equivalent total fatty acid (TFA) content increasing steadily from 6.7% DW to 22.9% DW in Pt1 8.6 and from 8.2% DW to 18.8% DW in Pt4 over 21 days cultivation (Figure 4-9 A & C and Table 4-2). By contrast, there was no significant change in TFA content from oval cell cultures which stabilised at around 8% DW in Pt1 8.6 and 7% DW in Pt4 under the tested conditions (Figure 4-9 B & D and Table 4-2).

Microalgal lipid is composed of neutral lipids (NLs) and polar lipids (PLs). It is widely reported that NLs, primarily TAGs, were significantly accumulated upon N starvation in microalgae, representing up to 90% of TFA content and

over 40% of dry weight (Breuer et al., 2012). TAGs, a storage pool of lipid, are precursors for biodiesel production (Al hattab and Ghaly, 2015). PLs including glycolipids and phospholipids are important components of various cellular membrane structures (van Meer et al., 2008). Membrane lipid remodelling from phospholipids to nonphosphorus lipids followed by TAG accumulation has been previously reported under N and P starvation in *P. tricornutum* (Abida et al., 2015, Alipanah et al., 2015, Alipanah et al., 2018, de Carvalho et al., 2016). Our results suggested that N and P deprivation was reached first in f/2 medium, inducing NL accumulation in fusiform cells which exhibit a potential feedstock for biodiesel production. *P. tricornutum* was reported to have a lipid content of 18-57% DW depending on growth conditions and extraction and quantification methods, comparable to that in other commonly used microalgae species such as *Chlorella sp.* (10-48% DW), *Dunaliella sp.* (18-67% DW) and *Nannochloris sp.* (20-56% DW) and lower than that in *Botryococcus braunii* (25-75% DW) and *Schizochytrium sp.* (50-77% DW) (Saifullah et al., 2014). In addition, nutrient deficiency conditions are often associated with relatively low biomass yields, leading to low overall product productivities (Gao et al., 2017). Therefore, the trade-off between culture condition-based cell biomass yield and product productivity should be carefully considered at the industrial level. When comparing the TFA content on day 3 before NL accumulation, there were no significant differences observed between fusiform and oval cell cultures of both strains ($p>0.05$) (Figure 4-9). In order to gain a better understanding about the biochemical differences of the two cell morphotypes, the modified f/2 medium with added nitrate and phosphate as M & M medium, given that it had no effect on fusiform cell morphotype, could be used in the future to grow fusiform cells to eliminate the impacts of N and P limitation.

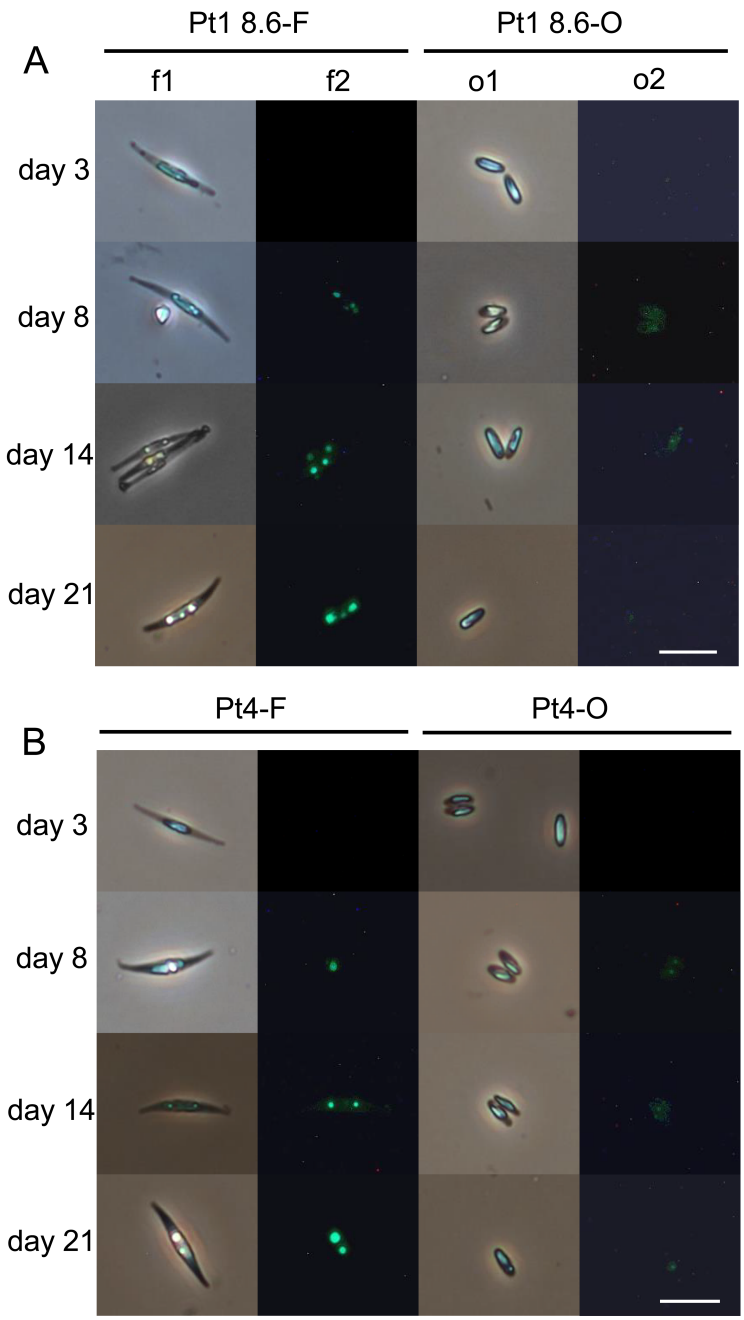

Figure 4-8 Neutral lipid content in two morphotypes of *P. tricornutum* cells.

Representative micrographs showing the neutral lipid bodies formation over time in fusiform (F) and oval (O) cells of Pt1 8.6 (A) and Pt4 (B) stained with BODIPY 505/515. Lanes of f1 and o1 show the bright-field images of cells. Lanes of f2 and o2 are the corresponding fluorescent images. Scale bars: 20 μm.

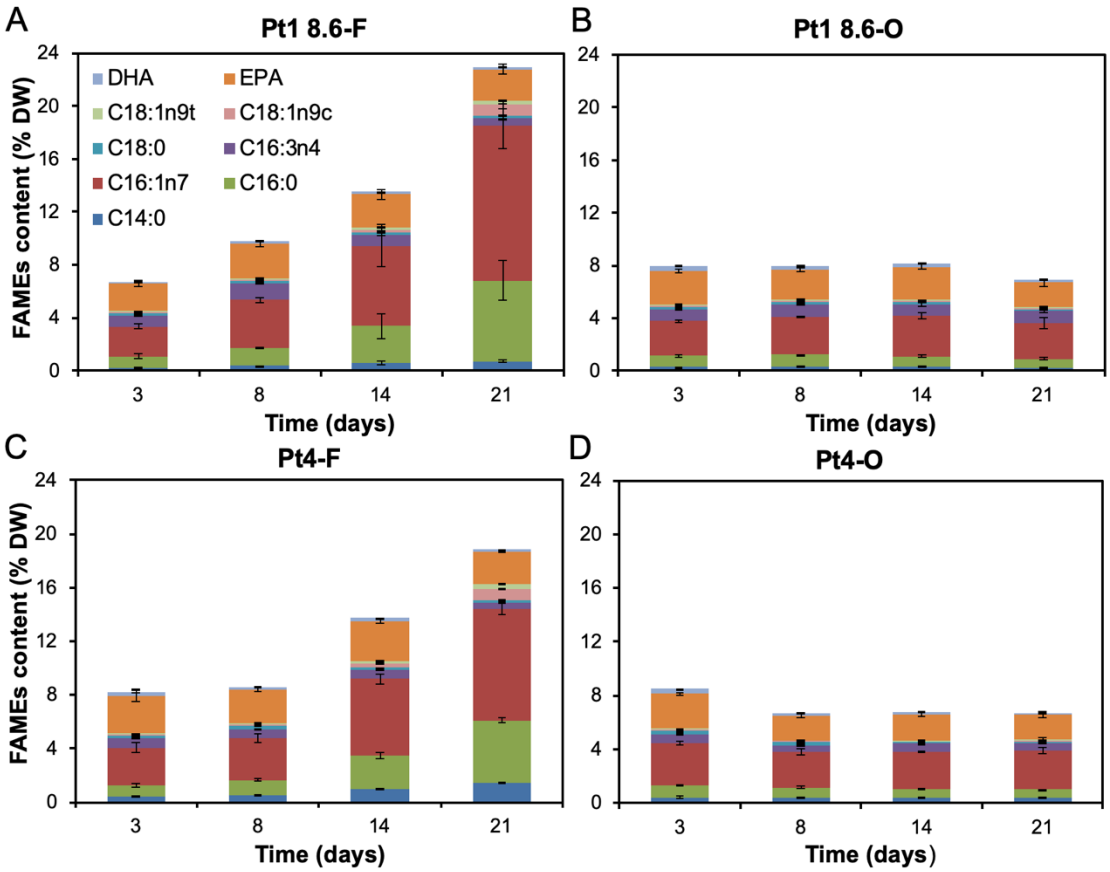

Figure 4-9 Fatty acid composition and content in two morphotypes of *P. tricornutum* cells.

Quantitative analysis of fatty acids by GC-FID from fusiform (F) or oval (O) cell cultures of Pt1 8.6 (A, B) and Pt4 (C, D). Data are shown as mean ± one standard deviation from three biological replicates. DW, dry weight.

Fatty acid composition of microalgal lipids represents an important evaluation index for biodiesel production. The major fatty acids detected from fusiform and oval *P. tricornutum* cultures were found to be C14:0, C16:0, C16:1, C16:3 and C20:5 (EPA), plus small amounts of C18 families and C22:6 (DHA) (Figure 4-9). C16:0, C16:1 and EPA were shown to be three predominant fatty acids in either fusiform or oval *P. tricornutum* cells, representing approximately 0.9%, 3% and 3% DW (11%, 34% and 34% of TFAs) respectively on day 3. Over 21 days cultivation, a marked increase in the amounts of C14:0, C16:0, C16:1 and C18:1 was observed in fusiform cell cultures of both strains, leading to the rise in TFA content (Figure 4-9 A & C). This outcome confirmed a general trend of increasing proportions of saturated fatty acids (SFAs) and monounsaturated fatty acids (MUFAs) but

decreasing proportion of polyunsaturated fatty acids (PUFAs) over culture age (Breuer et al., 2012, Gao et al., 2017). Fluorescent images showed the accumulation of NLs in fusiform cells (Figure 4-8), implying that NLs consisted mainly of SFAs and MUFAs in *P. tricornutum*. By contrast, no significant change in the amount of each individual fatty acid was observed in oval cell cultures of both strains in the tested conditions (Figure 4-9 B & D).

EPA was a major fatty acid detected in both fusiform and oval *P. tricornutum* cultures (Figure 4-9). As a high-value bioproduct, it is of great interest for nutraceutical and medical applications. EPA is present in all lipid classes, mainly in PLs. Among PLs, the highest EPA content was found in the glycolipid fraction of sulfoquinovosyl diacylglycerol (SQDG) (Yang et al., 2017). *P. tricornutum* has been reported to contain about 1.7-4.4% DW EPA depending on strains and growth conditions (Medina et al., 1998, Steinrucken et al., 2018). Our results showed an EPA content of 2.0-3.0% DW in fusiform cell cultures and 1.8-2.6% DW in oval cell cultures with little changes observed over the cultivation period.

4.3.5 Carbohydrate content from fusiform and oval *P. tricornutum* cells

When high-value bioproducts are extracted from the microalgae, it will be important that the remaining sugar in the cell can be converted to other value-added products like bioethanol or biobutanol. The polysaccharides from microalgae have also been shown to have multiple bioactivities such as antitumor, antibacterial and antioxidant for potential pharmaceutical application (Yang et al., 2019). In order to explore ways to improve the technoeconomic feasibility of *Phaeodactylum* biorefinery, the carbohydrates from the two morphotypes of *P. tricornutum* cells were characterised over time.

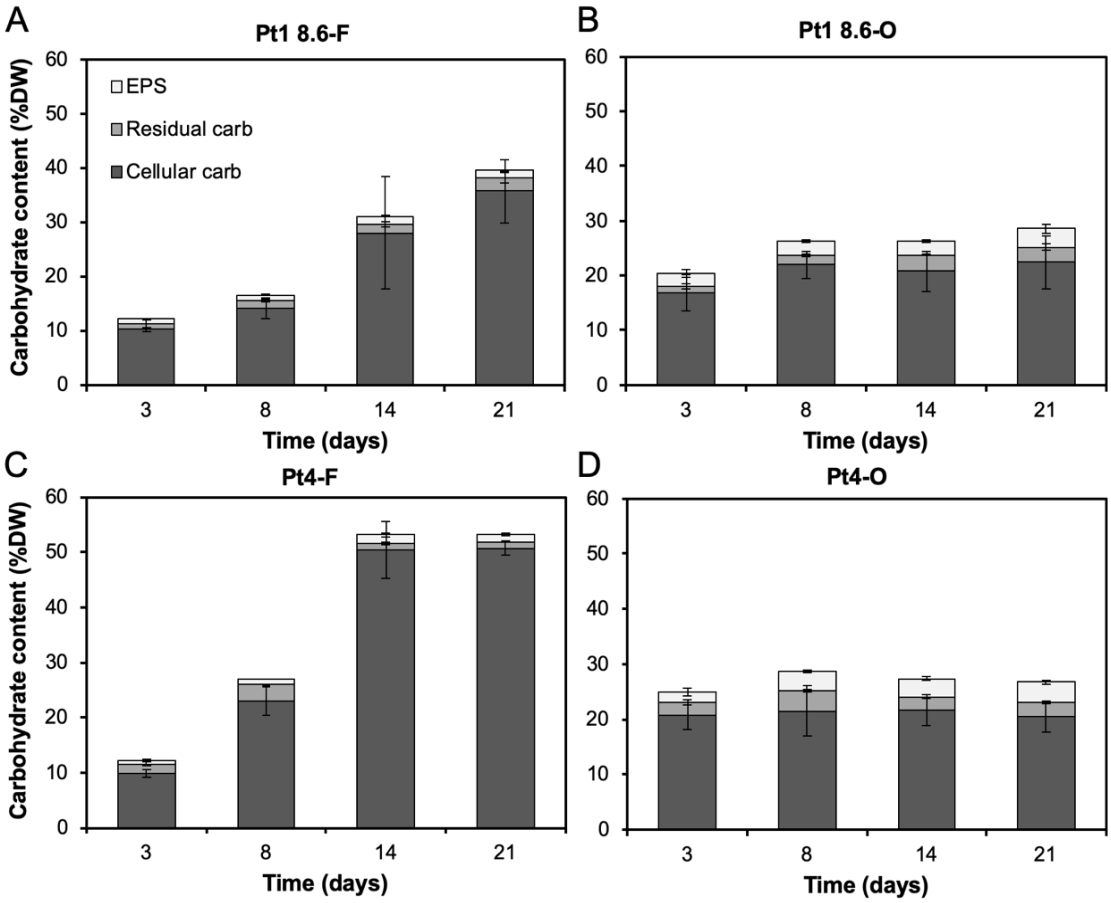

Figure 4-10 Carbohydrate content from two morphotypes of *P. tricornutum* cells quantified with the PSA method.

The cellular carbohydrate, residual carbohydrate and EPS content determined by the PSA assay on a dry weight (DW) basis from fusiform (F) or oval (O) cell cultures of Pt1 8.6 (A, B) and Pt4 (C, D). Data are shown as mean ± one standard deviation from three biological replicates.

With the PSA assay described in Chapter 2, section 2.2.5, the contents of three carbohydrate fractions including exopolysaccharides (EPS), soluble cellular carbohydrate and residual carbohydrate were determined. The cellular carbohydrate content in fusiform cell cultures grown in f/2 medium showed a 3.5-fold change, rising from 10.2% DW to 35.7% DW in Pt1 8.6 and a 5.1-fold change, increasing from 9.9% DW to 50.7% DW in Pt4 over 21 days cultivation (Figure 4-10 A & C and Table 4-2). However, no significant changes were observed in oval cell cultures, where the cellular carbohydrate content was stabilised at approximately 21% DW in both strains under the tested conditions (Figure 4-10 B & D and Table 4-2). The residual sugar remaining in the final pellet was quantified as well in order to check the

degree of carbohydrate extraction. As shown in Figure 4-10, a low residual carbohydrate amount of 1.0-3.8% DW was determined for both fusiform and oval *P. tricornutum* cultures, implying that almost all the carbohydrate was extracted from either fusiform or oval cells. Since oval cells are known to secrete exopolymers (Tesson et al., 2009a), the released media-soluble polysaccharides were investigated. It was found that oval cells produced more EPS than fusiform cells (1.9-3.8% DW versus 0.7-1.6% DW) in the tested conditions (Figure 4-10).

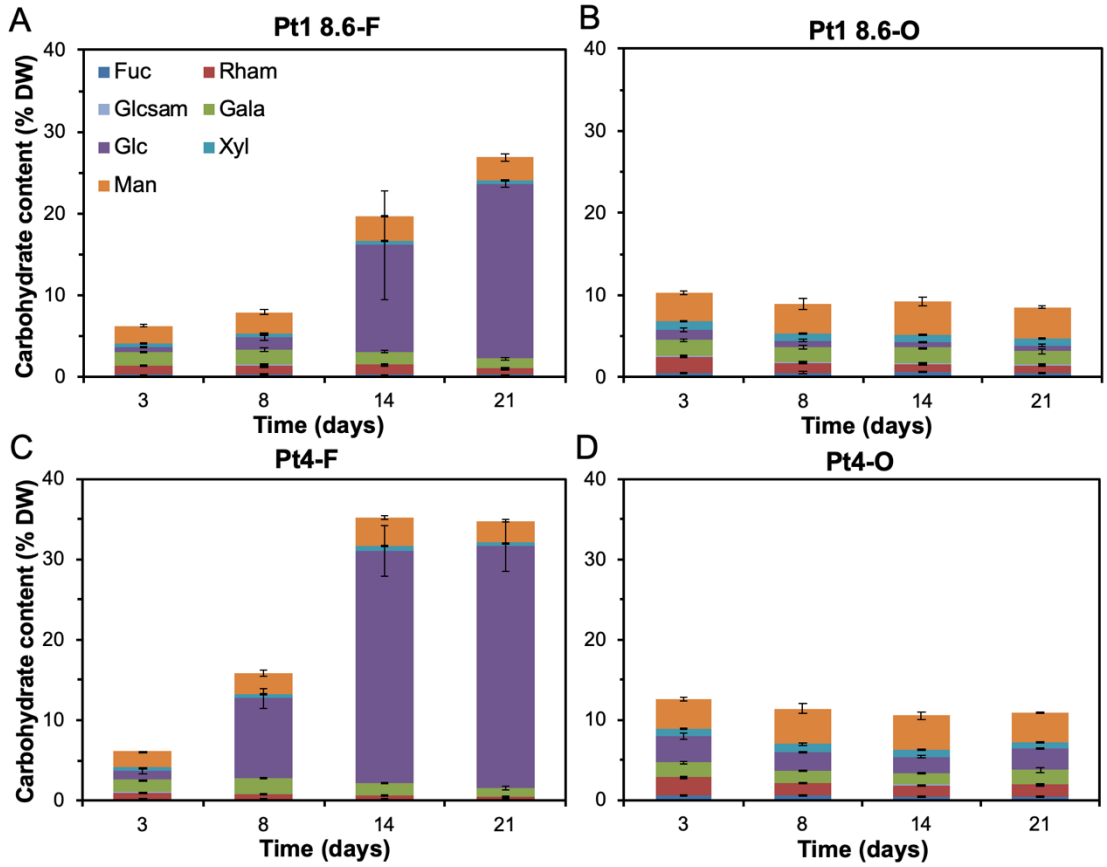

Figure 4-11 Carbohydrate content and profiles in two morphotypes of *P. tricornutum* cells.

Monosaccharide composition of the cellular carbohydrate fraction quantified by the HPAEC method from fusiform (F) or oval (O) cell cultures of Pt1 8.6 (A, B) and Pt4 (C, D). Fuc: fucose, Rham: rhamnose, Glcsam: glucosamine, Gala: galactose, Glc: glucose, Xyl: xylose and Man: mannose. Data are shown as mean ± one standard deviation from three biological replicates. DW, dry weight.

The cellular carbohydrate content is much higher than the other two detected carbohydrate fractions and its composition was further analysed using the

HPLC method in order to quantify the easily-fermentable carbohydrates in *P. tricornutum* and to gain some insights into differences between fusiform and oval cells. A similar trend of the rising total cellular carbohydrate content in fusiform cell cultures (6.3-26.9% DW in Pt1 8.6 and 6.1-35.2% DW in Pt4) but stable levels in oval cell cultures (~9% in Pt1 8.6 and ~11% in Pt4) over time was observed for both strains in the tested conditions (Figure 4-11). However, the values obtained by the HPLC method are lower than those quantified from the PSA assay (Figure 4-10). This is most probably due to the glucose-equivalent quantification of total sugar in the PSA method which could overestimate carbohydrate content (Templeton et al., 2012). Another reason might be due to the omission of tiny unclassifiable peaks and other undetectable carbohydrates from the HPLC method causing underestimation of carbohydrate content.

The results indicated that carbohydrate was accumulated significantly in fusiform *P. tricornutum* cells grown in f/2 medium with culture age, in agreement with previous observations in this species and other microalgae (Liang et al., 2006, Ho et al., 2013). This could also be induced by the nutrient limitation in f/2 medium during log phase, which has been shown to redirect the photosynthetic carbon flow into N-deficient compounds, resulting in enhanced biosynthesis and accumulation in storage compounds like carbohydrates and lipids in microalgal cells (Breuer et al., 2012, Pancha et al., 2014). Interestingly, before carbohydrate accumulation occurs (day 3), significantly higher total cellular carbohydrate content was observed in oval cell cultures than in fusiform cell cultures for both strains ($p<0.05$) (Figures 4-10 & 4-11), which might reflect the differences in structural carbohydrate between fusiform and oval cell morphotypes.

Carbohydrate profile analysis demonstrated that the major monosaccharides detected in either fusiform or oval cells of Pt1 8.6 and Pt4 were fucose, rhamnose, galactose, glucose, xylose and mannose (Figure 4-11), consistent with observations reported previously (Templeton et al., 2012). It was shown that the increase in cellular carbohydrate content from fusiform cell cultures resulted mainly from the accumulation of glucose, which constituted

approximately 80% and 87% of total cellular carbohydrate in Pt1 8.6 and Pt4 respectively by the end of cultivation (Figure 4-11 A & C). By contrast, no glucose accumulation was observed in oval cell cultures of both strains under the tested conditions. It is known that storage carbohydrate in *P. tricornutum* cells is present in the form of β-D-1,3-glucan, called chrysolaminarin which is a polymer of glucose molecules (Ford and Percival, 1965a). The result suggested that fusiform cells grown in f/2 medium have potential for bioethanol production through glucose fermentation. Additionally, Pt4 was found to accumulate higher levels of glucose more rapidly than Pt1 8.6. This implies that strains have different physiological properties and it is essential to conduct comparison to screen out the optimal strain for a specific application.

Interestingly, significantly higher amounts of mannose, xylose, and fucose were observed from oval cells (~ 4%, 1% and 0.6% DW respectively) compared to fusiform cells (~ 3%, 0.5% and 0.3% DW respectively) in both strains ($p<0.05$) (Figure 4-11). Mannose was the predominant monosaccharide prior to glucose accumulation in both fusiform and oval *P. tricornutum* cells. Detailed monosaccharide analysis in *P. tricornutum* has shown that mannose is generally dominant in alkali soluble fraction, residual insoluble fraction and cell frustule fraction (Willis et al., 2013, Abdullahi et al., 2006). Moreover, glucuronomannan is the main polysaccharide backbone of *P. tricornutum*'s cell wall (Le Costaouec et al., 2017, Ford and Percival, 1965b). In agreement with a previous report showing the activated biosynthesis of glucuronomannan in oval cells of Pt3 (Ovide et al., 2018), the observed higher mannose content from oval cells than from fusiform cells might suggest the differences in cell wall between fusiform and oval morphotypes.

4.3.6 Overview on biochemical profiles from fusiform and oval *P. tricornutum* cells

The profiles of total pigment, protein, lipid and carbohydrate from fusiform and oval *P. tricornutum* cultures over cultivation time were summarised in Table 4-2 to give an overview on the biochemical composition.

Table 4-2 Biochemical profile from fusiform and oval *P. tricornutum* cultures.

% DW	Time (day)	Pigment	Protein	Lipid	Carbohydrate [b]	Total
Pt1 8.6-F	3	2.31±0.25	14.94±1.34	6.71±0.36	10.17±0.36	34.13
	8	1.58±0.10 [a]	15.98±0.86	9.83±0.33	14.00±1.78	41.39
	14	0.95±0.06	12.36±0.62	13.51±1.94	27.94±10.38	54.76
	21	0.59±0.02	8.12±0.46	22.93±2.35	35.73±5.83	67.37
Pt1 8.6-O	3	1.90±0.18	17.98±1.40*	7.97±0.18	16.76±3.28*	44.61
	8	1.92±0.10 [a]	24.06±1.07	7.94±0.17	21.94±2.58	55.86
	14	2.76±0.09	23.27±1.48	8.17±0.39	20.81±3.62	55.01
	21	3.04±0.14	23.00±1.83	6.92±0.50	22.46±4.89	55.42
Pt4-F	3	2.10±0.17	13.85±1.01	8.25±0.62	9.88±0.74	34.08
	8	1.68±0.11 [a]	14.12±0.35	8.62±0.43	23.08±2.58	47.50
	14	1.17±0.08	11.69±0.94	13.72±0.50	50.35±5.14	76.93
	21	0.72±0.02	8.65±0.49	18.83±0.48	50.72±1.14	78.92
Pt4-O	3	1.83±0.10	19.39±1.45**	8.50±0.20	20.70±2.44**	50.42
	8	2.52±0.26 [a]	20.43±1.78	6.66±0.31	21.45±4.58	51.06
	14	3.14±0.25	20.78±1.28	6.74±0.15	21.68±2.74	52.34
	21	3.57±0.16	21.59±0.77	6.71±0.34	20.50±2.86	52.37

Data were shown as mean ± one standard deviation from three biological replicates.
[a] Cells were sampled on day 7 instead of day 8 for pigment content measurement.
[b] Carbohydrate content showed here is the cellular carbohydrate fraction quantified using the PSA method.
When compared the biochemical profiles on day 3 from oval cells with those from fusiform cells of each strain, * $p<0.05$, ** $p<0.01$.

Over 21 days cultivation in batch cultures, the total amount of pigment, protein, lipid and carbohydrate from fusiform *P. tricornutum* cells grown in f/2 medium increased from 34.1% DW to 67.4% DW in Pt1 8.6 and from 34.1% DW to 78.9% DW in Pt4. By contrast, for oval *P. tricornutum* cells maintained

in M & M medium, only 45-56% of the dry biomass was accounted for (Table 4-2). Other materials such as nucleic acids (DNA, RNA), intermediates of metabolism (e.g. citrate and malate), silicate/silica and mineral elements (e.g. Na, K, Ca, Mg, Fe, S, Zn) may account for the missing percentage of dry biomass (Rebolloso-Fuentes et al., 2001). A high ash (inorganic matter) content of up to 58% has been reported for *P. tricornutum* (Fernandez-Reiriz et al., 1989, de Ciencias, 1995). Ash-free dry weight (AFDW) is also generally used as a basis for quantification of biochemical composition. In addition, the extraction efficiency, incomplete hydrolysis, degradation and quantification methods could have a great influence on the amounts obtained.

The observed changes in cell morphotype and biochemical composition in *P. tricornutum* were induced by culture media. In order to gain an insight into the intrinsic link between cell morphotype and biochemical composition, the biochemical profiles from fusiform and oval *P. tricornutum* cultures sampled on day 3 were compared. Cells were at exponential phase on day 3, which minimises the effects of nutrient deficiency on biochemical composition. The results showed that for both Pt1 8.6 and Pt4, significantly higher protein and carbohydrate content (% DW) were obtained from oval cells than from fusiform cells ($p<0.05$) and no significant differences in total pigment and TFA content were observed between them ($p>0.05$) (Table 4-2). This implied the biochemical differences between fusiform and oval *P. tricornutum* cells. Despite the observations, the results are cofounded between cell shape and variables of N and P availability. From Chapter 3, there was no significant cell morphological change in f/2 medium with increased N or P (Figure 3-11). f/2 medium with added N and P could therefore be used in the future to maintain the fusiform morphotype for further comparison with the oval morphotype maintained in M & M medium. This would eliminate the effects of N and P limitation and direct the outcomes more to differences in *P. tricornutum* morphotypes.

Harvest time is one of the key parameters for optimal product yield. Here, the cultivation time was shown to have little effect on biomass composition in oval *P. tricornutum* cells, which could be attributed to the high initial nutrient

(11.76 mM nitrate and 0.57 mM phosphate) in M & M medium and implied the actively growing status of cells cultured in this medium under the conditions studied. However, from growth curves, early stationary phase seemed to be reached in oval *P. tricornutum* cultures after 21 days cultivation (Figure 4-1). This suggested again that oval cell growth under this relatively high nutrient condition might be limited by other factors like carbon and light as inorganic carbon would become limited rapidly in relatively high light and high cell density conditions and the high cell density in flasks would cause self-shading. In contrast to our results, a more than 5-fold higher dry biomass concentration of 4.05 g L^{-1}, a decrease in fucoxanthin content and an increase in total lipid content over time were observed in *P. tricornutum* grown under 14.5 mM nitrate and 0.88 mM phosphate at a large scale of 50 L aerated with 1% CO_2-enriched air (Gao et al., 2017). Further experiments such as an analysis of nutrient content, particularly nitrate and phosphate, remaining in culture media and optimisation of cultivation parameters would be helpful for understanding the morphological and biochemical responses of *P. tricornutum* to M & M medium and would also be important for scale-up bioprocess design.

4.4 Conclusion

In this chapter, the growth kinetics and biochemical profiles for fusiform and oval *P. tricornutum* cells maintained in f/2 medium and M & M medium respectively were investigated to gain insights into their industrial exploitation. Similar growth rates were observed for Pt1 8.6 fusiform and oval cell cultures whereas a higher maximum specific growth rate was obtained for Pt4 fusiform cell cultures compared to Pt4 oval cell cultures. Despite that, higher biomass yields were obtained from oval cell cultures than from fusiform cell cultures for both strains after three weeks cultivation. This indicated that cultivation in M & M medium under the constant shaking condition as proposed in Chapter 3 was an effective and practical method for high oval cell production in liquid cultures.

From the perspective of industrial application, fusiform *P. tricornutum* cells grown in f/2 medium were shown to be a potential feedstock for biodiesel and bioethanol production as lipids and carbohydrates, particularly neutral lipid and glucose, were significantly accumulated in fusiform cells with culture time. On the other hand, pigments, particularly chlorophyll *a* and fucoxanthin, were markedly accumulated in oval cell cultures over 21 days cultivation and higher protein content (% DW) was obtained from oval cells than from fusiform cells in the tested conditions. This suggested that oval *P. tricornutum* cells maintained in M & M medium may be preferable for high pigment and protein production. Additionally, both fusiform and oval cells can be used for EPA production. Knowledge on biochemical profiles in various cell morphotypes is essential for nutritional value evaluation and optimisation of *P. tricornutum* for industrial biotechnology. By characterising the product accumulation in different cell morphotypes grown in their respective culture medium, this work provides implications for the bioprocessing of *P. tricornutum* in terms of cultivation and harvest time and also provides a reference for further improvement of overall biomass and classes of product yields from *P. tricornutum.*

Statistical analysis of the biochemical profiles on day 3 showed that significantly higher protein and carbohydrate content (% DW) were obtained from oval cells than from fusiform cells and there were no significant differences in total pigment and TFA content between them. Particularly, higher amount of mannose (% DW) was observed from oval cells than from fusiform cells, implying the potential differences in cell wall between them. Our work offers an insight into the biochemical differences between oval and fusiform morphotypes and lays a foundation for deeper exploration at genetic levels.

5 Ultra scale-down mimics for cell harvest and disruption of two *Phaeodactylum tricornutum* morphotypes

5.1 Introduction

The polymorphic diatom, *P. tricornutum* appears to be an attractive platform for the manufacture of high-value compounds such as EPA, fucoxanthin and recombinant proteins for industrial, medical and nutritional applications. A novel way to regulate cell morphology of *P. tricornutum* in liquid cultures was developed in this study, as described in Chapters 3. Stable cultures predominantly oval cells of Pt1 8.6 and Pt4 ecotypes were well-maintained in Mann and Myers' medium. The subsequent biochemical composition analysis described in Chapter 4 showed the different bioproduct accumulation in different *P. tricornutum* morphotypes depending on growth conditions. Specifically, oval cells cultured in M & M medium were promising for high pigment and protein production whereas fusiform cells grown in f/2 medium were shown to highly accumulate carbohydrate and lipid over 21 days cultivation. In addition, successful genetic transformation of all three cell morphotypes by microparticle bombardment has been achieved at highly similar efficiencies (De Martino et al., 2007). Considering the potential of different *P. tricornutum* morphotypes for industrial biotechnology, it is important to understand the implications of cell morphotype on bioprocessing of *P. tricornutum*.

Downstream bioprocessing plays a significant role for economical *P. tricornutum* biotechnology. After cultivation, harvesting and cell disruption are the essential downstream steps for intracellular product recovery. Centrifugation remains one of the most commonly used methods for harvesting microalgae since large volume of culture broth can be easily processed in a fast and effective way with high recovery efficiency and chemical-free biomass obtained (Singh and Patidar, 2018). However, the high degree of shear forces generated in industrial centrifuges might cause cell damage to sensitive biological materials, and consequently lower the cell recovery and the attainable product productivity (Boychyn et al., 2001). Cell

disruption is a crucial pre-treatment step to rupture the cell wall thereby enhancing extraction efficiency of biomolecules from microalgae. However, the cell wall structure and composition of microalgae is complex and has a significant impact on the disruption efficiency (Alhattab et al., 2019).

Evaluation of the performance of large-scale bioprocessing by direct experimental method is material, time and cost consuming. Ultra scale-down (USD) technologies enable to use experimentation at the millilitre scale to rapidly evaluate the large-scale bioprocessing performance with greater ease and low cost (Rayat et al., 2016). An USD rotating-disc shear device was designed to mimic the hydrodynamic environments characterised in the feed zone of industrial centrifuges by computational fluid dynamics (CFD) (Boychyn et al., 2001, Boychyn et al., 2004). As a consequence, it enables to predict the recovery efficiency with a subsequent bench-top centrifugation. This approach has been successfully applied to assess the effects of shear stress on the physical properties of various biological materials and the effects on the performance of subsequent processing unit operations such as centrifugation, filtration and formulation (Rayat et al., 2016, Mccoy et al., 2010). An USD cell disruption method based on adaptive focused acoustics (AFA) has been used to mimic the high-pressure homogenisation of recombinant *E. coli* for recovery of an antibody fragment and this approach has been verified successfully at pilot scale (Li et al., 2012, Li et al., 2013).

Although *P. tricornutum* with diverse morphotypes exhibits great potential for industrial applications, there has not been a systematic study focusing on the downstream processing of different cell morphotypes. To our knowledge, little is known about the behaviour of diverse *P. tricornutum* morphotypes in response to shear stress occurring in downstream processing such as large-scale centrifugation and no study has been carried out to compare the rupture of various cell morphotypes. In this chapter, the initial steps of downstream processing including harvest and disruption of the obtained fusiform and oval *P. tricornutum* cells were investigated. The USD platform developed at UCL was employed to characterise the robustness of fusiform and oval cells against shear stresses and to predict the cell recovery in large-

scale centrifuges. Subsequently, the cell disruption efficiency of the two morphotypes was studied using the AFA-based USD cell disruption method. This work seeks to gain an insight into the early recovery stages of downstream processing of two *P. tricornutum* morphotypes considering their potential use as expression hosts.

5.2 Materials and methods

All chemicals were purchased from Sigma-Aldrich unless otherwise stated.

5.2.1 Cell cultivation for ultra scale-down studies

As described in Chapter 3, the strains Pt1 8.6 and Pt4 were grown in either f/2 medium (Guillard, 1975) for fusiform morphotype maintenance or in M & M medium (Mann and Myers, 1968) for oval cell maintenance without supplement of silicate. For experimental culture preparation, log-phase cells of Pt1 8.6 and Pt4 grown in f/2 medium or M & M medium were inoculated in 250 mL Erlenmeyer flasks containing 100 mL of respective culture medium with an initial cell density of approximately $1x10^6$ cells mL^{-1}. All cultures were grown under the conditions described in Chapter 2, section 2.2.1. Considering cell amount and time cost, as well as the maximum protein content obtained at late-log phase (section 4.3.3), cultures were sampled on day 7 for cell morphotype abundance, dry biomass concentration and USD bioprocessing analyses.

5.2.2 Ultra scale-down study on centrifugation

An USD rotating-disc shear device followed by bench-top centrifugation was used to evaluate large-scale centrifugation performance (Figure 1-7). The USD shear device (kompAs^{TM}, Gowerlabs Ltd., UK) consists of a 20 mL stainless-steel chamber of 50 mm internal diameter and 10 mm height, fitted with a stainless-steel rotating disc of 40 mm diameter and 1 mm thickness with disc speed 0–18,000 rpm. The disc speed (N, revs s^{-1}) was correlated to the maximum energy dissipation rate (ε, W kg^{-1}) using the CFD derived empirical equation: $\varepsilon=1.7x10^{-3}\ N^{3.17}$, $33<N<250$ (Chatel et al., 2014). Two

conditions, N=6,000 rpm, ε=0.45x10^5 W kg^{-1} and N=12,000 rpm, ε=5.3x10^5 W kg^{-1}, were used to mimic the low shear and high shear stress levels experienced by cells in the feed zone of hydro-hermetic and non-hermetic disc-stack centrifuges respectively. Culture samples (20 mL) were exposed to shear stress for 20 s in the USD shear device to characterise the shear susceptibility of fusiform and oval *P. tricornutum* morphotypes. Shear studies were conducted in biological duplicates.

The cell recovery efficiency was predicted with a following bench-top centrifugation based on the Sigma Theory (Equation 1-3), which was performed using a centrifuge 5424/5424R (Eppendorf, UK) equipped with a 1.5/2.0 mL 24-place rotor (FA-45-24-11). Aliquots of 2 mL (V_{USD}) of the sheared and non-sheared samples were centrifuged at rotational speeds (N) of 10,000 rpm, 8,000 rpm, 6,000 rpm and 4,000 rpm for times (t_{USD}) of 6 min, 5 min, 5 min and 6 min respectively (Table 5-1). The top 60% of the resulting supernatant was recovered without disturbing the sediment for clarification determination. The remaining sheared and non-sheared samples were used for particle size distribution measurement and microscopic examination. Centrifugation conditions used in this study and parameters calculated with Equations 1-3 & 1-4 were summarised in Table 5-1. An example calculation is presented in Appendix.

Table 5-1 Centrifugation conditions and parameters used for cell recovery study

N (rpm)	10,000	8,000	6,000	4,000
t_{USD} (min)	6	5	5	6
Σ_{USD} (m²)	0.648	0.409	0.230	0.104
$\frac{V_{USD}}{C_{USD}t_{USD}\Sigma_{USD}}$ (m s^{-1})	0.86x10^{-8}	1.6x10^{-8}	2.9x10^{-8}	5.4x10^{-8}

5.2.3 Ultra scale-down study on cell disruption

The cell disruption efficiency for the fusiform and oval morphotypes was investigated using a focused acoustic ultrasonicator (Covaris E210, Covaris, USA) (Figure 1-9), as described in previous studies (Blaha et al., 2018, Li et al., 2012). *P. tricornutum* cell pellets from 6-10 mL of cell cultures, corresponding to approximately 1.5 mg biomass in dry weight, were resuspended in 1 mL of PBS buffer (Gibco 10X PBS pH 7.4, Life Technologies, Thermo Fisher Scientific, UK). Cell suspensions were transferred into 1 mL millitubes with AFA fibres (Covaris, USA) and were then subjected to focused acoustic disruption with the following operation conditions: cycles per burst of 1000, power intensity of 10, duty factor of 20% (the percentage of "on" time of each acoustic burst) and water bath at 10 ^{o}C. The impact of treatment time on cell disruption efficiency of the two morphotypes was determined through counting the remaining intact cell number and measuring the released soluble protein content. Particle size distribution was also determined after cell disruption. Cell rupture experiment was conducted in biological triplicates.

5.2.4 Analytical methods

Cell morphotype abundance and dry biomass determination

The method for determining the proportion of each morphotype in *P. tricornutum* cultures was same as described in Chapter 3, section 3.2.1.

The final cell density and dry biomass concentration (g L^{-1}) were measured using the methods detailed in Chapter 2, section 2.2.2.

Clarification and solids remaining determination

The separation efficiency of centrifugation can be described by the degree of clarification (*C*) or the solids remaining (*S*), determined through optical density measurement at 750 nm as follows:

$$\boldsymbol{C}(\%) = \frac{\boldsymbol{OD_f - OD_s}}{\boldsymbol{OD_f - OD_w}} \times \mathbf{100} \qquad \textbf{Equation 5-1}$$

$$\boldsymbol{S}(\%) = \frac{\boldsymbol{OD_s - OD_w}}{\boldsymbol{OD_f - OD_w}} \times \mathbf{100} \qquad \textbf{Equation 5-2}$$

where OD_f is the optical density of the feed sample before shear treatment, OD_s is the optical density of the supernatant of centrifuged samples and OD_w is the optical density of the supernatant of a well-spun sample (prepared by centrifugation at 15,000 rpm for 30 min and used as a baseline measurement).

Particle size distribution, released protein and microscopic analyses

The methods for measuring the particle size distribution and the released protein content and for microscopic examination were described in Chapter 2, sections 2.2.6, 2.2.4 and 2.2.3.

5.3 Results and discussion

5.3.1 Growth of fusiform and oval *P. tricornutum* cells

Upon arrival from CCAP, both Pt1 8.6 and Pt4 strains were maintained in f/2 medium and displayed mainly the fusiform morphotype. Oval cell dominant cultures of the two strains were obtained and maintained in M & M medium, as described in Chapter 3. Fusiform and oval *P. tricornutum* cultures were grown in their respective medium for 7 days at approximately late-log phase (Figure 4-1) and were then sampled for USD studies. As detailed in Chapter 4, although the relatively young cells sampled on day 7 are different to older cells which seem to be more industrially relevant due to the accumulation of lipid and carbohydrate, their protein content reached maximum and meanwhile the lipid and carbohydrate content were more similar between fusiform and oval cells and may thus be suitable for sampling. After 7 days cultivation, the fusiform cell cultures of both Pt1 8.6 and Pt4 contained approximately 95% fusiform cells, plus a small proportion of oval and triradiate cells (Table 5-2). On the other hand, oval cells dominated in oval

cell cultures of Pt1 8.6 and Pt4, representing 75.6% and 100% respectively. In addition, fusiform cell cultures produced higher dry biomass concentration, but lower cell density compared to oval cell cultures on day 7 in both strains (Table 5-2), which is consistent with the growth profiles described in Chapter 4 (Figures 4-1 & 4-2). As demonstrated in Chapter 4, this could be due to the different cell size and biochemical composition between fusiform and oval cells (Table 4-2).

Table 5-2 *P. tricornutum* culture properties on day 7 for USD shear studies.

	Biomass (g L^{-1})	Cell density (x10^6 cells mL^{-1})	F (%)	O (%)
Pt1 8.6-F[a]	0.248±0.003	8.61±0.51	94.82±0.00	4.78±0.02
Pt1 8.6-O[b]	0.155±0.005	9.80±0.08	24.44±2.46	75.56±2.46
Pt4-F[a]	0.240±0.005	8.27±1.39	94.59±0.70	2.90±0.91
Pt4-O[b]	0.178±0.003	14.02±0.24	0.00±0.00	100.00±0.00

Data are shown as mean ± difference from the mean, representing the minimum and the maximum values from two biological replicates.
[a] Fusiform (F) cell cultures were grown in f/2 medium.
[b] Oval (O) cell cultures were grown in M & M medium.

5.3.2 Ultra scale-down prediction of cell recovery from large-scale centrifugation

An USD centrifugation method combining shear treatment in a high-speed rotating-disc device with lab-scale centrifugation has been successfully used for clarification performance prediction of various biological materials in industrial centrifuges (Boychyn et al., 2004, Hutchinson et al., 2006, Rayat et al., 2016, Stoffels et al., 2019). Here, the impact of shear stress depending on the choice of feed zone configuration of disc-stack centrifuges on recovery efficiency of fusiform and oval *P. tricornutum* cells were assessed employing the USD techniques.

Clarification efficiency

In order to mimic the performance of a continuous industrial disc-stack centrifuge operating at diverse flow rates, the USD centrifugation method was applied to determine the clarification efficiency of fusiform and oval cultures of Pt1 8.6 and Pt4 over a range of ratios of equivalent flow rate to settling area ($V/(t\Sigma)$=0.86-5.4x10^{-8} m s^{-1}, Table 5-1). As shown in Figure 5-1, the clarification efficiency decreased with the $V/(t\Sigma)$ ratio showing good linear correlation for non-sheared and sheared *P. tricornutum* samples, despite that such a decrease was not statistically significant for some conditions such as non-sheared and sheared Pt4 oval cell cultures due to the tested narrow $V/(t\Sigma)$ range. Within the range studied, an overall high degree of cell recovery was achieved with the minimum clarification values of 95.9% and 93.4% obtained for Pt1 8.6 fusiform and oval cell cultures, and 97.1% and 97.3% obtained for Pt4 fusiform and oval cell cultures, respectively. A reduction in the clarification performance was observed for *P. tricornutum* cultures after exposure to shear stresses, except for the Pt4 oval cell cultures. Specifically, exposure of cultures to a maximum energy dissipation rate of up to 5.3x10^{5} W kg^{-1} induced an up to 1.03-fold decrease in the clarification efficiency, with a corresponding up to 4.4-fold increase in the level of solids remaining in the supernatant in the range studied (Figure 5-1 A, B & C). The loss of clarification with shear treatment could be attributed to shear stresses leading to breakage of cells or cell aggregates, and consequently an increased proportion of fine particles (Boychyn et al., 2001). However, no significant further reduction in clarification efficiency was observed for high-sheared samples compared to low-sheared samples (Figure 5-1), which is probably due to the declined number of shear-sensitive particles in cultures. An exception is the Pt4 pure oval cell cultures for which little evidence of the clarification performance being affected by the applied shear stresses was observed (Figure 5-1 D), suggesting that oval cells might be potentially more shear tolerant than fusiform cells. Contrastingly, Pt1 8.6 oval cell cultures seemed to be sensitive to shear treatment, which might be attributed to the presence of 24% fusiform cells in the cultures.

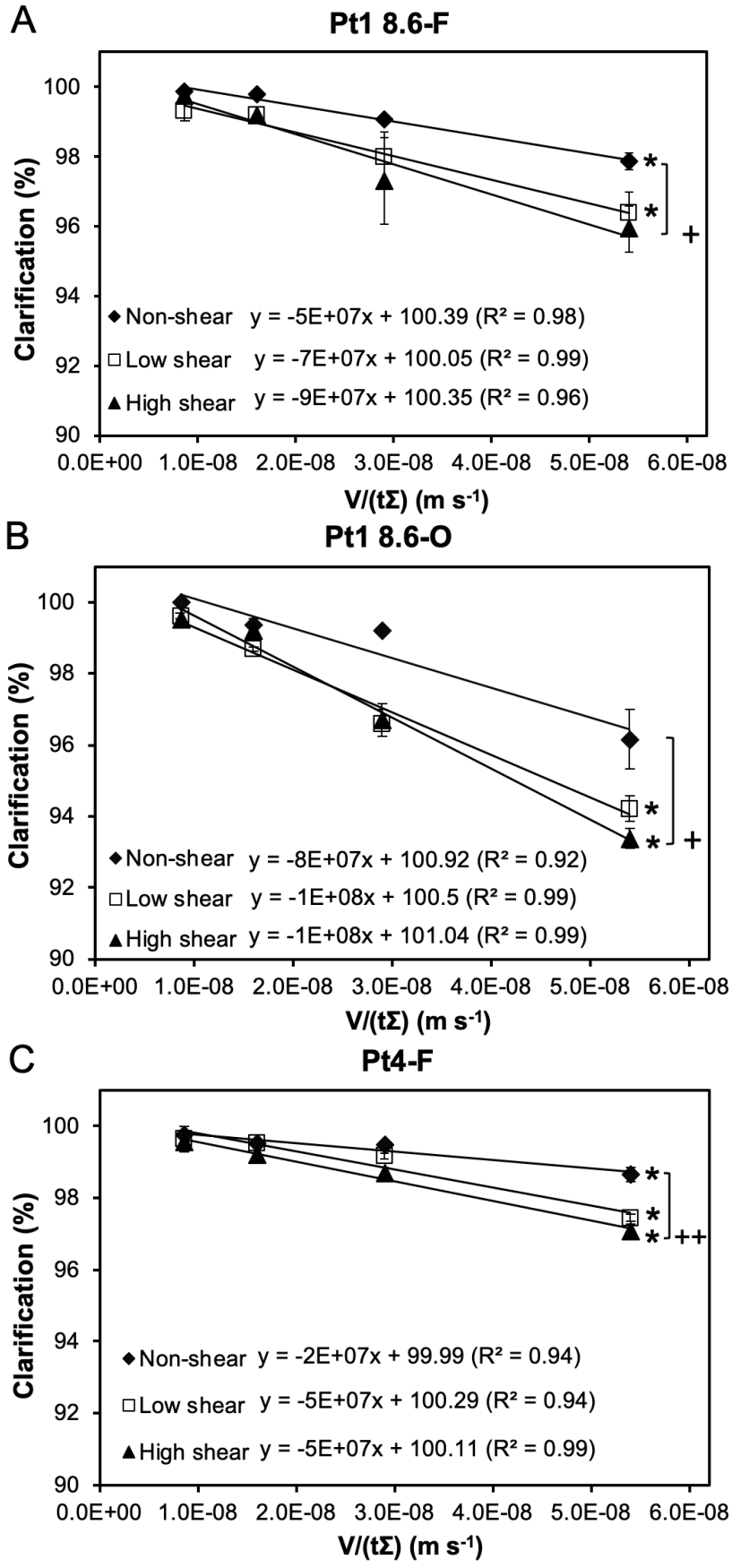
A
Pt1 8.6-F
Clarification (%)
100
98
96
94
92
90
0.0E+00
1.0E-08
2.0E-08
3.0E-08
4.0E-08
5.0E-08
6.0E-08
V/(tΣ) (m s-1)
Non-shear y = -5E+07x + 100.39 (R² = 0.98)
Low shear y = -7E+07x + 100.05 (R² = 0.99)
High shear y = -9E+07x + 100.35 (R² = 0.96)
*
*
+
B
Pt1 8.6-O
Clarification (%)
100
98
96
94
92
90
0.0E+00
1.0E-08
2.0E-08
3.0E-08
4.0E-08
5.0E-08
6.0E-08
V/(tΣ) (m s-1)
Non-shear y = -8E+07x + 100.92 (R² = 0.92)
Low shear y = -1E+08x + 100.5 (R² = 0.99)
High shear y = -1E+08x + 101.04 (R² = 0.99)
*
*
+
C
Pt4-F
Clarification (%)
100
98
96
94
92
90
0.0E+00
1.0E-08
2.0E-08
3.0E-08
4.0E-08
5.0E-08
6.0E-08
V/(tΣ) (m s-1)
Non-shear y = -2E+07x + 99.99 (R² = 0.94)
Low shear y = -5E+07x + 100.29 (R² = 0.94)
High shear y = -5E+07x + 100.11 (R² = 0.99)
*
*
*
++

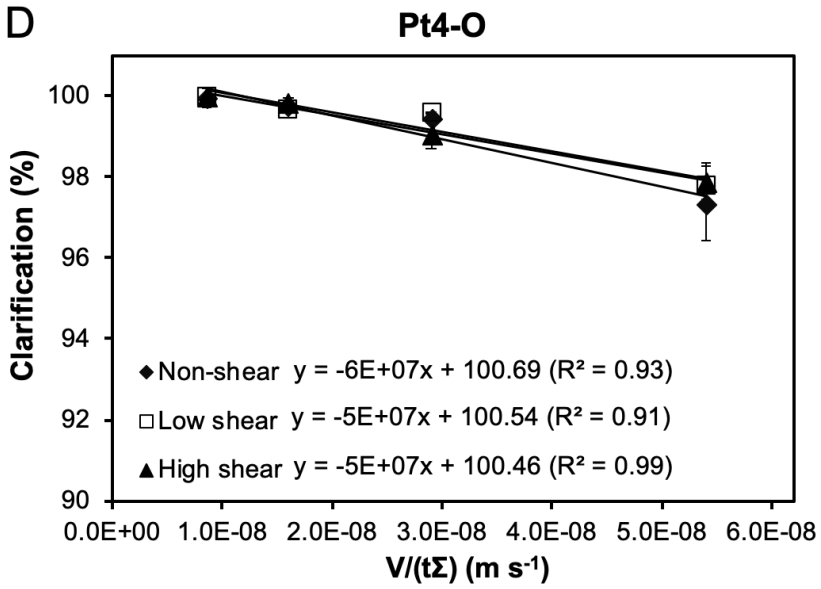

Figure 5-1 Clarification efficiency of two morphotypes of *P. tricornutum* cultures after ultra scale-down centrifugation.

The degree of clarification obtained over a range of ratios of equivalent flow rate to settling area for fusiform (F) or oval (O) cell cultures of Pt1 8.6 (A, B) and Pt4 (C, D), which were exposed to shear conditions: Non-shear (◆); Low shear (□), 0.45×10^5 W kg^{-1} and High shear (▲), 5.3×10^5 W kg^{-1} followed by bench-top centrifugation. Symbols shown are averages from two biological replicates. Error bars represent differences from the means, indicating the minimum and the maximum values. Lines represent the trendline of best fit for each data set with the equation and R^2 value shown. *p<0.05 showing the significant decrease in clarification with increasing V/(tΣ). +p<0.1, ++p<0.05 when comparing the clarification of high-sheared samples to that of non-sheared samples at V/(tΣ)=5.4×10^{-8} m s^{-1}.

Typical values of V/(tΣ) ranging from 10^{-9} m s^{-1} to 10^{-7} m s^{-1} are used to mimic an industrial centrifuge operating at low to high flow rates and typical values of Σ_{LS} for large-scale centrifuges are 500-5000 m^2 (Rayat et al., 2016). Our results indicated a high recovery efficiency of *P. tricornutum* cells under industrial centrifugation conditions. Recovery of Pt4 oval cells through centrifugation was shown to be highly effective irrespective of shear stress. According to Stokes' law (Equation 1-1), the sedimentation rate of a particle is influenced by the density difference between the solids and liquid phase, the viscosity and the particle size and shape. It has been reported that oval cells with smaller size tend to sink, having a higher sedimentation rate compared to fusiform and triradiate cells which are larger and more buoyant (De Martino et al., 2011). Due to the high centrifugation performance (>97%) obtained here, the differences in clarification between Pt4 oval and fusiform

cell cultures were not statistically significant (Figure 5-1 C & D). The superior separative advantage of Pt4 pure oval cell cultures during large-scale centrifugation might be exhibited at a lower separation capability (e.g., $V/(t\Sigma) > 6x10^{-8}$ m s^{-1}). Pt1 8.6 oval cell cultures are mixtures of oval and fusiform morphotypes (Table 5-2), which might influence the homogeneity leading to a hindered settling effect and thus a poorer clarification compared to the other three types of cell cultures (Figure 5-1).

Particle size distribution

In order to gain an insight into the susceptibility of *P. tricornutum* morphotypes to the applied shear stress, particle size distribution for non-sheared and sheared samples was analysed. Fusiform cell cultures of Pt1 8.6 and Pt4 were abundant with approximately 95% fusiform cells (Table 5-2) and showed a multimodal size distribution (Figure 5-2 A & C). The fusiform morphotype is approximately 15-35 µm in length and 2.5-5 µm in width (De Martino et al., 2007, Wilson, 1946). Therefore, the bimodal size distribution in the 2-35 µm range probably result from the distinct differences between the length and the width of fusiform cells. Particles larger than 35 µm could result from cell aggregation. Exposure of the fusiform cell cultures of both strains to a maximum energy dissipation rate of up to $5.3x10^5$ W kg^{-1} led to an increase in the volume of small particles and the disappearance of large particle aggregates. For example, the volume of particles in the 2-10 µm range increased from 59.1% to 74.2% in Pt1 8.6 and from 57.1% to 72.1% in Pt4 and the percentage of particles smaller than 35 µm increased from 87.5% to 97.8% in Pt1 8.6 and from 94.9% to 99.8% in Pt4 after high shear treatment.

The oval cell is two to three times smaller than the fusiform one, being 6-10 µm in length and 2.5-5 µm in width (De Martino et al., 2007). The Pt1 8.6 oval cell cultures had a larger volume of particles in the 2-10 µm range (70.9%) compared to those from fusiform cell cultures (Figure 5-2 A, B & C). Furthermore, a second discernible peak in the 10-35 µm range was observed (Figure 5-2 B), which could be derived from the fusiform cells (24%) and cell aggregates present in Pt1 8.6 oval cell cultures. By contrast, only oval cells

were observed in Pt4 oval cell cultures (Table 5-2), which showed a sharp peak in the 2-10 μm range containing 89.6% of particles. The second peak observed in the 10-100 μm range is likely due to oval cell aggregation (Figure 5-2 D). Similar to fusiform cell cultures, shear stress induced an increase in the proportion of small particles and the disappearance of large particle aggregation in oval cell cultures. After high shear treatment, the volume of particles in the 2-10 μm range increased to 85.4% in Pt1 8.6 and to 99.5% in Pt4, resulting in a monomodal size distribution for Pt4 pure oval cultures. The volume of particles smaller than 35 μm increased from 97.3% to 99.9% in Pt1 8.6 oval cell cultures.

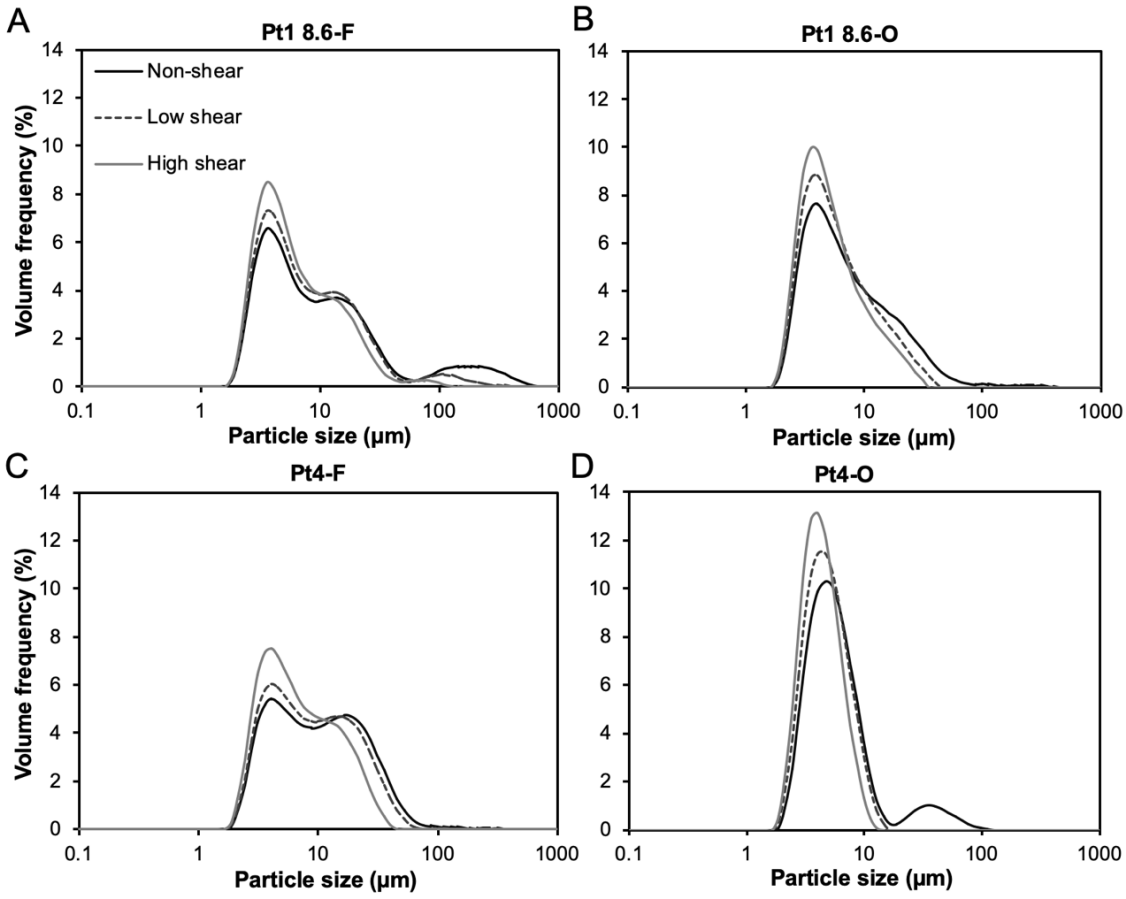

Figure 5-2 Particle size distribution of two morphotypes of *P. tricornutum* cultures after shear treatment in the USD shear device.

Representative particle size distribution for fusiform (F) or oval (O) cell cultures of Pt1 8.6 (A, B) and Pt4 (C, D) after being exposed to shear conditions: Non-shear (black solid line); Low shear (dash line), 0.45×10^5 W kg^{-1} and High shear (grey solid line), 5.3×10^5 W kg^{-1}.

The obtained changes in clarification efficiency could be reflected by the changes in particle size. For instance, the volume of particles in the 2-10 μm range increased by more than 14.5% for Pt1 8.6 cultures and Pt4 fusiform cell cultures, compared to the smaller change of 9.8% for Pt4 oval cell cultures after high shear treatment. This trend becomes more evident when it comes to the change in the parameter of D_{90} (the size value below which 90% of the particles lies) induced by shear stress (Table 5-3). After high shear treatment, the D_{90} value decreased by only 4 μm for Pt4 oval cell cultures, compared to the change of more than 10 μm for the other three types of cultures. Therefore, the observed little change in clarification efficiency for Pt4 oval cell cultures after shear treatment (Figure 5-1 D) may be attributed to its smaller change in particle size.

Table 5-3 Effect of shear stress on the parameter of D_{90} for fusiform (F) or oval (O) cell cultures of Pt1 8.6 and Pt4.

D_{90}, μm	Pt1 8.6-F	Pt1 8.6-O	Pt4-F	Pt4-O
Non-shear	55.7±27.6	24.0±0.8	30.7±2.2	11.7±0.8
Low shear	27.2±0.5	16.1±0.8	25.9±2.0	8.9±0.1
High shear	20.6±0.5	13.8±0.1	19.7±0.6	7.5±0.0

D_{90}, the size value below which 90% of the particles in a sample suspension lies. Data are shown as mean ± difference from the mean, representing the minimum and the maximum values from two biological replicates.

Microscopy and released protein

The particle size distribution analysis suggested the disruption of large particle aggregates (>35 μm) by shear stress. However, there is little evidence of cell breakage under the tested shear conditions as no distribution of fine particles below 2 μm which would be typical of cell debris was observed for either fusiform or oval cell cultures (Figure 5-2). Microscopic examination confirmed the presence of cell aggregates in non-sheared cultures and their dissociation in high-sheared samples (Figure 5-3). Similarly, no evident cell damage was observed under microscopy, except that one Pt1

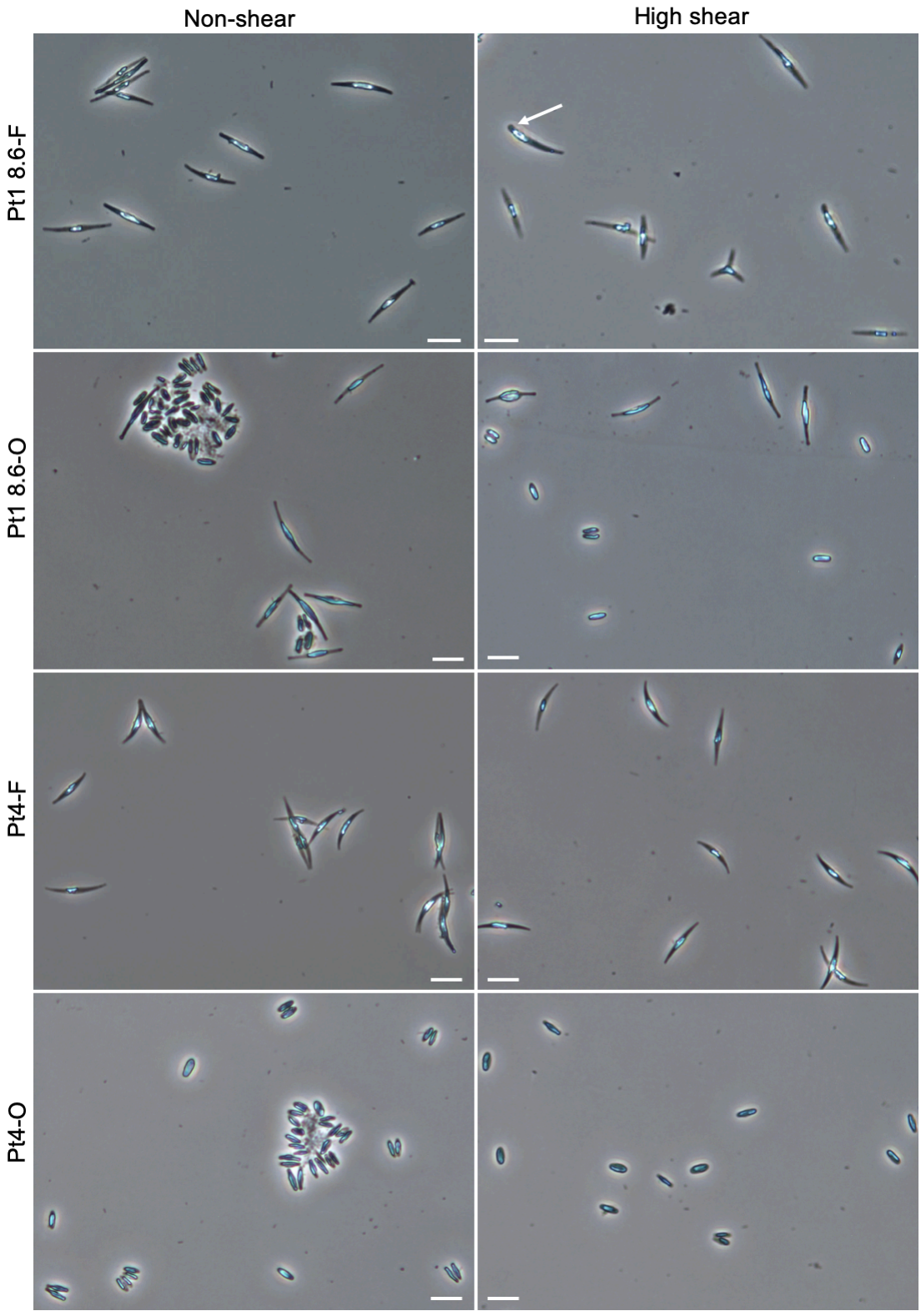

Figure 5-3 Microscopic images of *P. tricornutum* cells before and after shear treatment.

Representative micrographs of cells sampled from fusiform (F) or oval (O) cell cultures of Pt1 8.6 and Pt4 after exposure to Non-shear and High shear (5.3×10^5 W kg^{-1}) conditions. White arrow indicates the observed one-arm fusiform cell. Scale bars, 20 μm.

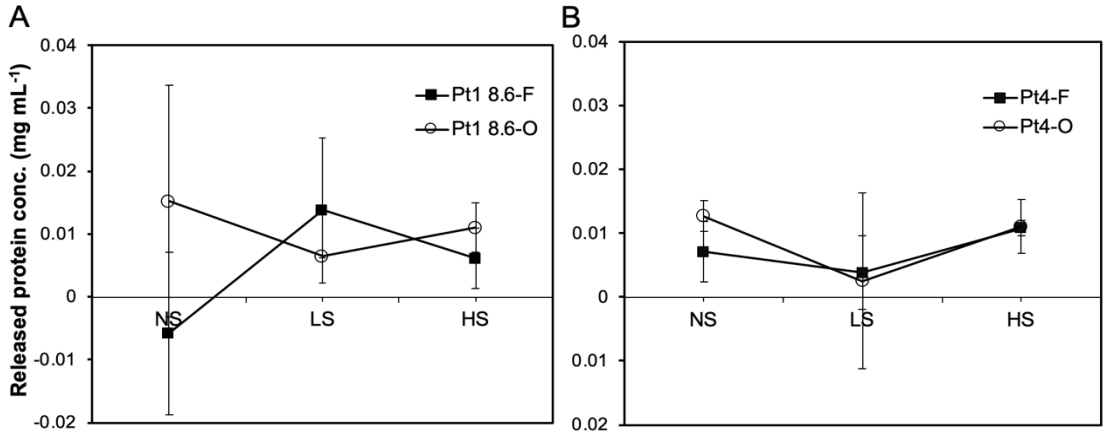

Figure 5-4 Released protein concentration detected in *P. tricornutum* cultures before and after shear treatment.

The released protein content detected in the supernatant of fusiform (F) or oval (O) cell cultures of Pt1 8.6 (A) and Pt4 (B) after being exposed to shear conditions: NS, non-shear; LS, low shear, 0.45×10^5 W kg^{-1} and HS, high shear, 5.3×10^5 W kg^{-1} followed by centrifugation at 21,000 x g for 20 min at 4 ^oC. Protein was measured with Milli-Q water as blank. Data are shown as mean ± one standard deviation from two biological replicates and two technical replicates (n=4). The protein content obtained in the cell-free media (<0.02 mg mL^{-1}) was even lower than the detection limit (0.025 mg mL^{-1}) of the used Bradford assay with high noises when blanked with Milli-Q water. This also reflects that little cell damage occurred after shear treatment as no significant release of protein was observed.

8.6 fusiform cell with one arm was found in the high-sheared fusiform cell cultures (Figure 5-3, white arrow), probably resulting from retraction of arm by cells in response to shear stress or cell damage. The results of protein detection in the supernatant of non-sheared and sheared samples showed no significant increase in the content of released protein after exposure to shear stresses from either fusiform or oval cell cultures (Figure 5-4), as may have been expected if cells were disrupted. The results suggested that both fusiform and oval *P. tricornutum* cells were resistant to the studied shear conditions and the reduced clarification efficiency observed might be indicative of disruption of cell aggregates, which are shear sensitive.

It can be predicted from our results that a high cell recovery efficiency without evident cell damage could be obtained for both fusiform and oval *P. tricornutum* cells when using either a hermetically (low shear stress feed zone) or a non-hermetically (high shear stress feed zone) sealed disc-stack centrifuge. Our results also suggested that fusiform cell cultures were more

shear sensitive than pure oval cell cultures, displaying a reduced clarification efficiency and a larger change in particle size due to the disruption of cell aggregation after exposure to shear stresses. However, both fusiform and oval *P. tricornutum* cells themselves were shown to be resistant to the applied shear conditions (a maximum energy dissipation rate of up to 5.3×10^5 W kg^{-1}) with no significant cell damage and protein release observed. The results do not permit a definite conclusion to be drawn regarding the relative shear sensitivity of the two cell morphotypes. A higher maximum energy dissipation rate of $6\text{-}14 \times 10^5$ W kg^{-1} has previously been reported for other types of industrial centrifuges including multichamber-bowl centrifuge and CARR Powerfuge centrifuge (Boychyn et al., 2001, Boychyn et al., 2004). Exposure of cells to a higher shear stress level in the future may help to characterise the relative shear sensitivity of fusiform and oval *P. tricornutum* morphotypes.

The shear stress tolerance of fusiform *P. tricornutum* cultures has been previously evaluated in photobioreactors (PBRs) during cultivation. In pilot-scale bubble columns and airlift PBRs, an aeration rate of >0.01 m s^{-1} (a specific power input of >98 W m^{-3}) was damaging to Pt3 cells, leading to a decline in biomass concentration (Mirón et al., 2003, Camacho et al., 2001). An agitation speed of >350 rpm (an impeller tip speed of >1.56 m s^{-1}) damaged fusiform Pt3 cells assessed by a decrease in the steady state biomass concentration in aerated (at 1.5 L min^{-1}) continuous cultures (Sobczuk et al., 2006). These studies demonstrated that *P. tricornutum* cells can be damaged by hydrodynamic forces depending on the energy dissipation rate experienced by cells. In addition, solids discharge from large-scale centrifuges could also produce cell damage due to the high impact velocity (Stoffels et al., 2019, Chan et al., 2006). Pilot scale studies of centrifugation would be required to confirm the results predicted from USD centrifugation and confirm that the shear experienced on the discharge would not be problematic.

5.3.3 Ultra scale-down investigation on cell disruption of two *P. tricornutum* morphotypes

The different *P. tricornutum* morphotypes are likely to behave very differently in bioprocessing due to the different cell properties (Martin-Jezequel and Tesson, 2013). Cell disruption is an important step of downstream processing for efficient recovery of intracellular products. However, little is known about the impact of cell morphotypes on disruption of *P. tricornutum*. Here, the Covaris E210 fitted with millitubes was used, enabling the investigation of cell disruption for fusiform and oval morphotypes through focused acoustic ultrasonication at the scale of one millilitre.

Cell breakage and released protein

The effectiveness of *P. tricornutum* cell disruption using acoustics is dependent on the loaded biomass concentration, power input, exposure time, cell morphotype and growth conditions. In this work, fusiform and oval cell pellet suspensions with approximately 1.5 g L^{-1} biomass were treated under the same acoustic conditions except for the sonication time. The degree of cell breakage increased with the sonication time for both fusiform and oval cells of Pt1 8.6 and Pt4 (Figure 5-5). Specifically, exposure of fusiform cells to focused acoustics for 60 s allowed an efficient fusiform cell disruption, with the degree of cell breakage achieving 97.0% for Pt1 8.6 and 95.8% for Pt4 (Figure 5-5 a & e). Accordingly, the released protein content from fusiform cell suspensions increased from 0.06 mg mL^{-1} to 0.22 mg mL^{-1} for Pt1 8.6 and from 0.04 mg mL^{-1} to 0.17 mg mL^{-1} for Pt4 (Figure 5-5 b & f). Further extension of sonication time to 90 s did not lead to a statistically significant increase in either the degree of cell breakage or the released protein content for fusiform cells of the two strains.

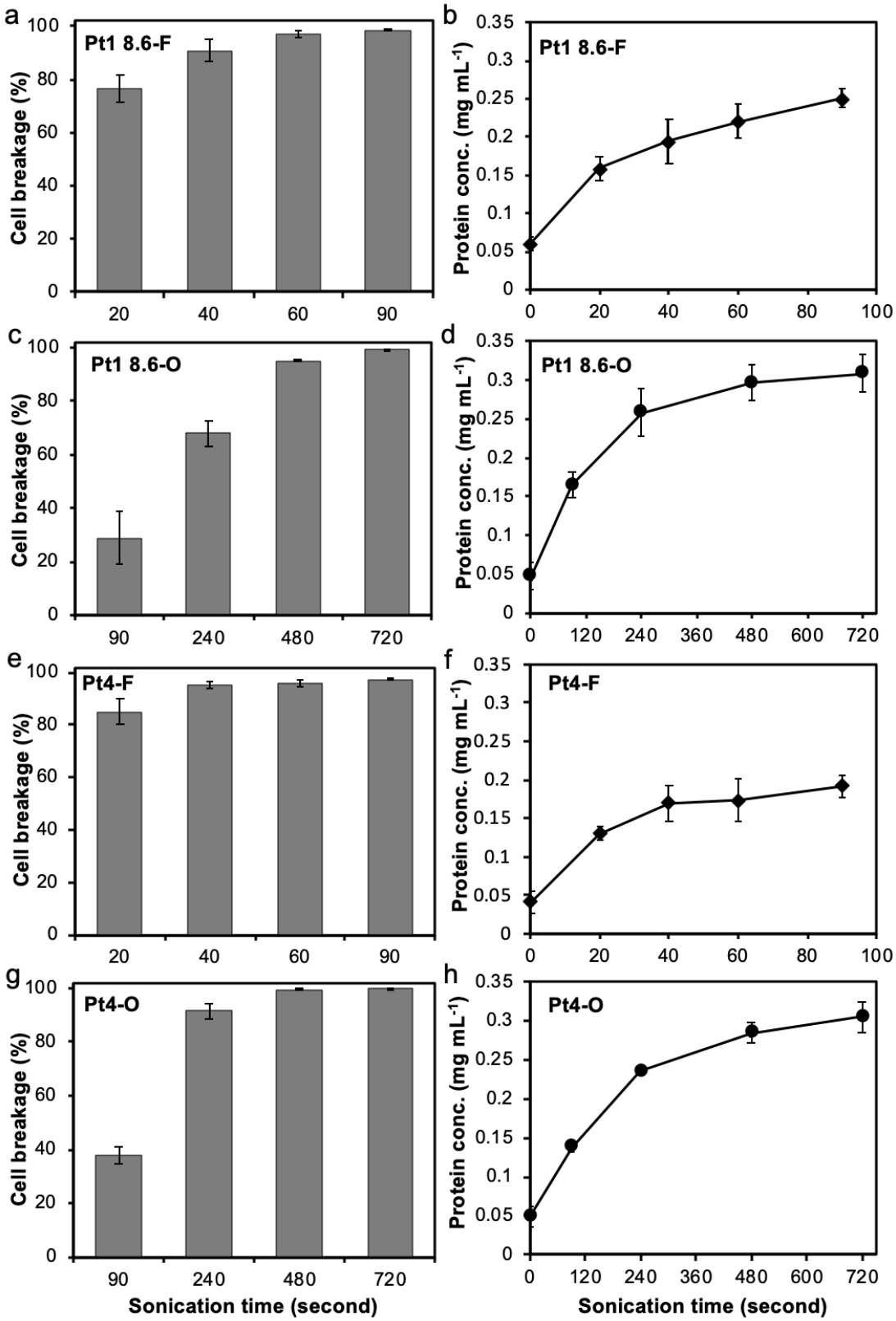

Figure 5-5 Impact of sonication time on cell disruption of two *P. tricornutum* morphotypes by focused acoustics.

Cell breakage efficiency (a, c, e, g) and released protein content (b, d, f, h) detected for fusiform (F) or oval (O) cell suspensions of Pt1 8.6 and Pt4 after being subjected

to focused acoustics for different time. Values are shown as mean± one standard deviation from three biological replicates.

Compared to the high cell breakage levels achieved for fusiform cells at 90 s (98.6% for Pt1 8.6, 97.2% for Pt4), exposure of oval cell samples to focused acoustics for 90 s only gave a cell disruption efficiency of 28.9% for Pt1 8.6 and 38.1% for Pt4 (Figure 5-5 c & g). Meanwhile, the released protein content from oval cell samples was lower than that from fusiform cell samples for both Pt1 8.6 and Pt4. With the extension of sonication time to 8 min, there was a marked increase in the cell breakage efficiency to 95.2% for Pt1 8.6 oval cell samples (containing 88.8% oval cells) and to 99.4% for Pt4 pure oval cell samples. Accordingly, the released protein content from oval cell suspensions increased from 0.05 mg mL^{-1} to 0.30 mg mL^{-1} for Pt1 8.6 and from 0.05 mg mL^{-1} to 0.28 mg mL^{-1} for Pt4 (Figure 5-5 d & h), higher than the maximum released protein content detected from fusiform cell suspensions. This result is consistent with our previous observations described in Chapter 4 showing that oval cells grown in M & M medium produced higher amount of protein than fusiform cells grown in f/2 medium (Figure 4-7).

Particle size distribution

The particle size distribution of the sonicated *P. tricornutum* suspensions was also evaluated for both fusiform and oval morphotypes. The cell suspensions before ultrasonication displayed a similar particle size distribution pattern (Figure 5-6) as observed for the non-sheared cell cultures in the USD centrifugation study (Figure 5-2). Clearly, after treatment of fusiform cells by focused acoustics, there is a shift in the size distribution towards smaller particles. With the sonication time, the second peak in the 10-35 μm range and the third large cell aggregation peak disappeared, resulting in a significant increase in the first peak and in the volume of sub 2 μm fine particles (Figure 5-6 A & C). Combining this result with cell breakage from microscopic cell counting (Figure 5-5 a & e), it was suggested that the disappearance of the second peak in the 10-35 μm range, similar size to the length of fusiform cells, is indicative of fusiform cell breakage and the peak in

the 1-10 µm range after complete cell disruption is probably derived from cell debris and their aggregation.

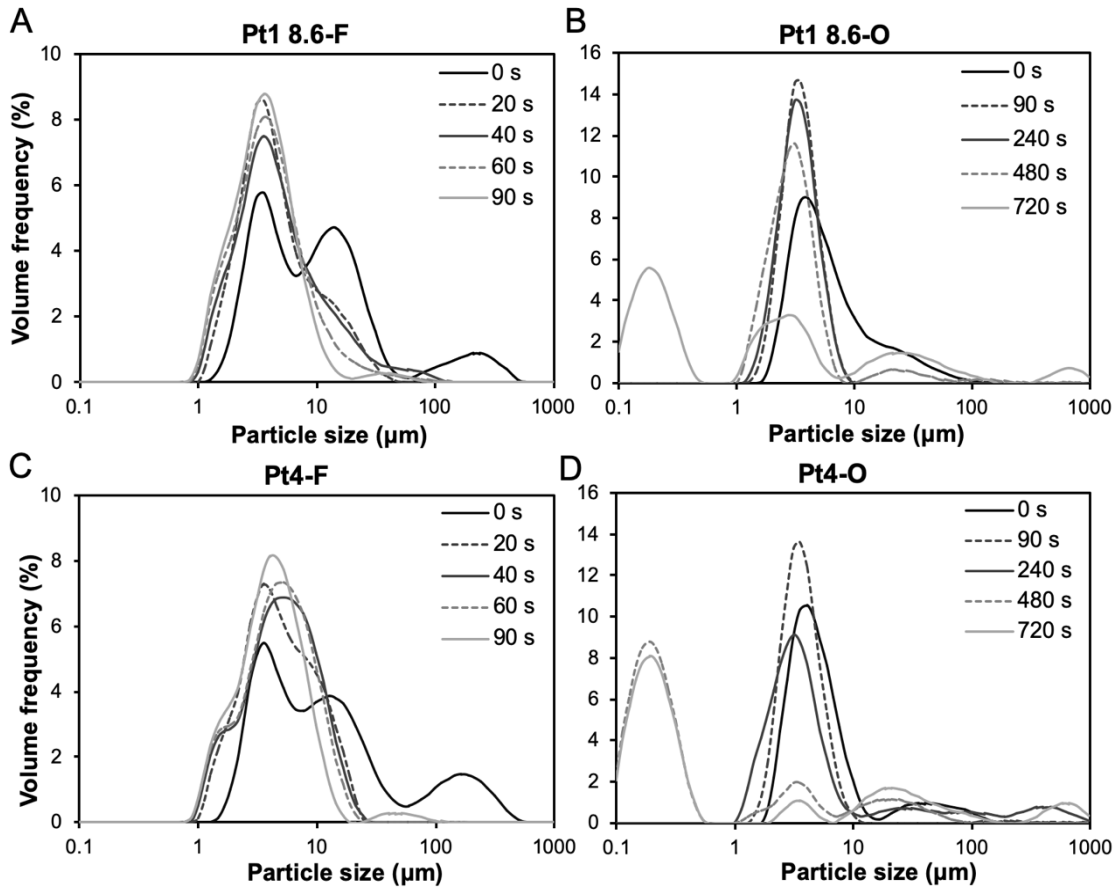

Figure 5-6 Particle size distribution of two morphotypes of *P. tricornutum* suspensions after cell disruption by focused acoustics.

Representative particle size distribution for fusiform (F) or oval (O) cell suspensions of Pt1 8.6 (A, B) and Pt4 (C, D) after exposure to focused acoustic ultrasonication for different time.

Similarly, after treatment of oval cell suspensions by focused acoustics for 90 s, the particles larger than 10 µm were disrupted leading to a sharp peak in the 1-10 µm range (Figure 5-6 B & D), which also implied the breakage of fusiform cells present in Pt1 8.6 oval cell samples. As expected, longer treatment time resulted in a shift towards smaller sizes for oval cell samples of both strains. A large proportion of submicron particles in the 0.1-1 µm range was observed in Pt1 8.6 after 12 min treatment (43.0%) and in Pt4 after 8 min treatment (69.2%), where a cell breakage level of 99% was achieved for both strains (Figure 5-5 c & g). The remaining particles could be

derived from cell debris, aggregation of fine debris or macromolecular precipitation (Figure 5-7, white arrows) (Chatel et al., 2014). Notably, a cell breakage efficiency of above 91% without generation of submicron particles was observed after Pt1 8.6 and Pt4 oval cell samples were sonicated for 8 min and 4 min respectively (Figure 5-5 & 5-6). These results suggest that the trade-off between complete cell disruption to achieve near complete intracellular product release and generation of submicron cell debris needs to be considered, as the subsequent micronised debris removal by centrifugation is challenging.

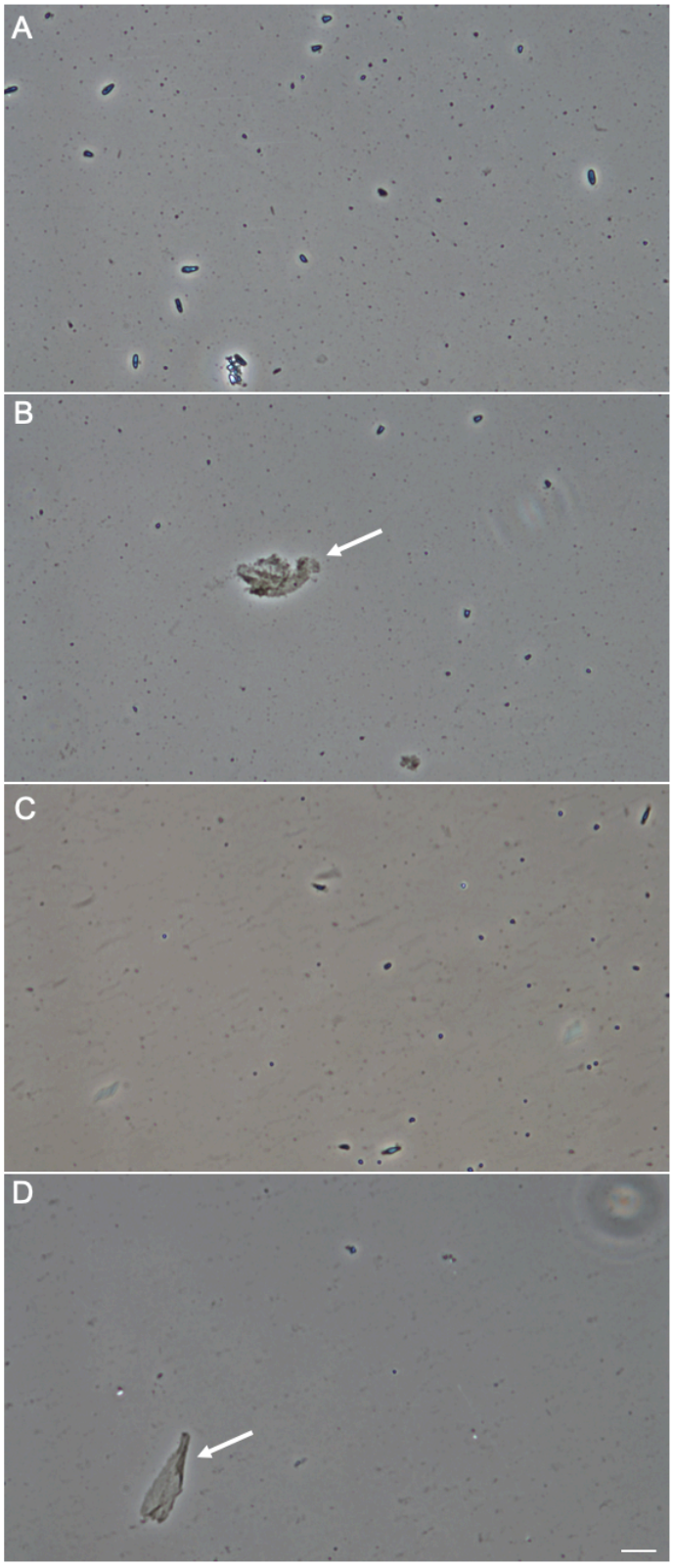

Figure 5-7 Microscopic images of oval *P. tricornutum* suspensions after treatment by focused acoustic ultrasonication.

Representative micrographs of oval cell disruptate of Pt1 8.6 sonicated for 8 min (A) or 12 min (B), and Pt4 sonicated for 4 min (C) or 8 min (D). Note the presence of large aggregation (white arrows) after complete cell disruption. Scale bar, 20 μm.

Robustness of fusiform and oval *P. tricornutum* cells

With approximately 1.5 g L^{-1} cell biomass loaded, 40 s was required for the fusiform morphotype to reach a cell breakage level of >90%, while more than 4 min was needed for the oval form to achieve a comparable cell disruption level by focused acoustic ultrasonication. This result clearly showed that oval cells were much more robust, requiring a greater amount of energy for complete cell rupture than fusiform cells. Major factors determining the shear sensitivity of a microalga include the size and morphology of the cell, the composition and thickness of the cell wall, and the growth environment (Alias et al., 2004, Chisti, 2009). As mentioned above, the oval cell is about three times smaller than the fusiform one in length. Longer microalgae were demonstrated to be more susceptible to shear damage when recirculated through pumps (Vandanjon et al., 1999). For a given power supply producing turbulence within the flow, if the length scale of microeddies is equal or below the length of the cells, this turbulence causes cell damage (Camacho et al., 2000, Alias et al., 2004). In this case, fusiform cells with larger size could be more sensitive to shear damage than oval cells for otherwise fixed conditions.

The fusiform morphotype is commonly found under normal culture conditions while the oval form is characterised by its resistance to unfavourable conditions such as low temperature, low salinity and red light (De Martino et al., 2007, De Martino et al., 2011, Ovide et al., 2018, Herbstova et al., 2017). This suggested that oval cells might possess some special protection mechanisms against external damaging effects. The cellular organisation and structure is similar among *P. tricornutum* morphotypes except for the cell wall and vacuolar organisation (Borowitzka and Volcani, 1978). The space within the arms of fusiform and triradiate morphotypes was occupied by large vacuoles whereas almost the whole space inside the oval cell was taken up by plastids or chromatophores (Wilson, 1946). Mechanical analysis by atomic force microscopy has shown that the triradiate arms are softer than the core region probably due to the localisation of cell organelles (Francius et al., 2008). Therefore, the large vacuolar volume in the fusiform morphotype

might be another contributor to its easier disruption compared to the oval form.

The differences in cell wall structure and composition between fusiform and oval morphotypes could largely account for their different susceptibility to mechanical forces. *P. tricornutum* has a three-layered cell wall structure (Reimann and Volcani, 1967, Tesson et al., 2009a), mainly composed of polysaccharides, proteins, lipids, polyamines and silicon (Tesson et al., 2009b). The frustule of fusiform and triradiate morphotypes is characterised being organic whereas the oval form cultured with a supplement of silicate is able to synthesise the siliceous frustule with the degree of silicification ranging from a raphe to a silicified valve with a raphe (Tesson et al., 2009a). Non-silicified valves were observed in oval cells grown in the absence of silicic acid (De Martino et al., 2007). A previous study showed that in the presence of silicate, the valve of oval cells provides higher mechanical resistance, being about five times stiffer than the valves of the other two morphotypes (Francius et al., 2008). Although silicate was not added for the cultivation of either fusiform or oval cells in this study, it has been hypothesised that *P. tricornutum* cells grown in glass vessels could potentially obtain sufficient silicon from the slow dissolution of glass at the alkaline pH of marine media (Lewin et al., 1958, Silkina et al., 2015). Therefore, further confirmation is needed for the degree of cell wall silicification and its contribution to the high mechanical resistance of oval cells detected in this work.

Apart from the possibly synthesised silica shell depositing at the mid-layer of cell wall structure, the oval cell surface is known to be coated with mucilaginous exopolymeric substances (EPS), which showed moderate stiffness, comparable with that of the fusiform valve (Francius et al., 2008), and might also help to protect oval cells from external damages. Sulphated glucuromannan has been shown to constitute the polysaccharide backbone of *P. triornutum* cell wall, which seems conserved among cell morphotypes (Ford and Percival, 1965b, Le Costaouec et al., 2017). However, variations in the amount and linkages of cell wall components occur depending on cell

morphotypes in acclimation to environmental changes. A detailed study on the polysaccharide composition of Pt1 fusiform and oval morphotypes revealed the higher proportion of mannose in the cell frustule fraction and in the residual insoluble fraction from oval cells than from fusiform cells (Willis et al., 2013). Furthermore, monosaccharide analysis in Chapter 4 also showed the higher content of mannose and xylose from oval cells than from fusiform cells (Figure 4-11). These might reflect the differences in cell wall and be associated with the observed stiffer cell wall of oval cells compared to fusiform cells. In summary, the fusiform morphotype is larger in size, has a larger vacuolar volume, lacks a silica frustule and EPS coating and showed a lower mannose content, and may therefore be more susceptible to mechanical forces compared to the oval morphotype.

As described in Chapter 4, fusiform cells grown in f/2 medium had quite different biochemical composition across 21 days cultivation. The relatively young cells sampled on day 7 have more protein and less lipid and carbohydrate so are likely to have a different cell structure and shear sensitivity compared to older stressed cells, which are with relevance to industrial bioproduction of particularly biofuels. There have been studies showing that the shear tolerance of microalgal cells varies with cell cultivation age (Wang and Lan, 2018). It would be worth to further investigate the effect of culture age on shear sensitivity of *P. tricornutum* morphotypes in the future. Oval cells hold the potential to be used as a host to produce proteins. Its high robustness increases the difficulty of cell disruption, which would increase the cost for the downstream processing of *P. tricornutum*. However, oval cells might be advantageous for recovery of whole cell products where the application needs a degree of resilience, e.g. edible vaccines (Embregts and Forlenza, 2016). On the contrary, fusiform cells are easier to be disrupted and might hence be more applicable for intracellular products where cell disruption is required. Conceivably, it may be possible to culture *P. tricornutum* in morphotypes considering the particular applications to balance between resistance to damage-causing forces and ease of cell disruption.

5.4 Conclusions

This chapter compared for the first time the downstream processing including cell harvest by centrifugation and cell disruption by ultrasonication of two *P. tricornutum* morphotypes: fusiform and oval, and assessed their relative robustness during these bioprocesses. The employment of ultra scale-down (USD) techniques based on a high-speed rotating disc shear device and a focused acoustic ultrasonicator provided important insights into the large-scale centrifugation and cell disruption processes. From the USD centrifugation, it was predicted that a high clarification efficiency (>93%) without evident cell damage could be obtained for both fusiform and oval *P. tricornutum* cells when using either a hermetically or a non-hermetically sealed disc-stack centrifuge operating over a range of flow rates ($Q/\Sigma \leq 5.4 \times 10^{-8}$ m s^{-1}). Both fusiform and oval morphotypes demonstrated robustness against the applied shear conditions (a maximum energy dissipation rate of $\leq 5.3 \times 10^{5}$ W kg^{-1}) without significant cell damage and protein release observed. However, fusiform cell cultures appeared more shear sensitive than pure oval cell cultures, displaying a reduced clarification efficiency and a larger change in particle size with shear stress due to the disruption of shear-sensitive cell aggregation.

Interesting results were obtained with regard to the cell disruption of fusiform and oval *P. tricornutum* morphotypes using the focused acoustic ultrasonication method. The impact of sonication time on cell rupture efficiency was described through measurement of cell breakage, released protein and particle size distribution. It was found that oval cells were much more robust, requiring a longer sonication time for complete cell rupture compared to fusiform cells. With approximately 1.5 g L^{-1} cells loaded, 40 s was required for the fusiform morphotype to reach a cell breakage level of above 90% while more than 4 min was needed for the oval form to achieve a comparable cell disruption level. This work provides new insights into the impact of cell morphotype on early recovery stages of *P. tricornutum* downstream bioprocessing. *P. tricornutum* is currently under development as an expression host for therapeutic proteins, bioplastics, etc. The findings

might offer significant implications for upstream cultivation strategies and downstream bioprocessing to optimise the manufacture of different classes of products in *P. tricornutum* with diverse morphotypes.

6 Conclusions and future work

6.1 Conclusions

In this thesis, a medium called Mann and Myers' medium was first identified as eliciting significant cell morphotype conversion from fusiform to oval in *P. tricornutum*. After five subculturing treatments in liquid M & M medium representing a cultivation period of approximately four months, oval cells were enriched reaching 90.8% and 99.9% in cultures of Pt1 8.6 and Pt4 respectively. The oval morphotype could be well-maintained in liquid M & M medium under the constant shaking condition, allowing high cell concentration and dry biomass yield to be achieved. The reversibility of this morphological change was also investigated by growing the obtained stable oval cells back in f/2 medium. It turned out that the cell morphotype conversion induced by M & M medium was reversible in Pt1 8.6 and might be irreversible in Pt4 under the tested conditions. This is the first report indicating that M & M medium could trigger cell morphological change to oval in *P. tricornutum.*

The following exploration on factors affecting morphotype change of *P. tricornutum* was performed by modifying f/2 medium to the components of M & M medium. It indicated that a single modification of low salinity, addition of Tris, increased concentration of nitrate or phosphate, M & M trace elements or omission of vitamins had no significant influence on cell morphotype of both Pt1 8.6 and Pt4 after two successive transfers lasting for 55 days. The addition of Tris in f/2 medium led to apparent cell aggregation in Pt1 8.6. Interestingly, an evident increase of oval cells to 72.5% was observed in Pt1 8.6 grown in a modified f/2 medium with increased nitrate and phosphate content and Tris addition (N P T) after two subculturing treatments, while Pt4 was not significantly affected.

The obtainment of stable oval cells enables us to characterise the bioproduct accumulation in them compared to fusiform cells to have a systematic analysis of biochemical composition in different *P. tricornutum* morphotypes.

It was found that fusiform *P. tricornutum* cells grown in f/2 medium were a potential feedstock for biodiesel and bioethanol production as lipid and carbohydrate, particularly neutral lipid and glucose, were significantly accumulated over 21 days cultivation. By contrast, pigments, particularly fucoxanthin and chlorophyll *a*, were markedly accumulated in oval *P. tricornutum* cultures gown in M & M medium under the tested conditions. Meanwhile, higher protein content (% DW) was obtained in oval cell cultures than in fusiform cell cultures. Additionally, both fusiform and oval cells can be used for EPA production. By characterising the different product accumulation in different cell morphotypes maintained in their respective culture medium, this work provides implications for the bioprocess design of *P. tricornutum* in terms of cultivation and harvest time. Noteworthy, higher amount of mannose (% DW) was observed from oval cells than from fusiform cells, implying the possible differences in cell wall between them.

The initial steps of downstream processing of fusiform and oval morphotypes were further investigated using ultra scale-down (USD) approaches. The USD centrifugation indicated that a high cell recovery efficiency (>93%) without evident cell damage could be obtained for both morphotypes when using either a hermetically or a non-hermetically sealed disc-stack centrifuge operating over a range of flow rates ($Q/\Sigma \leq 5.4 \times 10^{-8}$ m s^{-1}). Moreover, cell disruption analysis by focused acoustics demonstrated that oval cells were much more robust, requiring a longer treatment time for complete cell rupture than fusiform cells. This work reported for the first time the downstream processing including cell harvest by centrifugation and cell disruption by ultrasonication of different *P. tricornutum* morphotypes. These findings in this thesis provided significant implications for upstream cultivation strategies and downstream bioprocessing to optimise the manufacture of different classes of products in *P. tricornutum* with diverse morphotypes for industrial biotechnology.

6.2 Future work

Short-term future work

In this thesis, Mann and Myers' medium has been found to trigger significant cell morphotype conversion from fusiform to oval in strains Pt1 8.6 and Pt4. This is a novel way to regulate cell morphology of *P. tricornutum*. It would be interesting to apply this method to other *P. tricornutum* strains to verify its universality. A preliminary investigation has been carried out in this thesis to identify the factors inducing the morphological change of *P. tricornutum* grown in M & M medium. Although f/2 medium with increased nitrate and phosphate content and Tris addition was found to trigger evident morphotype change to oval in Pt1 8.6, this was not observed in Pt4. The specific conditional reasons capable of initiating oval cell production still remain unknown. Further systematic studies such as nutrient analysis remaining in the medium are required to address this. In addition, investigation on dynamics of bacterial community symbiotic with *P. tricornutum* by DNA sequencing or OMICs techniques (e.g. transcriptomics, proteomics) might provide an insight into the role of bacteria on morphotype, growth and biofilm formation of *P. tricornutum*.

The oval morphotype could be enriched and well-maintained in liquid M & M medium under the constant shaking condition, reaching high dry biomass concentration over 21 days cultivation. The biochemical profiles including pigment, protein, lipid and carbohydrate in oval cells were also examined over culture time. However, stationary phase was not reached after 21 days cultivation and culture time was shown to have little impact on biochemical composition in ovals. Furthermore, the highest biomass concentration obtained in this thesis for oval cells was much lower than that reported for *P. tricornutum* grown in the same medium with 1% CO_2-enriched air supply. This indicates that there is still the space for further improvement in the overall biomass and classes of product yields from oval cells through optimisation of cultivation parameters such as inorganic carbon supply and light. This would be very useful for scale-up bioprocess design and for

understanding the biochemical changes in oval cells during a whole growth cycle.

Finally, the initial steps of downstream bioprocessing were characterised for fusiform and oval morphotypes. Cell recovery using a disc-stack centrifuge with different feed zones was predicted in this study with the USD centrifugation method. Large scale verification of the results may be required. Higher levels of shear stress (e.g. $12x10^5$ W kg^{-1}) over a wider range of Q/Σ ratio (e.g. 10^{-7} m s^{-1}) to mimic other types of industrial centrifuges operating at diverse flow rates could be applied to assess the shear sensitivity and recovery efficiency of the two morphotypes. In addition, solid discharge from industrial centrifuges could produce an additional cell damage. The impact of discharge on cells can be investigated using the capillary shear device and verified at scale. Flocculation prior to centrifugation is commonly used for microalgal cell harvest. It may be interesting to know the impact of shear stress occurring in centrifugation on flocs of *P. tricornutum* morphotypes. The focused acoustic disruption at microscale was used in this thesis to investigate the rupture of *P. tricornutum* morphotypes. Oval cells were found to be harder to break compared with fusiform cells. This USD method has been successfully used to mimic high-pressure homogenisation. Thus, high-pressure homogeniser may be used in the future to confirm the obtained results. Optimisation of disruption method and conditions is needed for the two cell morphotypes considering the end product for specific applications.

Long-term future work

An aim for future studies would be to investigate scale-up of cultivation. This study has shown that oval and fusiform cells could be maintained in different culture media with diverse product accumulation. A preliminary scale-up cultivation in hanging plastic bags under aeration was conducted with Pt4 (Appendix, Figure A-2, A-3 & Table A-1). Microscopic examination confirmed that Pt4 cells grown in M & M medium displayed the oval morphotype (data not shown). However, since aeration and mixing were not optimised, cells, particularly oval cells were observed to accumulate in the bottom corners of

the bags. Therefore, a larger, more systematic study on the mechanism of scale-up with the two morphotypes will need to take into account reactor geometric design like “V” shaped bottom and fluid flow as well as illumination and medium nutrient design. Exploration of scale-up cultivation for natural product formation in the two morphotypes of cells would be necessary for practical application of *P. tricornutum* in industry. It would also be interesting to check if the obtained oval cells could be well-maintained during large-scale cultivation, and can this technique be applied in batch, fed-batch or continuous mode. In order to reduce the footprint of algal operations, it could be advantageous to move towards continuous cultivation. This may also have other benefits, including keeping algal cultures in steady state (Henley, 2019). Such experiments will also enable a greater understanding of the physiology of oval versus fusiform cultures.

As detailed in Chapter 1, *P. tricornutum* is a model organism for synthetic biology and a promising host for recombinant protein expression due to the advanced genetic toolkit available. Successful genetic transformation of fusiform and oval morphotypes has been reported using the biolistic method, and metabolic engineering approaches have been tested to improve yields of desired lipid classes. It would therefore be useful to explore the expression of recombinant proteins in the two cell morphotypes to evaluate and compare product yields. Factorial or Design of Experiments approaches might be used to examine the interplay of physical and biological factors, as well as the role of media design. For instance, this may enable a biorefinery approach by improving yields of EPA and fucoxanthin.

In terms of recombinant protein expression, algal synthetic biology is still at a nascent stage. One growing area of interest is whole cell or edible vaccines where the host cell encapsulates the product and enables delivery to the harsh gastric environment. Successful production of vaccines has been achieved in *Chlamydomonas reinhardtii* (Taunt et al., 2018), however scale-up poses a significant challenge. As shown in Chapter 5, *P. tricornutum* oval morphotype was more resistant to mechanical forces. This might be advantageous for two reasons. Firstly, it enables the use of centrifugation

and may make cells more resilient to spray drying. Previous studies have relied on lyophilised cells, however this is too expensive for applications such as aquaculture (Kwon et al., 2019). Secondly, a more resilient morphotype may be valuable for transport to the correct part of the digestive system. For instance, in some species of commercially farmed fish, it is necessary to protect the antigen from digestion in the stomach and foregut (Embregts and Forlenza, 2016).

Oval cells are known to secrete and be coated with exopolymeric substances (EPS) involving in cell adhesion and motility. EPS contain diverse biopolymers possessing multiple bioactivities and thus have high-value medical applications (Xiao and Zheng, 2016). Therefore, large-scale cultivation of the EPS producing oval morphotype of *P. tricornutum* could be examined for EPS properties. Another interesting application of EPS is the aggregation and capture of microplastic waste, which has been shown in other species to be able to flocculate small particles. Given the salinity tolerance of *P. tricornutum*, demonstrated in Chapter 3, this could be a robust organism to explore for wastewater treatment. Finally, oval *P. tricornutum* cells might be cultivated in the future to investigate EPS production for biofilm formation to gain some insights into diatom biofouling processes.

Predicting the commercial viability and sustainability credentials of a biorefinery based on *P. tricornutum* will rely on a detailed economic and environmental evaluation as well as life cycle assessment. For example, life cycle assessment of EPA production from *P. tricornutum* at pilot scale showed that significant environmental improvements could be achieved when sodium nitrate was substituted by nitrogen-based fertilizers such as urea, calcium nitrate or ammonium nitrate (Perez-Lopez et al., 2014). By conducting a thorough investigation of media components and uptake of nutrients by different morphotypes, it may be possible to reduce the amount of some components like Tris required. Building on the findings presented here, further elucidation of the key factors controlling cell morphotype could enable a move away from a system that is based on M & M medium. Reducing process inputs upstream may lead to gains both in economic terms

as well as environmental footprint. The tendency of oval morphotype cells to sink may expedite harvesting and dewatering, thus reducing energy input. Novel strategies to make use of this property could be compared with a decisional support tool.

This study revealed the morphological and biochemical responses of *P. tricornutum* to M & M medium. However, the molecular mechanisms behind the observed phenomena remain unclear. It will be interesting to study the differential gene expression involved in pleiomorphism and morphogenesis in acclimation to new environment. Furthermore, only oval cells can form siliceous frustule and possess a raphe. Techniques like quantitative reverse transcription polymerase chain reaction (qRT-PCR), OMICs, isotope labelling and epigenetics could be employed to explore the genetic mechanisms of morphogenesis, frustule silicification, raphe formation and EPS synthesis. This would be important for better understanding of diatom biology and gene function and would provide molecular insights into the resilience of diatoms and their ecological success in global oceans.

Reference

ABDULLAHI, A. S., UNDERWOOD, G. J. C. & GRETZ, M. R. 2006. Extracellular matrix assembly in diatoms (bacillariophyceae). v. environmental effects on polysaccharide synthesis in the model diatom, Phaeodactylum tricornutum 1. *Journal of Phycology,* 42**,** 363-378.

ABIDA, H., DOLCH, L. J., MEI, C., VILLANOVA, V., CONTE, M., BLOCK, M. A., FINAZZI, G., BASTIEN, O., TIRICHINE, L., BOWLER, C., REBEILLE, F., PETROUTSOS, D., JOUHET, J. & MARECHAL, E. 2015. Membrane glycerolipid remodeling triggered by nitrogen and phosphorus starvation in Phaeodactylum tricornutum. *Plant Physiology,* 167**,** 118-36.

ACIEN FERNANDEZ, F. G., HALL, D. O., CANIZARES GUERRERO, E., KRISHNA RAO, K. & MOLINA GRIMA, E. 2003. Outdoor production of Phaeodactylum tricornutum biomass in a helical reactor. *Journal of Biotechnology,* 103**,** 137-52.

AI HATTAB, M. & GHALY, A. 2015. Microalgae oil extraction pre-treatment methods: Critical review and comparative analysis. *J. Fundam. Renew. Energy Appl,* 5**,** 1-26.

ALHATTAB, M., KERMANSHAHI-POUR, A. & BROOKS, M. S. L. 2019. Microalgae disruption techniques for product recovery: influence of cell wall composition. *Journal of Applied Phycology,* 31**,** 61-88.

ALIAS, C. B., LOPEZ, M. C. G. M., FERNANDEZ, F. G. A., SEVILLA, J. M. G., SANCHEZ, J. L. G. & GRIMA, E. M. 2004. Influence of power supply in the feasibility of Phaeodactylum tricornutum cultures. *Biotechnology and Bioengineering,* 87**,** 723-733.

ALIPANAH, L., ROHLOFF, J., WINGE, P., BONES, A. M. & BREMBU, T. 2015. Whole-cell response to nitrogen deprivation in the diatom Phaeodactylum tricornutum. *Journal of Experimental Botany,* 66**,** 6281-6296.

ALIPANAH, L., WINGE, P., ROHLOFF, J., NAJAFI, J., BREMBU, T. & BONES, A. M. 2018. Molecular adaptations to phosphorus deprivation and comparison with nitrogen deprivation responses in the diatom Phaeodactylum tricornutum. *Plos One,* 13**,** e0193335.

ALLEN, A. E., LAROCHE, J., MAHESWARI, U., LOMMER, M., SCHAUER, N., LOPEZ, P. J., FINAZZI, G., FERNIE, A. R. & BOWLER, C. 2008. Whole-cell response of the pennate diatom Phaeodactylum tricornutum to iron starvation. *Proceedings of the National Academy of Sciences of the United States of America,* 105**,** 10438-10443.

AMBLER, C. M. 1959. The Theory of Scaling up Laboratory Data for the Sedimentation Type Centrifuge. *Journal of Biochemical and Microbiological Technology and Engineering,* 1**,** 185-205.

APT, K. E., KROTH-PANCIC, P. G. & GROSSMAN, A. R. 1996. Stable nuclear transformation of the diatom Phaeodactylum tricornutum. *Mol Gen Genet,* 252**,** 572-9.

AUCAMP, J. P., DAVIES, R., HALLET, D., WEISS, A. & TITCHENER-HOOKER, N. J. 2014. Integration of Host Strain Bioengineering and Bioprocess Development Using Ultra-Scale Down Studies to Select the Optimum Combination: An Antibody Fragment Primary Recovery Case Study. *Biotechnology and Bioengineering,* 111**,** 1971-1981.

AXELSSON, L., MERCADO, J. & FIGUEROA, F. 2000. Utilization of HCO3− at high pH by the brown macroalga Laminaria saccharina. *European Journal of Phycology,* 35**,** 53-59.

AXELSSON, M. & GENTILI, F. 2014. A Single-Step Method for Rapid Extraction of Total Lipids from Green Microalgae. *Plos One,* 9.

BAÏET, B., BUREL, C., SAINT-JEAN, B., LOUVET, R., MENU-BOUAOUICHE, L., KIEFER-MEYER, M.-C., MATHIEU-RIVET, E., LEFEBVRE, T., CASTEL, H. & CARLIER, A. 2011. N-glycans of Phaeodactylum tricornutum diatom and functional characterization of its N-acetylglucosaminyltransferase I enzyme. *Journal of Biological Chemistry,* 286**,** 6152-6164.

BALASUBRAMANIAN, R. K., DOAN, T. T. Y. & OBBARD, J. P. 2013. Factors affecting cellular lipid extraction from marine microalgae. *Chemical Engineering Journal,* 215**,** 929-936.

BARKER, H. A. 1935. Photosynthesis in diatoms. *Archives of Microbiology,* 6**,** 141-156.

BARTUAL, A., GÁLVEZ, J. A. & OJEDA, F. 2008. Phenotypic response of the diatom Phaeodactylum tricornutum Bohlin to experimental changes in the inorganic carbon system. *Botanica Marina,* 51.

BARTUAL, A. & GALVEZ, L. A. 2002. Growth and biochemical composition of the diatom Phaeodactylum tricornutum at different pH and inorganic carbon levels under saturating and subsaturating light regimes. *Botanica Marina,* 45**,** 491-501.

BEGUM, H., YUSOFF, F. M., BANERJEE, S., KHATOON, H. & SHARIFF, M. 2016. Availability and Utilization of Pigments from Microalgae. *Critical Reviews in Food Science and Nutrition,* 56**,** 2209-2222.

BERRILL, A., HO, S. V. & BRACEWELL, D. G. 2008. Ultra scale-down to define and improve the relationship between Flocculation and disc-stack centrifugation. *Biotechnology Progress,* 24**,** 426-431.

BERTRAND, E. M., ALLEN, A. E., DUPONT, C. L., NORDEN-KRICHMAR, T. M., BAI, J., VALAS, R. E. & SAITO, M. A. 2012. Influence of cobalamin scarcity on diatom molecular physiology and identification of a cobalamin acquisition protein. *Proceedings of the National Academy of Sciences,* 109**,** E1762-E1771.

BILBAO, P. S., SALVADOR, G. A. & LEONARDI, P. I. J. F. A. 2017. Fatty Acids from Microalgae: Targeting the Accumulation of Triacylglycerides. 119.

BLAHA, B. A. F., MORRIS, S. A., OGONAH, O. W., MAUCOURANT, S., CRESCENTE, V., ROSENBERG, W. & MUKHOPADHYAY, T. K. 2018. Development of a high-throughput microscale cell disruption platform for Pichia pastoris in rapid bioprocess design. *Biotechnology Progress,* 34**,** 130-140.

BLAS, P., TOLNER, B., WARD, J., CHESTER, K. & HOARE, M. 2018. The use of a surface active agent in the protection of a fusion protein during bioprocessing. *Biotechnology and Bioengineering,* 115**,** 2760-2770.

BOROWITZKA, M. A. & VOLCANI, B. E. 1978. The Polymorphic Diatom Phaeodactylum tricornutum: Ultrastructure of Its Morphotypes1, 2. *Journal of Phycology,* 14**,** 10-21.

BOWLER, C., ALLEN, A. E., BADGER, J. H., GRIMWOOD, J., JABBARI, K., KUO, A., MAHESWARI, U., MARTENS, C., MAUMUS, F., OTILLAR, R. P., RAYKO, E., SALAMOV, A., VANDEPOELE, K., BESZTERI, B., GRUBER, A., HEIJDE, M., KATINKA, M., MOCK, T., VALENTIN, K., VERRET, F., BERGES, J. A., BROWNLEE, C., CADORET, J. P., CHIOVITTI, A., CHOI, C. J., COESEL, S., DE MARTINO, A., DETTER, J. C., DURKIN, C., FALCIATORE, A., FOURNET, J., HARUTA, M., HUYSMAN, M. J., JENKINS, B. D., JIROUTOVA, K., JORGENSEN, R. E., JOUBERT, Y., KAPLAN, A., KROGER, N., KROTH, P. G., LA ROCHE, J., LINDQUIST, E., LOMMER, M., MARTIN-JEZEQUEL, V., LOPEZ, P. J., LUCAS, S., MANGOGNA, M., MCGINNIS, K., MEDLIN, L. K., MONTSANT, A., OUDOT-LE SECQ, M. P., NAPOLI, C., OBORNIK, M., PARKER, M. S., PETIT, J. L., PORCEL, B. M., POULSEN, N., ROBISON, M., RYCHLEWSKI, L., RYNEARSON, T. A., SCHMUTZ, J., SHAPIRO, H., SIAUT, M., STANLEY, M., SUSSMAN, M. R., TAYLOR, A. R., VARDI, A., VON DASSOW, P., VYVERMAN, W., WILLIS, A., WYRWICZ, L. S., ROKHSAR, D. S., WEISSENBACH, J., ARMBRUST, E. V., GREEN, B. R., VAN DE PEER, Y. & GRIGORIEV, I. V. 2008. The Phaeodactylum genome reveals the evolutionary history of diatom genomes. *Nature,* 456**,** 239-44.

BOWLER, C., VARDI, A. & ALLEN, A. E. 2010. Oceanographic and Biogeochemical Insights from Diatom Genomes. *Annual Review of Marine Science,* 2**,** 333-365.

BOYCHYN, M., YIM, S. S. S., BULMER, M., MORE, J., BRACEWELL, D. G. & HOARE, M. 2004. Performance prediction of industrial centrifuges using scale-down models. *Bioprocess and Biosystems Engineering,* 26**,** 385-391.

BOYCHYN, M., YIM, S. S. S., SHAMLOU, P. A., BULMER, M., MORE, J. & HOARE, M. 2001. Characterization of flow intensity in continuous centrifuges for the development of laboratory mimics. *Chemical Engineering Science,* 56**,** 4759-4770.

BRADFORD, M. M. 1976. A rapid and sensitive method for the quantitation of microgram quantities of protein utilizing the principle of protein-dye binding. *Anal Biochem,* 72**,** 248-54.

BRANYIKOVA, I., PROCHAZKOVA, G., POTOCAR, T., JEZKOVA, Z. & BRANYIK, T. 2018. Harvesting of Microalgae by Flocculation. *Fermentation-Basel,* 4.

BRENNAN, L. & OWENDE, P. 2010. Biofuels from microalgae-A review of technologies for production, processing, and extractions of biofuels and co-products. *Renewable & Sustainable Energy Reviews,* 14**,** 557-577.

BREUER, G., LAMERS, P. P., MARTENS, D. E., DRAAISMA, R. B. & WIJFFELS, R. H. 2012. The impact of nitrogen starvation on the dynamics of triacylglycerol accumulation in nine microalgae strains. *Bioresource Technology,* 124**,** 217-226.

BUHMANN, M. T., SCHULZE, B., FORDERER, A., SCHLEHECK, D. & KROTH, P. G. 2016. Bacteria May Induce the Secretion of Mucin-Like Proteins by the Diatom Phaeodactylum Tricornutum. *Journal of Phycology,* 52**,** 463-474.

CALDER, P. C. 2006. n-3 polyunsaturated fatty acids, inflammation, and inflammatory diseases. *American Journal of Clinical Nutrition,* 83**,** 1505s-1519s.

CAMACHO, F. G., GOMEZ, A. C., SOBCZUK, T. M. & GRIMA, E. M. 2000. Effects of mechanical and hydrodynamic stress in agitated, sparged cultures of Porphyridium cruentum. *Process Biochemistry,* 35**,** 1045-1050.

CAMACHO, F. G., GRIMA, E. M., MIRON, A. S., PASCUAL, V. G. & CHISTI, Y. 2001. Carboxymethyl cellulose protects algal cells against hydrodynamic stress. *Enzyme and Microbial Technology,* 29**,** 602-610.

CAPORGNO, M. P. & MATHYS, A. 2018. Trends in Microalgae Incorporation Into Innovative Food Products With Potential Health Benefits. *Frontiers in Nutrition,* 5.

CARLUCCI, A. F. & BOWES, P. M. 1970. VITAMIN PRODUCTION AND UTILIZATION BY PHYTOPLANKTON IN MIXED CULTURE 1. *Journal of Phycology,* 6**,** 393-400.

CHAN, G., BOOTH, A. J., MANNWEILER, K. & HOARE, M. 2006. Ultra scale-down studies of the effect of flow and impact conditions during E-coli cell processing. *Biotechnology and Bioengineering,* 95**,** 671-683.

CHAPMAN, R. L. 2013. Algae: the world's most important "plants"-an introduction. *Mitigation and Adaptation Strategies for Global Change,* 18**,** 5-12.

CHATEL, A., KUMPALUME, P. & HOARE, M. 2014. Ultra Scale-Down Characterization of the Impact of Conditioning Methods for Harvested Cell Broths on Clarification by Continuous Centrifugation-Recovery of Domain Antibodies from rec E. coli. *Biotechnology and Bioengineering,* 111**,** 913-924.

CHEN, X., QIU, C. E. & SHAO, J. Z. 2006. Evidence for K+-dependent HCO3− utilization in the marine diatom Phaeodactylum tricornutum. *Plant physiology,* 141**,** 731-736.

CHIBA, Y. & JIGAMI, Y. 2007. Production of humanized glycoproteins in bacteria and yeasts. *Curr Opin Chem Biol,* 11**,** 670-6.

CHISTI, Y. 2009. Shear sensitivity. *Encyclopedia of industrial biotechnology: bioprocess, bioseparation, and cell technology***,** 1-40.

CHISTI, Y. 2016. Large-Scale Production of Algal Biomass: Raceway Ponds. *Algae Biotechnology: Products and Processes***,** 21-40.

CONNAN, S. 2015. Spectrophotometric Assays of Major Compounds Extracted from Algae. *Methods Mol Biol,* 1308**,** 75-101.

COOKSEY, K. E. & COOKSEY, B. 1974. CALCIUM DEFICIENCY CAN INDUCE THE TRANSITION FROM OVAL TO FUSIFORM CELLS IN CULTURES OF PHAEODACTYLUM TRICORNUTUM BOHLIN1, 2. *Journal of Phycology,* 10**,** 89-90.

COOPER, M. S., HARDIN, W. R., PETERSEN, T. W. & CATTOLICO, R. A. 2010. Visualizing "green oil" in live algal cells. *Journal of Bioscience and Bioengineering,* 109**,** 198-201.

CRUZ, Y. R., ARANDA, D. A. G., SEIDL, P. R., DIAZ, G. C., CARLIZ, R. G., FORTES, M. M., DA PONTE, D. A. & DE PAULA, R. C. 2018. Cultivation Systems of Microalgae for the Production of Biofuels. *Biofuels: State of Development***,** 199.

CUELLAR-BERMUDEZ, S. P., AGUILAR-HERNANDEZ, I., CARDENAS-CHAVEZ, D. L., ORNELAS-SOTO, N., ROMERO-OGAWA, M. A. & PARRA-SALDIVAR, R. 2015. Extraction and purification of high-value metabolites from microalgae: essential lipids, astaxanthin and phycobiliproteins. *Microbial Biotechnology,* 8**,** 190-209.

CURRIE, J. A., DUNNILL, P. & LILLY, M. D. 1972. Release of Protein from Bakers-Yeast (Saccharomyces-Cerevisiae) by Disruption in an Industrial Agitator Mill. *Biotechnology and Bioengineering,* 14**,** 725-&.

D'ADAMO, S., DI VISCONTE, G. S., LOWE, G., SZAUB-NEWTON, J., BEACHAM, T., LANDELS, A., ALLEN, M. J., SPICER, A. & MATTHIJS, M. 2019. Engineering the unicellular alga Phaeodactylum tricornutum for high-value plant triterpenoid production. *Plant Biotechnology Journal,* 17**,** 75-87.

DABOUSSI, F., LEDUC, S., MARECHAL, A., DUBOIS, G., GUYOT, V., PEREZ-MICHAUT, C., AMATO, A., FALCIATORE, A., JUILLERAT, A., BEURDELEY, M., VOYTAS, D. F., CAVAREC, L. & DUCHATEAU, P. 2014. Genome engineering empowers the diatom Phaeodactylum tricornutum for biotechnology. *Nature Communications,* 5.

DE CARVALHO, M. H. C., SUN, H. X., BOWLER, C. & CHUA, N. H. 2016. Noncoding and coding transcriptome responses of a marine diatom to phosphate fluctuations. *New Phytologist,* 210**,** 497-510.

DE CIENCIAS, F. 1995. Culture of the marine diatom Phaeodactylum tricornutum with different nitrogen sources: growth, nutrient conversion and biochemical composition. *Cah. Biol. Mar,* 36**,** 165-173.

DE JONG, E., VAN REE, R. & KWANT, I. K. 2009. Biorefineries: adding value to the sustainable utilisation of biomass. *IEA Bioenergy,* 1**,** 1-16.

DE MARTINO, A., BARTUAL, A., WILLIS, A., MEICHENIN, A., VILLAZAN, B., MAHESWARI, U. & BOWLER, C. 2011. Physiological and Molecular Evidence that Environmental Changes Elicit Morphological Interconversion in the Model Diatom Phaeodactylum tricornutum. *Protist,* 162**,** 462-481.

DE MARTINO, A., MEICHENIN, A., SHI, J., PAN, K. H. & BOWLER, C. 2007. Genetic and phenotypic characterization of Phaeodactylum tricornutum (Bacillariophyceae) accessions. *Journal of Phycology,* 43**,** 992-1009.

DEL REAL, G. E. G., DAVIES, J. & BRACEWELL, D. G. 2014. Scale-Down Characterization of Post-Centrifuge Flocculation Processes for High-Throughput Process Development. *Biotechnology and Bioengineering,* 111**,** 2486-2498.

DEVI, K. U., SWAPNA, G. & SUNEETHA, S. 2014. Microalgae in Bioremediation: Sequestration of Greenhouse Gases, Clearout of Fugitive Nutrient Minerals, and Subtraction of Toxic Elements from Waters. *Microbial Biodegradation and Bioremediation.* Elsevier.

DROOP, M. R. 1958. Requirement for thiamine among some marine and supra-littoral protista. *Journal of the Marine Biological Association of the United Kingdom,* 37**,** 323-329.

DUBOIS, M., GILLES, K. A., HAMILTON, J. K., REBERS, P. A. & SMITH, F. 1956. Colorimetric Method for Determination of Sugars and Related Substances. *Analytical Chemistry,* 28**,** 350-356.

DUMONTIER, R., MARECK, A., MATI-BAOUCHE, N., LEROUGE, P. & BARDOR, M. 2018. Toward Future Engineering of the N-Glycosylation Pathways in Microalgae for Optimizing the Production of Biopharmaceuticals. *Microalgal Biotechnology.* IntechOpen.

EIGEMANN, F., HILT, S., SALKA, I. & GROSSART, H. P. 2013. Bacterial community composition associated with freshwater algae: species specificity vs. dependency on environmental conditions and source community. *FEMS microbiology ecology,* 83**,** 650-663.

EILERS, U., BIKOULIS, A., BREITENBACH, J., BUCHEL, C. & SANDMANN, G. 2016. Limitations in the biosynthesis of fucoxanthin as targets for genetic engineering in Phaeodactylum tricornutum. *Journal of Applied Phycology,* 28**,** 123-129.

EL-BAZ, F. K. & EL BAKY, H. H. A. 2018. Pilot Scale of Microalgal Production Using Photobioreactor. *Photosynthesis: From Its Evolution to Future Improvements in Photosynthetic Efficiency Using Nanomaterials***,** 53.

EMBREGTS, C. W. E. & FORLENZA, M. 2016. Oral vaccination of fish: Lessons from humans and veterinary species. *Developmental and Comparative Immunology,* 64**,** 118-137.

ERDENE-OCHIR, E., SHIN, B. K., KWON, B., JUNG, C. & PAN, C. H. 2019. Identification and characterisation of the novel endogenous promoter HASP1 and its signal peptide from Phaeodactylum tricornutum. *Scientific Reports,* 9.

FÁBREGAS, J., VÁZQUEZ, V., CABEZAS, B. & OTERO, A. J. J. O. A. P. 1993. Tris not only controls the pH in microalgal cultures, but also feeds bacteria. 5**,** 543-545.

FALCIATORE, A., CASOTTI, R., LEBLANC, C., ABRESCIA, C. & BOWLER, C. 1999. Transformation of Nonselectable Reporter Genes in Marine Diatoms. *Mar Biotechnol (NY),* 1**,** 239-251.

FALKOWSKI, P. G., BARBER, R. T. & SMETACEK, V. 1998. Biogeochemical controls and feedbacks on ocean primary production. *Science,* 281**,** 200-206.

FERNANDEZ-CEREZO, L., RAYAT, A. C. M. E., CHATEL, A., POLLARD, J. M., LYE, G. J. & HOARE, M. 2019. An ultra scale-down method to investigate monoclonal antibody processing during tangential flow filtration using ultrafiltration membranes. *Biotechnology and Bioengineering,* 116**,** 581-590.

FERNANDEZ-REIRIZ, M. J., PEREZ-CAMACHO, A., FERREIRO, M. J., BLANCO, J., PLANAS, M., CAMPOS, M. J. & LABARTA, U. 1989. Biomass Production and Variation in the Biochemical Profile (Total Protein, Carbohydrates, RNA, Lipids and Fatty Acids) of Seven Species of Marine Microalgae. *Aquaculture,* 83**,** 17-37.

FIELD, C. B., BEHRENFELD, M. J., RANDERSON, J. T. & FALKOWSKI, P. 1998. Primary production of the biosphere: Integrating terrestrial and oceanic components. *Science,* 281**,** 237-240.

FOLCH, J., LEES, M. & STANLEY, G. H. S. 1957. A Simple Method for the Isolation and Purification of Total Lipides from Animal Tissues. *Journal of Biological Chemistry,* 226**,** 497-509.

FOLLOWS, M., HETHERINGTON, P. J., DUNNILL, P. & LILLY, M. D. 1971. Release of Enzymes from Bakers Yeast by Disruption in an Industrial Homogenizer. *Biotechnology and Bioengineering,* 13**,** 549-+.

FORD, C. & PERCIVAL, E. 1965a. 1298. The carbohydrates of phaeodactylum tricornutum. Part I. Preliminary examination of the organism, and characterisation of low molecular weight material and of a glucan. *Journal of the Chemical Society (Resumed)***,** 7035-7041.

FORD, C. W. & PERCIVAL, E. 1965b. 1299. Carbohydrates of Phaeodactylum tricornutum. Part II. A sulphated glucuronomannan. *Journal of the Chemical Society (Resumed)***,** 7042-7046.

FRANCIUS, G., TESSON, B., DAGUE, E., MARTIN-JEZEQUEL, V. & DUFRENE, Y. F. 2008. Nanostructure and nanomechanics of live Phaeodactylum tricornutum morphotypes. *Environmental Microbiology,* 10**,** 1344-1356.

FUENTES, J. L., GARBAYO, I., CUARESMA, M., MONTERO, Z., GONZALEZ-DEL-VALLE, M. & VILCHEZ, C. 2016. Impact of Microalgae-Bacteria Interactions on the Production of Algal Biomass and Associated Compounds. *Mar Drugs,* 14.

GANGL, D., ZEDLER, J. A., RAJAKUMAR, P. D., MARTINEZ, E. M., RISELEY, A., WLODARCZYK, A., PURTON, S., SAKURAGI, Y., HOWE, C. J., JENSEN, P. E. & ROBINSON, C. 2015. Biotechnological exploitation of microalgae. *Journal of Experimental Botany,* 66**,** 6975-90.

GAO, B. Y., CHEN, A. L., ZHANG, W. Y., LI, A. F. & ZHANG, C. W. 2017. Co-production of lipids, eicosapentaenoic acid, fucoxanthin, and chrysolaminarin by Phaeodactylum tricornutum cultured in a flat-plate photobioreactor under varying nitrogen conditions. *Journal of Ocean University of China,* 16**,** 916-924.

GARCIA, J. L., DE VICENTE, M. & GALAN, B. 2017. Microalgae, old sustainable food and fashion nutraceuticals. *Microbial Biotechnology,* 10**,** 1017-1024.

GARCIA, M. C., MIRÓN, A. S., SEVILLA, J. F., GRIMA, E. M. & CAMACHO, F. G. 2005. Mixotrophic growth of the microalga Phaeodactylum tricornutum: influence of different nitrogen and organic carbon sources on productivity and biomass composition. *Process Biochemistry,* 40**,** 297-305.

GARY, P. P., DUNNILL, P. & LILLY, M. D. 1972. The continuous-flow isolation of enzymes. *In:* G., T. (ed.) *Fermentation technology today.* Kyoto: Society of Fermentation Technology.

GATENBY, C. M., ORCUTT, D. M., KREEGER, D. A., PARKER, B. C., JONES, V. A. & NEVES, R. J. 2003. Biochemical composition of three algal species proposed as food for captive freshwater mussels. *Journal of Applied Phycology,* 15**,** 1-11.

GIRALDO, J. B., STOCK, W., DOW, L., ROEF, L., WILLEMS, A., MANGELINCKX, S., KROTH, P. G., VYVERMAN, W. & MICHIELS, M. 2019. Influence of the algal microbiome on biofouling during industrial cultivation of Nannochloropsis sp. in closed photobioreactors. *Algal Research,* 42**,** 101591.

GOLDMAN, J. C., RILEY, C. B. & DENNETT, M. R. 1982. The effect of pH in intensive microalgal cultures. II. Species competition. *Journal of experimental marine biology and ecology,* 57**,** 15-24.

GONÇALVES, A. L., FERREIRA, C., LOUREIRO, J. A., PIRES, J. C. & SIMÕES, M. 2015. Surface physicochemical properties of selected single and mixed cultures of microalgae and cyanobacteria and their relationship with sedimentation kinetics. *Bioresources and Bioprocessing,* 2**,** 21.

GONG, Y. M., LIU, J., JIANG, M. L., LIANG, Z., JIN, H., HU, X. J., WAN, X. & HU, C. J. 2015. Improvement of Omega-3 Docosahexaenoic Acid Production by Marine Dinoflagellate Crypthecodinium cohnii Using Rapeseed Meal Hydrolysate and Waste Molasses as Feedstock. *Plos One,* 10.

GONZALEZ-DELGADO, A. D. & KAFAROV, V. 2011. Microalgae Based Biorefinery: Issues to Consider. *Ct&F-Ciencia Tecnologia Y Futuro,* 4**,** 5-21.

GRIFFITHS, M. J., GARCIN, C., VAN HILLE, R. P. & HARRISON, S. T. L. 2011. Interference by pigment in the estimation of microalgal biomass concentration by optical density. *Journal of Microbiological Methods,* 85**,** 119-123.

GRIMA, E. M., BELARBI, E. H., FERNANDEZ, F. G. A., MEDINA, A. R. & CHISTI, Y. 2003. Recovery of microalgal biomass and metabolites: process options and economics. *Biotechnology Advances,* 20**,** 491-515.

GUIDHE, A., ANSARI, F. A., SINGH, P. & BUX, F. 2017. Heterotrophic cultivation of microalgae using aquaculture wastewater: A biorefinery concept for biomass production and nutrient remediation. *Ecological Engineering,* 99**,** 47-53.

GUILLARD, R. R. L. 1975. Culture of phytoplankton for feeding marine invertebrates.

GUNERKEN, E., D'HONDT, E., EPPINK, M. H. M., GARCIA-GONZALEZ, L., ELST, K. & WIJFFELS, R. H. 2015. Cell disruption for microalgae biorefineries. *Biotechnology Advances,* 33**,** 243-260.

GUO, L. & YANG, G. P. 2015. Predicting the reproduction strategies of several microalgae through their genome sequences. *Journal of Ocean University of China,* 14**,** 491-502.

GUTENBRUNNER, S. A., THALHAMER, J. & SCHMID, A. M. M. 1994. PROTEINACEOUS AND IMMUNOCHEMICAL DISTINCTIONS BETWEEN THE OVAL AND FUSIFORM MORPHOTYPES OF PHAEODACTYLUM TRICORNUTUM (BACILLARIOPHYCEAE) 1. *Journal of Phycology,* 30**,** 129-136.

HALIM, R., HILL, D. R. A., HANSSEN, E., WEBLEY, P. A., BLACKBURN, S., GROSSMAN, A. R., POSTEN, C. & MARTIN, G. J. O. 2019. Towards sustainable microalgal biomass processing: anaerobic induction of autolytic cell-wall self-ingestion in lipid-rich Nannochloropsis slurries. *Green Chemistry,* 21**,** 2967-2982.

HALLMANN, A. 2015. Algae biotechnology–green cell-factories on the rise. *Current Biotechnology,* 4**,** 389-415.

HAMILTON, M. L., HASLAM, R. P., NAPIER, J. A. & SAYANOVA, O. 2014. Metabolic engineering of Phaeodactylum tricornutum for the enhanced accumulation of omega-3 long chain polyunsaturated fatty acids. *Metabolic Engineering,* 22**,** 3-9.

HAN, P. P., SHEN, S. G., GUO, R. J., ZHAO, D. X., LIN, Y. H., JIA, S. R., YAN, R. R. & WU, Y. K. 2019. ROS Is a Factor Regulating the Increased Polysaccharide Production by Light Quality in the Edible Cyanobacterium Nostoc flagelliforme. *J Agric Food Chem,* 67**,** 2235-2244.

HARRIS, L., TOZZI, S., WILEY, P., YOUNG, C., RICHARDSON, T. M. J., CLARK, K. & TRENT, J. D. 2013. Potential impact of biofouling on the photobioreactors of the Offshore Membrane Enclosures for Growing Algae (OMEGA) system. *Bioresource technology,* 144**,** 420-428.

HARRISON, P. J., WATERS, R. E. & TAYLOR, F. J. R. 1980. A broad spectrum artificial sea water medium for coastal and open ocean phytoplankton 1. *Journal of phycology,* 16**,** 28-35.

HE, L. Y., HAN, X. T. & YU, Z. M. 2014. A Rare Phaeodactylum tricornutum Cruciform Morphotype: Culture Conditions, Transformation and Unique Fatty Acid Characteristics. *Plos One,* 9.

HEMAISWARYA, S., RAJA, R., KUMAR, R. R., GANESAN, V. & ANBAZHAGAN, C. 2011. Microalgae: a sustainable feed source for aquaculture. *World Journal of Microbiology and Biotechnology,* 27**,** 1737-1746.

HEMPEL, F., BOZARTH, A. S., LINDENKAMP, N., KLINGL, A., ZAUNER, S., LINNE, U., STEINBUCHEL, A. & MAIER, U. G. 2011a. Microalgae as bioreactors for bioplastic production. *Microbial Cell Factories,* 10.

HEMPEL, F., LAU, J., KLINGL, A. & MAIER, U. G. 2011b. Algae as protein factories: expression of a human antibody and the respective antigen in the diatom Phaeodactylum tricornutum. *Plos One,* 6**,** e28424.

HEMPEL, F., MAURER, M., BROCKMANN, B., MAYER, C., BIEDENKOPF, N., KELTERBAUM, A., BECKER, S. & MAIER, U. G. 2017. From hybridomas to a robust microalgal-based production platform: molecular design of a diatom secreting monoclonal antibodies directed against the Marburg virus nucleoprotein. *Microb Cell Fact,* 16**,** 131.

HENLEY, W. J. 2019. The past, present and future of algal continuous cultures in basic research and commercial applications. *Algal Research-Biomass Biofuels and Bioproducts,* 43.

HERBSTOVA, M., BINA, D., KANA, R., VACHA, F. & LITVIN, R. 2017. Red-light phenotype in a marine diatom involves a specialized oligomeric red-shifted antenna and altered cell morphology. *Scientific Reports,* 7.

HO, S. H., HUANG, S. W., CHEN, C. Y., HASUNUMA, T., KONDO, A. & CHANG, J. S. 2013. Characterization and optimization of carbohydrate production from an indigenous microalga Chlorella vulgaris FSP-E. *Bioresource Technology,* 135**,** 157-165.

HORST, I., PARKER, B. M., DENNIS, J. S., HOWE, C. J., SCOTT, S. A. & SMITH, A. G. 2012. Treatment of Phaeodactylum tricornutum cells with papain facilitates lipid extraction. *Journal of Biotechnology,* 162**,** 40-9.

HOSSAIN, G. S., LIU, L. B. & DU, G. C. 2017. Industrial bioprocesses and the biorefinery concept. *Current Developments in Biotechnology and Bioengineering.* Elsevier.

HUTCHINSON, N., BINGHAM, N., MURRELL, N., FARID, S. & HOARE, M. 2006. Shear stress analysis of mammalian cell suspensions for prediction of industrial centrifugation and its verification. *Biotechnology and Bioengineering,* 95**,** 483-491.

INSKEEP, W. P. & BLOOM, P. R. 1985. Extinction Coefficients of Chlorophyll-a and Chlorophyll-B in N,N-Dimethylformamide and 80-Percent Acetone. *Plant Physiology,* 77**,** 483-485.

JHA, D., JAIN, V., SHARMA, B., KANT, A. & GARLAPATI, V. K. 2017. Microalgae‐based Pharmaceuticals and Nutraceuticals: An Emerging Field with Immense Market Potential. *ChemBioEng Reviews,* 4**,** 257-272.

JOSEPH, A., KENTY, B., MOLLET, M., HWANG, K., ROSE, S., GOLDRICK, S., BENDER, J., FARID, S. S. & TITCHENER-HOOKER, N. 2016. A Scale-Down Mimic for Mapping the Process Performance of Centrifugation, Depth, and Sterile Filtration. *Biotechnology and Bioengineering,* 113**,** 1934-1941.

KARAS, B. J., DINER, R. E., LEFEBVRE, S. C., MCQUAID, J., PHILLIPS, A. P. R., NODDINGS, C. M., BRUNSON, J. K., VALAS, R. E., DEERINCK, T. J., JABLANOVIC, J., GILLARD, J. T. F., BEERI, K., ELLISMAN, M. H., GLASS, J. I., HUTCHISON, C. A., SMITH, H. O., VENTER, J. C., ALLEN, A. E., DUPONT, C. L. & WEYMAN, P. D. 2015. Designer diatom episomes delivered by bacterial conjugation. *Nature Communications,* 6.

KEELING, P. J. 2010. The endosymbiotic origin, diversification and fate of plastids. *Philosophical Transactions of the Royal Society B-Biological Sciences,* 365**,** 729-748.

KHAN, M. I., SHIN, J. H. & KIM, J. D. 2018. The promising future of microalgae: current status, challenges, and optimization of a sustainable and renewable industry for biofuels, feed, and other products. *Microbial Cell Factories,* 17.

KHANRA, S., MONDAL, M., HALDER, G., TIWARI, O. N., GAYEN, K. & BHOWMICK, T. K. 2018. Downstream processing of microalgae for pigments, protein and carbohydrate in industrial application: A review. *Food and Bioproducts Processing,* 110**,** 60-84.

KIM, J., YOO, G., LEE, H., LIM, J., KIM, K., KIM, C. W., PARK, M. S. & YANG, J. W. 2013. Methods of downstream processing for the production of biodiesel from microalgae. *Biotechnology Advances,* 31**,** 862-876.

KIM, S. M., JUNG, Y. J., KWON, O. N., CHA, K. H., UM, B. H., CHUNG, D. & PAN, C. H. 2012. A Potential Commercial Source of Fucoxanthin Extracted from the Microalga Phaeodactylum tricornutum. *Applied Biochemistry and Biotechnology,* 166**,** 1843-1855.

KOLADE, O. O., JIN, W. B., TENGROTH, C., GREEN, K. D. & BRACEWELL, D. G. 2015. Shear Effects on Aluminum Phosphate Adjuvant Particle Properties in Vaccine Drug Products. *Journal of Pharmaceutical Sciences,* 104**,** 378-387.

KOOISTRA, W. H. C. F., GERSONDE, R., MEDLIN, L. K. & MANN, D. G. 2007. The origin and evolution of the diatoms: their adaptation to a planktonic existence. *Evolution of primary producers in the sea.* Elsevier.

KOSAKOWSKA, A., LEWANDOWSKA, J., STON, J. & BURKIEWICZ, K. 2004. Qualitative and quantitative composition of pigments in Phaeodactylum tricornutum (Bacillariophyceae) stressed by iron. *Biometals,* 17**,** 45-52.

KROGER, N. & POULSEN, N. 2008. Diatoms-From Cell Wall Biogenesis to Nanotechnology. *Annual Review of Genetics,* 42**,** 83-107.

KWON, K. C., LAMB, A., FOX, D. & JEGATHESE, S. J. P. 2019. An evaluation of microalgae as a recombinant protein oral delivery platform for fish using green fluorescent protein (GFP). *Fish & Shellfish Immunology,* 87**,** 414-420.

LARSSON, S. C., KUMLIN, M., INGELMAN-SUNDBERG, M. & WOLK, A. 2004. Dietary long-chain n-3 fatty acids for the prevention of cancer: a review of potential mechanisms. *American Journal of Clinical Nutrition,* 79**,** 935-945.

LE COSTAOUEC, T., UNAMUNZAGA, C., MANTECON, L. & HELBERT, W. 2017. New structural insights into the cell-wall polysaccharide of the diatom Phaeodactylum tricornutum. *Algal Research-Biomass Biofuels and Bioproducts,* 26**,** 172-179.

LEAF, A., KANG, J. X., XIAO, Y. F. & BILLMAN, G. E. 2003. Clinical prevention of sudden cardiac death by n-3 polyunsaturated fatty acids and mechanism of prevention of arrhythmias by n-3 fish oils. *Circulation,* 107**,** 2646-2652.

LEBEAU, T. & ROBERT, J. M. 2003. Diatom cultivation and biotechnologically relevant products. Part II: Current and putative products. *Applied Microbiology and Biotechnology,* 60**,** 624-632.

LEIGH-CLARE, J. L. 1927. A search for vitamin D in the diatom Nitzschia closterium (W. Sm.). *Biochemical Journal,* 21**,** 368-372.

LEVY, M. S., CICCOLINI, L. A. S., YIM, S. S. S., TSAI, J. T., TITCHENER-HOOKER, N., SHAMLOU, P. A. & DUNNILL, P. 1999. The effects of material properties and fluid flow intensity on plasmid DNA recovery during cell lysis. *Chemical Engineering Science,* 54**,** 3171-3178.

LEWIN, J. C. 1958. The Taxonomic Position of Phaeodactylum-Tricornutum. *Journal of General Microbiology,* 18**,** 427-&.

LEWIN, J. C., LEWIN, R. & PHILPOTT, D. 1958. Observations on Phaeodactylum tricornutum. *Microbiology,* 18**,** 418-426.

LI, Q., AUCAMP, J. P., TANG, A., CHATEL, A. & HOARE, M. 2012. Use of focused acoustics for cell disruption to provide ultra scale‐down insights of microbial homogenization and its bioprocess impact—recovery of antibody fragments from rec E. coli. *Biotechnology and Bioengineering,* 109**,** 2059-2069.

LI, Q., MANNALL, G. J., ALI, S. & HOARE, M. 2013. An ultra scale-down approach to study the interaction of fermentation, homogenization, and centrifugation for antibody fragment recovery from rec E. coli. *Biotechnology and Bioengineering,* 110**,** 2150-2160.

LIANG, Y., BEARDALL, J. & HERAUD, P. 2006. Changes in growth, chlorophyll fluorescence and fatty acid composition with culture age in batch cultures of Phaeodactylum tricornutum and Chaetoceros muelleri (Bacillariophyceae). *Botanica Marina,* 49**,** 165-173.

LOPES, A. G. & KESHAVARZ-MOORE, E. 2012. Prediction and verification of centrifugal dewatering of P. pastoris fermentation cultures using an ultra scale-down approach. *Biotechnology and Bioengineering,* 109**,** 2039-2047.

LORENTE, E., FARRIOL, X. & SALVADO, J. 2015. Steam explosion as a fractionation step in biofuel production from microalgae. *Fuel Processing Technology,* 131**,** 93-98.

MACLEOD, R. A. & ONOFREY, E. 1954. Cation antagonism of the antibacterial action of amines. *Journal of Biological Chemistry,* 210**,** 193-201.

MAEDA, H. 2015. Nutraceutical Effects of Fucoxanthin for Obesity and Diabetes Therapy: A Review. *Journal of Oleo Science,* 64**,** 125-132.

MAHESWARI, U., JABBARI, K., PETIT, J. L., PORCEL, B. M., ALLEN, A. E., CADORET, J. P., DE MARTINO, A., HEIJDE, M., KAAS, R., LA ROCHE, J., LOPEZ, P. J., MARTIN-JEZEQUEL, V., MEICHENIN, A., MOCK, T., SCHNITZLER PARKER, M., VARDI, A., ARMBRUST, E. V., WEISSENBACH, J., KATINKA, M. & BOWLER, C. 2010. Digital expression profiling of novel diatom transcripts provides insight into their biological functions. *Genome Biol,* 11**,** R85.

MAHESWARI, U., MOCK, T., ARMBRUST, E. V. & BOWLER, C. 2009. Update of the Diatom EST Database: a new tool for digital transcriptomics. *Nucleic Acids Res,* 37**,** D1001-5.

MAHESWARI, U., MONTSANT, A., GOLL, J., KRISHNASAMY, S., RAJYASHRI, K. R., PATELL, V. M. & BOWLER, C. 2005. The Diatom EST Database. *Nucleic Acids Res,* 33**,** D344-7.

MANN, J. E. & MYERS, J. 1968. On Pigments Growth and Photosynthesis of Phaeodactylum Tricornutum. *Journal of Phycology,* 4**,** 349-&.

MARKOU, G., VANDAMME, D. & MUYLAERT, K. 2014. Microalgal and cyanobacterial cultivation: The supply of nutrients. *Water Research,* 65**,** 186-202.

MARTIN-JEZEQUEL, V. & TESSON, B. 2013. Phaeodactylum tricornutum polymorphism : an overview. *Advances in Algal Cell Biology***,** 43-80.

MATA, T. M., MARTINS, A. A. & CAETANO, N. S. 2010. Microalgae for biodiesel production and other applications: A review. *Renewable & Sustainable Energy Reviews,* 14**,** 217-232.

MAYBURY, J. P., HOARE, M. & DUNNILL, P. 2000. The use of laboratory centrifugation studies to predict performance of industrial machines: Studies of shear-insensitive and shear-sensitive materials. *Biotechnology and Bioengineering,* 67**,** 265-273.

MCCOY, R., HOARE, M. & WARD, S. 2009. Ultra Scale-Down Studies of the Effect of Shear on Cell Quality; Processing of a Human Cell Line for Cancer Vaccine Therapy. *Biotechnology Progress,* 25**,** 1448-1458.

MCCOY, R., WARD, S. & HOARE, M. 2010. Sub-Population Analysis of Human Cancer Vaccine Cells-Ultra Scale-Down Characterization of Response to Shear. *Biotechnology and Bioengineering,* 106**,** 584-597.

MCMILLAN, J. R., WATSON, I. A., ALI, M. & JAAFAR, W. 2013. Evaluation and comparison of algal cell disruption methods: Microwave, waterbath, blender, ultrasonic and laser treatment. *Applied Energy,* 103**,** 128-134.

MEDINA, A. R., GRIMA, E. M., GIMENEZ, A. G. & GONZALEZ, M. J. I. 1998. Downstream processing of algal polyunsaturated fatty acids. *Biotechnol Adv,* 16**,** 517-580.

MEDIPALLY, S. R., YUSOFF, F. M., BANERJEE, S. & SHARIFF, M. 2015. Microalgae as sustainable renewable energy feedstock for biofuel production. *BioMed research international,* 2015.

MILLEDGE, J. & HEAVEN, S. 2013. A review of the harvesting of micro-algae for biofuel production. *Reviews in Environmental Science and Bio-Technology,* 12**,** 165-178.

MILLER, J., ROGOWSKI, M. & KELLY, W. 2002. Using a CFD model to understand the fluid dynamics promoting E-coli breakage in a high-pressure homogenizer. *Biotechnology Progress,* 18**,** 1060-1067.

MIRÓN, A. S., GARCIA, M. C. C., GÓMEZ, A. C., CAMACHO, F. G., GRIMA, E. M. & CHISTI, Y. 2003. Shear stress tolerance and biochemical characterization of Phaeodactylum tricornutum in quasi steady-state continuous culture in outdoor photobioreactors. *Biochemical Engineering Journal,* 16**,** 287-297.

MIYAGAWA, A., OKAMI, T., KIRA, N., YAMAGUCHI, H., OHNISHI, K. & ADACHI, M. 2009. Research note: High efficiency transformation of the diatomPhaeodactylum tricornutumwith a promoter from the diatomCylindrotheca fusiformis. *Phycological Research,* 57**,** 142-146.

MIYAHARA, M., AOI, M., INOUE-KASHINO, N., KASHINO, Y. & IFUKU, K. 2013. Highly efficient transformation of the diatom Phaeodactylum tricornutum by multi-pulse electroporation. *Biosci Biotechnol Biochem,* 77**,** 874-6.

MOBIN, S. & ALAM, F. 2017. Some promising microalgal species for commercial applications: A review. *1st International Conference on Energy and Power, Icep2016,* 110**,** 510-517.

MOEJES, F. W., SUCCURRO, A., POPA, O., MAGUIRE, J. & EBENHOH, O. 2017. Dynamics of the Bacterial Community Associated with Phaeodactylum tricornutum Cultures. *Processes,* 5.

MSANNE, J., XU, D., KONDA, A. R., CASAS-MOLLANO, J. A., AWADA, T., CAHOON, E. B. & CERUTTI, H. 2012. Metabolic and gene expression changes triggered by nitrogen deprivation in the photoautotrophically grown microalgae Chlamydornonas reinhardtii and Coccomyxa sp C-169. *Phytochemistry,* 75**,** 50-59.

NEILSON, A. H. & LARSSON, T. 1980. The Utilization of Organic Nitrogen for Growth of Algae - Physiological-Aspects. *Physiologia Plantarum,* 48**,** 542-553.

NELSON, D. M., TRÉGUER, P., BRZEZINSKI, M. A., LEYNAERT, A. & QUÉGUINER, B. J. G. B. C. 1995. Production and dissolution of biogenic silica in the ocean: revised global estimates, comparison with regional data and relationship to biogenic sedimentation. 9**,** 359-372.

NGUYEN, T. T., BUI, X. T., PHAM, M. D., GUO, W. S. & NGO, H. H. 2016. Effect of Tris-(hydroxymethyl)-amino methane on microalgae biomass growth in a photobioreactor. *Bioresource Technology,* 208**,** 1-6.

NIU, Y. F., YANG, Z. K., ZHANG, M. H., ZHU, C. C., YANG, W. D., LIU, J. S. & LI, H. Y. 2012. Transformation of diatom Phaeodactylum tricornutum by electroporation and establishment of inducible selection marker. *Biotechniques,* 52.

ODJADJARE, E. C., MUTANDA, T. & OLANIRAN, A. O. 2017. Potential biotechnological application of microalgae: a critical review. *Critical Reviews in Biotechnology,* 37**,** 37-52.

OUDOT-LE SECQ, M. P., GRIMWOOD, J., SHAPIRO, H., ARMBRUST, E. V., BOWLER, C. & GREEN, B. R. 2007. Chloroplast genomes of the diatoms Phaeodactylum tricornutum and Thalassiosira pseudonana: comparison with other plastid genomes of the red lineage. *Molecular Genetics and Genomics,* 277**,** 427-439.

OVIDE, C., KIEFER-MEYER, M.-C., BÉRARD, C., VERGNE, N., LECROQ, T., PLASSON, C., BUREL, C., BERNARD, S., DRIOUICH, A. & LEROUGE, P. 2018. Comparative in depth RNA sequencing of P. tricornutum's morphotypes reveals specific features of the oval morphotype. *Scientific Reports,* 8**,** 14340.

OWCZAREK, B., GERSZBERG, A. & HNATUSZKO-KONKA, K. 2019. A brief reminder of systems of production and chromatography-based recovery of recombinant protein biopharmaceuticals. *BioMed Research International,* 2019.

PANCHA, I., CHOKSHI, K., GEORGE, B., GHOSH, T., PALIWAL, C., MAURYA, R. & MISHRA, S. 2014. Nitrogen stress triggered biochemical and morphological changes in the microalgae Scenedesmus sp CCNM 1077. *Bioresource Technology,* 156**,** 146-154.

PENG, J., YUAN, J. P., WU, C. F. & WANG, J. H. 2011. Fucoxanthin, a Marine Carotenoid Present in Brown Seaweeds and Diatoms: Metabolism and Bioactivities Relevant to Human Health. *Marine Drugs,* 9**,** 1806-1828.

PEREZ, E. B., PINA, I. C. & RODRIGUEZ, L. P. 2008. Kinetic model for growth of Phaeodactylum tricornutum in intensive culture photobioreactor. *Biochemical Engineering Journal,* 40**,** 520-525.

PEREZ-LOPEZ, P., GONZALEZ-GARCIA, S., ALLEWAERT, C., VERWEEN, A., MURRAY, P., FEIJOO, G. & MOREIRA, M. T. 2014. Environmental evaluation of eicosapentaenoic acid production by Phaeodactylum tricornutum. *Science of the Total Environment,* 466**,** 991-1002.

PICAZO, A., ROCHERA, C., VICENTE, E., MIRACLE, M. R. & CAMACHO, A. 2013. Spectrophotometric methods for the determination of photosynthetic pigments in stratified lakes: a critical analysis based on comparisons with HPLC determinations in a model lake. *Limnetica,* 32**,** 139-158.

POTVIN, G. & ZHANG, Z. 2010. Strategies for high-level recombinant protein expression in transgenic microalgae: a review. *Biotechnol Adv,* 28**,** 910-8.

PRIEGO-CAPOTE, F. & DE CASTRO, M. D. L. 2007. Ultrasound-assisted digestion: A useful alternative in sample preparation. *Journal of Biochemical and Biophysical Methods,* 70**,** 299-310.

PROVASOLI, L., MCLAUGHLIN, J. J. & DROOP, M. R. 1957. The development of artificial media for marine algae. *Arch Mikrobiol,* 25**,** 392-428.

PUDNEY, A., GANDINI, C., ECONOMOU, C. K., SMITH, R., GODDARD, P., NAPIER, J. A., SPICER, A. & SAYANOVA, O. 2019. Multifunctionalizing the marine diatom Phaeodactylum

tricornutum for sustainable co-production of omega-3 long chain polyunsaturated fatty acids and recombinant phytase. *Scientific Reports,* 9.

PUETZ, J. & WURM, F. M. 2019. Recombinant proteins for industrial versus pharmaceutical purposes: a review of process and pricing. *Processes,* 7**,** 476.

QIAO, H., CONG, C., SUN, C., LI, B., WANG, J. & ZHANG, L. 2016. Effect of culture conditions on growth, fatty acid composition and DHA/EPA ratio of Phaeodactylum tricornutum. *Aquaculture,* 452**,** 311-317.

RAGNI, M. & D'ALCALA, M. R. 2007. Circadian variability in the photobiology of Phaeodactylum tricornutum: pigment content. *Journal of Plankton Research,* 29**,** 141-156.

RAJA, R., HEMAISWARYA, S., KUMAR, N. A., SRIDHAR, S. & RENGASAMY, R. 2008. A perspective on the biotechnological potential of microalgae. *Crit Rev Microbiol,* 34**,** 77-88.

RAMANAN, R., KIM, B. H., CHO, D. H., OH, H. M. & KIM, H. S. 2016. Algae–bacteria interactions: evolution, ecology and emerging applications. *Biotechnology advances,* 34**,** 14-29.

RAYAT, A. C. M. E., CHATEL, A., HOARE, M. & LYE, G. J. 2016. Ultra scale-down approaches to enhance the creation of bioprocesses at scale: impacts of process shear stress and early recovery stages. *Current Opinion in Chemical Engineering,* 14**,** 150-157.

REBOLLOSO‐FUENTES, M. M., NAVARRO‐PÉREZ, A., RAMOS‐MIRAS, J. J. & GUIL‐GUERRERO, J. L. 2001. Biomass nutrient profiles of the microalga Phaeodactylum tricornutum. *Journal of Food Biochemistry,* 25**,** 57-76.

REDFIELD, A. C. 1958. The Biological Control of Chemical Factors in the Environment. *American Scientist,* 46**,** 205-221.

REIMANN, B. E. F. & VOLCANI, B. E. 1967. Studies on the biochemistry and fine structure of silica shell formation in diatoms: III. The structure of the cell wall of Phaeodactylum tricornutum Bohlin. *Journal of ultrastructure research,* 21**,** 182-193.

RIDLEY, C. J. A., PARKER, B. M., NORMAN, L., SCHLARB-RIDLEY, B., DENNIS, R., JAMIESON, A. E., CLARK, D., SKILL, S. C., SMITH, A. G. & DAVEY, M. P. 2018. Growth of microalgae using nitrate-rich brine wash from the water industry. *Algal Research-Biomass Biofuels and Bioproducts,* 33**,** 91-98.

ROSALES-MENDOZA, S., ANGULO, C. & MEZA, B. 2016. Food-Grade Organisms as Vaccine Biofactories and Oral Delivery Vehicles. *Trends in Biotechnology,* 34**,** 124-136.

SAIFULLAH, A. Z. A., KARIM, M. A. & AHMAD-YAZID, A. 2014. Microalgae: An Alternative Source of Renewable Energy. *American Journal of Engineering Research,* 3**,** 330-338.

SCHEFFEL, A., POULSEN, N., SHIAN, S. & KROGER, N. 2011. Nanopatterned protein microrings from a diatom that direct silica morphogenesis. *Proceedings of the National Academy of Sciences of the United States of America,* 108**,** 3175-3180.

SCHERHOLZ, M. L. & CURTIS, W. R. 2013. Achieving pH control in microalgal cultures through fed-batch addition of stoichiometrically-balanced growth media. *Bmc Biotechnology,* 13.

SEO, S., JEON, H., HWANG, S., JIN, E. & CHANG, K. S. 2015. Development of a new constitutive expression system for the transformation of the diatom Phaeodactylum tricornutum. *Algal Research-Biomass Biofuels and Bioproducts,* 11**,** 50-54.

SHAH, M. M., LIANG, Y., CHENG, J. J. & DAROCH, M. 2016. Astaxanthin-Producing Green Microalga Haematococcus pluvialis: From Single Cell to High Value Commercial Products. *Front Plant Sci,* 7**,** 531.

SHAMLOU, P. A., SIDDIQI, S. F. & TITCHENERHOOKER, N. J. 1995. A Physical Model of High-Pressure Disruption of Bakers-Yeast Cells. *Chemical Engineering Science,* 50**,** 1383-1391.

SHARMA, K. K., GARG, S., LI, Y., MALEKIZADEH, A. & SCHENK, P. M. 2013. Critical analysis of current microalgae dewatering techniques. *Biofuels,* 4**,** 397-407.

SHI, F., WEI, X., FENG, J., SUN, Y. & ZHU, L. 2018. Variation of bacterial community associated with Phaeodactylum tricornutum in response to different inorganic nitrogen concentrations. *Acta Oceanologica Sinica,* 37**,** 118-128.

SIAUT, M., HEIJDE, M., MANGOGNA, M., MONTSANT, A., COESEL, S., ALLEN, A., MANFREDONIA, A., FALCIATORE, A. & BOWLER, C. 2007. Molecular toolbox for studying diatom biology in Phaeodactylum tricornutum. *Gene,* 406**,** 23-35.

SIDDIQI, S. F., TITCHENERHOOKER, N. J. & SHAMLOU, P. A. 1996. Simulation of particle size distribution changes occurring during high-pressure disruption of bakers' yeast. *Biotechnology and Bioengineering,* 50**,** 145-150.

SILKINA, A., FLYNN, K., LLEWELLYN, C. & BAYLISS, C. 2015. Standard Operating Procedures for Analytical Methods and Data Collection in Support of Pilot-Scale Cultivation of Microalgae. *Public Output report WP1A3.01 of the EnAlgae project.* Swansea.

SINGH, G. & PATIDAR, S. K. 2018. Microalgae harvesting techniques: A review. *Journal of Environmental Management,* 217**,** 499-508.

SIRIN, S., TROBAJO, R., IBANEZ, C. & SALVADO, J. 2012. Harvesting the microalgae Phaeodactylum tricornutum with polyaluminum chloride, aluminium sulphate, chitosan and alkalinity-induced flocculation. *Journal of Applied Phycology,* 24**,** 1067-1080.

SMITH, D. J. & UNDERWOOD, G. J. C. 2000. The production of extracellular carbohydrates by estuarine benthic diatoms: The effects of growth phase and light and dark treatment. *Journal of Phycology,* 36**,** 321-333.

SMITH, J. P., HUGHES, A. D., MCEVOY, L. & DAY, J. G. 2020. Tailoring of the biochemical profiles of microalgae by employing mixotrophic cultivation. *Bioresource Technology Reports,* 9**,** 100321.

SMITH, R. V. & FOY, R. H. 1974. Improved hydrogen ion buffering of media for the culture of freshwater algae. *British Phycological Journal,* 9**,** 239-245.

SOBCZUK, T. M., CAMACHO, F. G., GRIMA, E. M. & CHISTI, Y. 2006. Effects of agitation on the microalgae Phaeodactylum tricornutum and Porphyridium cruentum. *Bioprocess and Biosystems Engineering,* 28**,** 243-250.

SPOLAORE, P., JOANNIS-CASSAN, C., DURAN, E. & ISAMBERT, A. 2006. Commercial applications of microalgae. *Journal of Bioscience and Bioengineering,* 101**,** 87-96.

STANLEY, M. S. & CALLOW, J. A. 2007. Whole cell adhesion strength of morphotypes and isolates of Phaeodactylum tricornutum (Bacillariophyceae). *European Journal of Phycology,* 42**,** 191-197.

STEINRUCKEN, P., PRESTEGARD, S. K., DE VREE, J. H., STORESUND, J. E., PREE, B., MJOS, S. A. & ERGA, S. R. 2018. Comparing EPA production and fatty acid profiles of three Phaeodactylum tricornutum strains under western Norwegian climate conditions. *Algal Research-Biomass Biofuels and Bioproducts,* 30**,** 11-22.

STOFFELS, L., FINLAN, A., MANNALL, G., PURTON, S. & PARKER, B. 2019. Downstream Processing of Chlamydomonas reinhardtii TN72 for Recombinant Protein Recovery. *Frontiers in Bioengineering and Biotechnology,* 7.

SULEIMAN, M., ZECHER, K., YÜCEL, O., JAGMANN, N. & PHILIPP, B. 2016. Interkingdom cross-feeding of ammonium from marine methylamine-degrading bacteria to the diatom Phaeodactylum tricornutum. *Applied and environmental microbiology,* 82**,** 7113-7122.

TAN, J. S., LEE, S. Y., CHEW, K. W., LAM, M. K., LIM, J. W., HO, S. H. & SHOW, P. L. 2020. A review on microalgae cultivation and harvesting, and their biomass extraction processing using ionic liquids. *Bioengineered,* 11**,** 116-129.

TANDON, P., JIN, Q. & HUANG, L. 2017. A promising approach to enhance microalgae productivity by exogenous supply of vitamins. *Microb Cell Fact,* 16**,** 219.

TAUNT, H. N., STOFFELS, L. & PURTON, S. 2018. Green biologics: The algal chloroplast as a platform for making biopharmaceuticals. *Bioengineered,* 9**,** 48-54.

TEMPLETON, D. W., QUINN, M., VAN WYCHEN, S., HYMAN, D. & LAURENS, L. M. L. 2012. Separation and quantification of microalgal carbohydrates. *Journal of Chromatography A,* 1270**,** 225-234.

TESSON, B., GAILLARD, C. & MARTIN-JEZEQUEL, V. 2009a. Insights into the polymorphism of the diatom Phaeodactylum tricornutum Bohlin. *Botanica Marina,* 52**,** 104-116.

TESSON, B., GENET, M. J., FERNANDEZ, V., DEGAND, S., ROUXHET, P. G. & MARTIN-JEZEQUEL, V. 2009b. Surface Chemical Composition of Diatoms. *Chembiochem,* 10**,** 2011-2024.

TITCHENER-HOOKER, N. J., DUNNILL, P. & HOARE, M. 2008. Micro biochemical engineering to accelerate the design of industrial-scale downstream processes for biopharmaceutical proteins. *Biotechnology and Bioengineering,* 100**,** 473-487.

TREGUER, P., NELSON, D. M., VAN BENNEKOM, A. J., DEMASTER, D. J., LEYNAERT, A. & QUEGUINER, B. 1995. The silica balance in the world ocean: a reestimate. *Science,* 268**,** 375-9.

TRIPATHI, N. K. & SHRIVASTAVA, A. 2019. Recent Developments in Bioprocessing of Recombinant Proteins: Expression Hosts and Process Development. *Front Bioeng Biotechnol,* 7**,** 420.

UDUMAN, N., QI, Y., DANQUAH, M. K., FORDE, G. M. & HOADLEY, A. 2010. Dewatering of microalgal cultures: A major bottleneck to algae-based fuels. *Journal of Renewable and Sustainable Energy,* 2.

UMMALYMA, S. B., PANDEY, A., SUKUMARAN, R. K. & SAHOO, D. 2018. Bioremediation by Microalgae: Current and Emerging Trends for Effluents Treatments for Value Addition of Waste Streams. *Biosynthetic Technology and Environmental Challenges***,** 355-375.

URSI, S., GUIMARAES, M. & PLASTINO, E. M. 2008. Deleterious effect of TRIS buffer on growth rates and pigment content of Gracilaria birdiae Plastino & EC Oliveira (Gracilariales, Rhodophyta). *Acta Botanica Brasilica,* 22**,** 891-896.

VAN MEER, G., VOELKER, D. R. & FEIGENSON, G. W. 2008. Membrane lipids: where they are and how they behave. *Nature Reviews Molecular Cell Biology,* 9**,** 112-124.

VANDANJON, L., ROSSIGNOL, N., JAOUEN, P., ROBERT, J. M. & QUEMENEUR, F. 1999. Effects of shear on two microalgae species. Contribution of pumps and valves in tangential flow filtration systems. *Biotechnology and Bioengineering,* 63**,** 1-9.

VANIER, G., HEMPEL, F., CHAN, P., RODAMER, M., VAUDRY, D., MAIER, U. G., LEROUGE, P. & BARDOR, M. 2015. Biochemical Characterization of Human Anti-Hepatitis B Monoclonal Antibody Produced in the Microalgae Phaeodactylum tricornutum. *Plos One,* 10.

VARDI, A., THAMATRAKOLN, K., BIDLE, K. D. & FALKOWSKI, P. G. 2008. Diatom genomes come of age. *Genome Biology,* 9.

VARGA, E. G., TITCHENER-HOOKER, N. J. & DUNNILL, P. 1998. Use of scale-down methods to rapidly apply natural yeast homogenisation models to a recombinant strain. *Bioprocess Engineering,* 19**,** 373-380.

VARTANIAN, M., DESCLES, J., QUINET, M., DOUADY, S. & LOPEZ, P. J. 2009. Plasticity and robustness of pattern formation in the model diatom Phaeodactylum tricornutum. *New Phytologist,* 182**,** 429-442.

VILLANOVA, V., FORTUNATO, A. E., SINGH, D., BO, D. D., CONTE, M., OBATA, T., JOUHET, J., FERNIE, A. R., MARECHAL, E., FALCIATORE, A., PAGLIARDINI, J., LE MONNIER, A., POOLMAN, M., CURIEN, G., PETROUTSOS, D. & FINAZZI, G. 2017. Investigating mixotrophic metabolism in the model diatom Phaeodactylum tricornutum. *Philos Trans R Soc Lond B Biol Sci,* 372.

VOULGARIS, I., CHATEL, A., HOARE, M., FINKA, G. & UDEN, M. 2016. Evaluation of options for harvest of a recombinant E-Coli fermentation producing a domain antibody using ultra scale-down techniques and pilot-scale verification. *Biotechnology Progress,* 32**,** 382-392.

VUONG, T. T., KWON, B. R., EOM, J. I., SHIN, B. K. & KIM, S. M. 2019. Interaction between marine bacterium Stappia sp. K01 and diatom Phaeodactylum tricornutum through extracellular fatty acids. *Journal of Applied Phycology***,** 1-12.

WALKER, T. L., PURTON, S., BECKER, D. K. & COLLET, C. 2005. Microalgae as bioreactors. *Plant Cell Rep,* 24**,** 629-41.

WANG, C. & LAN, C. Q. 2018. Effects of shear stress on microalgae - A review. *Biotechnol Adv,* 36**,** 986-1002.

WANG, M., YUAN, W. Q., JIANG, X. N., JING, Y. & WANG, Z. C. 2014. Disruption of microalgal cells using high-frequency focused ultrasound. *Bioresource Technology,* 153**,** 315-321.

WELLBURN, A. R. 1994. The Spectral Determination of Chlorophyll-a and Chlorophhyll-B, as Well as Total Carotenoids, Using Various Solvents with Spectrophotometers of Different Resolution. *Journal of Plant Physiology,* 144**,** 307-313.

WENZL, S., HETT, R., RICHTHAMMER, P. & SUMPER, M. 2008. Silacidins: Highly acidic phosphopeptides from diatom shells assist in silica precipitation in vitro. *Angewandte Chemie-International Edition,* 47**,** 1729-1732.

WILLIS, A., CHIOVITTI, A., DUGDALE, T. M. & WETHERBEE, R. 2013. Characterization of the Extracellular Matrix of Phaeodactylum Tricornutum (Bacillariophyceae): Structure, Composition, and Adhesive Characteristics. *Journal of Phycology,* 49**,** 937-949.

WILSON, D. P. 1946. The triradiate and other forms of Nitzschia closterium (Ehrenberg) Wm. Smith, forma minutissima of Allen and Nelson. *Journal of the Marine Biological Association of the United Kingdom,* 26**,** 235-270.

WRIGHT, S. W., JEFFREY, S. W., MANTOURA, R. F. C., LLEWELLYN, C. A., BJORNLAND, T., REPETA, D. & WELSCHMEYER, N. 1991. Improved Hplc Method for the Analysis of Chlorophylls and Carotenoids from Marine-Phytoplankton. *Marine Ecology Progress Series,* 77**,** 183-196.

WU, H., LI, T., WANG, G., DAI, S., HE, H. & XIANG, W. 2016. A comparative analysis of fatty acid composition and fucoxanthin content in six Phaeodactylum tricornutum strains from diff erent origins. *Chinese journal of oceanology and limnology,* 34**,** 391-398.

XIAO, R. & ZHENG, Y. 2016. Overview of microalgal extracellular polymeric substances (EPS) and their applications. *Biotechnology Advances,* 34**,** 1225-1244.

XIE, W. H., ZHU, C. C., ZHANG, N. S., LI, D. W., YANG, W. D., LIU, J. S., SATHISHKUMAR, R. & LI, H. Y. 2014. Construction of novel chloroplast expression vector and development of an efficient transformation system for the diatom Phaeodactylum tricornutum. *Mar Biotechnol (NY),* 16**,** 538-46.

XU, Y., IBRAHIM, I. M., WOSU, C. I., BEN-AMOTZ, A. & HARVEY, P. J. 2018. Potential of New Isolates of Dunaliella Salina for Natural beta-Carotene Production. *Biology (Basel),* 7.

XUE, J., NIU, Y. F., HUANG, T., YANG, W. D., LIU, J. S. & LI, H. Y. 2015. Genetic improvement of the microalga Phaeodactylum tricornutum for boosting neutral lipid accumulation. *Metabolic Engineering,* 27**,** 1-9.

YAN, N., FAN, C., CHEN, Y. & HU, Z. 2016. The Potential for Microalgae as Bioreactors to Produce Pharmaceuticals. *Int J Mol Sci,* 17.

YANG, S. F., WAN, H. T., WANG, R. & HAO, D. J. 2019. Sulfated polysaccharides from Phaeodactylum tricornutum: isolation, structural characteristics, and inhibiting HepG2 growth activity in vitro. *Peerj,* 7.

YANG, Y. H., DU, L., HOSOKAWA, M., MIYASHITA, K., KOKUBUN, Y., ARAI, H. & TARODA, H. 2017. Fatty Acid and Lipid Class Composition of the Microalga Phaeodactylum tricornutum. *Journal of Oleo Science,* 66**,** 363-368.

YANG, Z. K., NIU, Y. F., MA, Y. H., XUE, J., ZHANG, M. H., YANG, W. D., LIU, J. S., LU, S. H., GUAN, Y. F. & LI, H. Y. 2013. Molecular and cellular mechanisms of neutral lipid accumulation in diatom following nitrogen deprivation. *Biotechnology for Biofuels,* 6.

YAO, S., LYU, S., AN, Y., LU, J., GJERMANSEN, C. & SCHRAMM, A. 2019. Microalgae-bacteria symbiosis in microalgal growth and biofuel production: a review. *J Appl Microbiol,* 126**,** 359-368.

YAO, Y., LU, Y., PENG, K. T., HUANG, T., NIU, Y. F., XIE, W. H., YANG, W. D., LIU, J. S. & LI, H. Y. 2014. Glycerol and neutral lipid production in the oleaginous marine diatom Phaeodactylum tricornutum promoted by overexpression of glycerol-3-phosphate dehydrogenase. *Biotechnology for Biofuels,* 7.

YELLAPU, S. K., BHARTI, KAUR, R., KUMAR, L. R., TIWARI, B., ZHANG, X. L. & TYAGI, R. D. 2018. Recent developments of downstream processing for microbial lipids and conversion to biodiesel. *Bioresource Technology,* 256**,** 515-528.

YONGMANITCHAI, W. & WARD, O. P. 1991. Growth of and Omega-3-Fatty-Acid Production by Phaeodactylum-Tricornutum under Different Culture Conditions. *Applied and Environmental Microbiology,* 57**,** 419-425.

YOO, G., YOO, Y., KWON, J. H., DARPITO, C., MISHRA, S. K., PAK, K., PARK, M. S., IM, S. G. & YANG, J. W. 2014. An effective, cost-efficient extraction method of biomass from wet microalgae with a functional polymeric membrane. *Green Chemistry,* 16**,** 312-319.

ZAMAN, F., ALLAN, C. M. & HO, S. V. 2009. Ultra Scale-Down Approaches for Clarification of Mammalian Cell Culture Broths in Disc-Stack Centrifuges. *Biotechnology Progress,* 25**,** 1709-1716.

ZASLAVSKAIA, L. A., LIPPMEIER, J. C., KROTH, P. G., GROSSMAN, A. R. & APT, K. E. 2000. Transformation of the diatom Phaeodactylum tricornutum (Bacillariophyceae) with a variety of selectable marker and reporter genes. *Journal of Phycology,* 36**,** 379-386.

ZASLAVSKAIA, L. A., LIPPMEIER, J. C., SHIH, C., EHRHARDT, D., GROSSMAN, A. R. & APT, K. E. 2001. Trophic conversion of an obligate photoautotrophic organism through metabolic engineering. *Science,* 292**,** 2073-2075.

ZERIOUH, O., REINOSO-MORENO, J. V., LOPEZ-ROSALES, L., CERON-GARCIA, M. D. C., SANCHEZ-MIRON, A., GARCIA-CAMACHO, F. & MOLINA-GRIMA, E. 2017. Biofouling in photobioreactors for marine microalgae. *Crit Rev Biotechnol,* 37**,** 1006-1023.

ZHAN, J., RONG, J. F. & WANG, Q. 2017. Mixotrophic cultivation, a preferable microalgae cultivation mode for biomass/bioenergy production, and bioremediation, advances and prospect. *International Journal of Hydrogen Energy,* 42**,** 8505-8517.

ZHANG, C. & HU, H. 2014. High-efficiency nuclear transformation of the diatom Phaeodactylum tricornutum by electroporation. *Mar Genomics,* 16**,** 63-6.

ZHANG, H., KONG, S., BOOTH, A., BOUSHABA, R., LEVY, M. S. & HOARE, M. 2007a. Prediction of shear damage of plasmid DNA in pump and centrifuge operations using an ultra scale-down device. *Biotechnology Progress,* 23**,** 858-865.

ZHANG, P. Y., ZHANG, G. M. & WANG, W. 2007b. Ultrasonic treatment of biological sludge: Floc disintegration, cell lysis and inactivation. *Bioresource Technology,* 98**,** 207-210.

ZHAO, P., GU, W., WU, S., HUANG, A., HE, L., XIE, X., GAO, S., ZHANG, B., NIU, J., LIN, A. P. & WANG, G. 2014. Silicon enhances the growth of Phaeodactylum tricornutum Bohlin under green light and low temperature. *Scientific reports,* 4**,** 3958.

ZHOU, X., YUAN, S., CHEN, R. & OCHIENG, R. M. 2015. Sustainable production of energy from microalgae: review of culturing systems, economics, and modelling. *Journal of Renewable*

Sustainable Energy, 7**,** 012701.

ZIOLKOWSKA, J. R. & SIMON, L. 2014. Recent developments and prospects for algae-based fuels in the US. *Renewable and Sustainable Energy Reviews,* 29**,** 847-853.

Appendix

Example sigma calculation

In Chapter 5, an Eppendorf centrifuge 5424/5424R equipped with a 1.5/2.0 mL 24-place rotor (FA-45-24-11) was used for the clarification study. The variables and constants for this bench-top centrifuge are as follows:

V_{USD} (mL)	2.0
R_1 (mm)	48
R_2 (mm)	68
Acceleration time (s)	15
Deceleration time (s)	16

Example calculation (centrifuged at 10,000 rpm for 6 min):

$$\omega = 2\pi N = \frac{2 \times \pi \times 10000\ rpm}{60\ s\ min^{-1}} = 1047.198\ rad\ s^{-1}$$

$$x = \frac{15\ s}{6 \times 60\ s} = 0.0417$$

$$y = \frac{16\ s}{6 \times 60\ s} = 0.0444$$

$$3 - 2x - 2y = 3 - 2 \times 0.0417 - 2 \times 0.0444 = 2.828$$

$$\Sigma_{USD} = \frac{V_{USD}\omega^2(3 - 2x - 2y)}{6gln\left(\frac{2R_2}{R_2 + R_1}\right)} = \frac{(2.0 \times 10^{-6}\ m^3) \times (1047.2\ rad\ s^{-1})^2 \times 2.828}{6 \times (9.81\ m\ s^{-2}) \times \ln(\frac{2 \times 0.068\ m}{0.068\ m + 0.048\ m})} = 0.648\ m^2$$

$$\frac{V_{USD}}{C_{USD}t_{USD}\Sigma_{USD}} = \frac{2.0 \times 10^{-6}\ m^3}{1 \times 6 \times 60\ s \times 0.648\ m^2} = 0.86 \times 10^{-8}\ m\ s^{-1}$$

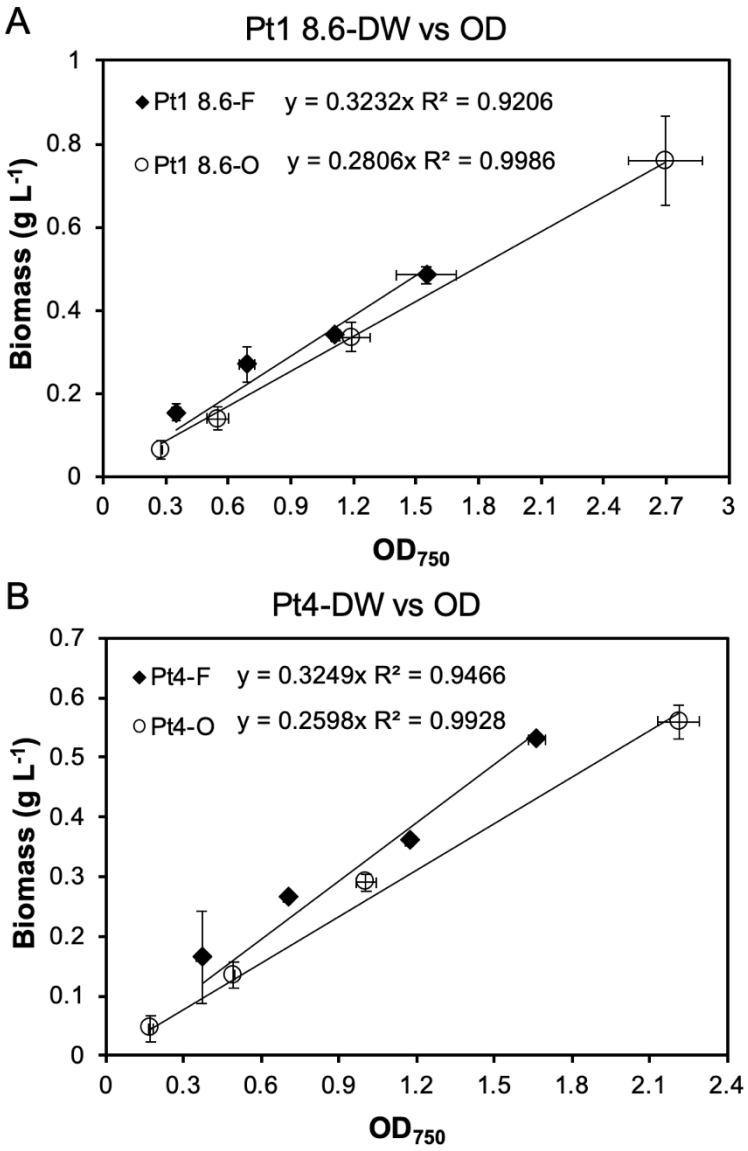

Figure A-1 Calibration curves of dry biomass concentration versus OD_{750} readings for *P. tricornutum*.

Calibration curves for fusiform (F) cell cultures grown in f/2 medium or oval (O) cell cultures grown in M & M medium of Pt1 8.6 (A) and Pt4 (B). Symbols are shown as mean ± one standard deviation from three biological replicates. Lines represent the trendline of best fit for each data set with the equation and R^2 value shown.

Scale-up cultivation with hanging bags

Figure A-2 Scale-up cultivation of Pt4 in hanging plastic bags.

A preliminary test for scale-up cultivation of fusiform (F) cells grown in f/2 medium or oval (O) cells grown in M & M medium of Pt4. Cultures were grown in hanging

plastic (polythene) bags with the working volume of 5 L at room temperature under continuous illumination at 100-200 µmol photons m^{-2} s^{-1} from three LED panels and aeration at 0.8-1.2 L min^{-1}. Cells were observed to accumulate in the bottom corners of the bags as mixing was not optimal and some ghost cells were observed under microscopy.

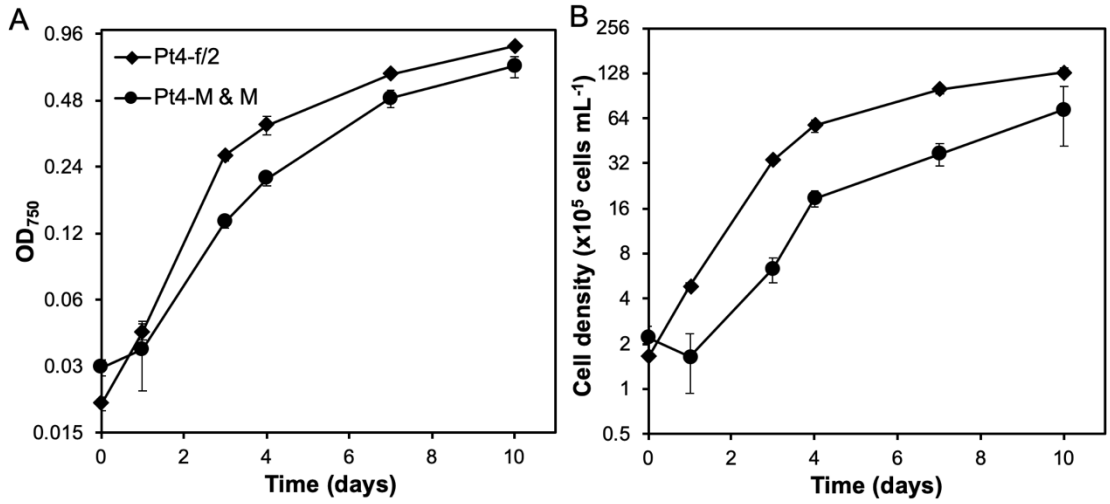

Figure A-3 Growth profiles of Pt4 from scale-up cultivation in hanging bags.

Growth curves measured by OD_{750} (A) or cell density (B) for fusiform cell cultures grown in f/2 medium or oval cell cultures grown in M & M medium of Pt4 (Figure A-2). Data are shown as mean ± one standard deviation from three biological replicates. Microscopic examination showed that Pt4 cells grown in M & M medium in hanging bags displayed the oval morphotype (Data not shown).

Table A-1 Dry biomass concentration, maximum specific growth rate and doubling time of fusiform (F) and oval (O) Pt4 cultures.

	DW (g L^{-1})	Maximum specific growth rate (d^{-1})	Doubling time (d)
Pt4-F	0.40±0.02	1.08±0.02	0.64±0.01
Pt4-O	0.26±0.02	1.09±0.16	0.65±0.10

Data are shown as mean ± one standard deviation from three biological replicates.
Dry biomass concentration (DW) was measured on day 10.
All cultures were grown in hanging bags (Figure A-2) with the working volume of 5 L.

Publication list

1. **Song, Z**., Lye, G. J., and Parker, B. M. 2020. Morphological and biochemical changes in *Phaeodactylum tricornutum* triggered by culture media: Implications for industrial exploitation. *Algal Research*, 47, 101822.

2. **Song, Z**., Vilatte, A., Lye, G. J., and Parker, B. M. 2020. Ultra scale-down mimics for cell harvest and disruption of fusiform and oval *Phaeodactylum tricornutum* morphotypes. *Manuscript preparation*.